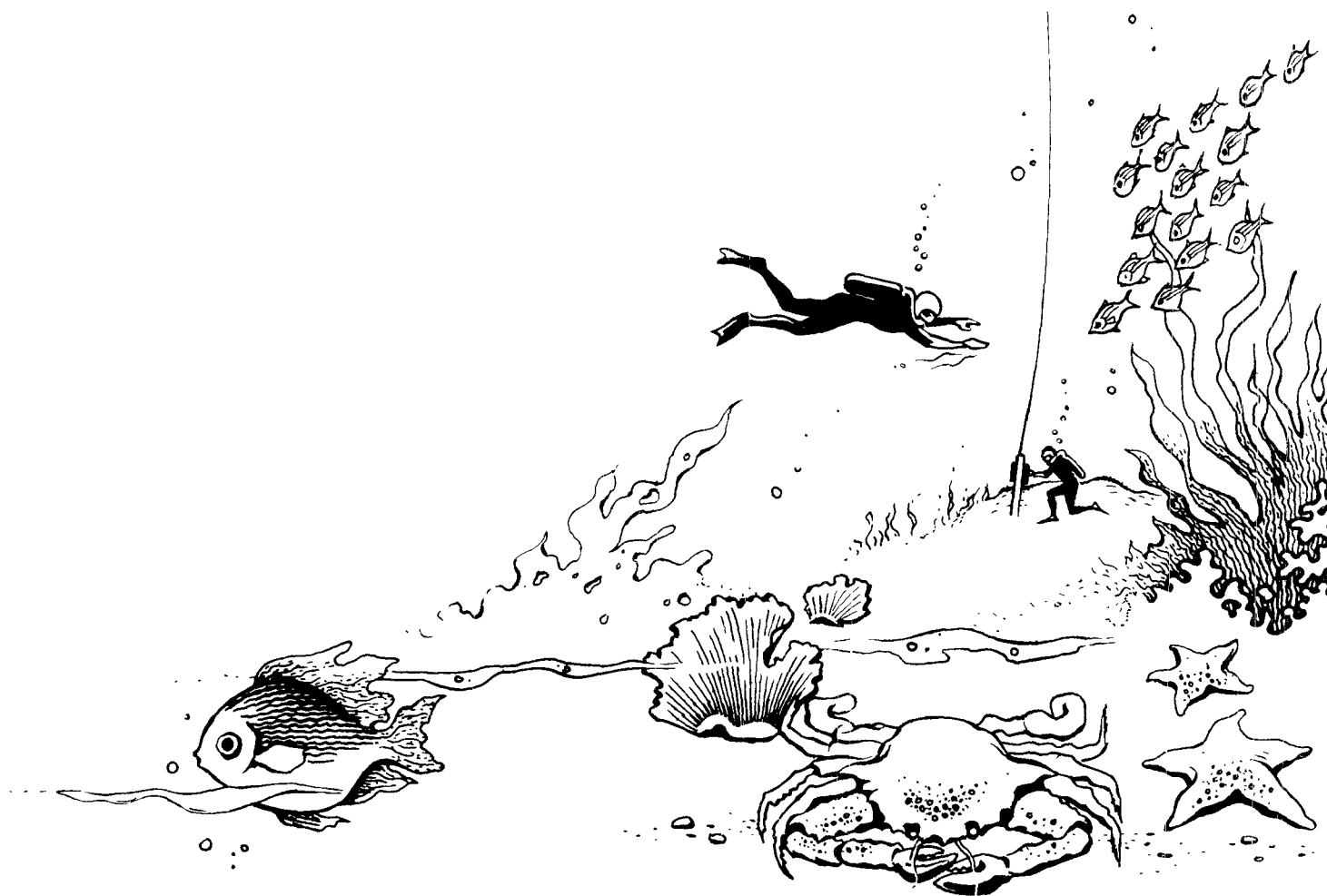
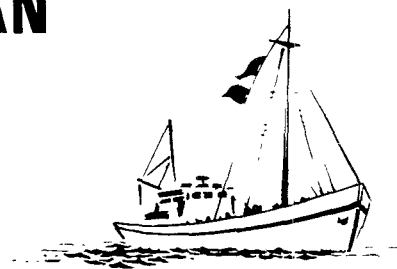




# AIRPHOTO ANALYSIS OF OCEAN OUTFALL DISPERSION



U.S. ENVIRONMENTAL PROTECTION AGENCY

## WATER POLLUTION CONTROL RESEARCH SERIES

The Water Pollution Control Research Series describes results and progress in the control and abatement of pollution in our Nation's waters. They provide a central source of information on the research, development and demonstration activities in the Environmental Protection Agency, through inhouse research and grants and contracts with Federal, State, and local agencies, research institutions, and industrial organizations.

Inquiries pertaining to Water Pollution Control Research Reports should be directed to the Chief, Publications (Water), Research Information Division, R&M, Environmental Protection Agency, Washington, D.C. 20460.

AIRPHOTO ANALYSIS  
OF  
OCEAN OUTFALL DISPERSION

by

Oregon State University  
Fred J. Burgess, Principal Investigator  
Dean, School of Engineering  
Wesley P. James, Research Associate  
Corvallis, Oregon 97331

for the

ENVIRONMENTAL PROTECTION AGENCY

Program No. 16070 ENS  
June, 1971

Environmental Protection Agency  
Library, Region V  
1 North Wacker Drive  
Chicago, Illinois 60606

EPA Review Notice

This report has been reviewed by the Water Quality Office, EPA, and approved for publication. Approval does not signify that the contents necessarily reflect the views and policies of this office, nor does mention of commercial products constitute endorsement for use.

ENVIRONMENTAL PROTECTION AGENCY



## ABSTRACT

Aerial photography was taken of the ocean outfall waste plume at Newport, Oregon, during the summers of 1968, 1969, and the period extending from September 1970 through May 1971. Computerized techniques to analyze the photos were developed by combining the principles of photogrammetry and photo interpretation. This remote sensing system involving multispectral photography was utilized to yield waste concentrations, water currents and diffusion coefficients.

Conventional boat sampling of the waste field was conducted concurrently with the photography during the 1968 and 1969 field seasons. The waste concentrations determined by the two methods were compared by matching ground coordinates. The correlation coefficient for the comparison ranged from 0.85 to 0.95. The photographic technique is more comprehensive than conventional boat sampling and permits waste concentrations to be measured throughout the plume in one instant. Discrepancies between concentrations determined by boat sampling and concentrations determined from aerial photography appear to be due primarily to changing and shifting of the waste field during the two hour boat sampling period.

Procedures were developed to evaluate proposed ocean outfall sites by using dye drops from an airplane. Diffusion coefficients and water current velocities were determined from aerial photography. A minimum of two photographic flights over the area were required to show the transport and spread of the dye patches.

When the hydrography of the receiving water allowed the formation of a surface plume, the water current velocity was found to be the dominant factor in the resulting plume pattern. The steady state form of the Fickian diffusion equation with a unidirectional transport velocity was not applicable to the majority of the observations. The equation for a line source in a uniform stream provided the x and y velocity components for a two-dimensional diffusion model with the losses to the lower layers being considered by including a decay coefficient. The second model was found to be more applicable to the diffusion process.

Characteristic airphoto pattern elements are given for visual interpretation of the photography. Wind velocity, sea state, current velocity, wave height and diffusion coefficients can be estimated from the aerial photography.

Key Words: Ocean outfall, aerial photography, remote sensing, marine disposal, diffusion, water currents.

## CONTENTS

<u>Section</u>		<u>Page</u>
I	Conclusions	1
II	Recommendations	3
III	Introduction	5
IV	Background	7
V	Rationale	13
VI	Diffusion Studies	43
VII	Sampling Procedures	47
VIII	Dye Patch Studies	55
IX	Data Processing	59
X	Sampling Results	77
XI	Discussion of the Results	153
XII	Summary	175
XIII	Acknowledgments	179
XIV	References	181
XV	Publications	185
XVI	Appendices	187

## FIGURES

	<u>Page</u>
1. Camera filtered to absorption band of rhodamine WT dye.	8
2. Camera filtered to fluorescence band of rhodamine WT dye.	8
3. Infrared black and white photo of algal bloom in a lake.	11
4. Infrared black and white photo of a waste plume.	11
5. Spectral distribution of radiant energy.	14
6. Direct sunlight and skylight on a horizontal plane.	17
7. Sunlight reflection from a sloping water surface.	18
8. Light penetration into the sea.	19
9. Typical attenuation coefficients.	21
10. Volume scattering function.	22
11. Variation in the scattering angle.	23
12. Effect of contaminant on the scattering function.	24
13. Light from the sea.	26
14. Depth of light return from the sea.	28
15. Typical spectral signature.	31
16. Geometry of exposure calculation.	32
17. Typical characteristic curve of an aerial positive film.	34
18. Spectral response curves.	37
19. Aerial view of Newport area.	48
20. Sketch of the Newport outfall.	49
21. Multiple camera unit.	53
22. Dye patch on July 7, 1969.	56
23. Data processing flow diagram.	60

	<u>Page</u>
24. Waste concentrations from boat sampling on August 12, 1969.	61
25. Surface water temperature on August 12, 1969.	61
26. Water temperature profiles on August 12, 1969.	62
27. Flow diagram for photographic processing.	64
28. Symbolic plots from two flights August 16, 1968.	67
29. Isoconcentration plot, flight on August 16, 1968.	67
30. Digitizing aerial film.	73
31. Scanning densitometer.	73
32. Infrared black and white photo on July 7, 1969.	79
33. Plume on July 8, 1969 at 15:21 from 4000 feet.	79
34. Temperature profiles July 7 and 8, 1969.	80
35. Plume July 8, 1969 at 15:56 from 4000 feet.	81
36. Plot of residuals - 1968.	86
37. Plot of residuals - 1969.	87
38. Comparison of boat and photo values on August 8, 1968.	88
39. Comparison of boat and photo values on August 16, 1968.	89
40. Comparison of boat and photo values July 8, 1969.	90
41. Comparison of boat and photo values August 12, 1969.	91
42. Chart of the outfall area at Newport, Oregon.	99
43. Aerial photo of outfall area on September 9, 1970 from 8000 feet at 14:30.	100
44. Data for September 9, 1970.	101
45. Aerial photo of outfall area on September 23, 1970 from 8000 feet at 15:30.	102
46. Data for September 23, 1970.	103

	Page
47. Aerial photo of outfall area on September 30, 1970 from 5000 feet at 14:54.	104
48. Data for September 30, 1970.	105
49. Aerial photo of outfall area on October 7, 1970 from 3000 feet at 14:32.	106
50. Data for October 7, 1970.	107
51. Aerial photo of outfall area on October 12, 1970 from 4000 feet at 14:10.	108
52. Data for October 12, 1970.	109
53. Aerial photo of outfall area December 21, 1970 from 6000 feet at 13:15.	110
54. Data for December 21, 1970.	111
55. Aerial photo of outfall area on December 23, 1970 from 3000 feet at 11:25.	112
56. Data for December 23, 1970.	113
57. Aerial photo of outfall area on December 31, 1970 from 3000 feet at 12:10.	114
58. Data for December 31, 1970.	115
59. Aerial photo of outfall area on January 2, 1971 from 4000 feet at 11:40.	116
60. Data for January 2, 1971.	117
61. Aerial photo of outfall area on February 6, 1971 from 6000 feet at 11:55.	118
62. Data for February 6, 1971 AM.	119
63. Aerial photo of outfall area on February 6, 1971 from 4000 feet at 14:18.	120
64. Data for February 6, 1971 PM.	121
65. Aerial photo of outfall area on March 16, 1971 from 4250 feet at 12:20.	122

	<u>Page</u>
66. Data for March 16, 1971.	123
67. Aerial photo of outfall area on March 17, 1971 from 4000 feet at 14:25.	124
68. Data for March 17, 1971.	125
69. Aerial photo of outfall area on March 18, 1971 from 8000 feet at 11:42.	126
70. Data for March 18, 1971.	127
71. Aerial photo of outfall area on March 19, 1971 from 8000 feet at 11:27.	128
72. Data for March 19, 1971 AM.	129
73. Aerial photo of outfall area on March 19, 1971 from 6000 feet at 13:50.	130
74. Data for March 19, 1971 PM.	131
75. Aerial photo of outfall area on March 24, 1971 from 6000 feet at 16:00.	132
76. Data for March 24, 1971.	133
77. Aerial photo of outfall area on April 12, 1971 from 6000 feet at 14:45.	134
78. Data for April 12, 1971.	135
79. Aerial photo of outfall area on April 15, 1971 from 4000 feet at 14:07.	136
80. Data for April 15, 1971.	137
81. Aerial photo of outfall area on April 21, 1971 from 4000 feet at 13:46.	138
82. Data for April 21, 1971.	139
83. Aerial photo of outfall area on April 26, 1971 from 6000 feet at 14:20	140
84. Data for April 26, 1971.	141
85. Aerial photo of outfall area on May 7, 1971 from 4000 feet at 15:13.	142

	<u>Page</u>
86. Data for May 7, 1971.	143
87. Aerial photo of outfall area on May 10, 1971 from 4000 feet at 16:10.	144
88. Data for May 10, 1971.	145
89. Aerial photo of outfall area on May 13, 1971 from 6000 feet at 14:10.	146
90. Data for May 13, 1971.	147
91. Aerial photo of outfall area on May 14, 1971 from 4000 feet at 14:48.	148
92. Data for May 14, 1971.	149
93. Photos of sea conditions.	150
94. Plume patterns for a unidirectional transport velocity.	154
95. Isoconcentration plot, August 8, 1968.	155
96. Geometry for a line source in a uniform stream.	158
97. Plots of a source in a uniform stream.	160
98. Potential flow solutions for a line source.	161
99. Isoconcentration plots from diffusion model.	163
100. Typical diurnal thermoclines.	165
101. Development of current velocity profile.	166
102. Mottled photo pattern from surface waves.	173

## TABLES

<u>No.</u>		<u>Page</u>
1	Preliminary diffusion coefficients, flight 1, August 16, 1968.	70
2	Nonsteady-state diffusion coefficients, August 16, 1968.	71
3.	1968-1969 sampling summary for Newport.	78
4.	Summary of the 1968 vertical aerial photography.	83
5.	Summary of the 1969 oblique aerial photography.	84
6.	Wind scales and sea descriptions.	151
7.	Summary of the 1970-71 data.	152
8.	Preliminary diffusion coefficients, flight 2, August 8, 1968.	157
9.	Sea state due primarily to wind.	168
10.	Sea state due primarily to swell.	169
11.	Sea state due to wind and swell.	170
12.	Conditions in fully developed seas.	172



## SECTION I

### CONCLUSIONS

1. Aerial photography provides an effective method for a comprehensive analysis of the dispersion of wastes that are discharged into the ocean.
2. Aerial photographs showing the transport and spread of dye patches will provide detailed design information for evaluating proposed ocean outfall sites throughout the year.
3. Characteristic airphoto pattern elements can be utilized to estimate wind velocity, sea state, water current velocities and diffusion coefficients in the nearshore areas.
4. In addition to being technically feasible, aerial photography has been shown to be an economically feasible method for acquiring ocean outfall design data prior to discharge.
5. The surface water current is a dominant factor in the resulting plume pattern. The currents were primarily generated by the wind with tide playing a minor role.
6. A two dimensional Fickian diffusion model was usually adequate to explain the resulting plume pattern. The surface spreading of the waste field was considered in the model by including the equations for a line source in a uniform stream while vertical diffusion was considered by including a decay coefficient.
7. There was no indication that the diffusion coefficients varied to the  $4/3$  power of the scale.

## SECTION II

### RECOMMENDATIONS

1. It is recommended that aerial photography be used to obtain information for evaluation of requests for waste discharge permits that involve ocean outfalls.
2. It is recommended that aerial photography be used in establishing surveillance programs and in conducting surveillance programs on operating waste discharge outfalls.
3. It is recommended that future studies be conducted to establish the importance of both the vertical diffusion coefficient and the vertical stability on the waste disposal process. Such a study should include continuous recording of wind, water current profiles for several locations, and wave profiles in order to better understand the response of the sea to the wind forces. The effect of the scale of the turbulence on the rate of diffusion needs additional study.
4. It is also recommended that a critical analysis of actual field conditions versus the original design predictions be made for the several ocean outfalls in Oregon and at Eureka, California. Such a study will indicate areas of design deficiencies and will improve the technology of ocean outfall disposal.

## SECTION III

### INTRODUCTION

The objective of this research is to develop a remote sensing tool for the evaluation of dispersion of wastes from existing or proposed ocean outfalls. Photogrammetric and photo interpretation methods are used to determine dispersion patterns, diffusion coefficients, waste concentrations and nearshore currents. This study is unique in that the aerial photography is not only used to determine the position of points and the size of objects as in normal photogrammetry, but the photograph is also used as an energy sensor. The amount of light reflected from an object is recorded by the photograph as the film density of the image. The light scattered from within the sea is measured from the film with a photo densitometer and can be related to certain water quality parameters.

An ocean outfall is a pipeline that is used for discharging waste into the ocean. The pipeline extends into the receiving body of water and usually terminates with a diffuser section where the flow is divided into a number of small jets.

The discharging jets of waste are subjected to momentum forces and to a buoyant force which is proportional to the density difference between the effluent and the receiving water. As the jet of liquid rises towards the surface, it mixes with the ambient fluid and both its momentum and buoyance per unit volume decrease. The mixing causes a waste field to be formed either at the surface or submerged below the sea surface depending on the hydrography of the site and initial dilution.

If there is little density stratification in the receiving water, the effluent, being less dense than sea water, will rise to the surface to form a surface waste field. After the initial dilution due to jet diffusion, the waste is transported from the site by current action and continues to mix and spread by natural turbulence in the receiving body.

The conventional method of studying the waste field from an outfall has been by boat sampling with the tracer technique. The use of this method for water quality studies has been enhanced by the development of highly sensitive instruments and new dye tracers during the past several years.

The use of radioactive tracers has been limited by handling problems and misunderstanding by the public. The use of fluorescent dyes as tracers avoids these objections and gives satisfactory results in most quality studies. Fluorescein dye has been used for the past 50 years but has the disadvantage of a high photochemical decay rate (Wilson, 1968). Rhodamine B has a low decay rate but tends to adhere to suspended particles. This may result in a low recovery of the dye.

Rhodamine WT and pontacyl pink dyes both have low sorptive tendency, but the pontacyl pink is about four times as expensive as the rhodamine WT solution.

The general procedure for tracing waste discharged from an existing outfall is to meter the dye tracer into the pipeline. Complete mixing of the tracer and waste is required. By knowing the tracer injection rate and the waste discharge rate, the tracer concentration within the pipeline can be determined. This mixture passes through the diffusers and forms the waste field. Tracer concentrations in the waste plume are measured by sampling from a boat. The waste concentration at any point in the waste field can then be computed from the samples on the basis of the dye concentration.

Ocean outfall sewers for the disposal of waste along the Pacific Northwest coastline are, in general, located on the relatively shallow coastal shelf which is subjected to heavy seas. Sampling from a boat in these areas is dangerous at all times and impossible much of the time due to rough water. The use of aerial photography and photogrammetric methods presents a possible method for overcoming this difficulty. From two to eight hours of continuous sampling from a boat is required to adequately define the waste field in the vicinity of an ocean outfall. The waste field is usually shifting thus making a comprehensive study nearly impossible by conventional methods. The aerial photographic technique presents a method where concentrations throughout the waste field can be measured in one instant. Consideration of these factors suggest that photogrammetry can be a most useful tool for water quality investigations. Prior to this time the use of aerial photography for water quality studies has been limited to identifying pollution sources, but has not been used for making quantitative measurements from the photographs.

The field work was conducted at the Georgia-Pacific Kraft pulp mill outfall at Newport because of its convenient location. This site provided an additional advantage since the natural color of the waste effluent was visible on aerial photography. However, the results of this study are not limited to Kraft pulp mill outfalls. If the effluent from an outfall has the same light scattering and light absorption properties as the receiving water, dye can be added to the effluent to distinguish the waste field from the receiving body of water. The natural color characteristics of the Kraft pulp waste will vary with time while the addition of dye to a colorless waste will give greater control over the test.

In order to obtain design information at proposed outfall locations, aerial photography is taken of dye patches. The dye markers are dropped from the aircraft at selected locations in the waste disposal area. Current velocities and diffusion coefficients are determined from the change in position and size of the dye patches between two photographic flights over the proposed site.

## SECTION IV

### BACKGROUND

Both the color of the waste and the amount of light scattered from below the water surface can be recorded on aerial photography. Most black and white film used today for aerial photography is panchromatic film which is sensitive to the 400-700<sup>1</sup> nm region of the spectrum. By using lens filters on the camera, the exposure can be limited to a selected region of the spectrum. Generally the film-filter combination is sketched to give maximum contrast between the object and background. For example, when aerial photography is taken of a rhodamine WT dye patch in the ocean, high contrast can be obtained by either filtering the camera to the band of maximum light absorption of the dye or filtering the camera to the maximum fluorescence of the dye as shown in figures 1 and 2. For the first case, on a positive black and white print, the sea would appear light in tone while the dye patch would appear dark. However, if the camera is filtered to maximum fluorescence, the dye patch would be light in tone while the sea would appear dark.

Blue light with a wave length of about 480 nm has the greatest penetration in the deep ocean waters. In the turbid coastal waters the greatest penetration occurs at about 530 nm (Jerlov, 1968). As the composition, size or concentration of particles in the water vary, the band of greatest penetration and color of the sea may also change. Photography can, under certain conditions, be used to distinguish water masses, to delineate current patterns, to identify upwelled water along the coast and to track river plumes in the ocean.

Color photography divides the visible spectrum into three bands. The composition of the light is recorded as blue, green, and red colors on a positive transparency or print. For many applications of aerial photography the three bands are adequate. However, the color film has been designed to reproduce a natural land scene which is visually similar to the original view. The film may not give the best results possible if it is used for other than its designed purpose. Strandberg (1966, 1967) of Itek Data Analysis Center has published numerous examples of color photographs for water quality analysis. In these examples it was possible to detect the sources of pollution; however, no attempt was made to measure pollution concentration.

Color infrared film is sometimes called false color film. The blue, green and red colors on the photograph result from exposures to the green, red and infrared bands of the spectrum, respectively (Fritz, 1967). Besides military uses, the film has been used extensively in the detection of disease and insect pests in forest and agriculture

---

<sup>1</sup>Nanometers, 10<sup>-9</sup> meters

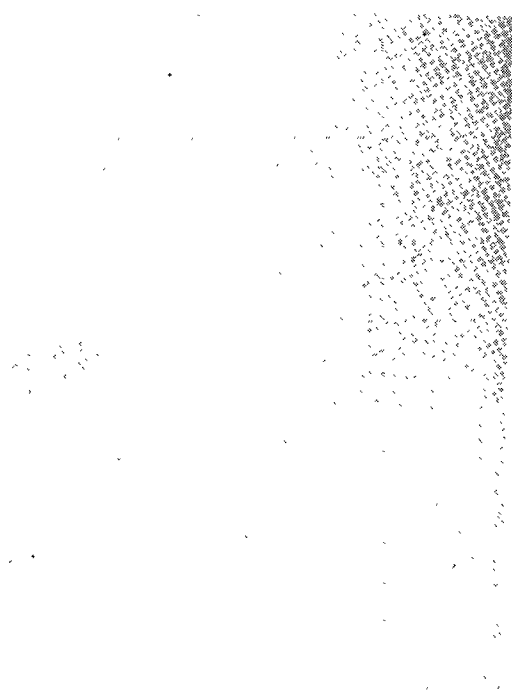


Figure 1. Camera filtered to absorption band of rhodamine WT dye.



Figure 2. Camera filtered to fluorescence band of rhodamine WT dye.

crops (American. . ., 1960). It also has been used advantageously in geological and soils interpretation. When using this film a yellow filter is needed to eliminate the blue light, thereby reducing the degrading effect of haze. As skylight reflection on the water surface is also predominantly blue, infrared color photography of underwater details will appear clearer than with ordinary color photography. Generally, the infrared layer on the film is underexposed when photographing a water body.

Narrow band filters permit the selection of the region of the spectrum that has minimum interference and maximum subject contrast. Interference filters have several advantages over absorption filters including high peak transmittance and sharp cutoffs. However, the peak wavelength of an interference filter is a function of the angle of incidence of the radiation impinging on the filter. If it is desired to record essentially the same band or region of the spectrum on the edges of the frame as in the center of the picture, interference filters can only be used with cameras having a narrow angle field of view. The color characteristics of waste from the Kraft pulp process vary causing the optimum film-filter combinations required to study the effluent plume to change. The same film-narrow band filter combinations used to study one waste can probably not be used to study a plume of a different waste or to study fluorescent dye concentrations in a dye patch.

Multiband camera systems have been developed by several organizations (Yost and Wenderoth, 1967; Molineux, 1965). This system has a number of film-filter combinations to take simultaneous photographs in several regions in the spectrum. This method not only allows the selection of several film-filter combinations for optimum results, but permits the proper exposure of each spectral band. For an example, on a normal color photograph of the sea, the blue sensitive layer is generally over exposed while the red sensitive is generally under exposed. A multiband camera system would allow the proper exposure of each band.

In research at the Allen Hancock Foundation it was found that high optical absorbance of millipore-filtered water to light at a wavelength of 230 nm is related to the concentration of sewage. In their study (Allen. . ., 1964), the ultraviolet absorbance was suggested as a possible method of tracing the sewage field by direct sampling without using a tracer. A film sensitive to the ultraviolet region of the spectrum might be used to trace the sewage field. However, the ultraviolet is also the region of maximum atmospheric interference.

Infrared film is sensitive to both the blue and infrared regions of the spectrum. It is, therefore, necessary to use lens filters in order to limit the exposure to the infrared region. Infrared photography will record energy in the 700-900 nm region. At normal temperatures the energy in this region is predominantly reflected energy, not emitted energy, and is not related to temperature. Due to

the high attenuation of water in the infrared band, water surfaces on an infrared black and white photograph will normally appear black. The high contrast between the water and land is used to advantage when mapping the water line of a body of water. Algae have high reflectance in this band and infrared photography is used to monitor blooms. The photo in figure 3 shows the aerial distribution of the algal bloom in the lake. Concentration and total mass can be estimated from the photography. An infrared photo of the waste field from an ocean outfall is shown in figure 4. When taking black and white photographs of water, the exposure is about two stops greater than ordinary land detail. As a result, the shore in figure 3 and the four boats in figure 4 are overexposed.

Objects at normal temperature radiate thermal infrared rays at a wavelength greater than can be recorded on ordinary infrared film. Suitable equipment is now available for measuring surface water temperatures by remote sensing. Infrared scanning of 4.5 - 5.5 micron wavelength has been used successfully by the U.S. Geological Survey to locate fresh water springs in Hawaii (Fisher, Davis, and Sousa, 1966). In this study the sea water temperature averaged 73.5 degrees F while the fresh water temperature was between 60 and 70 degrees F. Scanning in the 8-14 micron wavelength would be most suitable for water surface temperatures as this is the region of maximum radiation and the region relatively free of reflected sunlight interference. It is expected that temperature differences of 0.2 degrees C can be detected by scanning in this region (Ory, 1965). The temperature of the waste may provide a suitable tracer for a thermal effluent discharge. For cooler industrial wastes the use of heat as a tracer is unlikely since the thermal resolution of the scanning equipment is about the same magnitude as the expected maximum difference in temperature within the waste field. In the ocean, vertical thermal stratification will exist under certain conditions. Warm wastes discharged from the diffuser of an ocean outfall will mix with the colder subsurface water and by the time the mixture reaches the surface, the resulting plume temperature may be greater than, less than, or equal to the surrounding ocean temperature.

Surface currents have been measured successfully with aerial photography by a number of investigators. The Coast and Geodetic Survey has been using aerial photography to measure surface tidal currents for more than ten years (Keller, 1963). Waldichuk (1966) found long strips of buoyant paper provided an economical target for surface current measurement as long as the sea was not so rough that the paper would buckle and twist. A study by the Water Pollution Research Board of England (1964) indicated that drift cards released over the outlet of an ocean outfall did not in general follow the sewage field but were deflected by the wind; however, drift poles and surface floats with drogues at about five feet did follow the waste plume.

Romanousky (1966), from the Center for Oceanographic Research and Studies in Paris, has studied diffusion of wastewaters by photographing



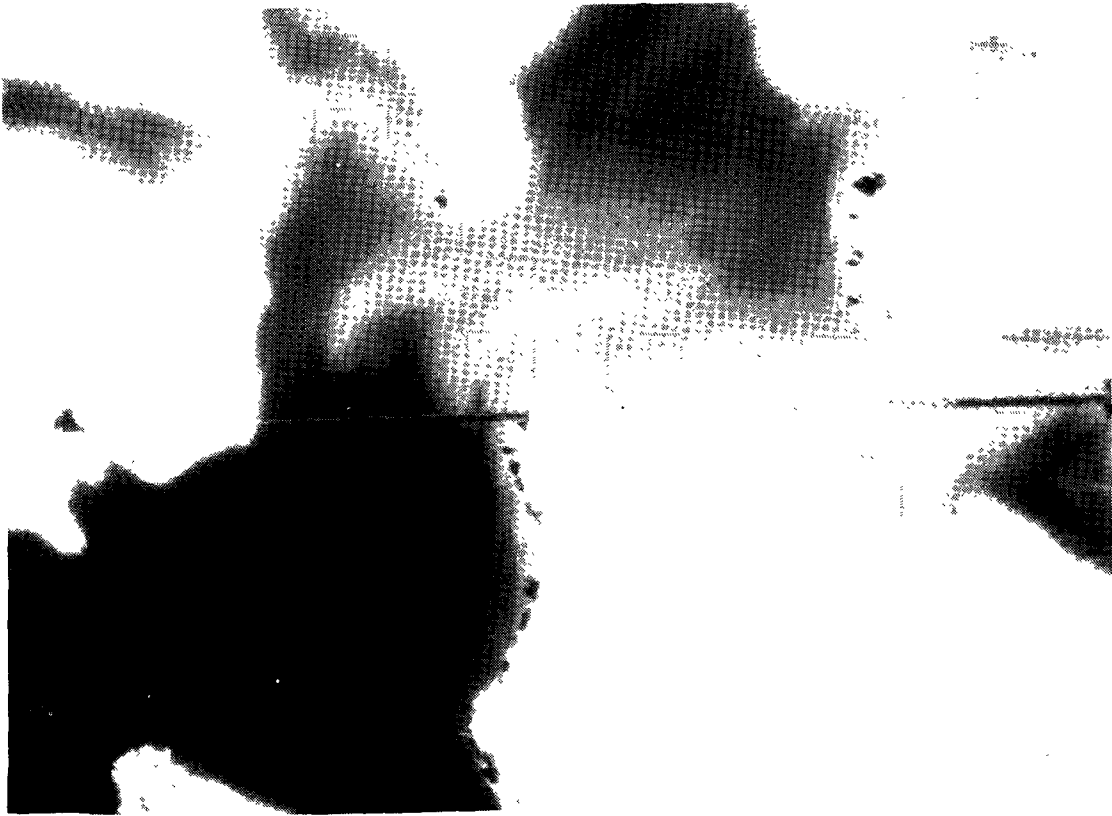


Figure 3. Infrared black and white photo of algal bloom in a lake.

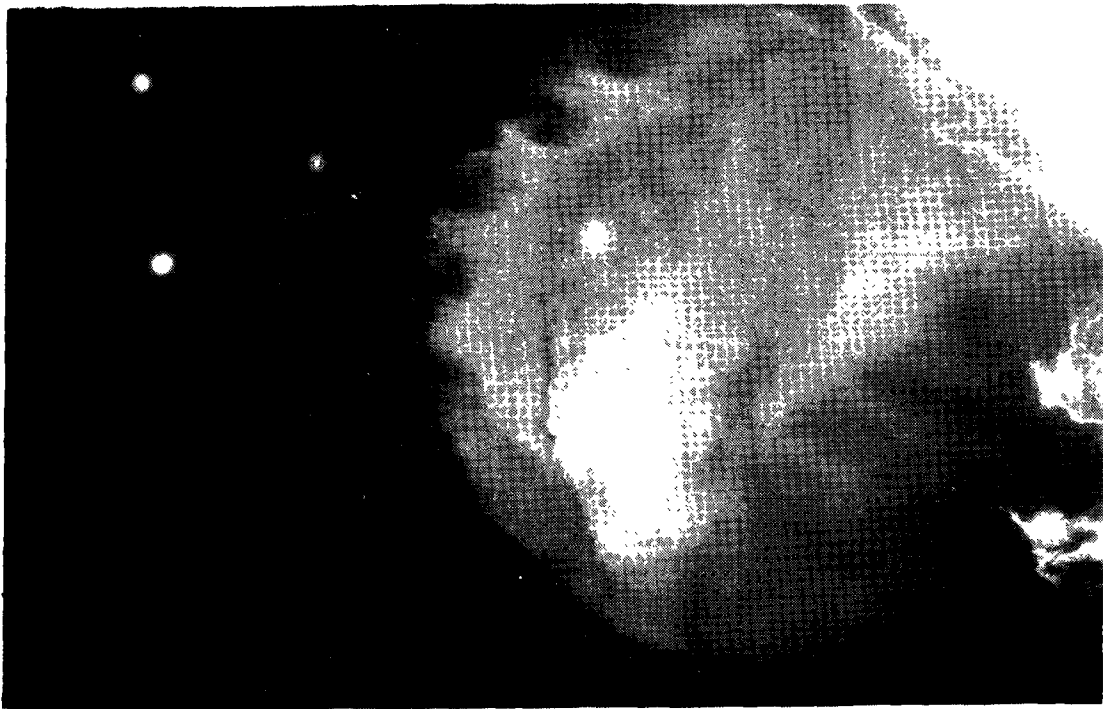


Figure 4. Infrared black and white photo of a waste plume.

dye releases from a balloon. Fresh water with rhodamine B or fluorescein dye added was pumped through a pipe to the bottom of the sea. The fresh water discharge rose to the surface where it spread under the influence of surface mixing and was then photographed. Ichiye and Plutchak (1966) of Columbia University have taken aerial photographs of rhodamine B dye patches and have found that the dye concentrations measured by a shipborne Turner fluorometer correlated very well with densitometer readings on the aerial negative.

Scherz (1967) at the University of Wisconsin has conducted work on pollution detection with aerial photography. In this work, aerial photographs were taken of various pollution sources using different film-filter combinations and the optimum film-filter was selected by visual observation. Cornell Aeronautical Laboratory (Neumaier et al., 1967) under project Aqua-Map has conducted studies on the reflectance of various polluted waters using test panels submerged below the water surface. Both laboratory studies with reflection spectrometer and field surveys with aerial cameras have been conducted. Their study indicated that industrial waste effluents can in some cases be identified photographically.

## SECTION V

### RATIONALE

Photographic films used in aerial photography are sensitive to the visible and near visible light. The main source of this light is the sun. Both the amount and composition of the light scattered from within the water are utilized in the study to determine the waste concentration in the effluent plume. The amount of light is recorded as the film density of the photographic image while the composition of the scattered light is determined from the film-filter combinations used for the photography. If the light scattering or light absorption properties of a waste are a function of the wave length of light, the ratio of the light return in the band of maximum absorption is a sensitive indicator of the waste concentration. However, if the waste is either black or white, the difference in the light returned in two bands divided by the sum will provide a sensitive indicator of the waste concentration. By using the ratio of light returned, the relationship between the film densities and the waste or dye concentration will be simplified as shown in the following sections.

### Sun Energy

Energy from the sun passes through the atmosphere to the sea. Upon reaching the water surface, the radiation is either reflected or transmitted through this interface. The refracted light is transmitted, scattered, or absorbed in the sea. Some of the scattered light is directed upwards and passes through the sea-air interface. A part of the light emerging from the sea reaches the aerial camera and exposes the photographic film.

The upper limit of the atmosphere receives energy at an average rate of about 0.135 watts per square cm perpendicular to the radiation. This value fluctuates about  $\pm 5\%$  during a yearly period due to the eccentricity of the earth's orbit about the sun. The extraterrestrial energy spectrum of the sun's radiation is shown in figure 5 (Hutchinson, 1957).

The normal spectrum of solar radiation that reaches the sea surface is also shown in figure 5. Solar radiation, when passing through the atmosphere, is reduced by scattering and absorption. The amount of radiation received at the earth's surface  $(H)^2$  can be estimated by

$$H = H_0 \exp(-KL) \quad (1)$$

where  $K$  is the attenuation coefficient which varies with wave length,  $H_0$  is the incoming radiation at the outer atmosphere and  $L$  is the

---

<sup>2</sup> Terms in this chapter are defined where first used. Definition of these terms are also listed in Appendix A.

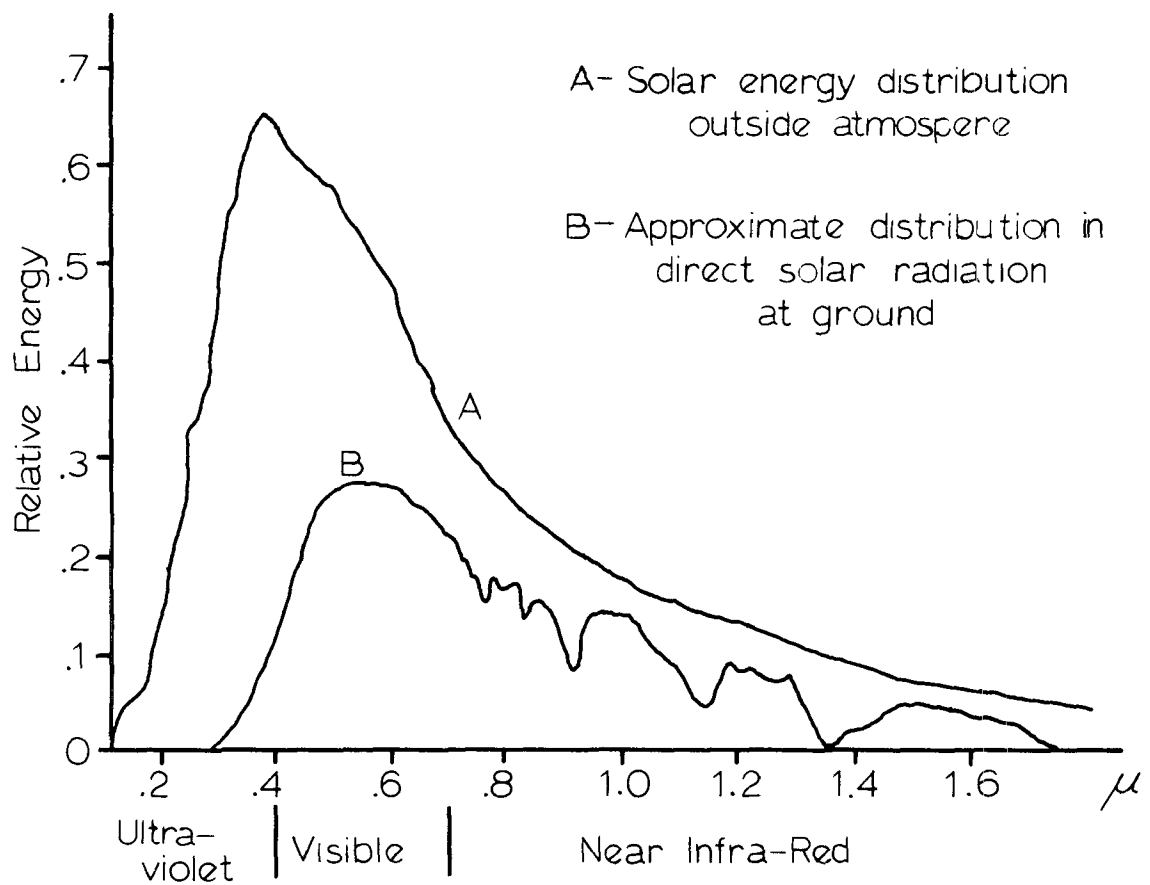


Figure 5. Spectral distribution of radiant energy.

light path length (Elterman and Toolin, 1965).

Absorption of light depends on the composition of the air, mainly water vapor, carbon dioxide and ozone, and the wave length of light. It can be seen in figure 5, that there are several zones of selective absorption. The ultraviolet part of the sun's radiation with a wave length of 290 nm or less is completely cut off by the atmospheric ozone layer and oxygen before it reaches the earth's surface. In the near infrared region (0.7 to 5 microns), the selective absorption is primarily due to water vapor and carbon dioxide (Holter, 1967).

The attenuation depends not only on the turbidity in the atmosphere but also on the length of path through the atmosphere. The length of the light path varies approximately as the secant of the zenith angle ( $i$ ). Hence, the zenith angle ( $i$ ) is involved in reducing illumination in two ways. First, the intensity on a horizontal surface is  $\cos(i)$  times the intensity on a plane normal to the radiation. Second, the path traversed by radiation through the atmosphere is greater for large angles than for the small angles. The irradiance on a horizontal plane at sea surface is

$$H_s = H_o \cos(i) \exp(-A \sec(i)) \quad (2)$$

where  $A$  is the extinction optical thickness and includes Rayleigh attenuation, aerosol attenuation, and ozone absorption for a standard atmosphere (Elterman and Toolin, 1965).

In clean, dry, air, molecular scattering is of primary importance. The scattering of very small particles of molecular dimensions is inversely proportional to the fourth power of the wavelength (Jensen, 1968) and, therefore, affects the shorter wavelengths more than the longer wavelengths. This is the reason most black and white aerial photography is taken with the minus-blue filter. As the particle sizes in the atmosphere increase, the wavelength of maximum scatter becomes less selective and extends into the green, yellow, etc., regions of the spectrum. Hence, the color of the sky changes toward cloud white as the particles increase from molecular to aerosol size. As a result, aerial photography taken under turbid atmospheric conditions requires filtering out of more of the spectrum, including green and possibly yellow light to produce a noticeable effect (Tarkington, 1966). Photographs taken in the near infrared wavelengths are better able to penetrate haze.

#### Light Reflection

Since the reflected light from the water surface will not contribute information on the material in the water, it should be reduced to a minimum. The incident light includes both direct sunlight and diffused skylight. The reflection of direct sunlight will be partially polarized and can be reduced from exposing the film by the proper

orientation of a polarized filter. On a cloudless day, the skylight will be predominantly blue and the surface reflection of diffused light can be reduced with a minus blue filter. Figure 6 shows the effect of the sun's altitude on the irradiance of skylight and direct sunlight (Jones and Condit, 1948).

The height of the sun above the horizon is critical for vertical aerial photography of a water surface. The maximum height determines the amount of reflected light reaching the film while the minimum height determines light penetration into the sea. If the sea surface were calm, a single mirror-like reflection of the sun would appear. As the sea surface is generally not smooth, the zenith angle of the sun must be greater than half the angular coverage of the camera to avoid photographing the sun spot glare. The width of the glitter pattern about the sun's reflection is an indication of the maximum slope of the sea surface. Cox and Munk (1955) have studied roughness of the sea surface by analyzing photographs of the sun's glitter. As shown in figure 7, a sloping water surface will require that the minimum zenith angle of the sun be at least half the angular coverage of the aerial camera plus twice the water surface slope if vertical photography is to be free of sun's glare. The slope of waves can vary from  $0^\circ$  to over  $90^\circ$  for breaking waves. It is, therefore, necessary to select a reasonable value of slope which will eliminate most of the sun spot glare for the expected sea conditions during photography. Studies (Cox and Munk, 1954) have indicated that for a 3-knot wind the maximum slope is about  $15^\circ$  and about  $25^\circ$  for an 18-knot wind. For photographing underwater objects Faas (1960) suggests that the slope  $18.5^\circ$  be used. This would indicate that the sun's zenith angle at the time of photography be at least  $37^\circ$  plus half the angular coverage of the aerial camera, if the sun's glitter is to be avoided on vertical photography. An alternate solution is to mount the camera to take oblique photography.

The light reaching the water surface is either reflected from or refracted through the air-sea interface. As shown in figure 8, the incident light ( $H_i$ ) is divided into that which penetrates the sea ( $H_w$ ) and that which is reflected from the interface. If  $i$  is the angle of incidence of the incoming radiation and  $j$  is the angle of refraction, then  $\sin(i)/\sin(j)$  is equal to the index of refraction for water or about  $4/3$ . The reflectivity of an optically flat water surface is theoretically obtained for unpolarized light from Fresnel's law (Jerlov, 1968) which gives the ratio ( $p_a$ ) of reflected energy to incoming radiation and is

$$p_a = \frac{1}{2} \left[ \frac{\tan^2(i-j)}{\tan^2(i+j)} + \frac{\sin^2(i-j)}{\sin^2(i+j)} \right] \quad (3)$$

where the terms inside the brackets are for the components of light parallels and perpendicular to the plane of incidence. A plot of the percent reflectivity for angles of incidence from 0 to 90 degrees is

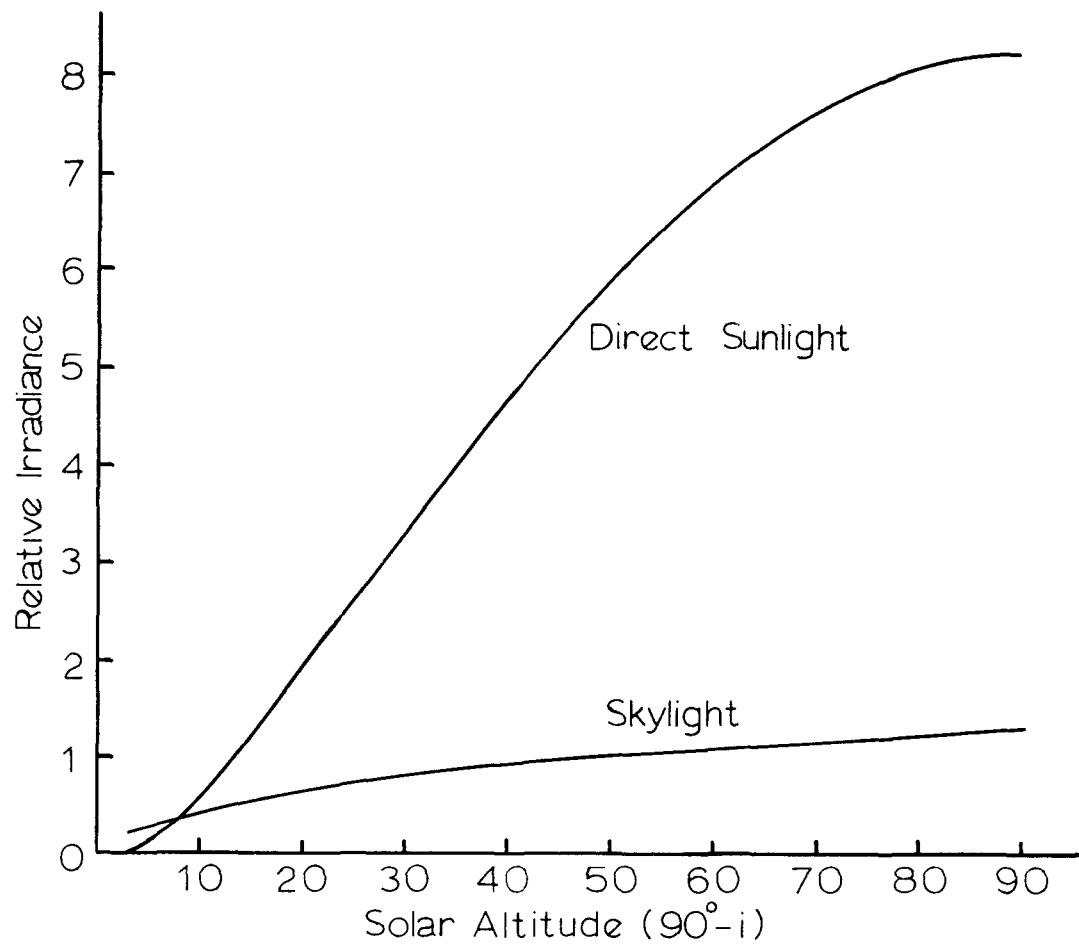


Figure 6. Direct sunlight and skylight on a horizontal plane.





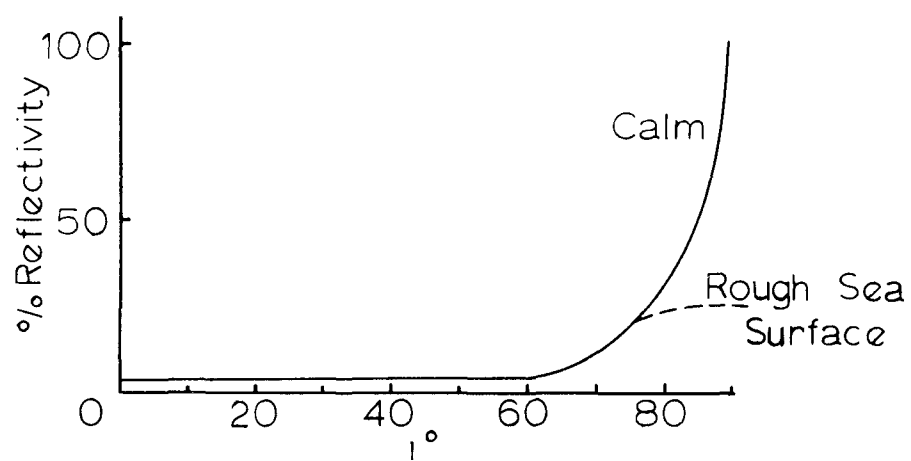
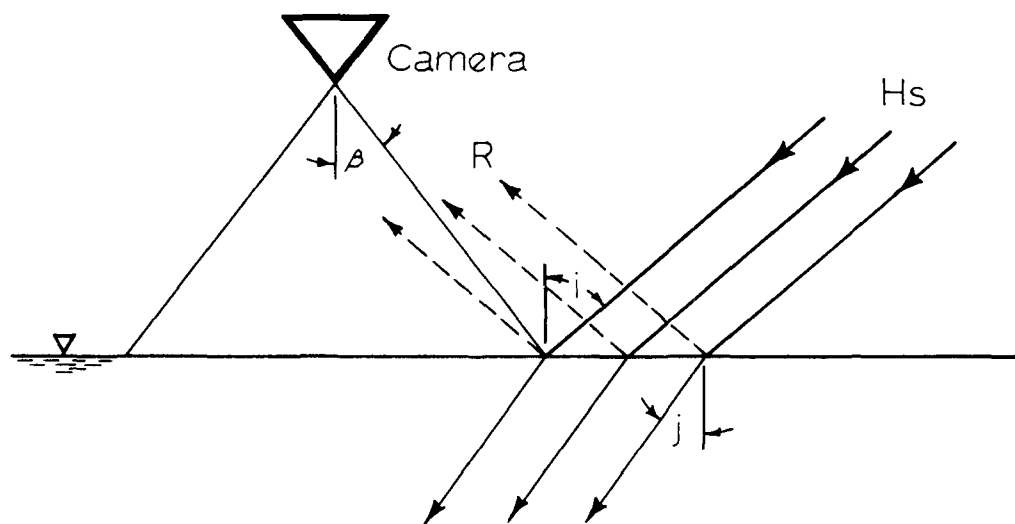


Figure 8. Light penetration into the sea.

shown in figure 8. It can be seen that the reflectivity increases rapidly when the angle of incidence exceeds 60 degrees. The irradiance ( $H_w$ ) below the sea surface and normal to the beam is

$$H_w = (1 - p_a) H_s \sec(j) \quad (4)$$

#### Light Attenuation in the Sea

The radiation that penetrates the surface of the sea is progressively diminished by extinction as it travels through the water. The attenuation of light is caused by scattering and absorption. By applying Lambert's and Beer's laws for monochromatic light the intensity  $H_z$  at some depth  $z$  below the sea surface is given by

$$H_z = H_w \exp(-Cz \sec(j)) \quad (5)$$

$$C = a + bW \quad (6)$$

where  $C$  is the attenuation coefficient for sea water and waste, ' $a$ ' is the sea water attenuation coefficient,  $b$  is the waste absorption coefficient and  $W$  is the waste concentration. The attenuation coefficients for sea water and Kraft pulp waste are shown in figure 9. Minimum attenuation of sea water occurs at about 540 nm while the minimum for the waste is about 700 nm.

#### Light Scattering in the Sea

The attenuation coefficients of both sea water and the waste can be divided into attenuation due to absorption and attenuation due to scattering. The scattering of light in a turbid medium is caused by reflection and diffraction light rays by small particles of suspended matter and colloidal solutions. As in the atmosphere, if the size of the particles is small compared to the wavelength of light, then the intensity of the scattering light is inversely proportional to the wavelength to the  $n^{\text{th}}$  power. The exponent  $n$  decreases with increasing particle size from the value of four for pure water to approaching zero for coarse suspended matter (Jensen, 1968). Thus for solutions with small particles, the blue light has the maximum scatter, while for solutions with larger particles all colors are scattered about the same amount.

By definition of the volume scattering function  $\beta(\alpha)$ , the scattered light intensity ( $dJ$ ) from an incremental volume  $dV$  is

$$dJ = H_z \beta(\alpha) dV \quad (7)$$

where  $\alpha$  is the angle between the incident beam and the scattered light.

Figure 10 shows the variation in the volume scattering function for both sea water and pure water (Jerlov, 1964). It can be seen that the curve

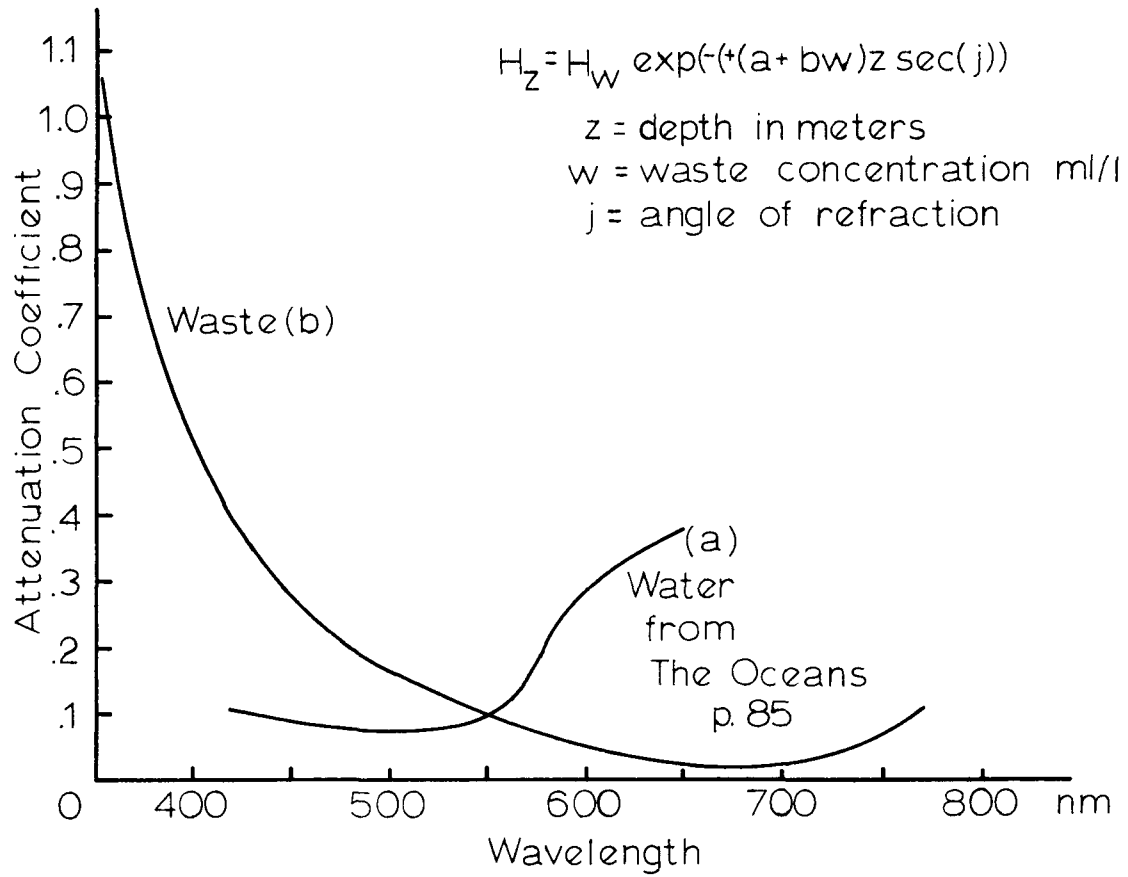


Figure 9. Typical attenuation coefficients.

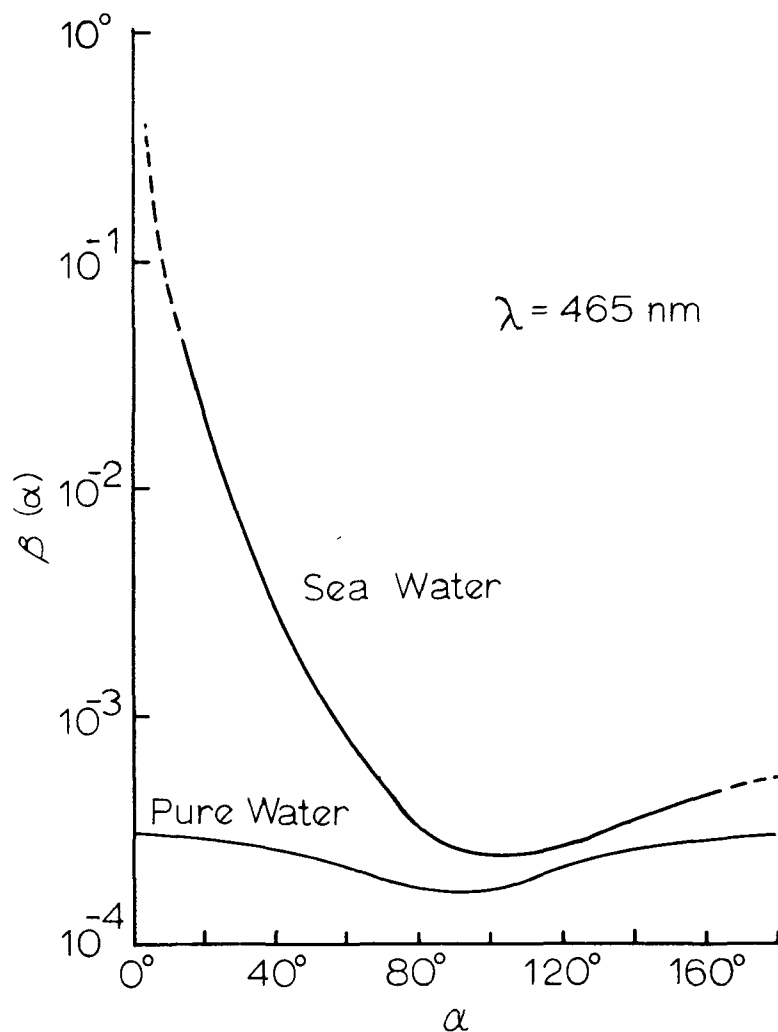


Figure 10. Volume scattering function.

for pure water is symmetrical with a minimum at  $\alpha$  equal to 90 degrees. The scattering function for sea water varies greatly with  $\alpha$ .

The variation of the scattering angle ( $\alpha$ ) on an aerial photograph is shown in figure 11. The angle between the incoming direct light in the sea and the scattered light reaching the camera changes with position; hence, the intensity of scattered light from below the sea surface will also vary. For a vertical photograph taken with a 6-inch aerial camera when the sun's zenith angle is 55 degrees, the angle " $\alpha$ " would vary from about 110 degrees to 170 degrees.

Figure 12 is a plot of data taken from work by Tyler and Richardson (1958). In this study a nephelometer was used to measure the radiant intensity scattered from a volume for various scattering angles ( $\alpha$ ). A

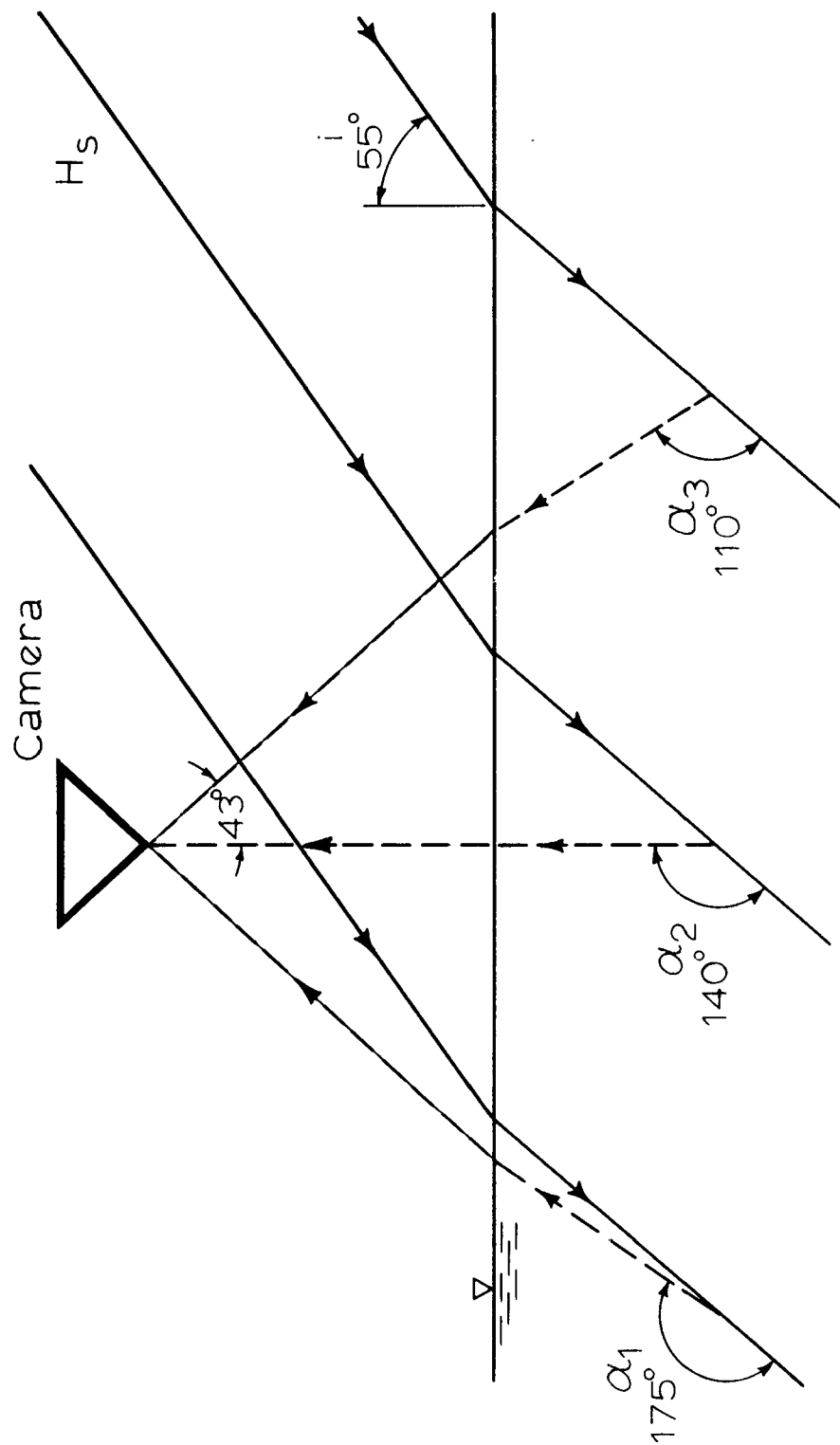


Figure 11. Variation in the scattering angle.

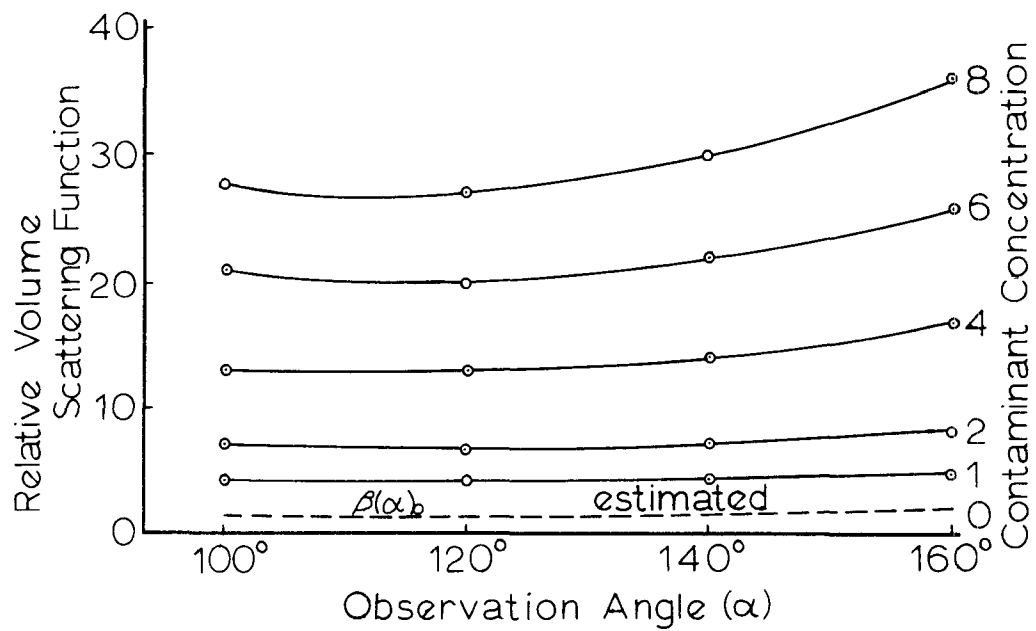
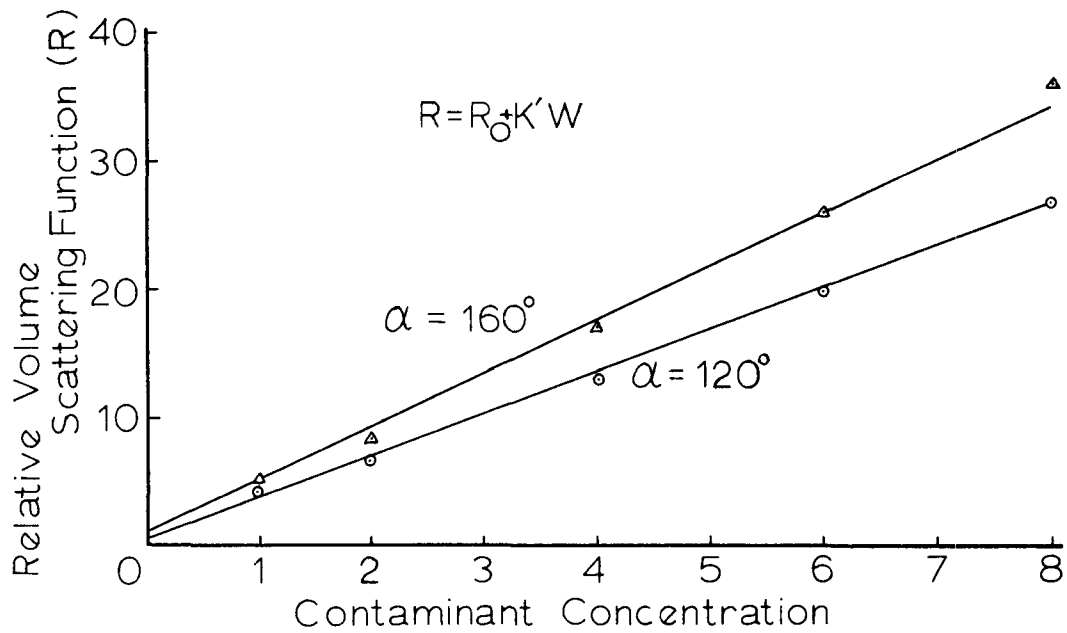


Figure 12. Effect of contaminant on the scattering function.

contaminant of skim milk was added at various concentrations. The light scattering for the various solutions is directly related to concentration of the contaminant.

For scattering by large particles, the intensity of the scattered light is proportional to the particle surface area that is exposed to the incident beam (Jerlov, 1968). If the particle size is uniform, then the intensity of the scattered light is proportional to the waste concentration. In the upper plot in figure 12 the volume scattering function is shown as a linear function of the waste concentration. From the lower plot in figure 12, it can be seen that the function  $\beta(\alpha)$  can be approximated by

$$\beta(\alpha) = \beta_o(\alpha)(1 + K'W) \quad (8)$$

where  $\beta_o(\alpha)$  is the volume scattering function of the sea water,  $K'$  is a constant for a particular waste and  $W$  is the waste concentration.

As shown in figure 13, if  $R$  is the distance from the volume element ( $dV$ ) to the point where the scattered light strikes the surface and  $d\Omega$  is the solid angle formed at the surface by  $dV$ , then

$$dV = R^2 d\Omega dR \quad (9)$$

In addition, the emerging ray of scattered light from the incremental volume will be augmented by diffused light of almost uniform intensity in all directions. As the intensity of the light which is scattered for the second time, will be approximately three orders of magnitude less than that of the direct lighting, the addition of the rescattered light to the emerging ray will not be considered. The intensity of the emerging ray  $dJ$  will be reduced by the absorption and scattering of the water and particles. From the inverse square law, the irradiance from the scattering volume incident on a normal plane to the beam at the surface is

$$dH_a \approx \frac{dJ}{R^2} \exp(-CR) \quad (10)$$

By combining equations and integrating, the irradiance at the surface is

$$H_a = \frac{H_o \beta_o(\alpha) \cos(i) (1 - p_a) \exp(-A \sec(i)) d\Omega}{\cos(i_2) \cos(j)} \int (1 + K'W) \exp(-(a+bW)(\sec(j) + \sec(i_2))z) dz \quad (11)$$

If the waste concentration is a known function of the depth ( $z$ ), then equation 11 can be integrated numerically. However, if the waste field forms a relatively stable layer at the surface and the waste concentra-

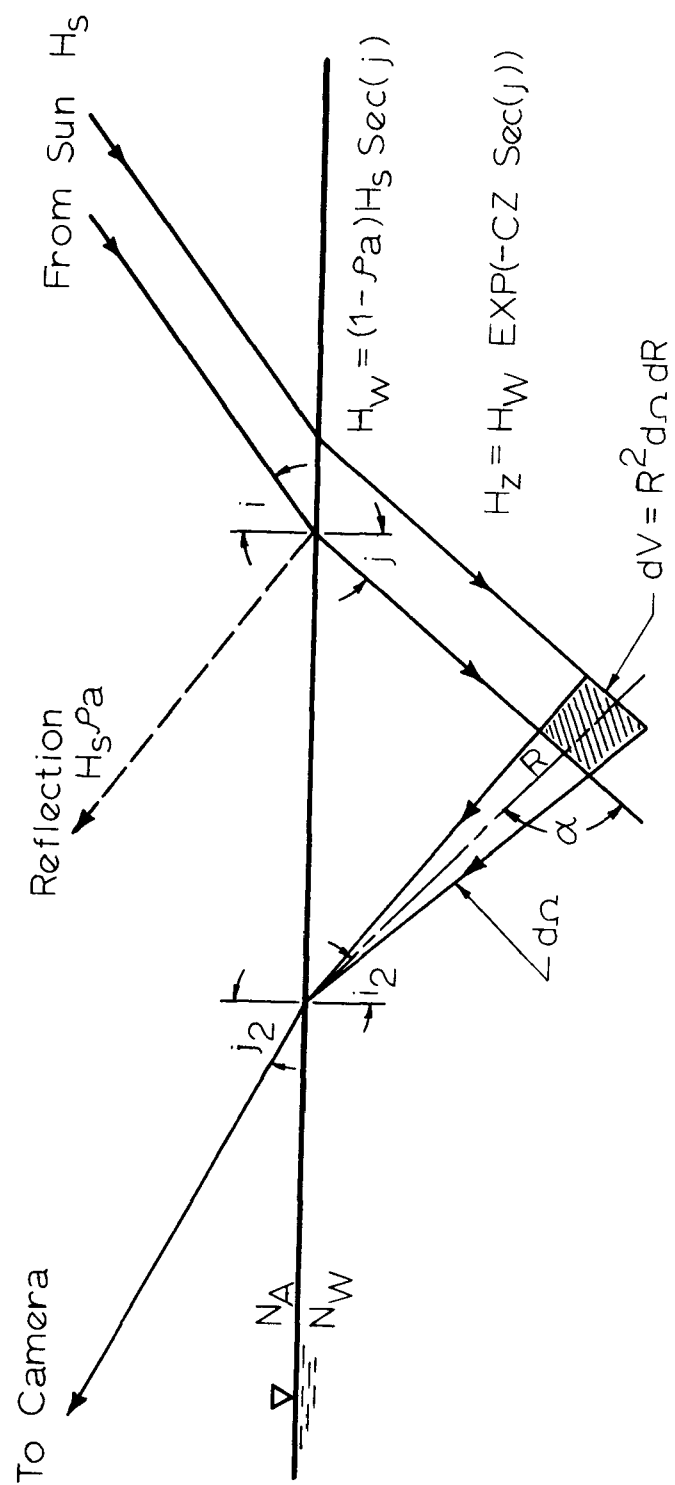


Figure 13. Light from the sea.



tion is approximately uniform throughout the depth of this layer, then equation 11 can be integrated directly.

If the waste concentration is not a function of depth and  $\exp(-(a + bW) z(\sec(j) + \sec(i_2)))$  approaches zero, equation 11 reduces to

$$H_a = \frac{(1 + K'W) H_0 \beta_0(\alpha) \cos(i)(1 - p_a) \exp(-A \sec(i)) d\Omega}{(a+bW) \cos(i_2) \cos(j)(\sec(i_2) + \sec(j))} \quad (12)$$

Evaluation of  $\exp(-Cz(\sec(j) + \sec(i_2)))$  is shown in figure 12 for the green, red, and infrared regions of the spectrum. The expression was evaluated for values of the angles  $j$  and  $i_2$  other than those listed in figure 14; however, the expression was relatively insensitive to changes in these angles. Average values of attenuation coefficients were selected from figure 9. It can be seen from the upper plot in figure 14 that 90% of the light returned in the infrared region is from the upper half meter of water. In the red and green bands the depth above which 90% of the light is returned is a function of the waste concentration. From the lower plot in figure 14, it can be seen that in the open sea 50% of the light in the red and green bands is returned from the upper two and four meters, respectively.

#### Radiance from the Sea

From equation 12 the radiance ( $N_w$ ) from the scattering volume below the sea surface is

$$N_w = \frac{H_a}{d\Omega} \quad (13)$$

The light spreads into a larger solid angle when passing through the sea-air interface (Jerlov, 1968) and the radiance in air is

$$N_a = \frac{N_w}{n^2} (1 - p_w) \quad (14)$$

where  $n$  is the refractive index of water and  $p_w$  is the reflectivity of light at the interface.

In addition to the upward radiance from the sea, the light reaching the photographic sensor includes skylight reflection, direct sunlight reflection and path radiance intensity. Reflectance of skylight from a rough sea surface can be approximated by a Lambert reflector while the direct sunlight is reflected specularly. Skylight radiance reflected from the surface is given by

$$N_{sky} = p_s \frac{H_{sky}}{\pi} \quad (15)$$

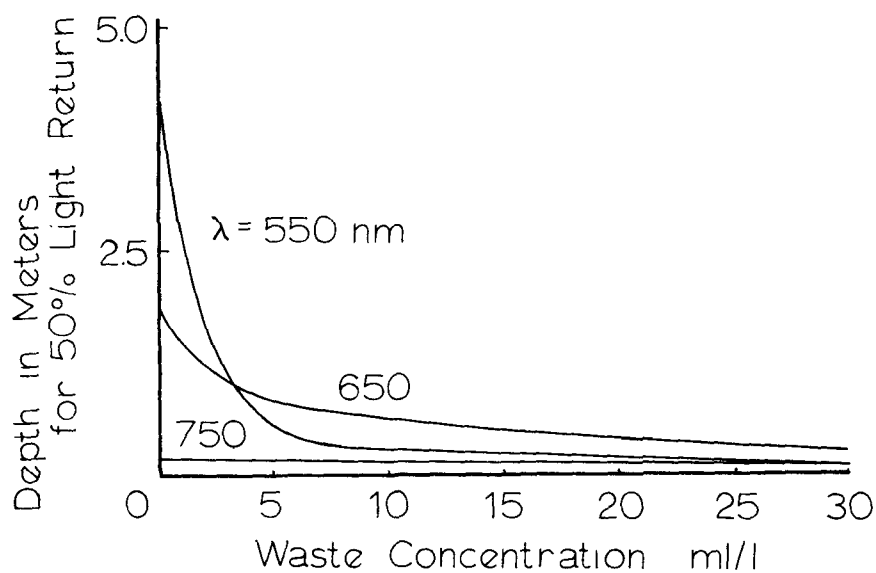
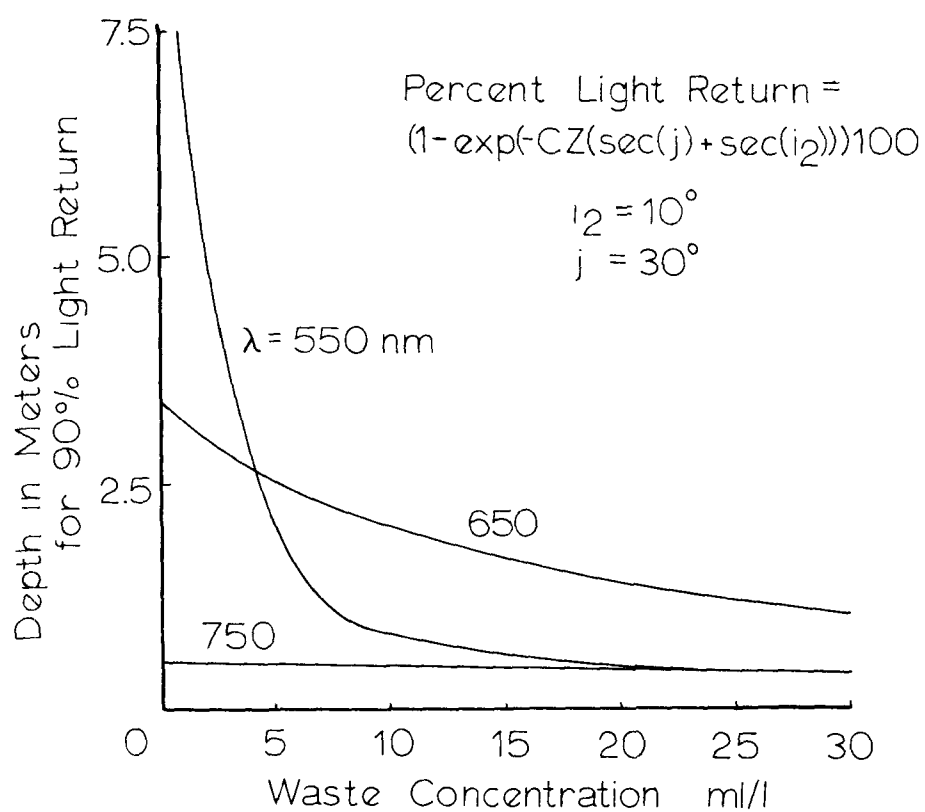


Figure 14. Depth of light return from the sea.

where  $p_s$  is reflectivity of the skylight and was found by Burt (1953) to be approximately 0.066. The skylight irradiance ( $H_{sky}$ ) is a function of solar altitude, atmospheric scattering and wave length of light. Path radiance intensity is a function of the length of sight ray, angle between sight and sun rays, atmospheric condition and wave length. For a clear atmosphere, skylight irradiance will be due predominantly to Rayleigh scattering and will have greatest influence on the shorter wave lengths. The reflection of direct sunlight is mathematically easier to estimate in magnitude by Fresnel's equations but its direction is difficult to predict without knowing the surface configuration of the sea. Since the Fresnel's equations are nearly independent of wave length, the magnitude of direct sunlight reflection will be proportional to each other in spectral bands of the sensor.

If  $N$  is the radiance from the sea surface and the path radiance is neglected then the radiance at the sensor is

$$N_c = N \exp(-E \sec(j_2)) \quad (16)$$

where  $E$  is the extinction optical thickness for the attenuation by the atmosphere from the sea to the camera.  $E$  is, therefore, a function of flying height and wave length.  $N$  includes the skylight reflection ( $N_{sky}$ ), direct sunlight reflection ( $N_d$ ), and upward radiance from the sea and the waste ( $N_a$ ) or

$$N = N_{sky} + N_d + N_a \quad (17)$$

By combining equations 12, 13, 14, 15, and 17 the radiance  $N$  is equal to

$$N = p_s \frac{H_{sky}}{\pi} + N_d + \frac{(1 - p_w)(1 + K'W)\beta_o(\alpha) H_o \exp(-A \sec(i)) \cos(i)(1 - p_a)}{n^2 (a + bW) \cos(j) \cos(i_2)(\sec(i_2) + \sec(j))} \quad (18)$$

The first term on the right is the skylight reflection, the second term is direct sunlight reflection and the last term is the uplighting from the sea ( $N_a$ ).

Equation 18 can be expanded by writing the equation for each of the spectral bands. The subscripts  $g$  and  $r$  refer to the bands of maximum absorption and scatter, respectively.

$$N_g = K_4 p_s \frac{H_{sky}}{\pi} + K_5 N_d + K_6 Y (\exp(-A_g \sec(i))) \frac{(1 + K'_g W)}{a_g + b_g W} \beta_o(\alpha) \quad (19)$$

$$N_r = K_7 p_s \frac{H_{sky}}{\pi} + K_8 N_d + K_9 Y (\exp(-A_r \sec(i))) \frac{(1 + K'_r W)}{a_r + b_r W} \beta_o(\alpha) \quad (20)$$

A typical spectral signature of both the open sea and the waste field is shown in figure 15. The effect of skylight, direct sunlight, and waste on the spectral signature is shown in the figure. Whenever possible direct sunlight reflection from the water surface should be avoided as it will cause interference with the data processing. Hence, the second term on the right of the three equations is zero. As skylight is predominantly blue

$$K_4 \sim 0, \quad K_7 \sim 0$$

Rewriting equations 19 and 20

$$N_g = K_6 Y \frac{(1 + K'_g W)}{a_g + b_g W} \exp(-A_g \sec(i)) \quad (21)$$

$$N_r = K_9 Y \frac{(1 + K'_r W)}{a_r + b_r W} \exp(-A_r \sec(i)) \quad (22)$$

Where Y is a constant for the two bands at a point on the photograph and is equal to

$$Y = \frac{H_o (1 - pw) (1 - pa) \cos(i) \beta_o(\alpha)}{n^2 \cos(j) \cos(i_2) (\sec(i_2) + \sec(j))} \quad (23)$$

The Y term can be eliminated by taking the ratio (Rp) of the radiance in the two bands

$$R_p = K_{10} \frac{1 + K'_r W}{1 + K'_g W} \frac{a_g + b_g W}{a_r + b_r W} \exp(-(A_r - A_g) \sec(i)) \quad (24)$$

where  $K_{10}$  is a constant.

$\frac{1 + K'_r W}{1 + K'_g W}$  is the scattering coefficient ratio and shows the effect of scattering on the composition of the scattered light. As the particle size is relatively large compared to the wavelength of light, the scattered light is of nearly the same composition as the incident light. Therefore, this term is approximately equal to one.

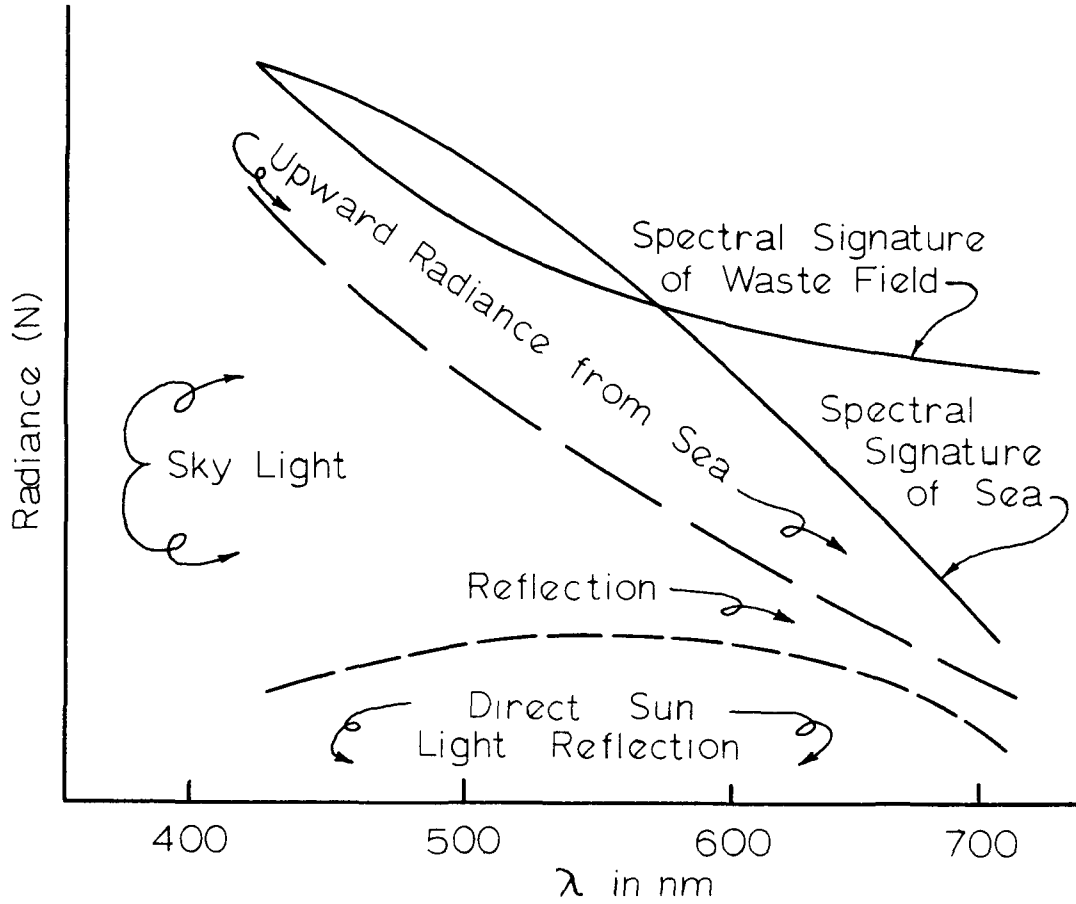


Figure 15. Typical spectral signature.

The term  $\frac{a_g + b_g W}{a_r + b_r W}$  represents the change in light composition due to the selective absorption of the waste and the sea water.

$\exp(-(A_r - A_g) \sec(i))$  is the atmospheric attenuation ratio and shows the effect of the sun's altitude on the incident light composition.

From equation 24, the ratio at the sea surface (Rph) is

$$R_{ph} = R_p \exp((A_r - A_g) \sec(i)) = K_{10} \frac{a_g + b_g W}{a_r + b_r W} \quad (25)$$

#### Photographic Measurement of Light

The aerial photograph is a light detector and can be used to measure the light return from objects. As shown in figure 16,  $j_2$  is the angle between the ray to the camera and the vertical. If the angle between

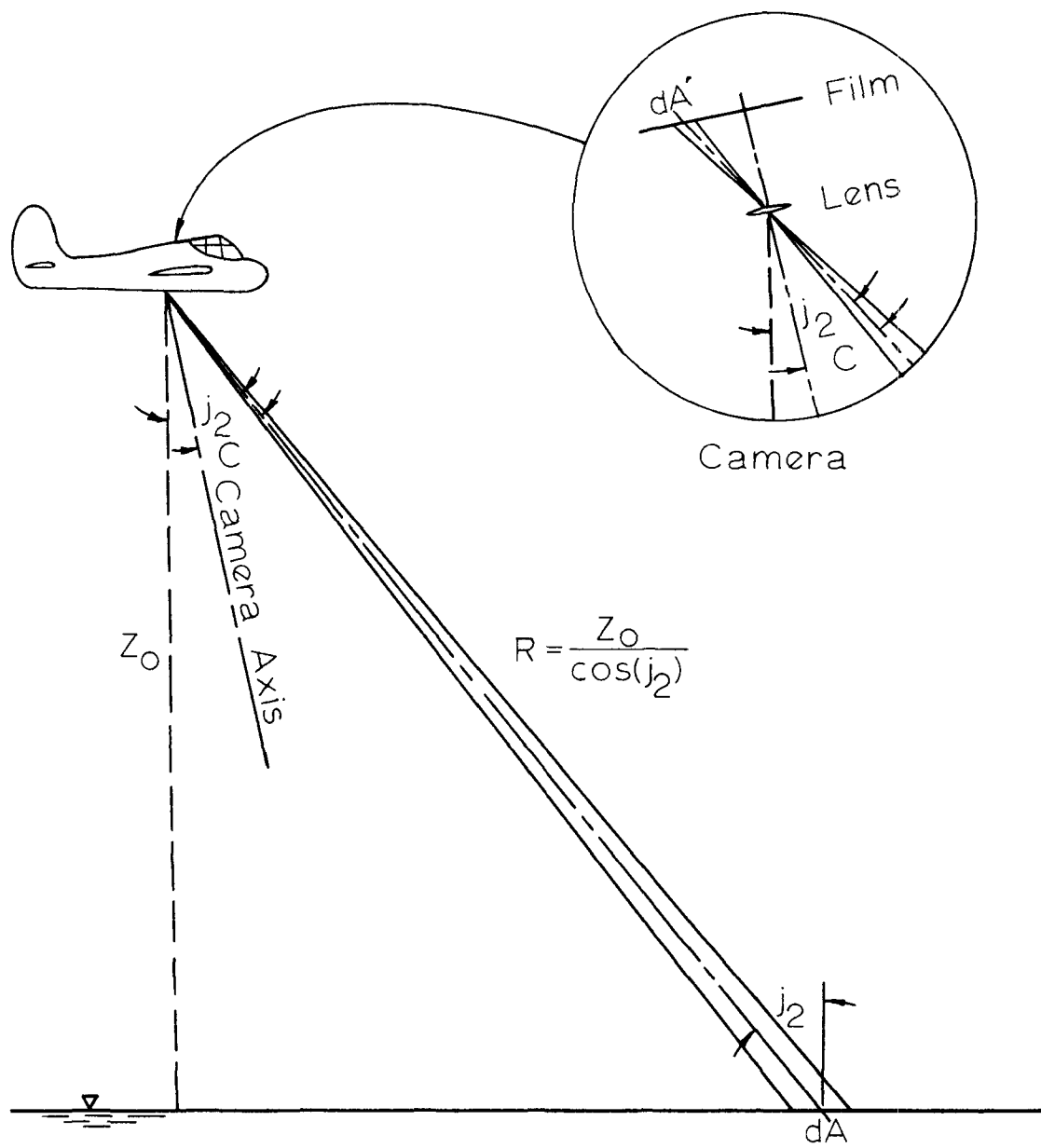


Figure 16. Geometry of exposure calculation.

the ray and the camera axis is represented by  $c$ , then by geometry

$$dA = dA' \left[ \frac{Z_o}{f} \right]^2 \left[ \frac{\cos(c)}{\cos(j_2)} \right]^3 \quad (26)$$

where  $dA$  is the area on the sea surface included in the densitometer aperture area  $dA'$  on the photographic film,  $Z_o$  is the flying height and  $f$  is the focal length of the camera. The solid angle subtended by the lens of diameter  $D$  is

$$d\Omega = \frac{\pi}{4} \left[ \frac{D \cos(j_2)}{Z_o} \right]^2 \cos(c) \quad (27)$$

The radiant flux ( $dp'$ ) collected by the camera lens is

$$dp' = N_c dA \cos(j_2) d\Omega \quad (28)$$

The irradiance of the film image is

$$H' = \frac{dp'}{dA'} = K_{12} \frac{TR N_c \cos^4(c)}{(FNO)^2} \quad (29)$$

where  $K_{12}$  is a constant,  $FNO$  is the relative aperture of the lens ( $f/D$ ),  $TR$  is the lens transmittance and  $N_c$  is the object radiance at the camera.

The photographic exposure ( $EX$ ) is the product of image irradiance ( $H'$ ) or the rate at which energy is incident upon a unit area of the film and the time ( $TIM$ ) during which it acts. The equation

$$EX = H' \times TIM \quad (30)$$

indicates that there are many combinations of  $H'$  and  $TIM$  that will give the same exposure. This is known as the Reciprocity Law and is correct for normal aerial photography where extremes in exposure times are not employed.

The density of a film is defined as the common logarithm of the reciprocal of the transmittance or the logarithm of the ratio of incident light on the film and the transmitted light through the film. The relationship between film density and exposure is shown by the characteristic curves of a film. The curve is a plot of log exposure against film density for a particular development. A typical characteristic curve is shown in figure 17 (American..., 1968).

The characteristic curve can be divided in three parts; the lower part of the curve  $AB$  which is concaved upward is known as the toe, the

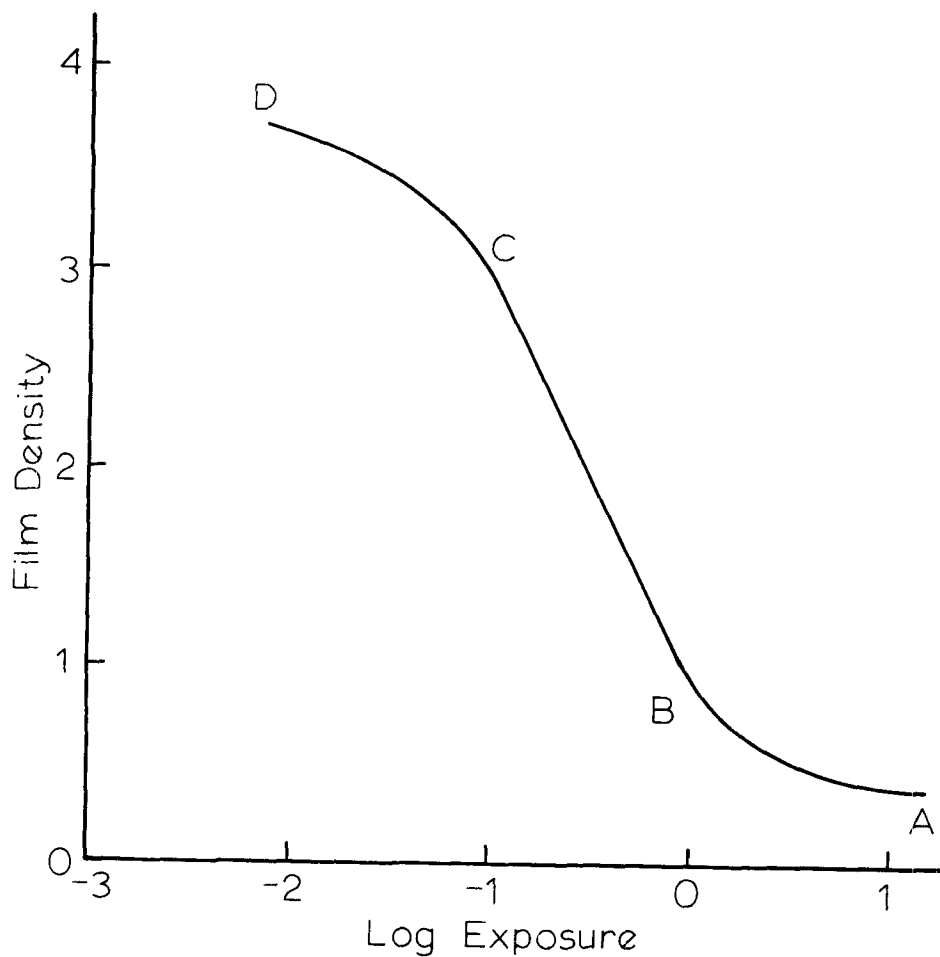


Figure 17. Typical characteristic curve of an aerial positive film.

the straight line portion of the curve BC, and the top part of the curve CD which is concave downward and is known as the shoulder region. The toe of the characteristic curve approaches a horizontal line at some value of density greater than zero. This value represents the density of the base of the film.

The slope of the straight line portion of the characteristic curve is known as the film gamma. The greater the gamma the greater the contrast or the greater the difference in densities on a given photograph. The gamma is a characteristic of the film but varies within limits with different development time. The speed or exposure index of the film is indicated by the horizontal position of the characteristic curve along the exposure axis.

If the exposure of the film is on the straight line portion of the D or E curve, then the film density can be expressed by



$$D(x, y) = M + G \ln (EX) \quad (31)$$

$D(x, y)$  is the film density at the point on the photo with film coordinates  $x$  and  $y$ ,  $M$  is a constant representing the film speed,  $G$  is the gamma or contrast of the film and  $EX$  is the exposure.

Combining equations 30 and 31 and solving for the image irradiance

$$H' = \frac{K_{13}}{TIM} \exp((D(x, y) - M)/G) \quad (32)$$

The radiance from the sea as measured at the camera station is determined from equations 29 and 32

$$N_c = \frac{K_{14} (FNO)^2 \exp((D(x, y) - M)/G)}{(TIM)(TR) \cos^4(c)} \quad (33)$$

By including the atmospheric attenuation, but neglecting light path radiance in the atmosphere, the radiance at the sea surface ( $N$ ) is equal to

$$N = \frac{K_{15} (FNO)^2}{(TIM)(TR) \cos^4(c)} \exp(D(x, y)/G + E \sec(j_2)) \quad (34)$$

where the term  $\exp(-M/G)$  has been included in the constant ( $K_{15}$ ). The factor  $\exp(E \sec(j_2))$  compensates for the atmospheric attenuation of the light from the sea surface to the camera. Writing equation 34 for two spectral bands:

$$N_g = \frac{K_{17} (FNO)^2 \exp(D_g(x, y)/G_g + E_g \sec(j_2))}{(TIM)(TR_g) \cos^4(c)} \quad (35)$$

$$N_r = \frac{K_{18} (FNO)^2 \exp(D_r(x, y)/G_r + E_r \sec(j_2))}{(TIM)(TR_r) \cos^4(c)} \quad (36)$$

The ratio ( $R$ ) of the radiance in the two bands is obtained by dividing equation 36 by 35

$$R_p = \frac{N_r}{N_g} = K_{19} \exp((D_r(x, y)/G_r - D_g(x, y))/G_g + (E_r - E_g) \sec(j_2)) \quad (37)$$

For the color films used on this project the gamma ( $G$ ) was nearly the same in the spectral bands. As in equation 25, the value of  $R_{ph}$  is

defined as

$$\begin{aligned}
 R_{ph} &= R_p \exp(A_r - A_g) \sec(i) \\
 &= K_{19} \exp((D_r(x,y)/G_r - D_g(x,y))/G_g + (E_r - E_g) \sec(j_2) \\
 &\quad + (A_r - A_g) \sec(i))
 \end{aligned} \tag{38}$$

where angle  $i$  is the angle of incidence for the direct sunlight and  $A_r$  and  $A_g$  are the extinction optical thickness of a standard atmosphere for the maximum absorption and scatter bands respectively.

If  $R_{pho}$  is the ratio of the radiance from the sea for the two bands where no waste is present and this value is adjusted for the atmospheric attenuation as in equation 38,  $R_{pho}$  can be estimated by the following regression model for any point on the photograph.

$$R_{pho} = B_0 + B_1 \text{ SUNR} + \epsilon \tag{39}$$

In this equation  $B_0$  and  $B_1$  are regression coefficients to be determined by a least squares fit of the model to the data points outside the waste field. SUNR is the angle between the ray from the sea to the camera station and the direct sunlight reflected from a horizontal surface.

The ratio anomaly (RA) is defined as

$$RA = R_{ph} - R_{pho} \tag{40}$$

and is the variation in the ratio of two bands of light returned from within the sea due to the presence of waste. The value of the ratio anomaly is determined from equations 38 and 39.

#### Waste Concentrations from Aerial Photography

The relationship between the photographic value RA and the concentration  $W$  can be developed from equation 25 as

$$RA = K_{10} \left[ \frac{(a_r b_g - a_g b_r)W}{a_r(a_r + b_r W)} \right] \tag{41}$$

Evaluation of the term in the brackets of equation 41 is shown in figure 18. The relationship between the photographic value RA and the waste concentration is a function of the sea water attenuation coefficients and the waste absorption coefficients. Average values of these coefficients were selected from figure 9. The upper curve in figure 18 is for the ratio of red to green radiance. For comparison

$$f(a,b) = \frac{(a_r b_g - a_g b_r)W}{a_r^2 + a_r b_r W}$$

Curve No.	Band Subscripts		Evaluated For
	<u>r</u>	<u>g</u>	
1	red	green	green at 550nm red at 650nm
2	infrared	green	infrared at 750nm
3	infrared	red	

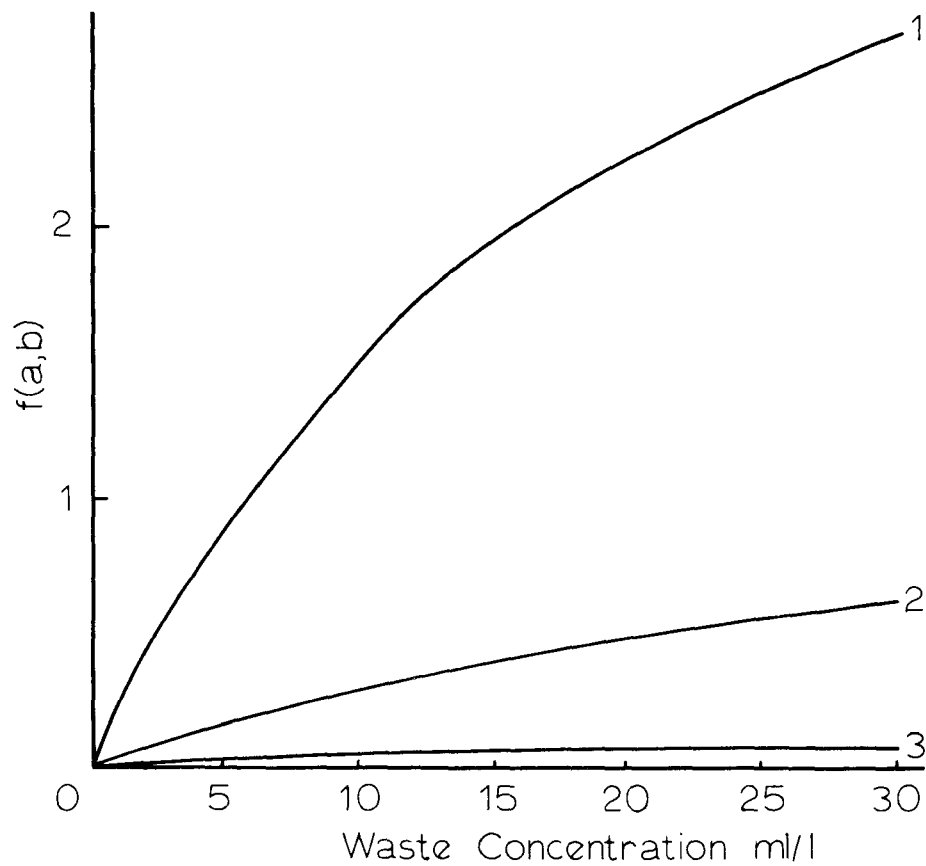


Figure 18. Spectral response curves.

two other curves were included. The lower curve is for the ratio of infrared to red and the center curve is for the ratio of infrared to green. While the ratio of red to green radiance is the most sensitive to changes in waste concentration, it is also the ratio with the greatest interference to skylight reflection and light path radiance.

Curves such as those shown in figure 18 are useful in predicting the response of different film-filter combinations for measuring waste concentrations; however, interference must be considered. If the two regions of the spectrum are measured with two cameras, the camera settings can be adjusted for optimum exposure in each band. By using high contrast developer and/or film, the sensitivity of the film density to the waste concentration can be increased.

From equation 41 the waste concentration can be expressed as

$$W = C_1 (RA) + C_2 (RA)^2 + \dots \quad (42)$$

where  $C_1$  and  $C_2$  are coefficients. A stepwise regression analysis of this model has shown that only the first two terms are significant.

The F level to enter the first term ranges between 500 to 1000 while the F level to enter the second term generally ranges from 1 to 5.

#### Photographic Orientation

Photographic orientation is accomplished by a non-linear solution to the collinearity condition equations (Keller and Tewinkel, 1966). Corrections are generally not required for atmospheric refraction, earth curvature, film shrinkage or lens distortion. The relationship between photo coordinates and ground coordinates is

$$\begin{bmatrix} x_p - x_0 \\ y_p - y_0 \\ -f \end{bmatrix} = K[RM] \begin{bmatrix} X_p - Y_c \\ Y_p - Y_c \\ Z_p - Z_c \end{bmatrix} \quad (43)$$

where  $x_p$  and  $y_p$  are photo coordinates of imagepoint p, f is the camera focal length,  $x_0$  and  $y_0$  are photo coordinates of the principal point, K is a scale factor, the X, Y, and Z subscripted p and c refer to ground coordinates of the object and camera station respectively, RM is the rotational matrix. The matrix is defined as

$$[RM] = \begin{bmatrix} m_{11} & m_{12} & m_{13} \\ m_{21} & m_{22} & m_{23} \\ m_{31} & m_{32} & m_{33} \end{bmatrix} \quad (44)$$

where

$$\begin{aligned}
m_{11} &= \cos(\phi) \cos(K_a) \\
m_{12} &= \cos(W_o) \sin(K_a) + \sin(W_o) \sin(\phi) \cos(K_a) \\
m_{13} &= \sin(W_o) \sin(K_a) - \cos(W_o) \sin(\phi) \cos(K_a) \\
m_{21} &= -\cos(\phi) \sin(K_o) \\
m_{22} &= \cos(W_o) \cos(K_a) - \sin(W_o) \sin(\phi) \sin(K_a) \\
m_{23} &= \sin(W_o) \cos(K_a) + \cos(W_o) \sin(\phi) \sin(K_a) \\
m_{31} &= \sin(\phi) \\
m_{32} &= \sin(W_o) \cos(\phi) \\
m_{33} &= \cos(W_o) \cos(\phi)
\end{aligned}$$

The three parameters  $W_o$ ,  $\phi$  and  $K_a$  are the photographic rotations about the X, Y and Z axis, respectively.

The collinearity equations are obtained by dividing the first and second rows of equation 43 by the third row hereby eliminating the scale factor.

$$\frac{x_p - x_o}{-f} = \frac{m_{11} (X_p - X_c) + m_{12} (Y_p - Y_c) + m_{13} (Z_p - Z_c)}{m_{31} (X_p - X_c) + m_{32} (Y_p - Y_c) + m_{33} (Z_p - Z_c)} \quad (45)$$

$$\frac{y_p - y_o}{-f} = \frac{m_{21} (X_p - X_c) + m_{22} (Y_p - Y_c) + m_{23} (Z_p - Z_c)}{m_{31} (X_p - X_c) + m_{32} (Y_p - Y_c) + m_{33} (Z_p - Z_c)} \quad (46)$$

These equations insure that the camera station, image and object lie on a straight line. For each point two collinearity equations can be written. As there are six unknowns ( $X_c, Y_c, Z_c, W_o, \phi$  and  $K_a$ ) a minimum of three noncollinear control points are required for their solution. However, a least squares solution permits the use of an unlimited number of control points.

Solution to the equations is obtained based on a set of initial approximations which are adjusted iteratively until the adjustments become small. The collinearity equations are linearized by the Taylor series with the expansion terminated at the first derivative.

When the initial approximations of  $B_j$  are close to the actual

parameters values (B)

$$f(B) = F(B_j) + \sum_{i=1}^6 \frac{\partial f(B)}{\partial B_i} \Delta B_i \quad (47)$$

Letting  $Y = f(B) - f(B_j)$  (48)

$$Z_i = \frac{\partial f(B)}{\partial B_i} \quad \text{for } B = B_j \quad (49)$$

then  $Y = \sum_{i=1}^6 Z_i \Delta B_i + \epsilon$

which is a linear form of the collinearity equations. The least squares solution in matrix notation is

$$B = [Z^T Z]^{-1} Z^T Y \quad (50)$$

The initial approximations of the parameters ( $B_j$ ) are replaced by

$$B_{j+1} = B_j + \Delta B_j \quad (51)$$

This iterative process is continued until the solution converges, that is, until all  $\Delta B$ 's are less than some prespecified amount. In this space resection problem no test is made on the linear adjustments but solution is terminated when the angular adjustments are less than about two seconds of arc.

By knowing the photo orientation, it is possible to determine the position vectors for any point on the photograph. The position vector ( $\bar{X}$ ) based on the state plane coordinate system axis is related to the photographic vector ( $\bar{X}_p$ ) by the equation

$$\bar{X} = [RM]^{-1} \bar{X}_p \quad (52)$$

The ground coordinate of any point on the photograph can be computed from the unit position vector and the camera station coordinate determined from the photographic orientation.

In order to compute the required angle between this position vector and the light rays, the sun's position must be determined. The altitude (h) and azimuth (Az) from true north of the sun are determined from

$$\sin(h) = \sin(L) \sin(D) + \cos(L) \cos(D) \cos(t) \quad (53)$$

$$\tan(Az) = \sin(t) / (\cos(L) \tan(D) - \sin(L) \cos(t)) \quad (54)$$

where    L = latitude  
           D = declination of the sun  
           t = hour angle of the sun

The vector representation of the light ray from the sun is

$$\bar{X}_s = \cos(h) \sin(AZ) i + \cos(h) \cos(AZ) j - \sin(h) k \quad (55)$$

AZ represents the azimuth of the sun from grid north and differs from the azimuth from true north by the state plane coordinate mapping angle. The position vector as defined by equation 52 and the sun ray vector as defined by equation 55 are based on the same coordinate system.

## SECTION VI

### DIFFUSION STUDIES

Numerous investigators have employed solutions to the diffusion equations for the estimation of waste concentrations in the waste plume that occurs at an outfall location. If the scale of the current eddies is much smaller than the dimensions of the waste field, then the Fickian form of diffusion equation can be applied. The basic equation is:

$$\begin{aligned} \frac{\partial W}{\partial T} = & \frac{\partial}{\partial Y} (D_y \frac{\partial W}{\partial Y}) + \frac{\partial}{\partial X} (D_x \frac{\partial W}{\partial X}) + \frac{\partial}{\partial Z} (D_z \frac{\partial W}{\partial Z}) - [ \frac{\partial}{\partial Y} (V_y W) \\ & + \frac{\partial}{\partial X} (V_x W) + \frac{\partial}{\partial Z} (V_z W) ] + S \end{aligned} \quad (56)$$

where V is velocity, W is waste concentration, D is eddy diffusivity. The first three terms on the right are the diffusion terms, the next three are convection terms and S represents the sources and sinks.

Solutions to the equations have required various assumptions such as steady state condition, no vertical or longitudinal mixing and unidirectional transport velocity in the x direction. With these assumptions, the equation becomes:

$$V_x \frac{\partial W}{\partial X} = \frac{\partial}{\partial Y} (D_y \frac{\partial W}{\partial Y}) + aW \quad (57)$$

Where "a" is a first order decay constant and "aW" represents a sink or loss in the system.

Investigators such as Pearson (1955-1967), Brooks (1960) and others have reported solutions to the diffusion equation for various conditions. Pearson points out that for point and line sources, steady unidirectional current, uniform mixing of the waste over a depth, d and continuous uniform flow from the source, solutions to the diffusion equation in terms of the minimum dilution,  $S_{om}$ , along the centerline axis of the waste sea water plume are as follows:

#### Point Source

$$S_{om} = \frac{2.35 \, d \, \sqrt{D_y V_x X}}{Q} \quad (58)$$

where  $S_{om}$  is the minimum dilution along axis of waste plume at distance X from source;  $D_y$  is the assumed diffusivity, ft<sup>2</sup>/sec; X is the distance from source, feet;  $V_x$  is the average velocity of water mass, ft/sec; Q is the waste discharge, MGD; and d is the assumed mixing depth, ft.



Including the decay function for bacterial dieaway for disappearance, and expressing the waste concentration in terms of coliform concentration, the above expression becomes:

$$MPN = \frac{0.425 Q C_o}{d \sqrt{D_y} V_x X \exp(aX V_x)} \quad (59)$$

where MPN is the most probable number of organisms per ml on plume centerline at X;  $C_o$  is the concentration of organisms in waste, MPN/ml; and  $a$  is the bacterial dieaway (decay) constant,  $\text{sec}^{-1}$ .

#### Line Source

$$S_{om} = \frac{0.622 V_x b d}{Q \operatorname{erf} [(b/4) \sqrt{V_x/D_y X}]} \quad (60)$$

where  $b$  is equal to the width of diffuser source, feet and

$$MPN = \frac{1.55 Q C_o \operatorname{erf} [(b/4) \sqrt{V_x/D_y X}]}{b d V_x \exp(aX/V_x)} \quad (61)$$

Pearson (1967) further points out that: "The above equations assume a constant eddy diffusivity; correspondingly, the value of  $D_y$  employed must be representative of the overall or average scale of the diffusion phenomenon.

Brooks has reported a solution to the diffusion equation with a variable coefficient of diffusivity. It is assumed that the diffusivity coefficient,  $D_y$ , varies as the four-thirds power of the scale of the diffusion phenomenon,  $D_y \approx \alpha l^{4/3}$ , where  $\alpha$  is a constant. Brooks' equation for a line source is as follows:

$$C_m = C_o e^{-at} \operatorname{erf} \left[ \frac{3/2}{(1 + 2BX/(3b))^3 - 1} \right]^{1/2} \quad (62)$$

Where:

$C_o$  = initial coliform concentration

$C_m$  = maximum coliform concentration at time,  $t$

$t$  = time of travel =  $\frac{X}{V_x}$

$B = \frac{12D_y}{V_x b}$

- a = decay constant
- $D_y$  = eddy diffusivity at source ( $X = 0$ )
- b = initial width of sewage field

Considering the foregoing solutions to the diffusion equation, the four characteristics of the receiving waters which have the major effect on waste concentration are the following:

1.  $V_x$ , average current speed
2.  $D_y$ , eddy diffusivity
3. d, average mixing depth
4. a, decay or dieaway constant of pollutant

The Allen Hancock Foundation conducted an investigation on the dilution and dispersion of a waste field in the sea (1965). In their study rhodamine B dye was introduced as slugs from a point source, continuous plume from a point source and continuous plume from a volume source. Dye concentration was measured with a Turner fluorometer. The mathematical models used for analysis of data were statistical models based on Gaussian distribution. The basic three-dimensional model for the dye slug was

$$W(x,y,z,t) = \frac{M}{\pi \sqrt{2\pi} [\bar{\sigma}_x^2 \bar{\sigma}_y^2 \bar{\sigma}_z^2]^{1/2}} \exp - \left[ \frac{X^2}{2\bar{\sigma}_x^2} + \frac{Y^2}{2\bar{\sigma}_y^2} + \frac{Z^2}{2\bar{\sigma}_z^2} \right] \quad (63)$$

where W is the average concentration of a point X, Y, Z, and time t, M is the amount of dye initially discharged from an instantaneous point source and  $\bar{\sigma}_x^2$ ,  $\bar{\sigma}_y^2$ ,  $\bar{\sigma}_z^2$  are the average values of the variances of the concentration distribution.

One of the two dimensional models used describe a continuous plume from point source neglecting diffusion in the direction of motion was

$$W(x,y,z) = \frac{Q}{\pi (\bar{\sigma}_y^2 \bar{\sigma}_z^2)^{1/2} V_x} \exp - \left[ \frac{Y^2}{2\bar{\sigma}_y^2} + \frac{Z^2}{2\bar{\sigma}_z^2} \right] \quad (64)$$

where Q is the continuous steady rate of discharge of material,  $V_x$  is the mean current velocity. The variances are a function of diffusion time or distance from the source, i.e., by making the substitution  $t = X/V_x$  the variances can be expressed approximately as functions of distance.

For volume source the basic equation was

$$\begin{aligned}
 W(x,y,z) &= \frac{2Q}{\pi V_x [2\bar{\sigma}_y^2 + \bar{\sigma}_y^2(0)]^{1/2} [2\bar{\sigma}_z^2 + \bar{\sigma}_z^2(0)]^{1/2}} \\
 &\quad \exp - \left[ \frac{y^2}{2\bar{\sigma}_y^2 + \bar{\sigma}_y^2(0)} + \frac{z^2}{2\bar{\sigma}_z^2 + \bar{\sigma}_z^2(0)} \right] \quad (65)
 \end{aligned}$$

where  $\bar{\sigma}^2(0)$  is the variance of the initial waste concentration distribution.

Several of the conclusions of this investigation are listed below.

1. The rate of vertical diffusion can contribute significantly to the overall diffusion process at wind speeds greater than eight knots and/or low water column stability.
2. The rate of longitudinal and lateral diffusion appeared to be influenced by wind speed but not by water column stability.
3. The "4/3 law" relating the lateral coefficient of eddy diffusion as a function of average eddy scale did not hold in the particular oceanic areas studied.

Vertical mixing does occur in the waste field as well as horizontal mixing. As indicated by Wiegel (1964), vertical mixing is difficult to study in the laboratory because of limitations of tank size. In these studies the wind drags the surface water to the down wind end of the tank producing a hydraulic head which causes a flow in the opposite direction.

Laboratory studies have indicated that wind drag on the water surface produces very little mixing. However, when wind generated waves appear, extremely rapid mixing occurs as wind waves are rotational in the generating area. On the other hand, there is some indication that swell is not important to the mixing process as it is apparently nearly irrotational (Wiegel, 1964).

Masch (1961) conducted a wave study in a wave tank and developed the following relationship for the coefficient of eddy diffusivity:

$$D_y = 0.0038 (V_s + Q_w)^{3.2}$$

where  $V_s$  is the surface current and  $Q_w$  is the water particle orbit speed ( $Q_w = H/T$ ,  $H$  = significant wave height and  $T$  = average wave period).

## SECTION VII

### SAMPLING PROCEDURES

In order to achieve the goals of this research project, the Kraft pulp mill outfall at Newport, Oregon was selected as the study site. The Georgia-Pacific pulp and paper plant at Toledo produces about 900 tons of pulp per day. Waste from the process is pumped through an eight-mile pipeline to the outfall at Newport. Flow rates vary from six to twelve million gallons per day. The aerial photograph of the Newport-Toledo area shown in figure 19 was taken looking east with the ocean in the foreground. The location of the outfall in this figure was sketched on the photo and is shown in white. The 21-inch diameter outfall was rebuilt and extended to 3500 ft. offshore in 1965. The outfall terminates with a wye diffuser in about 40 feet of water at low tide. A sketch of the outfall is shown in figure 20. Thirteen outlet ports are located at 20-foot intervals on each leg of the wye section. The three-inch diameter ports discharge horizontally into the sea. The ports are oriented so that they discharge alternately on opposite sides of the header.

Three different field procedures were used on the project. During the 1968 and 1969 field seasons, work was carried out by conducting simultaneous studies of the waste plumes by aerial photographic methods and by conventional boat sampling. Concentrations in the plume were determined by metering rhodamine WT tracer into the pipeline and measuring the tracer concentration in the waste field with a fluorometer aboard the survey boat.

During the first field season, two fluorometers were used to sample from one foot and five feet below the water surface. Since there was no significant difference in the concentration at these two depths, only one fluorometer was used during the following field season. A ten-foot sampling probe for the fluorometer intake was constructed for the 1969 field season. Sample intake ports were located along the length of a sampling probe mounted on the side of the boat. The probe was designed to hang vertically at five knots. By a sliding valve arrangement in the body of the probe, the sampling depth could be selected from one to ten feet below the water surface. Boat sampling was discontinued during the 1970-71 field season and field work continued throughout the fall, winter, and spring when boat operations were impossible due to rough sea conditions most of the time.

Vertical aerial photography was taken with a single camera by a commercial aerial photography firm during the 1968 field season. As the firm was located approximately 100 miles from the study area, scheduling of the photography was difficult. After the 1968 field season, the project purchased three aerial cameras and the photography was taken with the cameras mounted obliquely in a rented four-passenger aircraft.

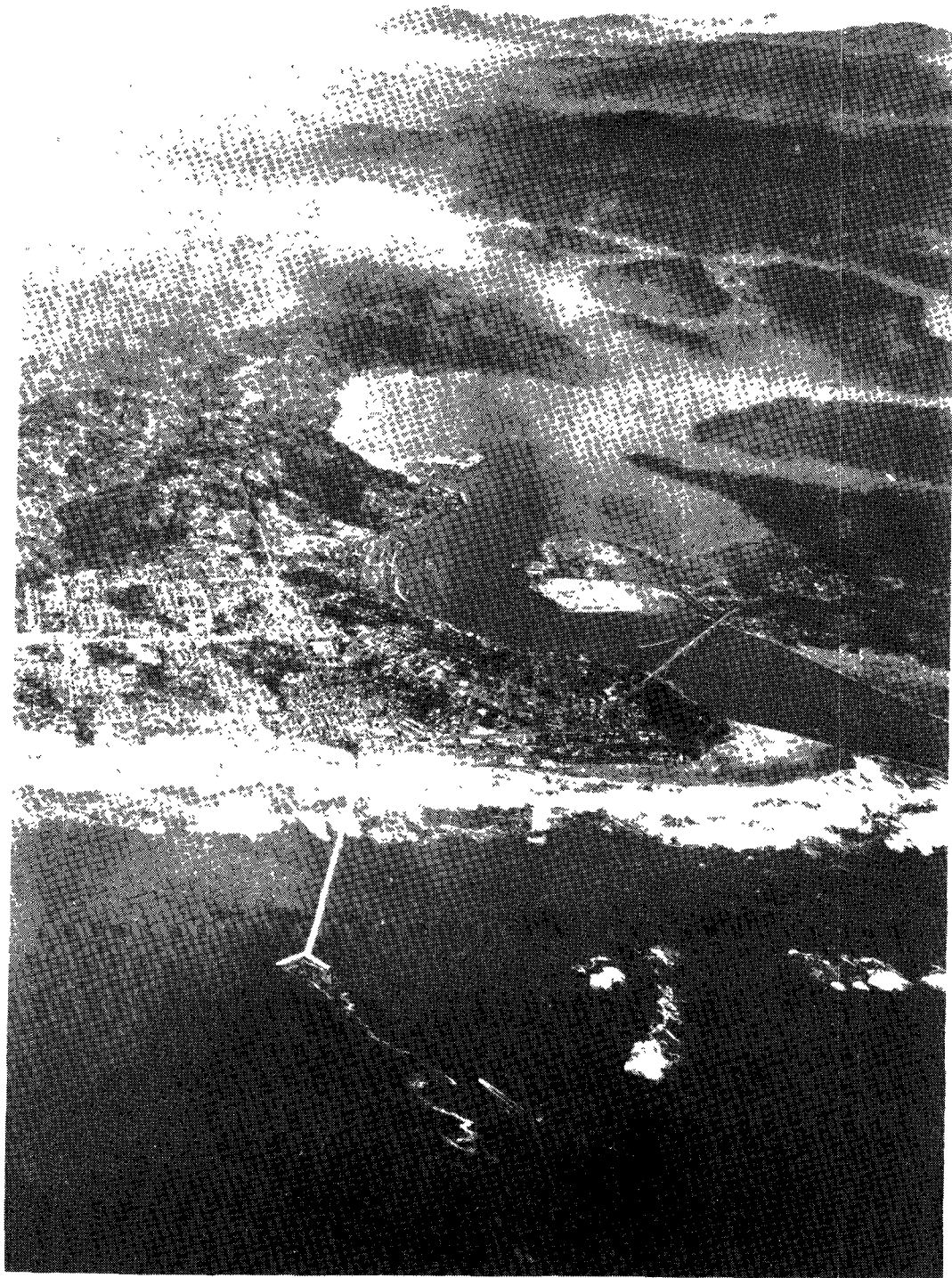


Figure 19. Aerial view of Newport area.

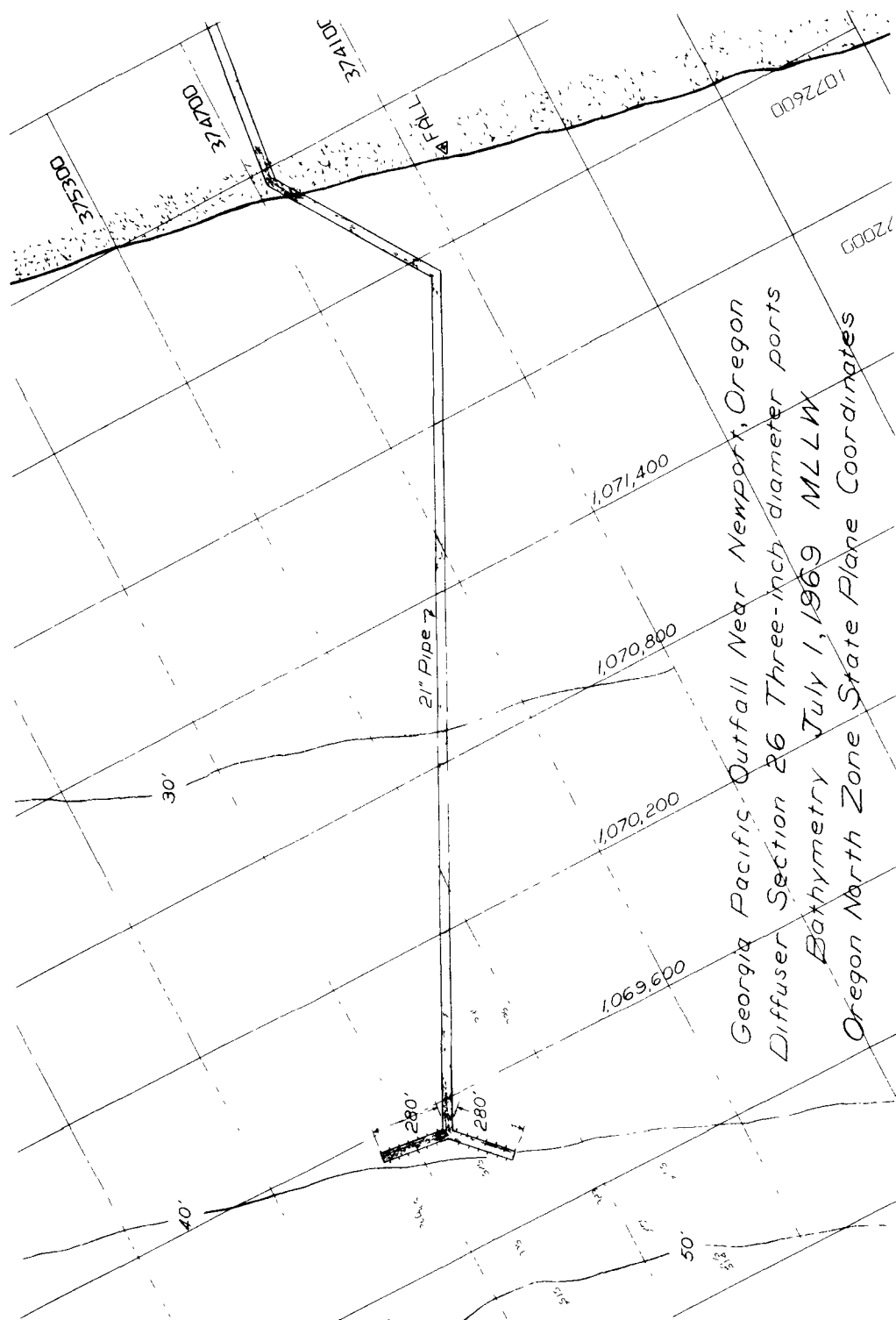


Figure 20. Sketch of the Newport outfall.

### Shore Control

Accurate control for positioning the boat and orientation of the photography was essential. Concentrations computed from the photographs are compared to those measured by sampling from the boat. Since the comparison requires matching of ground coordinates, an accurate control network was established, thus eliminating the possibility of discrepancies in concentration being due to error in positioning.

Shore control for boat location and photograph orientation was provided by a ten-mile tellurometer traverse between two USC & GS triangulation stations. The traverse extended from a triangulation station on the south to station Yaquina Head Lighthouse on the North. Six traverse stations were established and marked with three quarter-inch steel rods 30 inches long. Horizontal angles were measured with a Wild T-3 theodolite. Initially the distances were to be measured with a geodimeter but due to poor visibility, a tellurometer was used. As the tellurometer measures slope distance, the station elevations were determined by reciprocal vertical angles. The established stations were marked with white cloth for photo identification.

### Buoy Control

During the 1968 field season vertical, color photography was taken by a commercial aerial mapping firm. Photography was taken at scales of 1:6,000 and 1:12,000 using precise mapping cameras. In addition to the shore control, control buoys were required in the water for photographic orientation of the low altitude photography. The buoys were positioned so that each photo would contain a minimum of three control points for photographic orientation. Control buoys were four-foot square plywood floats three inches deep attached to 500 lb concrete anchors. The floats were constructed of a two-inch thick sheet of polyurethane between two sheets of half-inch plywood. To hold the float together a metal flashing was fastened around the edge and an eye bolt was placed through the center of the float. The mooring line was attached to the eye bolt. This line consisted of a ten-foot length of half-inch chain attached to each end of a half-inch polypropylene rope. A swivel was placed between the top section of chain and the rope. The weight of the chain added stability to the anchoring system. In addition, the top 10-foot section of chain prevented vandalism by boaters. The scope of the mooring line was made as short as possible to minimize movement of the float about the anchor yet long enough to prevent movement of the anchor during normal summer months. The mooring line was made equal to the depth of water at MLLW plus 20 feet. Summer storms did take out three of the near-shore buoys which were set in less than 20 feet of water.

The small scale photography taken during the 1968 field season was intended to be used for buoy location by analytical strip bridging. However, it was found more convenient to triangulate the position of

the buoys from the shore stations.

The oblique camera mounting used after the first field season reduced the requirement for horizontal control in the water. The large camera photographs included the horizon and two horizontal control points could be identified on shore. In addition, one buoy was desired near the outfall to provide a strong fix for the photographic orientation. During the 1969 field season, two temporary buoys were set near the outfall on each day that field work was conducted. The buoy floats were four feet square, two inches thick polyurthene board which were fibreglassed and painted orange. The 60-lb anchors were adequate to hold the floats in position for the sea conditions encountered during the field work. Since boat operations were stopped during the 1970-71 field season, control buoys were not used during this period and photo control was provided by identification of at least three shore stations on the photography.

#### Water Currents

During the 1968 field season, the survey boat would set two four foot square floats with drogues attached to measure the water currents. The drogues extended from one half foot below the water surface to five feet and were constructed of herculite material fitted over a conduit frame to form a cross banner 4-1/2 ft in length and in width. A ten pound weight was attached to the lower end of the drogue. The positions of the current floats were determined from the aerial photography. In addition, during the 1969 field season 500 ml of 20% rhodamine WT dye in a plastic bag were dropped from the aircraft. The change in location and size of the resulting dye patch provided information on both the current velocity and the diffusion coefficients. When boat sampling was discontinued after the 1969 field season, floats with drogues attached were no longer used but dye markers were used to determine water currents and diffusion coefficients.

#### Continuous Boat Sampling

Cooperative arrangements were made with Georgia-Pacific Corporation to maintain a nearly constant waste discharge rate while field work was in progress. In addition, they provided the project with a dye tracer injection station installed on their outfall line near the beach. The station was equipped with a tap to the pipeline for injecting the tracer. A positive displacement pump was employed for continuous tracer injection into the pipeline. Pressure in the pipeline at the station varied from zero at low tide to about five psi at high tide for the pipeline flow rates encountered during the study.

Measurement of waste concentrations in the ocean was accomplished by metering a dye tracer, rhodamine WT 20% solution, into the outfall pipeline on shore to produce a dye concentration of about one part per million in the effluent at the point of discharge. Dye concentrations



in the waste plume were measured with a Turner III Fluorometer aboard the survey boat. The fluorometer was equipped with a flow through sample cell and continuous readings were recorded with a chart recorder. The sample was drawn through the instrument with a pump on the discharge side of the fluorometer. By knowing the tracer injection rate and the effluent flow rate, the waste concentration was calculated from the measured tracer concentration. In order to eliminate the effect of temperature on the tracer fluorescence the instruments were standardized in the field.

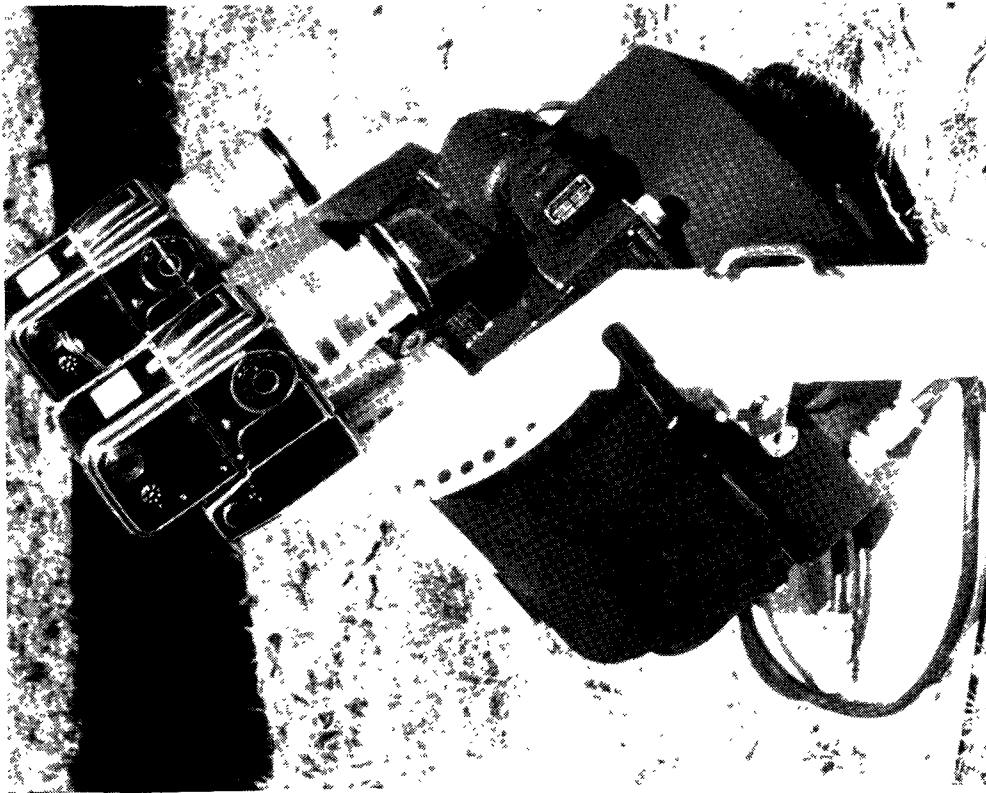
While continuous sampling was underway, the fluorometer operator would mark each position, record position number, indicate any fluorometer scale change and any sampling depth change on the chart record. The boat's position was determined at one-minute intervals by triangulation. Simultaneous horizontal angles were measured from two shore stations with Wild T-2 Theodolites. The radio operator aboard the boat would signal the theodolite operators when the position was to be taken.

#### Aerial Photography

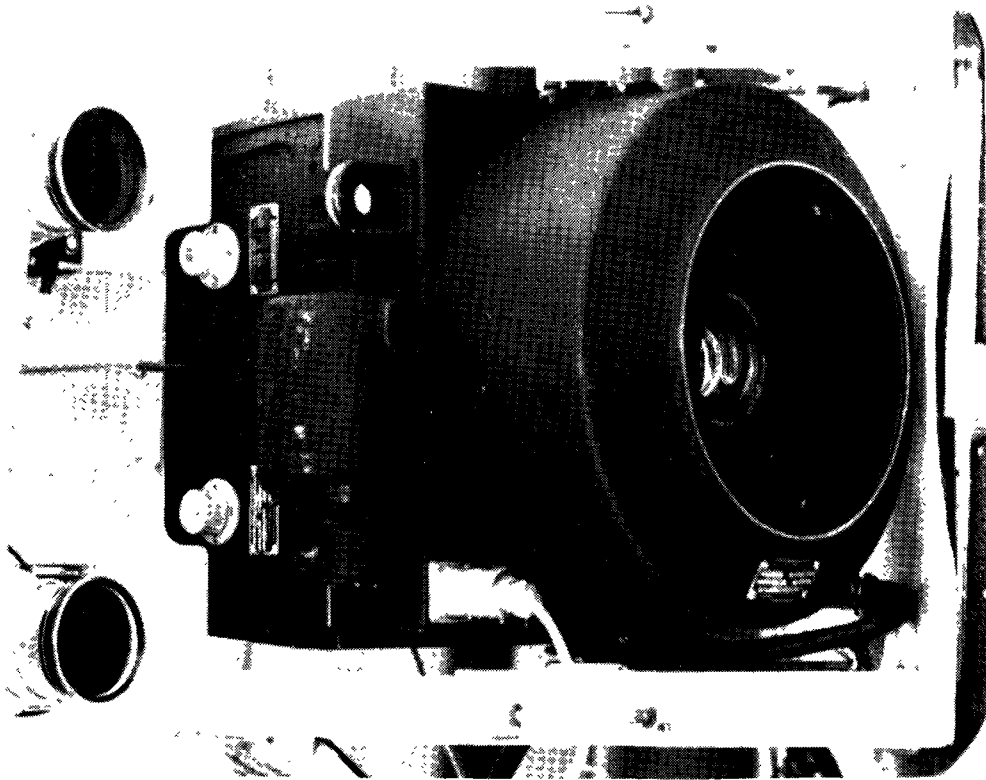
One of the primary problems encountered in processing the 1968 vertical photography was the direct sunlight reflection from the water surface. Photography after 1968 was taken with an oblique camera mounting to avoid the sun spot. Prior to the 1969 field season, three cameras were purchased and mounted in the baggage compartment of a small high wing aircraft. This eliminated the need for advance scheduling of commercial aerial photography and allowed flexible planning of the changing weather and sea conditions. The camera package shown in figure 21 consisted of a K-17 mapping camera and two 70 mm cameras. Multiple cameras allowed the selection of optimum film, filter and exposure combinations for several photographic bands. The mapping camera, because of its large angular coverage, permitted photographic orientation of the two smaller cameras. Films from the two 70 mm cameras were used for detailed analyses and measurements of the waste field. Polarizing filters on the 70 mm cameras reduced the skylight reflection from the water surface.

The cameras were synchronized to take simultaneous pictures with a timing device consisting of a capacitor in parallel with a variable resistor. The cameras were lined up end to end without their magazines and the variable resistor was adjusted until a light could be seen through the cameras when the shutters were activated at 1/100 of a second.

When the aerial photography was taken with a single vertical mapping camera, normal color film was used. Both Ektachrome 8442 film and Anscochrome D200 film were tested. There was no significant difference in the results of the two films. When aerial photography was taken with the three camera unit, generally the K-17 was loaded with black and white film, type 2402, with a Wratten 25A filter, while one 70 mm



Aerial cameras



Camera unit in aircraft

Figure 21. Multiple camera unit.

Hasselblad camera was loaded with normal color film, type 2448, and the second Hasselblad camera was loaded with infrared black and white film, type 5424. Because of the variable light scattering and absorbing characteristics of the pulp mill effluent, a broad band photographic system was used.

The photographic film was developed by project personnel in accordance with the film manufacturer's directions. The aerial film from the mapping camera was 9-1/2 inches wide and 100 ft long, and was processed with a Morse B-5 rewind processor while the 70 mm film was processed with a Nikor reel and tank processor.

## SECTION VIII

### DYE PATCH STUDIES

During the 1969 field season, several dye drops were made from the aircraft. The three pictures shown in figure 22 were taken July 7, 1969 using panchromatic film type 8401 with a Wratten 25A filter. While this is not the best film-filter combination for observing the dye patch, the change in shape of the dye patch can be seen. The dye was dropped at 12:19 and the first photo was taken at 12:25 from 3000 ft at which time the size of the dye field was 160 ft by 40 ft. The photo in figure 22b was taken at 13:13 from 4000 ft. After 54 minutes from the time the dye was dropped, the dye patch had grown to approximately 70 ft wide and an overall curved length of 1000 ft. The light reflection in 22b could have been reduced with a polarizing filter. The photo in figure 22c was taken an hour and a half later at 14:43 from 5000 ft. The dye field at this time is 2100 ft long and 1300 ft wide.

The example given in figure 22 was an extreme example of elongation, curvature and striation of a dye patch. The wind was downward and to the right in the pictures at 5 to 12 knots with a swell height of 4 to 6 ft and a water current velocity of 0.4 ft/sec. Most dye patches observed have been elongated in a direction nearly parallel to that of the water flow. Striations and curvature of the dye patch are common. However, in most experiments the overall shape of the patch resembles an ellipse.

The elongation of the dye patch in the direction of flow suggests dispersion due to a vertical velocity gradient can, at times, be an important consideration. The upper layers of water are first influenced by a change in wind velocity or direction and vertical velocity gradients would be expected. Wind waves and swell both have specific orientation that suggest diffusion will occur at different rates in a horizontal plane.

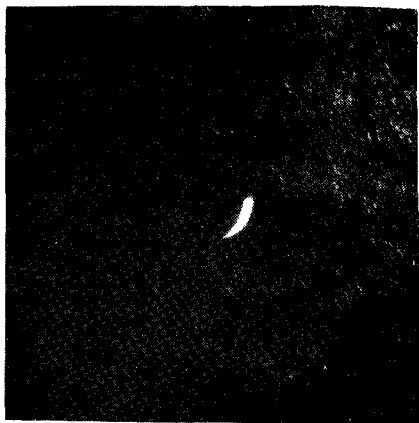
The basic diffusion equation given as equation 56 is reduced to a two dimensional model.

$$\frac{\partial W}{\partial t} = D_y \frac{\partial^2 W}{\partial Y^2} + D_x \frac{\partial^2 W}{\partial X^2} + aW \quad (67)$$

A solution is

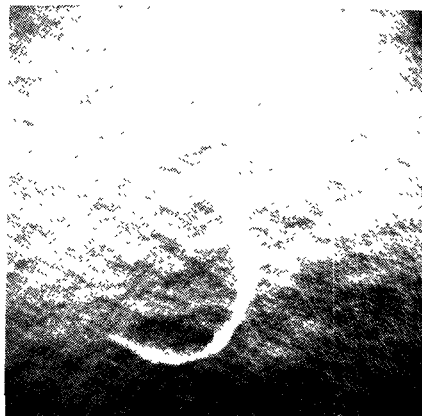
$$W(x, y, t) = W_{\max} \exp - \left[ \frac{X^2}{2\sigma_x^2} + \frac{Y^2}{2\sigma_y^2} \right] \quad (68)$$

where the coordinate axis is assumed to move with the dye patch. In



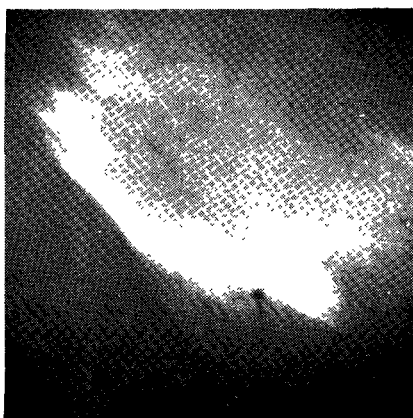
a

At 12:25 from 3000 ft



b

At 13:13 from 4000 ft



c

At 14:43 from 5000 ft

Figure 22. Dye patch on July 7, 1969.

the equation  $W$  represents the dye concentration,  $X$  and  $Y$  are the coordinates from the centroid of the dye patch parallel and transverse to the direction of flow,  $D_x$  and  $D_y$  are the longitudinal and lateral diffusion coefficients, " $a$ "<sup>x</sup> is a first order decay coefficient which includes the loss to the lower layers due to vertical diffusion and  $\sigma_x^2$  and  $\sigma_y^2$  represent the variances in the  $X$  and  $Y$  directions. The relationship between the change in variance and the diffusion coefficient is given by

$$D = \frac{1}{2} \frac{\Delta \sigma^2}{\Delta t} \quad (69)$$

The diffusion coefficient is equal to one half the change in variance ( $\Delta \sigma^2$ ) divided by the time interval ( $\Delta t$ ).

Dividing equation 68 by the maximum concentration at the centroid ( $W_{\max}$ ), taking the log of each side and multiplying by 2 the equation becomes

$$\frac{X^2}{\sigma_x^2} + \frac{Y^2}{\sigma_y^2} = 2 \ln \left[ \frac{W_{\max}}{W} \right] \quad (70)$$

by letting

$$a^2 = 2\sigma_x^2 \ln \left[ \frac{W_{\max}}{W} \right] \quad (71)$$

$$b^2 = 2\sigma_y^2 \ln \left[ \frac{W_{\max}}{W} \right] \quad (72)$$

equation 70 reduces to that of an ellipse

$$\frac{X^2}{a^2} + \frac{Y^2}{b^2} = 1 \quad (73)$$

where  $a$  and  $b$  are the major and minor semi axis of an ellipse fitted to a line of equal concentration about the dye patch. Since the edge of the dye patch is generally characterized by relatively steep concentration gradients, the visible boundary of the patch was assumed to have a concentration of  $W_{\max}/2$ . With this assumption equations 71 and 72 reduce to

$$\sigma_x^2 = 0.72 a_e^2 \quad (74)$$

$$\sigma_y^2 = 0.72 b_e^2 \quad (75)$$

By using equation 69, 74 and 75 the diffusion coefficients are related to the change in size of the dye patch between photographic flights over the area. Since the dye patches seldom form a perfect ellipse, the major and minor semi axes of the edge of the patch ( $a_e$  and  $b_e$ ) can not be measured directly from the aerial photography. The procedures employed in determining diffusion coefficients from the aerial photography are given in Section IX on Data Processing.

## SECTION IX

### DATA PROCESSING

The general scheme for processing the boat and photographic data during both the 1968 and 1969 field seasons is shown in figure 23. Data processing included reduction of shore angles to state plane coordinates, conversion of fluorometer strip chart records to waste concentrations and reduction of photographic information. A comparison was made between the waste concentrations determined by boat sampling with those determined from aerial photography by matching ground coordinates.

During the 1970-71 field season only aerial photography required processing. Aerial film taken during this period was not digitized using the densitometer. The processing techniques were modified to achieve the research objective of the original proposal, which was to develop a remote sensing tool for the evaluation of dispersion of wastes from existing or proposed ocean outfalls. Since the 1968 and 1969 field seasons were concerned with existing outfall sites, the final year of the project was concerned with the development of simplified procedures for proposed outfall sites.

#### 1968-1969 Boat Data

Angles from the shore stations to the photo control buoys and the boat were reduced to state plane coordinates. Boat positions were indexed by time for matching with waste concentration. Since theodolite sightings were made on the boat's mast, a correction was applied to determine the position of the fluorometer intake ports.

The fluorometer records were processed by 1) a least squares fit to the standardization data, 2) a shift of the index on the fluorometer reading to account for the time delay for the sample to pass from the intake port to the fluorometer, 3) reduction of the fluorometer reading to concentration of tracer and concentration of effluent, and 4) interpolating the ground coordinates from the processed shore control data.

Waste concentrations determined by boat sampling were displayed on a three dimensional plot. Figure 24 is a typical display of the boat sampling data where the grid represents the X and Y state plane coordinates and the Z axis represents the waste concentration in milliliters/liter. The waste concentration is represented by the length of a line drawn parallel to the z-axis. The state plane coordinate position of any sample point can be scaled from the grid to the base of the vertical line. The solid line on the plot is the boat's track. The plume in the plot extends upward and to the right.

The surface water temperature was also recorded along the boat's track and displayed on a three dimensional plot as shown in figure 25.



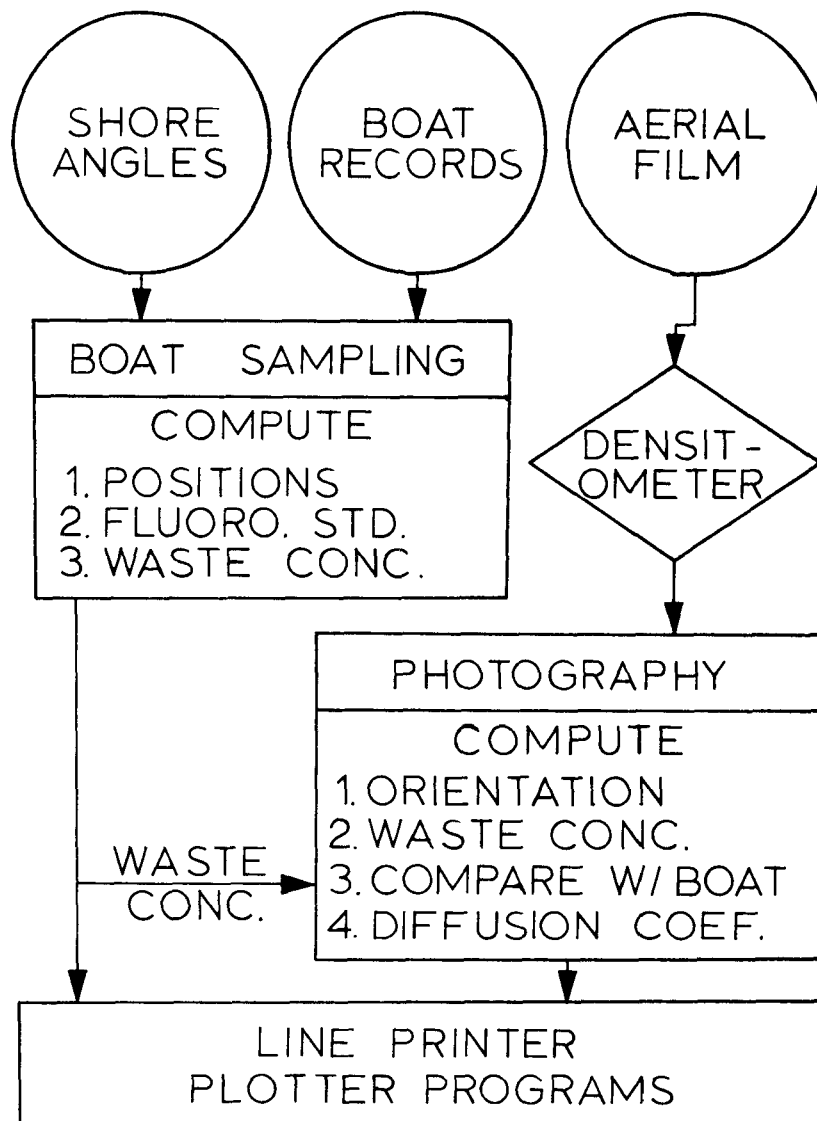


Figure 23. Data processing flow diagram.

# AIRPHOTO ANALYSIS OF OCEAN OUTFALL DISPERSION

PLST OF WASTE CONCENTRATIONS ML/L FROM BOAT

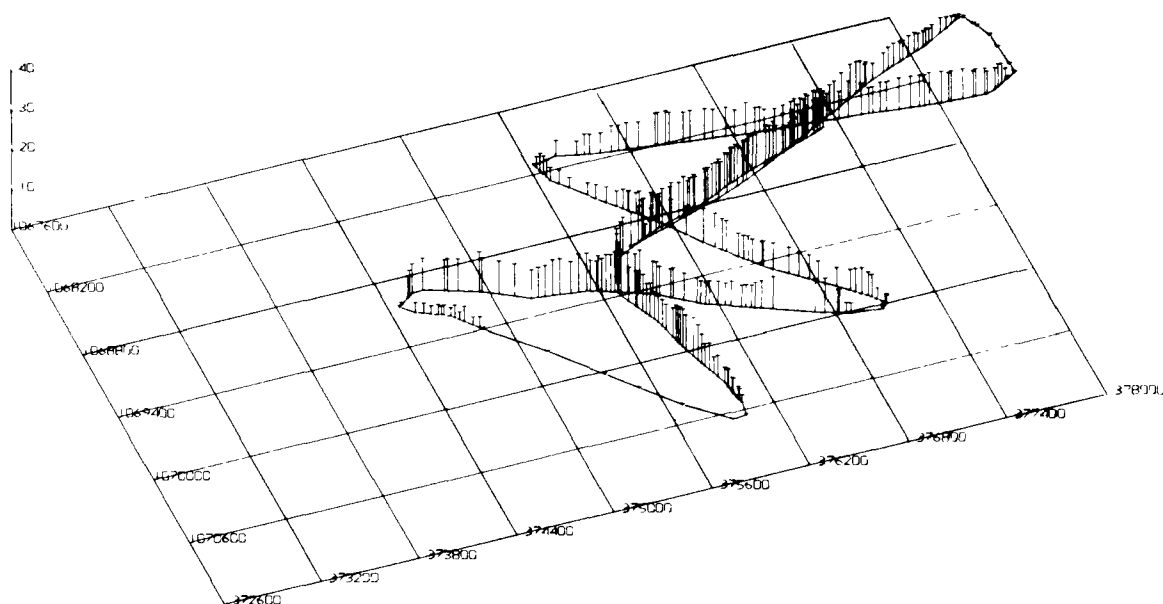


Figure 24. Waste concentrations from boat sampling on August 12, 1969.

# AIRPHOTO ANALYSIS OF OCEAN OUTFALL DISPERSION

PLST OF SURFACE WATER TEMPERATURE IN DEGREES C

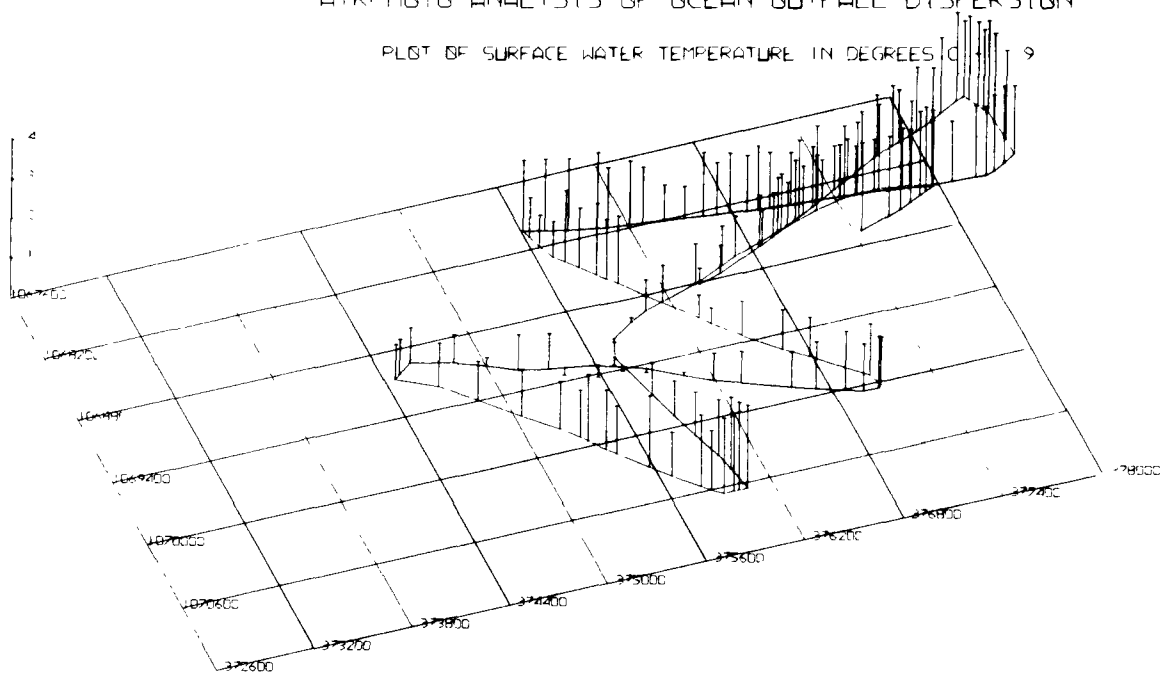


Figure 25. Surface water temperature on August 12, 1969.

In order to be able to show a smaller temperature variation, the values plotted in figure 25 were the surface temperatures minus nine degrees. The outfall in figures 24 and 25 is located near coordinates 1069400E, 375600N where the waste concentration is a maximum and the surface water temperature is a minimum. The temperature of the waste while in the pipeline is about 40°C. The waste discharged from the outfall ports mixes by jet diffusion with the colder subsurface water and the resulting mixture at the surface in this case was colder than the surrounding sea water.

A temperature profile taken over the outfall and one taken north of the waste field on August 12, 1969 are shown in figure 26. The temperature of the water near the bottom is 7.5°C while that near the surface over the outfall is 8.4°C and north of the waste field is 10°C.

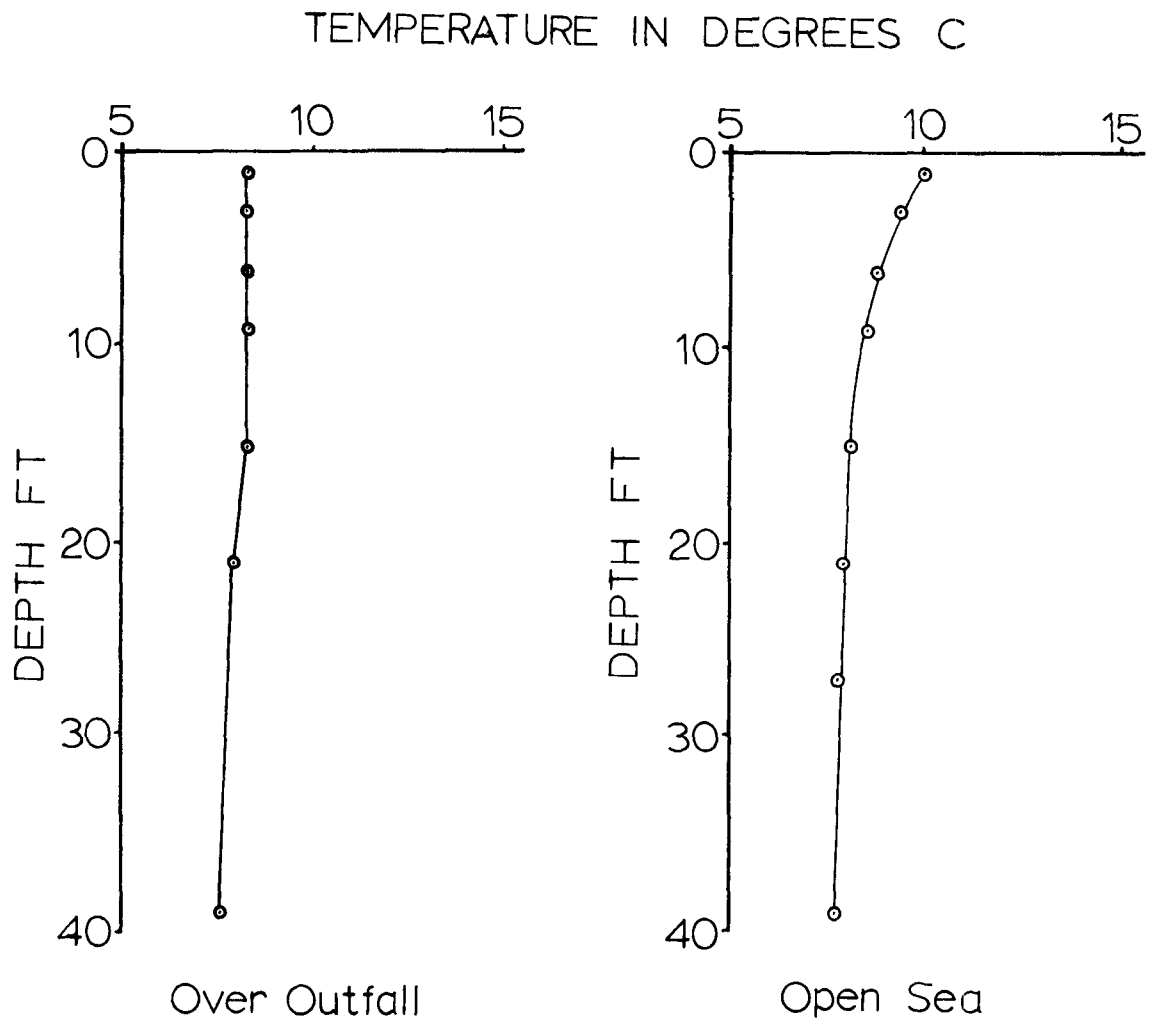


Figure 26. Water temperature profiles on August 12, 1969.

A detailed description including the computer program for processing the boat sampling data is given in Appendix C of the Water Pollution Control Research Series, 12040EBY on "Aerial Photographic Tracing of Pulp Mill Effluent in Marine Waters" by Burgess and James. Detailed description of the three dimensional plotting program was given in Appendix D of the "First Annual Progress Report" on this project (Burgess and James, 1969).

#### 1968 Photographic Data

During the 1968 field season, color aerial photography was taken with a single vertical aerial mapping camera. The photographic film was converted to digital data with a McBeth model TD-102 photo densitometer. The densitometer can measure the density of the three layers of the color photo. Wratten filters numbers 92, 93, and 94 are utilized to measure the red, green and blue film densities, respectively. The aerial film holder was attached to an x - y coordinatograph which measured the photo coordinates to  $\pm 0.001$  inches. At the same time, the film densities were measured with a digital voltmeter. Both the voltmeter and coordinatograph were connected to a digitizer which in turn was connected to a card punch. One card was required for each point and contained the photo identification number, point number, x and y coordinates and the film densities for the three spectral bands of the color photo. The position of each data point was selected manually. The three film densities on each card were measured at the same point on the photograph.

A generalized flow diagram of the photographic data processing is shown in figure 27. The photographic analysis phase of the data processing began with the photographic orientation which was accomplished by a non-linear least square solution to the collinearity condition equations. After the last photograph has been oriented, the water currents are computed. The sun altitude and azimuth are computed for the first photograph of each flight.

The photographic variable that was the most sensitive to changes in waste concentration was the ratio of red to green light reflected from the waste field. This ratio, adjusted for atmospheric attenuation and for light scattered from the sea water, was related to the waste concentration by a least squares fit of the boat sampling data. The comparison was made by matching ground coordinates at 60-foot intervals along the boat's path. Utilizing this regression equation waste concentrations were computed throughout the waste field.

Film densities and photo coordinates were measured with the photo densitometer for points outside both the waste field and the area of direct sunlight reflections. The data from these points were used to determine the regression coefficients for the model

$$ATR = A_0 + A_1 (j_2) + A_2 (j_2)^2 + \epsilon \quad (76)$$

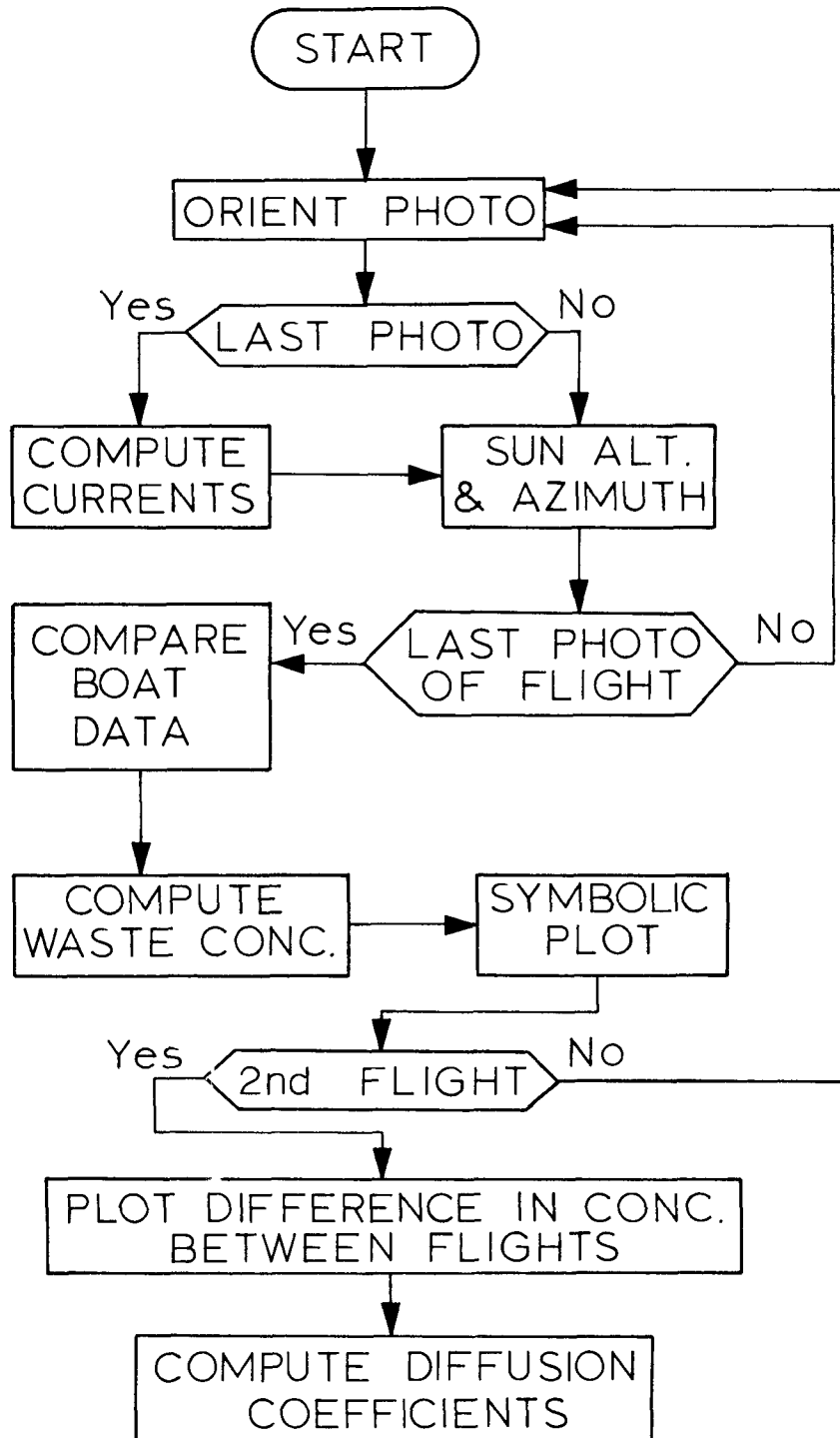


Figure 27. Flow diagram for photographic processing.

where  $\epsilon$  is the error term,  $j_2$  is the angle between the ray to the camera and the vertical, and the A's are the regression coefficients. ATR is determined for each point from

$$\text{ATR} = \frac{(\text{TIM}) \cos^4(c)}{(\text{FNO})^2 \exp(D_b(x,y)/G)} \quad (77)$$

TIM is the photographic exposure time,  $c$  is the angle between the camera axis and the ray, FNO is the f-number setting on the camera,  $D_b(x,y)$  is the blue film density as measured with the densitometer and  $G$  is the film gamma. The film gamma for the three spectral bands of the color photo was determined from sensometric curves made by Kodak and GAF for the film used on the project. The gamma to the base 10 was taken as -3.0 for the Ektachrome 8442 film and -2.4 for the anscochrome D200 film.

In the expression for the ratio ( $R_{\text{pho}}$ ), the values of the coefficients were determined from the following method in place of that given by equation 39

$$R_{\text{pho}} = B_0 + B_1 (\text{SUNR}) + B_2 (N_b) + \epsilon \quad (78)$$

The regression coefficients were determined by a least squares fit of data from selected points outside the waste field.  $N_b$  is the radiance in the blue band as determined from

$$N_b = \frac{\text{ATR} (\text{FNO})^2 \exp(D_b(x,y)/G)}{(\text{TIM}) \cos^4(c)} \quad (79)$$

SUNR is the angle between the ray to the camera and the reflected direct sunlight. For the model 78 the value of  $R_{\text{pho}}$  was determined from

$$R_{\text{pho}} = \exp[(D_r(x,y) - D_g(x,y))/G + (E_r - E_g)\sec(j_2) + (A_r - A_g)\sec(i)] \quad (80)$$

where  $D(x,y)$  is the film density,  $E$  is the atmospheric attenuation from the sea surface to the camera,  $j_2$  is the angle between the ray to the camera and the vertical axis,  $A$  is the atmospheric attenuation for a standard atmosphere and  $i$  is the angle of incidence for the direct sunlight. The subscripts  $r$  and  $g$  refer to the red and green bands, respectively. Atmospheric attenuation coefficients were determined from the Handbook of Geophysics and Space Environments for a standard atmosphere. The following coefficients and equations were used

$$A_r = 0.252$$

$$A_g = 0.331$$

$$E_r - E_g = 0.024 \ln (H + 1) \quad (81)$$

where H is the camera station altitude in kilometers. After the coefficients in model 78 were computed, the ratio anomaly (RA) for any point on the photograph, excluding kelp and shallow nearshore areas, was determined from

$$RA = R_{ph} - R_{pho} \quad (82)$$

where  $R_{pho}$  was estimated from the regression equation

$$R_{pho} = B_0 + B_1 (\text{SUNR}) + B_2 (N_b) \quad (83)$$

and  $R_{ph}$  was determined from

$$R_{ph} = \exp[ (D_r(x,y) - D_g(x,y)) / G + (E_r - E_g) \sec(j_2) + (A_r - A_g) \sec(i) ] \quad (84)$$

The ratio anomaly (RA) was computed for each data point on the aerial photo. The values were stored in a 120 by 60 array. The index on the array indicated the ground coordinates for each element of the array. Each element represented a 60-foot square area on the sea. After all the film density measurements were converted to RA values and stored in the array, missing values were interpolated from adjacent points.

Concentrations determined from the fluorometers aboard the boat were read into the computer program. Boat concentrations were interpolated at 60-foot intervals along the fluorometer track line. These values were matched by ground coordinates with the RA values in the array. A least square regression analysis was made on the data with the model

$$W = C_1 (RA) + C_2 (RA)^2 + \epsilon \quad (85)$$

where W is the waste concentration in milliliters per liter and  $C_1$  and  $C_2$  are regression coefficients.

The array was oriented so that the x-axis was along the center line of plume. Values of the waste concentration were computed from the above equation and stored in the array in place of the RA values. Waste concentrations were displayed as a symbolic plot on the line printer. In figure 28 are two plots from photographs taken August 16. The symbols on the plot represent different ranges in concentration and were selected so that the density of the plot increases with the concentration. The movement or change in shape of the waste field can be seen during the 22-minute period between the flights. The area of the waste field within each concentration range is determined by continuing the number of times each symbol is used to make the symbolic



Figure 28. Symbolic plots from two flights August 16, 1968.



Figure 29. Isoconcentration plot, flight on August 16, 1968.



plot.

The most visually useful form of displaying the photographic waste concentrations is the isoconcentration plot. This plot is similar to a topographic map with the elevation being replaced with the concentration. Figure 29 is a computer printout by this technique of the concentrations shown in the left plot of figure 28. The outfall is located at the top of the plot and the plume extends downward. The plume is 500 to 1000 ft wide and about 7000 ft long.

Steady state diffusion coefficients were determined for a steady state model with unidirectional transport velocity in the X direction. By neglecting the loss to the lower layers and assuming the diffusion in the Y direction was not a function of Y, the basic diffusion equation becomes

$$V_x \frac{\partial W}{\partial X} = D_y \frac{\partial^2 W}{\partial Y^2} \quad (86)$$

where X is the distance along the centerline of the plume, Y is the distance right or left of the plume center line,  $V_x$  is the velocity along the plume center line, W is the waste concentration, and  $D_y$  is the diffusion coefficient. A solution to equation is

$$W = \frac{K}{2(\pi D_y t)^{1/2}} \exp [-Y^2/rtD_y] \quad (87)$$

For computational purposes this equation can be reduced to

$$W = W_0 \exp [-Y^2/2\sigma_y^2] \quad (88)$$

where  $W_0$  is the concentration at the center line of the plume and  $\sigma_y^2$  is variance of normal curve. The diffusion coefficient is equal to one half the change in variance divided by the time interval or

$$D_y = \frac{1}{2} \frac{\Delta \sigma_y^2}{\Delta t} \quad (89)$$

In the computer program, the variance was computed every 300 feet along the center line of the plume. The change in time for this steady state model was equal to the distance between sections in feet divided by the velocity in feet per second. The velocity was determined photogrammetrically from the current floats or dye patches.

The variance ( $\sigma_y^2$ ) can be estimated for a normal distribution from the sample variance ( $S_y^2$ ). The concentration (W) is equivalent to the frequency of occurrence in the computations. The sample variance is

$$S_y^2 = \frac{\sum W(Y-\bar{Y})^2}{N} \quad (90)$$

where  $\bar{Y}$  is the mean distance from the origin and

$$N = \sum_{i=1}^n W_i \quad (91)$$

In computational form, equation 90 is

$$s_y^2 = \frac{1}{N} \left[ \sum_{i=1}^n W_i Y_i^2 - \frac{\left( \sum_{i=1}^n W_i Y_i \right)^2}{N} \right] \quad (92)$$

From equation 92 an estimate of the variance can be made for any section across the plume. Equation 89 was used to determine the diffusion coefficient.

Nonsteady-state diffusion coefficients were determined from two flights over the area using equation 89. In this equation for the non-steady state

$$\Delta \sigma_i^2 = \sigma_{1,i}^2 - \sigma_{2,i+c}^2 \quad (93)$$

where the subscripts 1 and 2 refer to the flight numbers, i refers to the section number across the plume in flight one and i+c is the section number in flight two adjusted for the movement of the waste field between flights. In solving equation 89 for the nonsteady-state case,  $\Delta t$  is the time difference between the flights.

The preliminary diffusion coefficients based on the steady state model are shown in table 1. The coefficients are determined from the change in variance along each flight at 300 ft intervals. Assuming a uniform concentration with depth, a vertical thickness of the waste field can be estimated. The columns listed in table 1 are 1) section number where each section represents 60 ft along the axis of the plume, 2) width of the waste field, 3) the estimated average depth of the waste field, 4) the estimate of the standard deviation of Y, 5) the maximum centerline concentration for a normal distribution, 6) and 7) the ground X and Y coordinates of the centerline of the plume, 8) the diffusion coefficient between each fifth section of the plume, and 9) the average diffusion coefficient from the head of the plume. Also shown in the tables are the flow rate, current velocity, sun azimuth from the south, sun altitude, and area within each concentration range.

Nonsteady-state diffusion coefficients are shown in table 2. The coefficients were determined from the change in variance between two photographic flights over the outfall area. Convection of the field was considered in making the comparison.

A detailed description of the computer program used to process the vertical color photography is given in Appendix B.

Table 1. Preliminary diffusion coefficients, flight 1, August 16, 1968.

Section	Width Ft	Eff. Depth Ft	Sigma Y Ft	Coefficient PPT	State Plane Coordinates X Y	Diffusion Coefficient Ft <sup>2</sup> /sec Fifth Sec. Average
13	660	3.0	1.541E 02	3.491E 01	1069872 376281	7.922E 00 7.992E 00
18	780	2.4	1.811E 02	3.695E 01	1070009 376549	6.352E 00 7.137E 00
23	1020	2.1	2.156E 02	3.515E 01	1070033 376863	9.565E 00 7.946E 00
28	1080	1.9	2.419E 02	3.458E 01	1070128 377148	8.441E 00 8.070E 00
33	1320	2.1	2.473E 02	3.007E 01	1070284 377409	1.827E 00 6.821E 00
38	840	2.9	1.685E 02	3.249E 01	1070516 377639	-2.292E 01 1.864E 00
43	840	3.7	1.602E 02	2.700E 01	1070662 377903	-1.900E 00 1.327E 00
48	840	3.5	1.696E 02	2.664E 01	1070703 378210	2.158E 00 1.431E 00
53	720	4.5	1.429E 02	2.459E 01	1070778 378503	-5.838E 00 6.230E-01
58	1200	4.0	2.338E 02	1.718E 01	1070783 378825	2.398E 01 2.959E 00
63	1140	3.5	2.604E 02	1.772E 01	1070808 379138	9.181E 00 3.524E 00
68	1020	3.4	2.394E 02	1.957E 01	1070886 379430	-7.349E 00 2.618E 00
73	1200	2.8	2.645E 02	2.142E 01	1071094 379670	8.883E 00 3.100E 00
78	1260	3.0	2.657E 02	1.979E 01	1071285 379916	4.818E-01 2.910E 00
83	960	5.7	2.194E 02	1.275E 01	1071227 380263	-1.573E 01 1.667E 00
88	660	7.3	1.314E 02	1.655E 01	1071232 380584	-2.159E 01 2.134E-01
93	720	6.6	1.389E 02	1.738E 01	1071337 380865	1.410E 00 2.838E-01
98	600	6.7	1.220E 02	1.960E 01	1071489 381127	-3.086E 00 9.654E-02
103	600	6.6	1.235E 02	1.955E 01	1071614 381400	2.587E-01 1.051E-01
108	780	5.8	1.453E 02	1.892E 01	1071700 381689	4.105E 00 3.051E-01
113	780	6.1	1.662E 02	1.582E 01	1071876 381942	4.554E 00 5.074E-01
Flow Rate 16.8 CFS						
Sun Az. from S. 1.013 Rad.						
Current Velocity .42 FPS						
Sun Altitude .790 Rad.						
Area Within Each Concentration Range						
Range ml/i						
Area Sq Ft						
0- 2						5.580E 05
2- 4						3.924E 04
4- 6						3.672E 05
6-10						9.468E 05
10-15						1.199E 06
15-20						1.188E 06
20-25						5.400E 05
GT25						6.948E 05

Table 2. Nonsteady-state diffusion coefficients, August 16, 1968.

Section No.	Width Feet	Diffusion Coefficients $\text{Ft}^2/\text{sec}$
13	660	10.1
18	780	4.8
23	1020	2.5
28	1080	1.9
33	1320	1.2
38	840	13.5
43	840	7.5
48	840	0.2
53	720	13.6
58	1200	38.0
63	1140	24.9
68	1020	12.6
73	1200	9.0
78	1260	8.9
83	960	9.0
88	660	10.3
93	720	11.6
98	600	16.6
103	600	13.2
108	780	7.6

#### 1969 Photographic Data

During the 1969 field season, the aerial photography was taken with two 70 mm Hasselblad cameras and a K-17 mapping camera. The large photos from the mapping camera were used for photographic orientation of the smaller cameras. Detailed analysis of the waste field was accomplished from the 70 mm photos.

The aerial film was digitized in the photogrammetry laboratory as shown in figure 30. The densitometer is located on the Kelsh plotter table. The film density is measured as voltage output from the densitometer with a digital voltmeter. The BCD digital voltmeter logic is transmitted through a logic converter to the Autotrol digital recorder. Output from the digitizer is recorded on computer cards by a card punch.

The densitometer and scanning table shown in figure 31 is processing a 70 mm picture. About all that can be seen of the densitometer is the white meter near the center of the figure. The scanning table is designed to handle film up to 9 1/2 inches wide and 250 feet long.

The film is loaded on the reel on the left of the scanning table and the take up reel is on the right. The arm that extends from the meter on the densitometer out over the scanning table contains the filters and the photomultiplier tube. A light source is located below the film. The amount of light that is transmitted through the film is measured by the photomultiplier tube and converted to D. C. voltage.

When digitizing aerial film, the scanning table continuously moves back and forth. The scan limits are marked on the photograph with a black tape or the dark border around the picture. The densitometer senses the end of the scan when its voltage output exceeds 750 volts. At the end of the scan, the scanning table stops and the film is advanced one scan by the take up reel on the table. The direction of the scan is reversed and the scanning table moves in the opposite direction.

The Y axis of the coordinatograph is attached to the scanning table. While scanning, the film density and Y photo coordinates are recorded at a selected interval along the scan. The X coordinate is computed from the scan number.

The operator shown in figure 29 is able to accomplish three processing steps at one time. While the densitometer is digitizing one photo, the operator is usually scanning the line printer listing of a previous photograph searching for illegal characters. At the same time, he can operate the teletype which preliminarily processes the data from another photograph with the computer using program EDIT. This program reduces the voltage output from the densitometer to film densities, rejects extreme values of densities, interpolates photo coordinates and displays the difference in film densities between adjacent bands on the line printer. Output from this program is stored on magnetic tape waiting final processing using program REMOTE. The basic details of this program are essentially the same as those for a single color photograph except that up to ten photographic bands or channels can be processed at one time. Program listings of EDIT and REMOTE are given in Appendix C.

#### 1970-71 Photographic Data

Field procedures and processing techniques were revised to include estimating diffusion coefficients from dye patch studies. Field work was conducted during the fall, winter, and spring. Boat sampling was not attempted due to rough sea conditions which generally prevail during this period. More specifically, the aims of this phase of the investigation were to develop a remote sensing tool for the evaluation of waste dispersion from proposed ocean outfalls and to develop a set of characteristic airphoto pattern elements for estimating diffusion coefficients.

Aerial film taken during this period was not digitized with the densitometer but photo coordinates were measured with the x-y coordinatograph about both the waste field and dye patch. The area of the waste field

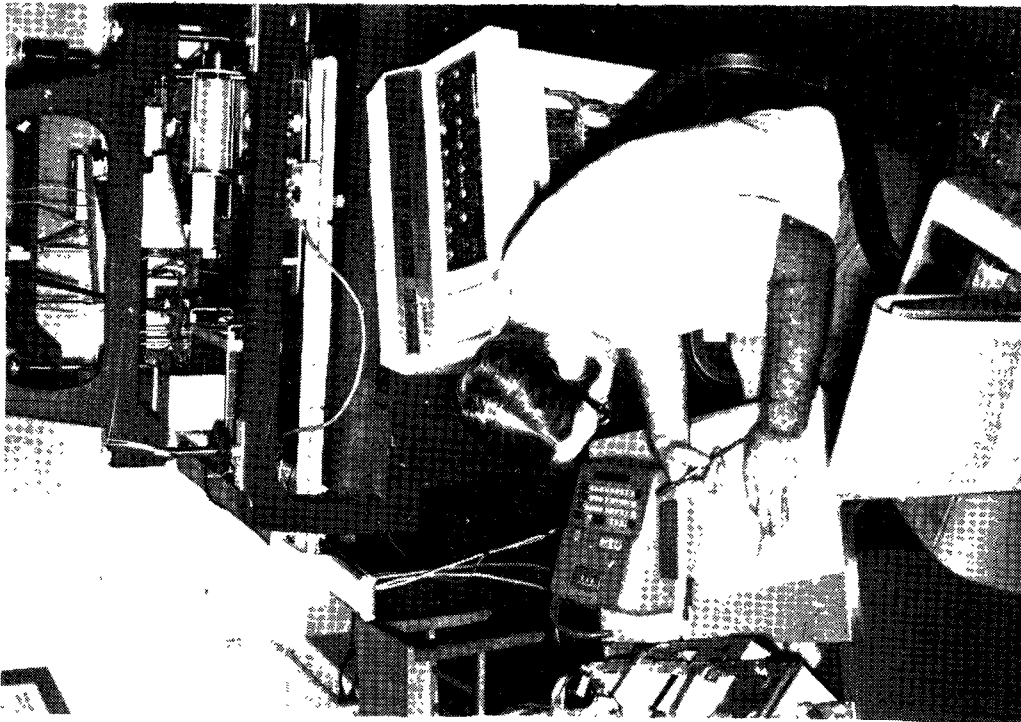


Figure 30. Digitizing aerial film.

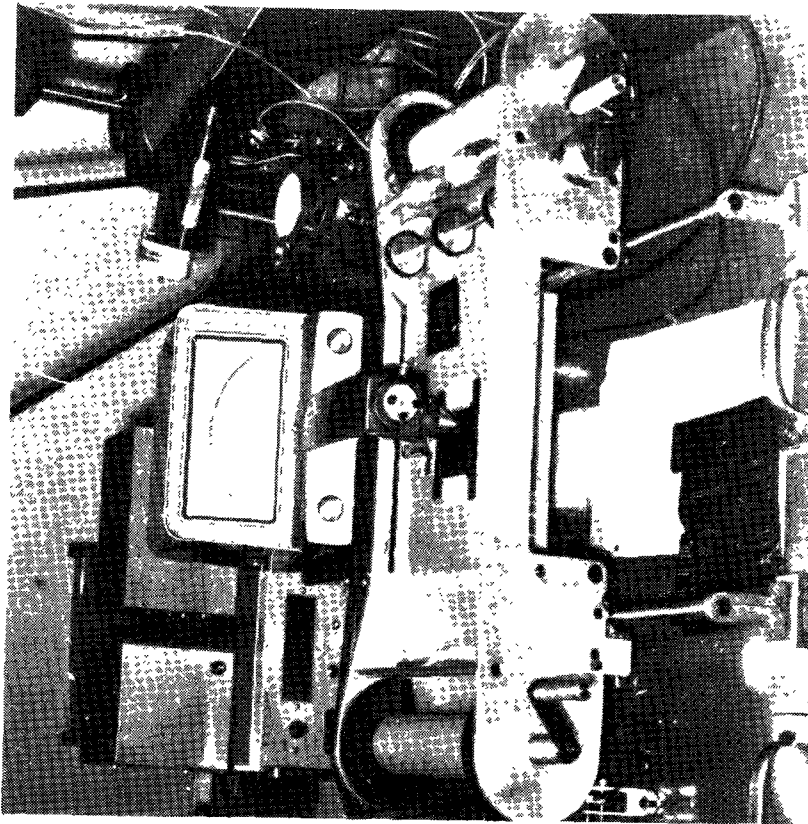


Figure 31. Scanning densitometer.

was computed from the photo coordinates about the plume. In addition, the water current velocity and direction and diffusion coefficients were determined from the dye patch photo coordinates.

The outline of the dye patch was digitized with the x and y coordinates along with sufficient ground control for photographic orientation. Photo coordinates about the dye patch were converted to state plane coordinates of the centroid and moments of inertia were computed from the following equations.

$$A = \frac{1}{2} \sum_{i=1}^n X_i (Y_{i-1} - Y_{i+1}) \quad (94)$$

$$\bar{X} = \frac{\sum \bar{X}_i \Delta A_i}{A} \quad (95)$$

$$\bar{Y} = \frac{\sum \bar{Y}_i \Delta A_i}{A} \quad (96)$$

$$I_x = \sum X_i^2 \Delta A_i \quad (97)$$

$$I_y = \sum Y_i^2 \Delta A_i \quad (98)$$

$$I_{xy} = \sum X_i Y_i \Delta A_i \quad (99)$$

Care must be taken when programming these equations to avoid roundoff error as state plane coordinates are typically six to seven digit numbers.

The rotation angle ( $\alpha$ ) of the axis to obtain the principal axis is given by

$$\tan (2\alpha) = \frac{2I_{xy}}{I_x - I_y} \quad (100)$$

The maximum and minimum moments of inertia about the principal axis are computed from

$$I_{\max} = \frac{I_x - I_y}{2} + \left[ \left( \frac{I_x - I_y}{2} \right)^2 + I_{xy}^2 \right]^{1/2} \quad (101)$$

$$I_{\min} = \frac{I_x - I_y}{2} - \left[ \left( \frac{I_x - I_y}{2} \right)^2 + I_{xy}^2 \right]^{1/2} \quad (102)$$

The irregular shaped dye patch is replaced with an ellipse that has the same horizontal area. In addition, the ratio of  $I_{\max}$  to  $I_{\min}$  are the same for the ellipse as for the dye patch. The principal moments of inertia for an ellipse are given by

$$I_{\max} = \frac{\pi b_e a_e^3}{4} \quad (103)$$

$$I_{\min} = \frac{\pi a_e b_e^3}{4} \quad (104)$$

where  $a_e$  and  $b_e$  are the major and minor semi axes of an equivalent ellipse. If the ratio (IR) of  $I_{\max}$  to  $I_{\min}$  remain the same for both the dye patch and the ellipse, the ratio of variances are also the same (equations 74 and 75).

$$IR = \frac{I_{\max}}{I_{\min}} = \frac{a_e^2}{b_e^2} = \frac{\sigma_x^2}{\sigma_y^2} \quad (105)$$

After computing the area (A) and the ratio of principal moments of inertia (IR) for the dye patch, the semi axes of the equivalent ellipse are determined from

$$a_e^2 = \frac{A}{\pi} (IR)^{-1/2} \quad (106)$$

$$b_e^2 = \frac{A}{\pi} (IR)^{1/2} \quad (107)$$

Equations 74 and 75 are utilized in determining the variances. Diffusion coefficients are determined from the change in variance between two photographic flights as given by equation 69.

Details of the computer program used for this phase of the study are given in Appendix D. In addition to the dye patch analysis, the program prepares the input coordinates for a plotting program. The outline of the waste field, current velocity vector, along with a state plane coordinate grid and displayed on a CRT plotter and a polaroid picture is taken of the face of the tube for a record of the results.



## SECTION X

### SAMPLING RESULTS

#### 1968-1969 Data

Detailed descriptions of the 1968-1969 boat sampling and aerial photography acquisition and processing were given by Burgess and James (August 1970). A summary of the results is given in table 3. Field work was conducted in late June, July, August and early September. Fourteen sampling runs were made during this period. For eight of the fourteen sampling runs, the waste field from the ocean outfall was at the sea surface. A submerged plume occurred during the remaining six sampling runs.

When the plume was submerged, both the swell height and the wind velocity were significantly less at a 90 percent confidence level than when the plume formed at the surface. On July 7 and 8, 1969, the sea and weather conditions were very nearly the same, yet on July 7, the plume submerged and on July 8 the plume was at the surface.

On both days the wind was from the north and a foam streak extended southward from the outfall for approximately 1.3 miles. The infrared black and white photo in figure 32 shows the foam streak on July 7, 1969. The photo was taken in a northwest direction with the shore in the foreground and the foam extending southward from the outfall.

The aerial photograph of the plume on July 8, 1969 in figure 33 was taken from 4000 ft with the camera tilted 45 degrees from vertical toward the east. The shore is off the upper edge of the photo and the foam streak extends south from the outfall. The direction from the outfall that the foam travels is not necessarily the same as that of the waste plume and in this case the plume is to the right of the foam.

Temperature profiles taken upstream of the outfall for July 7 and 8 are shown in figure 34. On the first day when the plume was submerged, the temperature profile did not show a definite thermocline but the temperature decreased with depth at a decreasing rate. On the second day a thermocline existed at about four feet below the surface. The wind on the 7th increased from 5 mph at 8:00 to 12 mph at 20:00. On July 8th the wind was stronger and increased from 6 mph at 8:00 to 15 mph at 15:00.

Both steady state and nonsteady state diffusion coefficients were computed when possible for each sampling run. Of the eight days that a surface plume occurred, a one dimensional diffusion model was applicable to the plume pattern on only three days. A two dimensional model was necessary to describe the plume when the current velocity was low. When the velocity was greater than 0.4 ft/sec, a one dimensional diffusion model was adequate.

Table 3. 1968-1969 sampling summary for Newport.

Date	Tide <sup>a</sup>		Wave		Wind		Effluent		PLUME					Remarks
	Range Ft.	Height Ft.	Dir.	Velocity mph	Flow Rate gpm	Area <sup>b</sup> Acres	Length Ft.	Max. Concen. ml/L	Current Vel. ft/sec	Dif. Coef. ft <sup>2</sup> /sec				
8-8-68	10.2	4	NE	10-20	5,550	100	4600	15	0.26	c				
8-10-68	-----	-----	-----	-----	-----	-----	-----	-----	-----	-----			Foggy	
8-14-68	6.0	4-6	SW	5-10	7,600	-----	3400	21	-----	c			No photography	
8-15-68	-----	-----	-----	-----	-----	-----	-----	-----	-----	-----			Foggy	
8-16-68	6.3	6-8	SW	10-15	7,550	142	7000	23	0.42	11.				
8-21-68	8.1	8-10	SW	0-5	7,400	-----	7500	20	-----	c				
8-22-68	-----	-----	-----	-----	-----	-----	-----	-----	-----	-----			Raining	
9-10-68	6.8	1-2	-----	0	7,450	0	-----	-----	0.0	-----			Plume submerged	
9-11-68	6.8	1-2	E	0-5	8,950	0	-----	-----	-----	-----			Plume submerged	
9-12-68 <sup>e</sup>	6.5	1-2	E	0-5	6,750	0	-----	-----	0.0	-----			Plume submerged	
9-12-68 <sup>f</sup>	6.5	4-6	NW	15-20	6,750	-----	3000	10	-----	-----			d	
6-30-69	11.5	1-2	N	5-10	8,100	0	-----	-----	-----	-----			Plume submerged	
7-1-69	11.3	2-4	NW	4-5	8,100	0	-----	-----	0.06	-----			Plume submerged	
7-7-69	6.4	4-6	N	5-12	9,000	5	-----	-----	0.4	-----			Plume submerged	
7-8-69	7.7	4-6	N	6-15	9,000	93	5500	10	0.5	14.				
7-21-69	-----	-----	-----	-----	-----	-----	-----	-----	-----	-----			Foggy	
7-22-69	-----	-----	-----	-----	-----	-----	-----	-----	-----	-----			Foggy	
8-12-69	8.4	2-3	W	3-5	8,300	127	4000	10	0.1	c				
8-13-69	-----	-----	-----	-----	-----	-----	-----	-----	-----	-----			Foggy	
9-8-69	7.2	4	SW	5	8,400	39	2000	10	0.2	c				
9-9-69	-----	-----	-----	-----	-----	-----	-----	-----	-----	-----			Foggy	

<sup>a</sup> Maximum difference between adjacent high and low tides during the day.<sup>b</sup> Area within the plume with concentrations greater than 2 ml/L.<sup>c</sup> One dimension model was not applicable.<sup>d</sup> Vertical photography not processed because of sunlight reflection.<sup>e</sup> a.m.<sup>f</sup> p.m.



Figure 32. Infrared black and white photo on July 7, 1969.

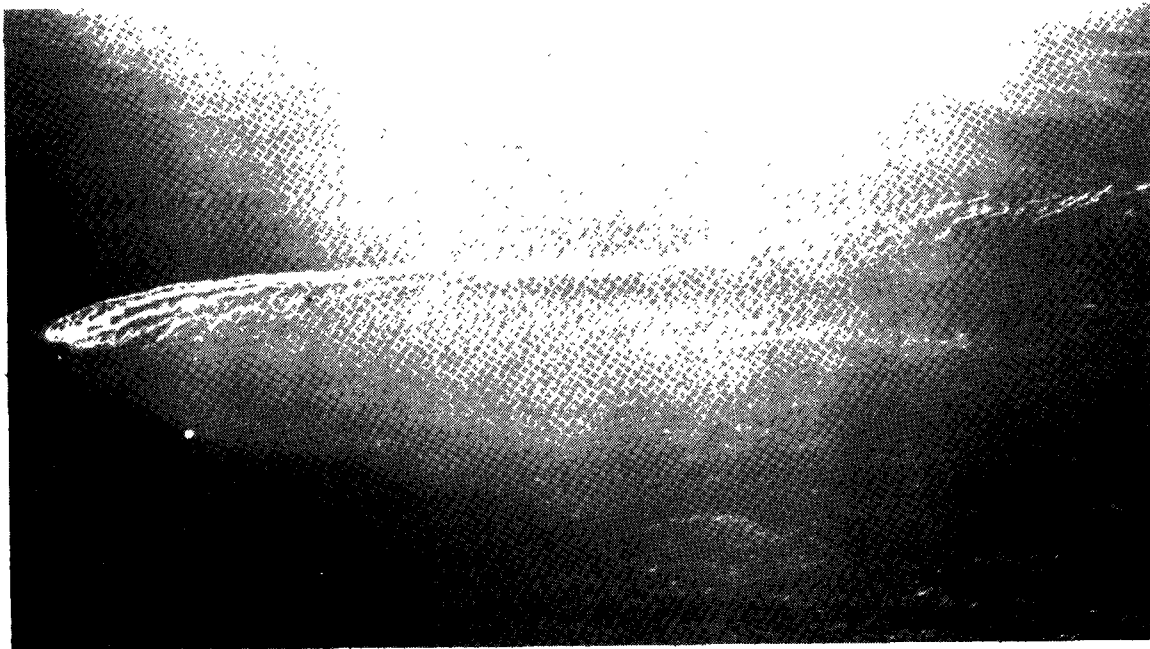


Figure 33. Plume on July 8, 1969 at 15:21 from 4000 feet.

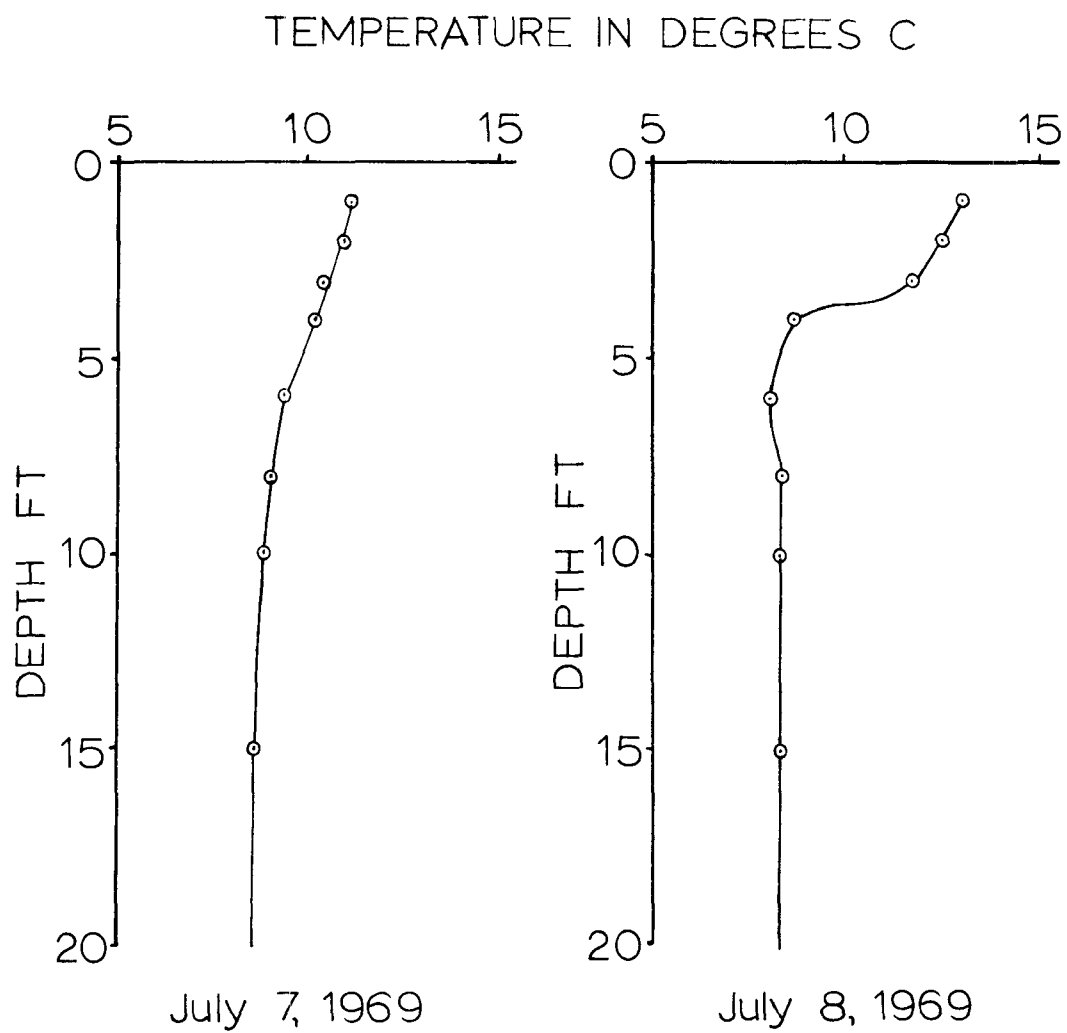


Figure 34. Temperature profiles July 7 and 8, 1969.

On August 16, 1968, the current velocity was 0.42 ft/sec and the waste field was long and narrow as the plume was generally about 600 ft wide; however, there were several locations along the plume that were up to 1200 ft wide. As a result of the nonuniform shape along the axis of the plume, the application of the steady state model to the data resulted in nearly half of the diffusion coefficients being negative. Diffusion coefficients determined from the change in concentrations between flights resulted in all positive values and the average nonsteady diffusion coefficient is listed in table 3 for August 16, 1968.

On July 8, 1969, the current velocity was 0.5 ft/sec and the steady state diffusion coefficient was listed. The nonsteady state model was not applicable. After the first flight, the width of the plume decreased due to horizontal density stratification. In figure 35 dark upwelled water can be seen below the plume. Measurements with the temperature probe indicated that this water was approximately two degrees C warmer than the inshore water. The upwelled water appears to have moved over the plume with limited mixing between masses.

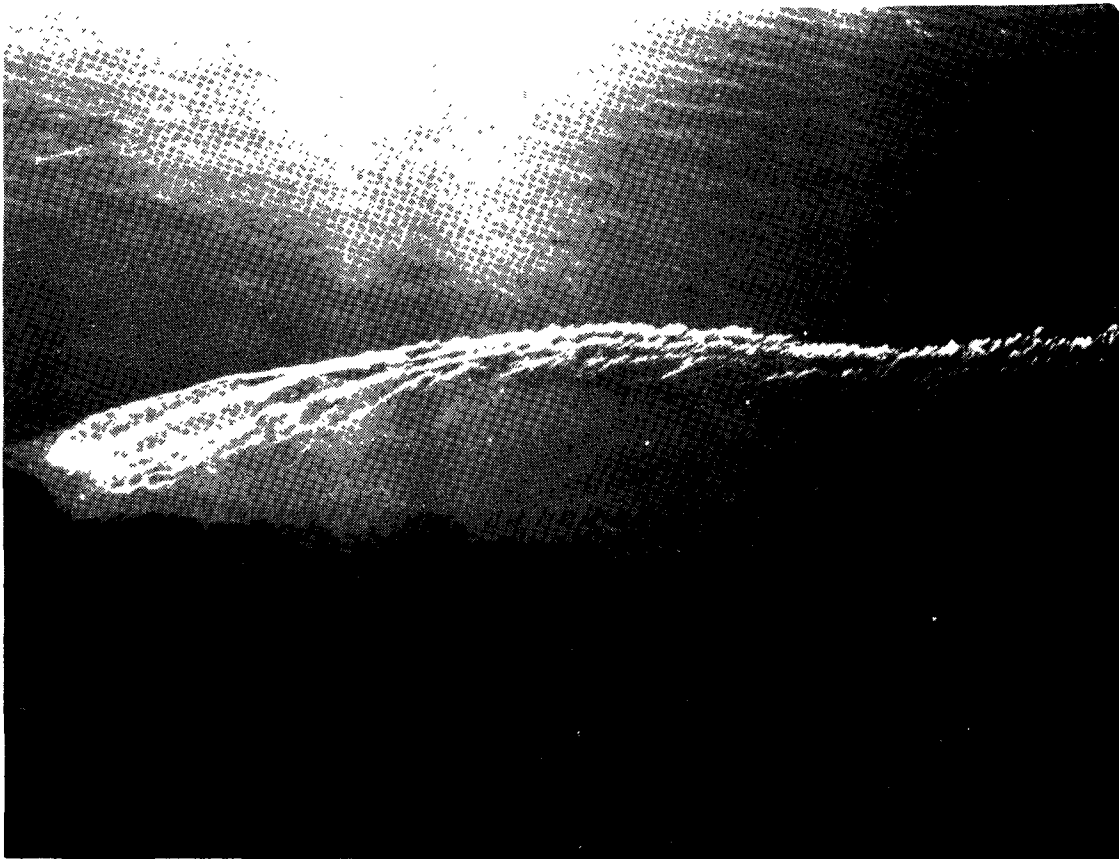


Figure 35. Plume July 8, 1969 at 15:56 from 4000 feet.

The plume was submerged on the morning of September 12, 1968. Weather and sea conditions were calm until 14:00 when a 15-20 mph wind began blowing. The waste field came to the surface and formed a long narrow plume which could have been described with a one dimensional diffusion model. The vertical aerial photography was taken with a six-inch focal length camera at 16:30. Interference caused by sunlight reflection on the choppy water surface made the photography impossible to process.

As listed in the original proposal, the first year of the study was divided into two phases:

- 1) Photographing the plume and current floats and
- 2) Photographing dye slugs introduced into the pipeline.

On August 22, 1968, one-gallon dye slugs were injected into the pipeline at 15-minute intervals using compressed air. It was raining on this day and no photography was taken. However, individual dye slugs were not observed from the boat. On September 10, 1968, the time interval was increased to one hour. Because of density stratification, the waste field and dye slugs were submerged. There was no wind on this day and the swell height was one to two ft. The dye slugs and waste field were visible on the aerial photography below the sea surface. The dye slugs did not move away from the outfall in discrete patches as planned, but accumulated about the outfall area. When the dye patches first appeared about the outfall they were doughnut shaped. Two-gallon dye slugs were introduced into the pipeline at one hour intervals on September 11, 1969; however, the aerial photography was cancelled due to cloudy skies. The plume was submerged but the individual boils over the outfall could be seen from the boat. Dye concentrations were detectable visually and with the fluorometers only directly over the outfall.

Had aerial photography been obtained of the dye patches under ideal conditions, it would have been difficult to process. Considering a nonsteady state dye patch within a nearly steady state waste field, the amount of dye, waste and sea water could occur in various combinations which would be impossible to distinguish by measuring the light return with the three broad bands of color photography. At a minimum, four individual narrow pass bands would have been required to obtain meaningful results. This phase of the study was replaced by dye slugs dropped from the airplane away from the waste field.

Summaries of the aerial photography for the 1968 and 1969 field seasons are shown in tables 4 and 5, respectively. The date, flight time, altitude, camera, and type of film are listed in the table.

As listed in the original proposal, water samples were collected during the first year of the study and tested for BOD, COD, PBI, dissolved oxygen and dye tracer concentration. The dissolved oxygen content of

Table 4. Summary of the 1968 vertical aerial photography.

Date	Photography			Boat-Photo <sup>a</sup>			Boat		
	Time PDT	Altitude (Ft.)	Camera	Film	MSE <sub>bp</sub>	d.f.	MSE <sub>b</sub>	d.f.	Sampling PDT
8-8-68	17:09	8250	8-1/4"	Ektachrome	---	---	12.	3	16:06- 18:09
	17:20	4125	Zeiss	8442	5.3	172	2.3	---	
	17:30	4125	RMKA	---	7.3	195	1.6	---	
	17:41	4125	---	---	7.3	142	1.6	---	
	17:50	8250	---	---	---	---	---	---	
8-16-68	15:51	8250	8-1/4"	Ektachrome	38.	178	2.4	4	14:25- 16:53
	16:00	4125	Zeiss	8442	31.	156	3.0	---	
	16:13	4125	RMKA	---	40	187	2.3	---	
	16:21	8250	---	---	---	---	---	---	
8-21-68	10:13	3500	3-1/2"	Anso	---	---	22.	5	12:10- 13:41
	10:21	1750	Wild	D200	---	---	---	---	
	10:36	1750	RC-9	---	---	---	---	---	
	10:44	3500	---	---	---	---	---	---	
9-10-68	10:10	5625	11-1/4"	Anso	---	---	---	---	10:30- 12:06
	10:25	11250	K-17	D200	---	---	---	---	
	10:35	5625	---	---	---	---	---	---	
9-10-68	15:56	5625	11-1/4"	Anso	---	---	---	---	16:15- 17:42
	16:11	11250	K-17	D200	---	---	---	---	
	16:21	5625	---	---	---	---	---	---	
9-12-68	10:12	5625	11-1/4"	Anso	---	---	---	---	9:25- 10:49
	10:30	11250	K-17	D200	---	---	---	---	
	10:43	5625	---	---	---	---	---	---	
9-12-68	16:31	3000	6"	Ektachrome	---	---	28.	6	15:49- 17:11
	16:46	6000	Zeiss	MS	---	---	---	---	
	16:54	3000	RMKA	Aerographic	---	---	---	---	

<sup>a</sup> Statistic from a comparison between boat data and photo results.

<sup>b</sup> Statistic from a comparison within boat data.

Table 5. Summary of the 1969 oblique aerial photography.

Date	Photography				Boat-Photo <sup>c</sup>		F		Boat	
	Time PDT	Altitude (ft.)	K-17 <sup>a</sup>	Film HB-1 <sup>b</sup>	HB-2 <sup>b</sup>	MSE <sub>bp</sub>	d.f.	MSE <sub>b</sub> MSE <sub>bp</sub>	MSE <sub>d</sub>	d.f. Sampling PDT
7-8-69	15:15	3000	8442	8401	5424	4.0	147	2.8	-----	-----
	15:21	4000	8442	8443	5424	2.9	130	3.7	11.1	5
	15:56	4000	8442	8443	5424	2.2	148	5.0	-----	-----
8-12-69	12:52	4000	5425	5424	8442	2.8	124	5.3	14.9	4
	13:01	6000	5425	5424	8442	3.5	193	4.3	-----	-----
9-8-69	11:21	3000	2402	5424	8443	7.3	110	-----	-----	-----
	11:38	6000	2402	5424	8443	4.8	181	-----	e	-----
	14:44	8000	2402	5424	8443	4.8	70	-----	-----	-----

- <sup>a</sup> Mapping camera with 6-inch focal length lens.  
<sup>b</sup> 70 mm Hasselblad camera with 150 mm focal length lens.  
<sup>c</sup> Statistic from a comparison between boat data and photo results.  
<sup>d</sup> Statistic from a comparison within boat data.  
<sup>e</sup> No cross lines for the boat sampling.



the water samples were consistently at or near saturation. However, the standard error in conducting the BOD, COD, and PBI tests were about the same magnitude as the test results and the chemical sampling phase of the study was discontinued after the first season.

Originally, nine surface floats with drogues attached at various depths were planned to be set in the receiving water prior to the aerial photography for determining the water currents. Because of the time required to set and retrieve the floats, only three floats were set after the first two sampling runs.

For each day that waste concentrations were computed from both the densitometer measurements taken on the aerial photography and the fluorometer records from the boat sampling, a comparison was made of the concentrations determined by the two methods by matching the ground coordinates. The mean square residuals for this comparison are listed under the column heading of Boat-Photo. Points for the comparison were selected at 60-ft along the boat's track. Only points inside the waste field were used in the comparison. On August 12, 1969, foam from the waste covered the water surface near the outfall and this area was deleted from the comparison.

Plots of the residuals for flight 1 on August 8, 1968, and flight 2 on August 16, 1968, are given in figure 36. In figure 37 are two plots of residuals for the second flights on July 8, 1969, and August 12, 1969. In general, maximum residuals occurred near median concentration values. Plots showing both the concentrations determined from the aerial photography and those measured by boat sampling are given in figures 39 through 41. The X axis of the plot represents distance along the boat's track when inside the waste field. The distance in feet would be equal to the position number times 60. The correlation coefficient between the two methods ranged from 0.85 to 0.95.

Continuous boat sampling of the waste field was conducted while the survey vessel was underway. Where the boat sampling lines crossed, concentrations were measured twice at one point within a relatively short period of time. Continuous boat sampling was generally conducted over a period of about one hour. A measure of the repeatability of the concentrations determined by boat sampling is given by the mean square residual for these observations as listed in tables 4 and 5 under the column heading -  $MSE_b$ .

The F statistic listed in the tables can be used to test for a significant difference in the residuals computed between the boat and photo data and within the boat data. Using a 95 percent confidence level, the F statistic would have to be greater than 2.5 to indicate that the residual within the boat data is significantly greater than the residual between the boat sampling and the photo values.

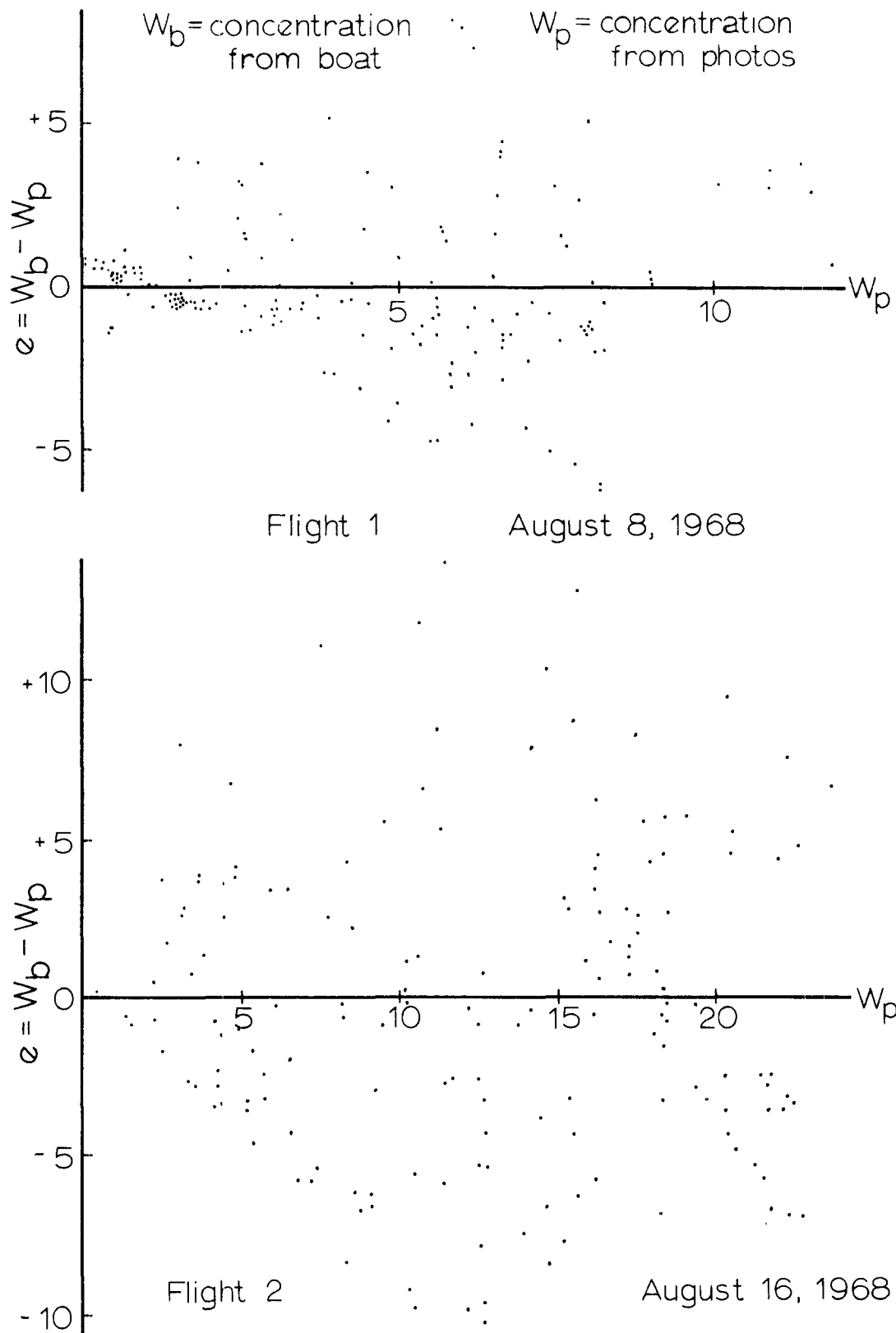


Figure 36. Plot of residuals - 1968

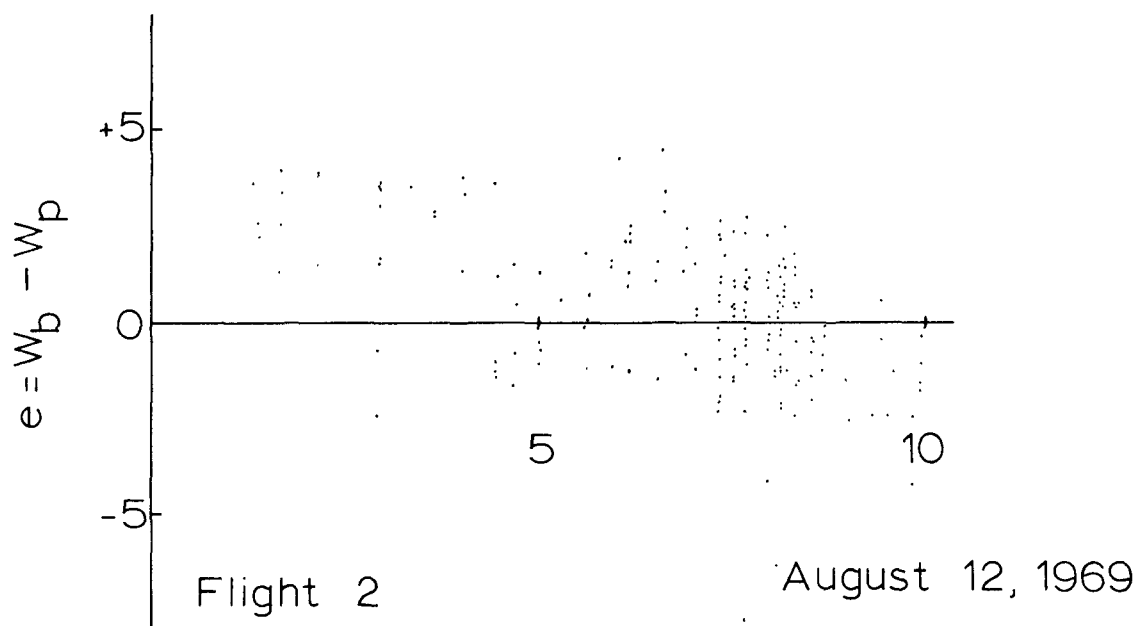
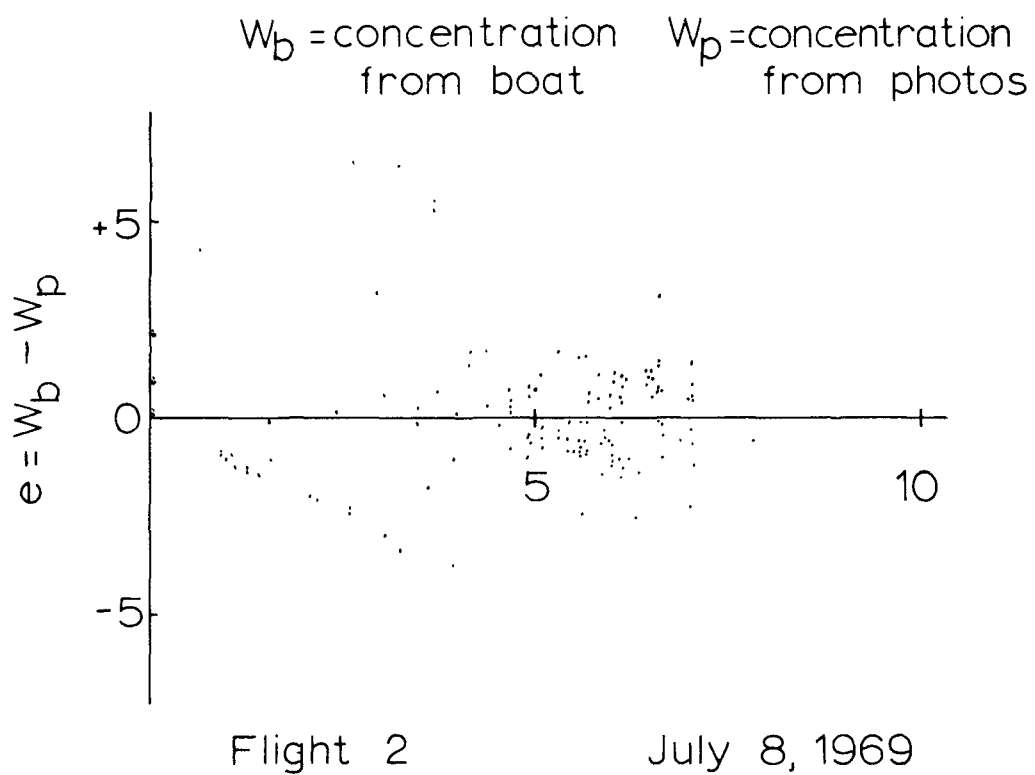


Figure 37. Plot of residuals - 1969

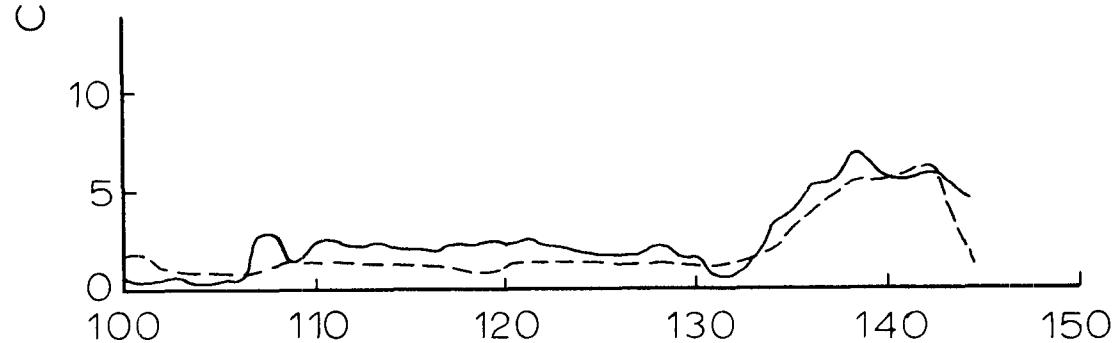
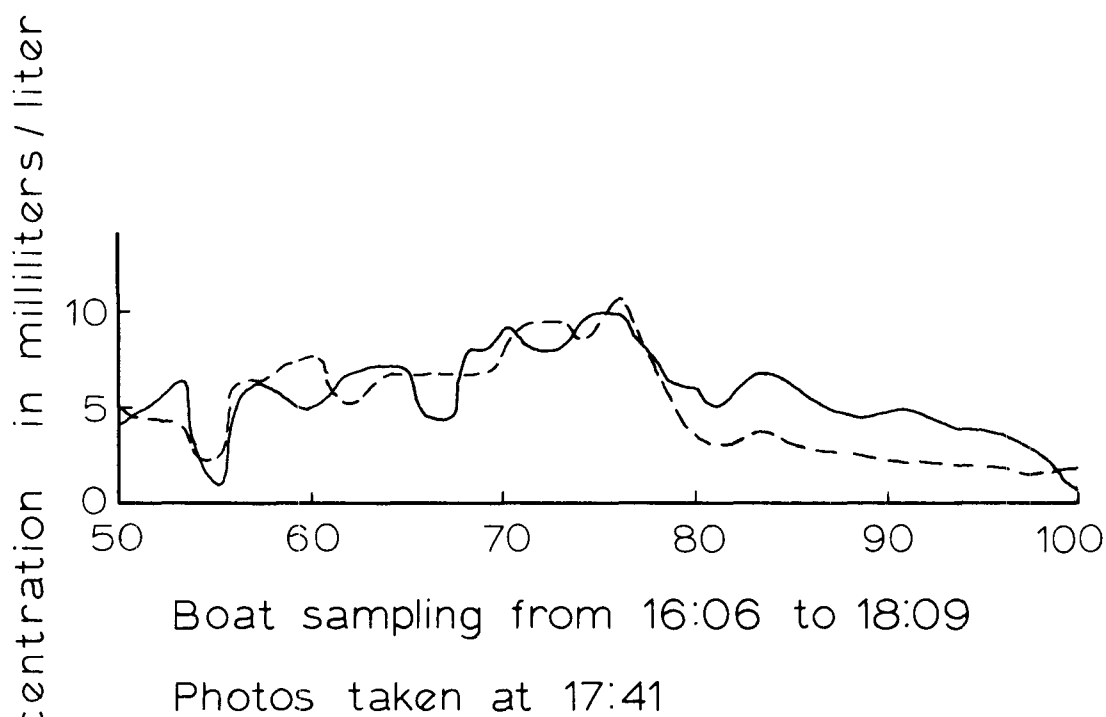
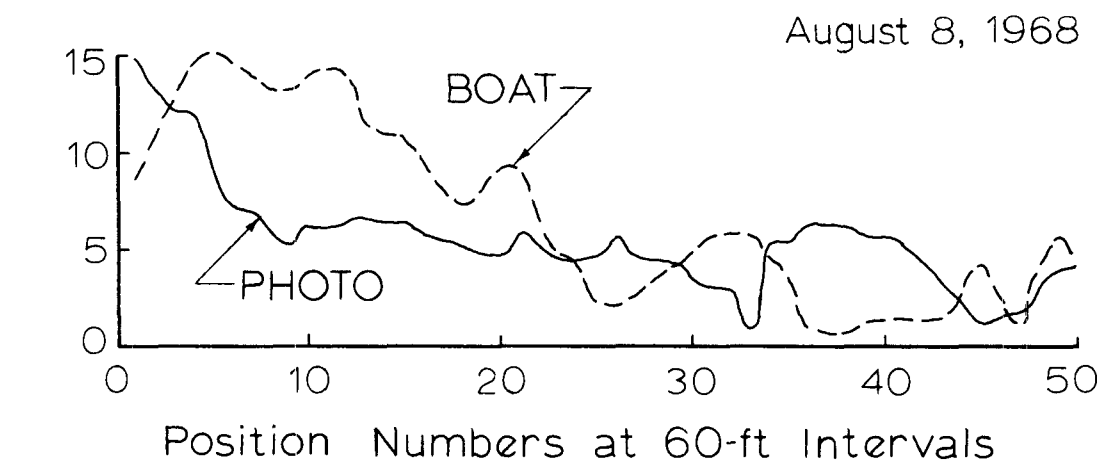


Figure 38. Comparison of boat and photo values on August 8, 1968.

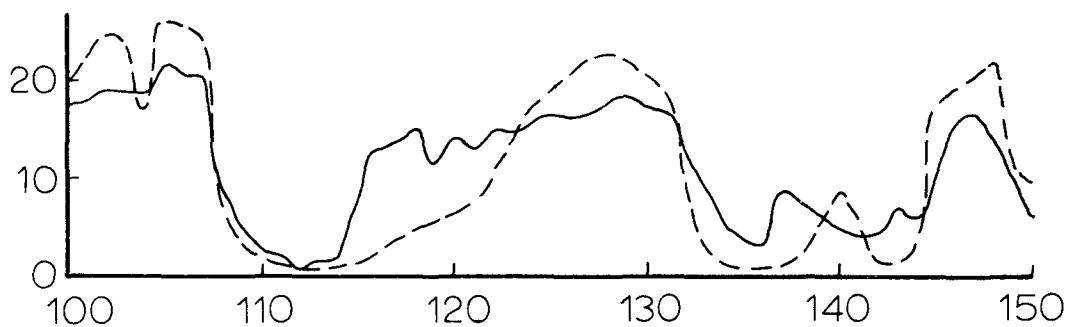
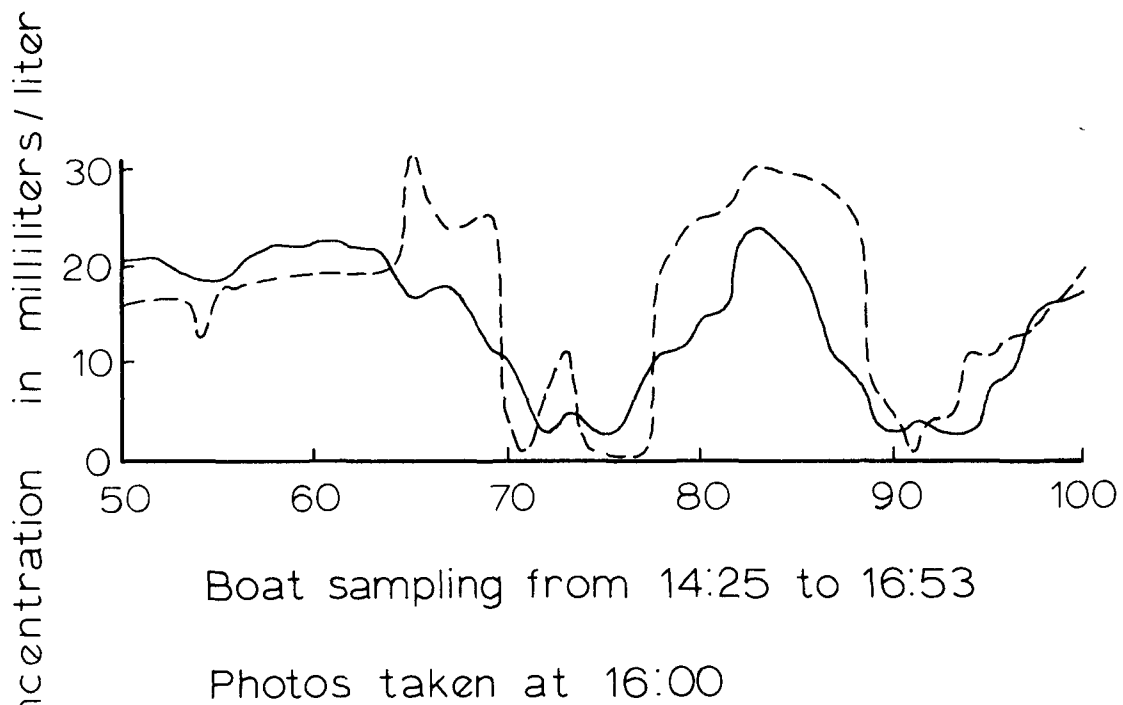
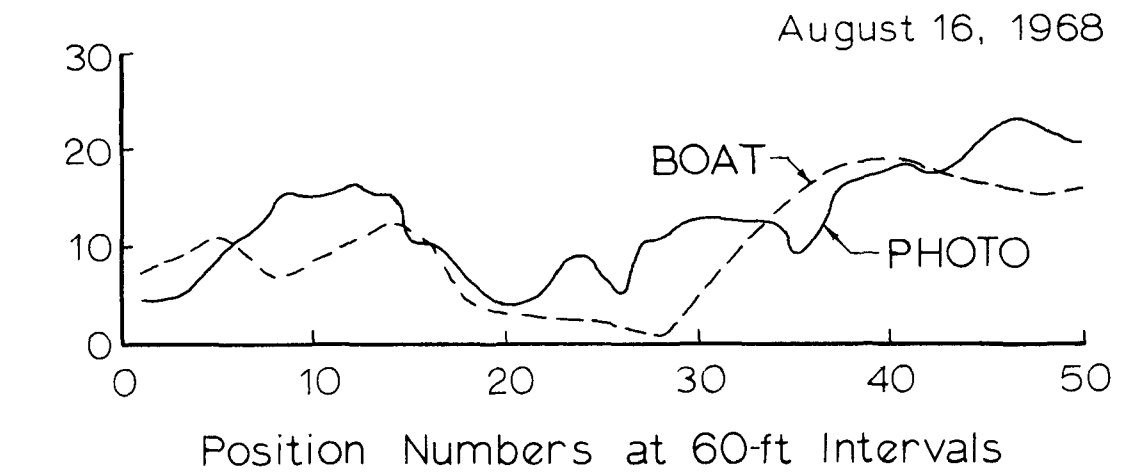


Figure 39. Comparison of boat and photo values on August 16, 1968.

July 8, 1969

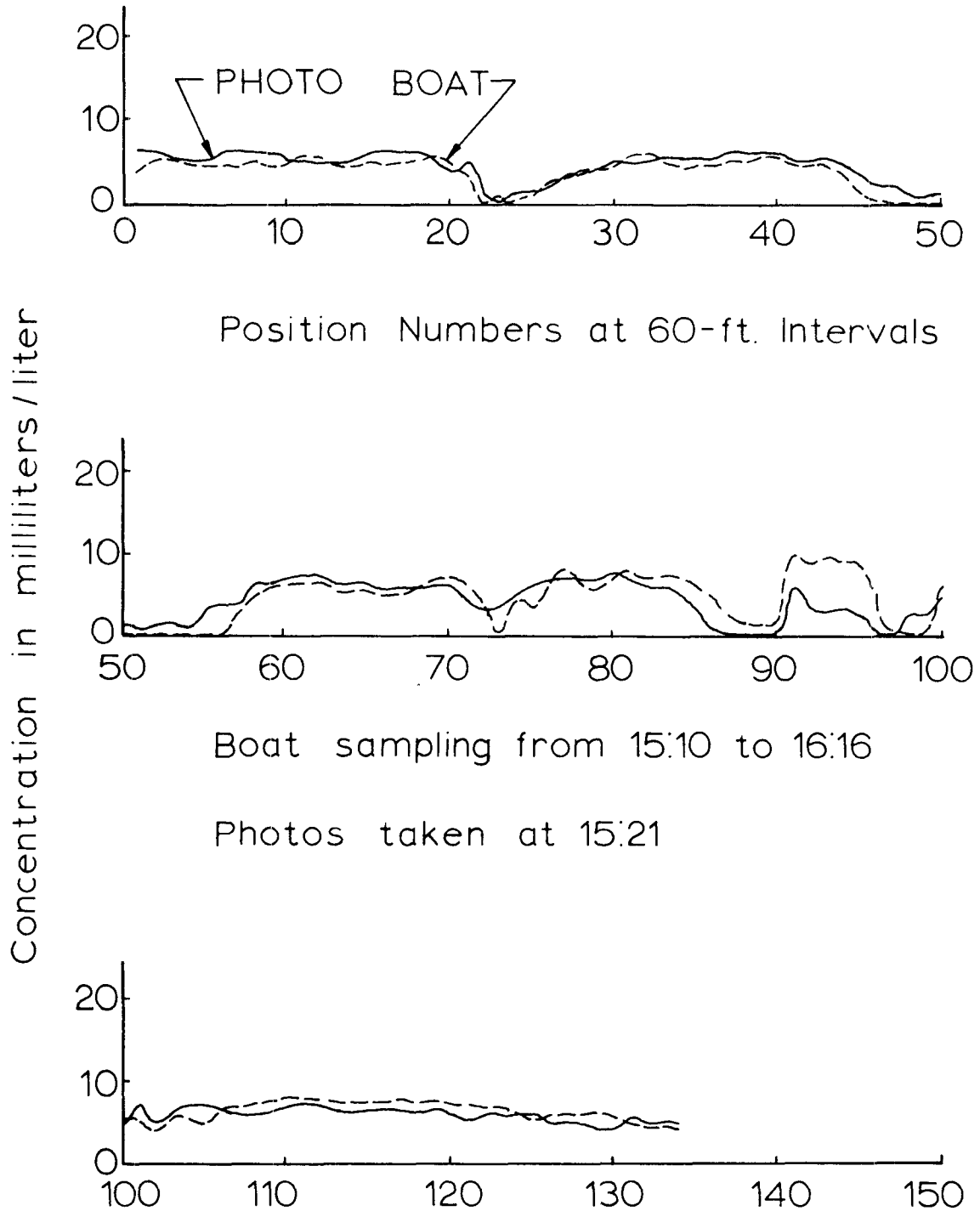


Figure 40. Comparison of boat and photo values July 8, 1969.

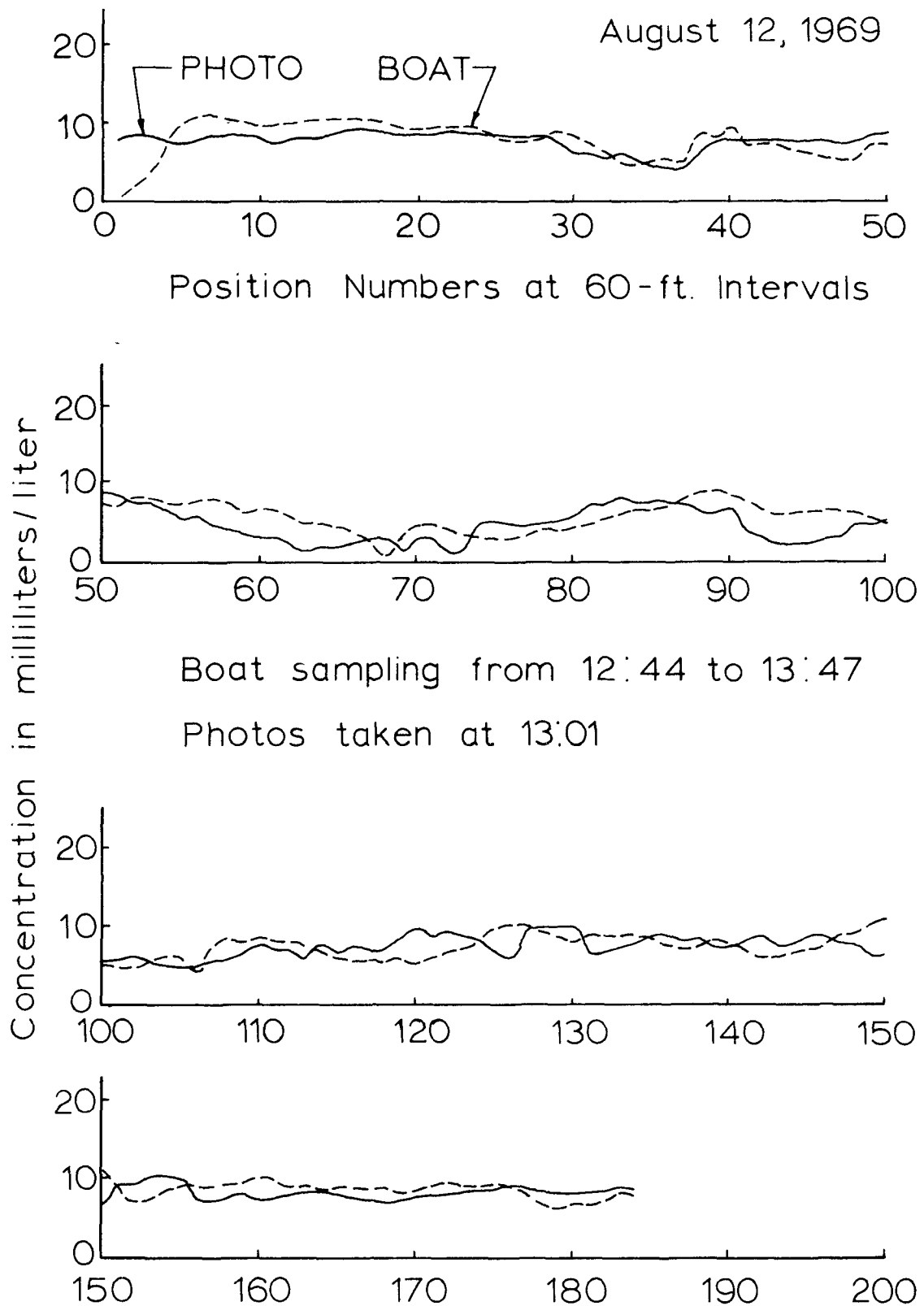


Figure 41. Comparison of boat and photo values August 12, 1969.

### 1970-1971 Data

The data acquired during the 1970-1971 field season are summarized on the following pages. The results of each sampling run are tabulated on two pages. On the left page is a contact print of the outfall area taken with the K-17 mapping camera using panchromatic, type 2402 film with a 25A wratten filter. The oblique photographs were taken with the axis of the camera oriented approximately 50 degrees from the vertical. The general orientation of the photographs can be visualized from the shoreline which extends almost due north and south along this section of the coast. A chart of the outfall area is shown in figure 42.

Depending upon the characteristics of the effluent, the location of the waste field is not always evident in these photographs. If the light scattering of the waste in the red band is high, the plume can be distinguished from the bluish-green background of sea water. However, when the seas are rough suspended sands and silts in the sea water can make the identification of the plume difficult in the red band. When the waste appears black instead of brown, the greatest contrast between the plume and the sea occurs around 500 nm. In this band the light return from the sea water is high while the light scattered in the plume is low.

The plot shown on the right page for a sampling run was made by photographing the CRT of the Tektronix T-4002 graphs display terminal. A state plane coordinate grid is drawn and labeled at 1000-ft intervals. The outline of the waste field is shown on the plot as a solid line. Foam from the effluent is indicated with x's on the plot. The area of the plume is computed in acres and displayed at the top of the plot.

When possible, the water current velocity is computed from the dye patch and the vector drawn on the plot at a scale of 1.0 ft/sec to 1000 ft. The position of the centroid of the dye patch during the first flight over the outfall area is shown on the plot at the tail of the velocity vector. The apparent position of the boil over the outfall is also shown on the plot as a triangle. The position of the outfall as determined from the 1968-1969 data and shown in figure is 1069400E, 375800N.

The wind velocity and direction were listed at the two-hour interval below the tekplot photo for the day of the observation and the previous day. Wind data were obtained from the continuously recording anemometer located on the south jetty. If this station was not in operation or for some other reason the data were not usable, manually recorded weather from the Newport station was plotted at 3 hr intervals. According to the Weather Bureau, the wind velocity at this station is less than that which would be recorded at the south jetty but the wind directions agree closely.

Tidal information is given on the data sheet below the wind vector



plot. Pacific Standard Time of day was used for both the wind and tide plots during the period October 25 through April 25. The tidal information was obtained from the Coast and Geodetic Survey tide tables.

Factors which influence the size of wind waves include the wind velocity, wind duration and the fetch. For a given outfall location, the fetch will vary with the direction of the wind. The effect of wind velocity on the condition of the sea is shown in figure 93. The photos show the condition of a developed sea for wind velocities of 15, 20, 25, 30, 40 and 50 kts, respectively. Energy from the wind is transferred to sea as transport velocity energy and turbulent energy. Descriptions of the sea for various wind scales are listed in table 6.

A summary of the 1970-71 data is given in table 7. Effluent discharge rates were not available for December 21 and 23, 1970. During the sampling period the current velocity ranged from 0.1 to 1.4 ft/sec while the area of the waste field ranged from 7 to 464 acres. The diffusion coefficients listed in the table were determined from the dye patch studies. The predicted tide stage at the time of the aerial photography is listed in column eight. In the last column of table 7 is the sea state which was estimated from the aerial photography with the aid of both the descriptions listed in table 6 and the photos of the sea state in figure 93. Detailed descriptions of the observations by dates follows.

The plume on September 9 was one of the largest observed with an area of 275 acres from an effluent discharge rate of 5850 gpm. A current velocity of 0.3 ft/sec was measured near the outfall. The tide was at 4 ft at the time the photo was taken and rising with a maximum of 7.5 ft reached 4 hours later. It can be seen in figure 43 that some foam is visible forming a striated pattern extending southeasterly toward the jetty. The current vector is shown in a southwesterly direction to the north in the afternoon. The waste plume extended northeast from the outfall at the time of the photography. The photo has a mottled tone with scattered whitecaps throughout the area. No definite linear pattern is present due to the wave crests aligned perpendicular to the wind. The diffusion coefficient parallel to the current vector was 12.9 ft<sup>2</sup>/sec and 0.4 ft<sup>2</sup>/sec perpendicular to the current.

On September 23, the plume was small with foam streaks originating from the boil over the outfall as shown in figure 45. The foam runs southward due to the prevailing northerly winds while the plume extends northward. The winds on the previous day were 20 kts from the southwest. The area of the waste field was 28 acres and the diffusion coefficients were 3.2 ft<sup>2</sup>/sec and 0.1 ft<sup>2</sup>/sec in the x and y directions, respectively. The current velocity was small (0.1 ft/sec), while the tide was 4 ft and rising with a maximum of 6.5 ft 4 hours later. The dye patch can be seen in figure 45 approximately 2000 ft southwest of the outfall. A light haze covers the nearshore area.

A very distinct plume pattern was observed on September 30. The width of the plume increases at a decreasing rate downstream from the outfall. The current velocity was 0.7 ft/sec which is higher than average. The area of the plume was 128 acres with an effluent discharge rate of 6950 gpm. Diffusion coefficients were  $7.5 \text{ ft}^2/\text{sec}$  and  $0.1 \text{ ft}^2/\text{sec}$  in the x and y directions. Although the wind was approximately 10 kts from the north only a small amount of foam was present. The tide was at 4 ft and decreasing with the minimum being reached 3 hours after the photos were taken. The photo in figure 47 shows the plume as a light area with two thin foam streaks parallel to the shore extending to the right. A few whitecaps can be seen in the photo. The sea has a finely mottled pattern with a definite linear trend normal to the shore due to the wind waves.

On October 7, the plume was one of the smallest observed despite the fact that the effluent flow rate was 7450 gpm. The plume is difficult to see in figure 49 but two small foam streaks can be seen extending southeast from the outfall. The area of the waste field was only 9 acres. At the time of the photo, the stage of the tide was 6.5 ft and rising. The peak was reached about an hour and a half after the flight. The dye patch can be seen in the lower right of figure 49.

A lake-like plume pattern with an area of 89 acres was observed on October 12. The waste discharge rate was 7650 gpm and the sea was choppy. The wind was from the north at 10-15 kts. The current velocity was not measured since only one flight was made over the outfall area. The tide was at 2.5 ft and decreasing, reaching a low of 0.5 ft two hours after the flight. The plume is visible in figure 51 as a lighter patch in the center of the picture just above the dye patch. The swell breaking on the reef can be seen in the lower right of figure 51. The sea has a mottled pattern with a number of whitecaps visible. There is a slight linear trend to the mottled pattern caused by the wind generated waves in the E-W direction.

On December 21, the plume was small and extended offshore from the outfall. Wind from the southwest at 40 kts generated large swell prior to the photography. Breakers can be seen all along the reef in figure 53. The tide stage was at low water. The winds changed and were 10-15 kts from the east for 24 hours before the current velocity was measured at 2.0 ft/sec to the west. The sea has a mottled pattern with a few whitecaps. The swell can be seen peaking throughout the area between the shore and the reef. The Coast Guard recorded a swell of ten ft at the mouth of the Yaquina River. Diffusion coefficients of  $7.3 \text{ ft}^2/\text{sec}$  and  $1.9 \text{ ft}^2/\text{sec}$  were measured for the x and y directions respectively.

The waste field on December 23 tended to lake about the outfall with an area of 26 acres. A current velocity of 1.1 ft/sec was measured inshore from the outfall. Diffusion coefficients were  $5.1 \text{ ft}^2/\text{sec}$  in the x direction and  $0.7 \text{ ft}^2/\text{sec}$  in the y direction. The sea was calm with

a slight northeasterly breeze. The tide was at 4 ft and falling to one ft 3-1/2 hours later. A long streak of foam extended from the outfall area to the northwest and can be seen in figure 55.

As can be seen in figure 57, the sea was extremely rough on December 31. Although the effluent discharge rate was 8700 gpm, the plume was not visible. While the wind was relatively calm, the swell height was eight feet from the Coast Guard records. The waves were breaking from the outer reef to the beach. A current velocity of 1.4 ft/sec was measured as were diffusion coefficients of 6.9 ft<sup>2</sup>/sec and 0.6 ft<sup>2</sup>/sec in the x and y directions. The plot from the Tektronix scope shows only the current vector extending from the position of the dye patch. The tide was at 7.5 ft and reached a maximum of 8 ft about one hour after the flight was taken.

A lake-like waste field was observed on January 2 with an area of 36 acres. The effluent flow rate was 6950 gpm. Diffusion coefficients were 1.7 ft<sup>2</sup>/sec and 0.5 ft<sup>2</sup>/sec in the x and y directions. The area near and to the north of the outfall is covered with foam as can be seen in figure 59. The lighter water near shore was caused by the turbulence from the large swell suspending the sand. Wind waves oriented NE-SW can be seen in the upper left. The tide was at 3 ft at the time the photo was taken and reached a peak of 7 ft approximately 3 hours later.

During the morning of the 6th of February, the plume was observed heading toward the north with an area of 193 acres. The current velocity near the outfall was 0.3 ft/sec. The effluent flow rate was 6450 gpm and diffusion coefficients in the area were 3.6 ft<sup>2</sup>/sec and 0.1 ft<sup>2</sup>/sec in the x and y directions. The wind had been from the east but was beginning to shift towards the northeast at the time of the photography. The tide stage was 0.5 ft and falling, reaching a minimum of 0.0 ft four hours later. The photo in figure 61 shows foam originating at the boil over the outfall and trailing off toward the northwest. The plume is the lighter area north of the outfall. A few whitecaps are present in the nearshore area but the sea surface when viewed from about 30 degrees from the vertical appears uniform in tone.

In the afternoon of the 6th of February, the plume had shifted approximately 180 degrees from the direction observed in the morning and was headed toward the south. The area of the waste field remained approximately the same as in the morning. The winds had shifted from easterly to northwesterly, and the long foam streak formed a U-shaped pattern, open to the northeast as can be seen in figure 63. The sea was relatively calm, and the tide was at 1.5 ft and nearly reached the minimum of 0.0 ft at 16:00.

The plume on March 16 was small, measuring 22 acres, and extended southward from the outfall. The sea was rough, as the photo in figure 65 shows, and the winds were approximately 20 knots out of the north.

The tide was at a stage of 4 ft and rising to a maximum of 6 ft three hours after the flight. The plume can be seen in figure 65 as the dark area near the lower center of the photo. Extensive whitecaps can be seen everywhere. The photo has a mottled pattern with turbid water near shore and in the shallow area between the outfall and the north jetty. The crests of the wind-generated waves show a linear pattern and the swell can be seen peaking outside the surf zone.

The plume on March 17 tended to lake about the outfall with a leg extending towards the southeast. As can be seen in figure 67, a foam streak extends southward from the outfall, apparently driven by the 15 kt wind from the north. The plume can be seen in figure 67 as the dark area surrounding the boil. Suspended silts and sands in the nearshore area give the water a lighter tone. The sea appears rough with numerous whitecaps in the area. There is a definite linear trend caused by the wind generated waves and the photo has a mottled pattern. A current velocity of 0.3 ft/sec toward the southeast was measured north of the outfall. The tide stage was 5 ft and about 1 hour before high tide.

The area of the plume observed on March 18 was 111 acres with a current velocity of 0.7 ft/sec driving the plume to the south. The effluent flow rate was 5950 gpm and diffusion coefficients of  $0.4 \text{ ft}^2/\text{sec}$  in the x and y directions were measured near the plume. The winds were shifting from northeasterly to northwesterly at the time the photo in figure 69 was taken and the tide was at low water. The lighter water near the shore is caused by sand being suspended by the turbulent action of the large waves. This turbulent action continues to suspend material to a depth of 35 ft near the north end of the reef. Waves are breaking on the reef near the outfall.

The lake-like plume in the morning of March 19 measured 73 acres and diffusion coefficients near the plume were determined to be  $1.2 \text{ ft}^2/\text{sec}$  in the x direction and  $0.4 \text{ ft}^2/\text{sec}$  in the y direction. The current velocity was 0.3 ft/sec in a generally westward direction. The winds were shifting from the northeast to the northwest at the time the observations were made and the tide was at 1 ft. The light water near the shore in figure 71 is caused by sand suspended in the water. The plume extended both onshore and offshore from the outfall. The sea has a mottled pattern with a few whitecaps visible. Waves were breaking on the reef both north and south of the outfall. Swell crests can be seen in the upper left of the photo and near shore. The turbid water along the coast both north and south of Yaquina Head shows a confused circulation pattern.

In the afternoon of March 19, the plume had begun to spread to the south, apparently due to the shifting of the wind from easterly to northerly. The tide had passed the minimum and was at 1 ft and rising. The photo in figure 73 shows the plume as the dark area extending both offshore and onshore. The photo was taken from 6000 ft at 13:50 and,

when compared with figure 71, shows the change which occurred. The swell had decreased and the wind had increased from morning and a number of whitecaps can be seen. The refraction wave pattern in the lower right of the photo was caused by a sunken barge on the reef. Photos of the outfall area on both March 18th and 19th showed very turbid water along the coast. Neither the swell height nor wind velocities during these days were particularly large. A heavy rain storm began March 9 and ended March 15. Turbid fresh water runoff from this storm may have caused these conditions in the nearshore coastal waters.

The plume on March 24 was somewhat elongated, extended southwest and covered an area of 58 acres. The current velocity north of the outfall was 0.3 ft/sec and diffusion coefficients were 1.2 ft<sup>2</sup>/sec in the x direction and 0.0 in the y direction. The wind had been blowing 15-25 kts and generated rough seas as can be seen in figure 75. The waves were breaking on the reef just offshore from the outfall located near the lower center of figure 75. A few whitecaps can be seen near the outfall. The tide was at low water when the photography was taken.

The plume on April 12 was the smallest observed, measuring only 7 acres and extended toward the northwest from the outfall, driven by a current of 0.4 ft/sec. While the wind was 10-15 kts from the east, the sea was calm as the photo in figure 77 shows. The light spot in the center of the photo is the dye patch from which diffusion coefficients of 8.07 ft<sup>2</sup>/sec and 0.19 ft<sup>2</sup>/sec were measured. The tide was at 5.5 ft and falling.

The plume on April 15 extended towards the southwest while a foam streak can be seen looping back toward shore in figure 79. The area of the plume was 68 acres with an effluent flow rate of 7700 gpm. The tide is at 4.5 ft and flooding. The wind had been from the east but had changed to the northwest at the time of the observations. The light area in figure 79 extending from shore to the foam streak appears to be a tide rip. Numerous whitecaps are visible and the sea has a mottled tone. A breaker is visible on the reef offshore from the outfall.

The plume on April 21 was long and narrow and extended northward approximately 13,000 ft. The effluent discharge rate was 5850 gpm and the area of the plume was 166 acres. Some foam appears to be generated in the waste by the 10 kt wind with foam streaks extending northeast near the upper left of figure 81. An eddy or a tide rip appears northeast of the outfall and may be the cause of the curved plume pattern. The current velocity was 0.5 ft/sec near the outfall while the x and y diffusion coefficients were only 0.3 and 0.02 ft<sup>2</sup>/sec, respectively. The observations were made at low tide and the wind was from the southwest.

The largest plume observed during the 1970-71 season was 464 acres on

April 26. The current velocity was 0.3 ft/sec towards the north. The boil over the outfall can be seen near the lower right of figure 83. The plume is the light area extending upwards and to the left from the outfall. The effluent discharge rate was 5800 gpm and diffusion coefficients were 14.0 and 0.2 ft<sup>2</sup>/sec in the x and y directions, respectively. The elongated dye patch can be seen in the photo just south of the boil. The photo of the sea appears to have a slightly mottled pattern with a few whitecaps present. The wind velocity was only ten knots at the time of the photography. Coast Guard records indicate that the swell was 2-4 ft.

Only one photographic flight was taken over the outfall on May 7 before the area was covered with fog. The fog can be seen on the left in figure 85. The plume was narrow and extended northward from the outfall. A foam streak can be seen along the nearshore edge of the plume. The light spot near the head of the plume is the dye patch. The observation was made during a falling tide when the wind was from the southwest 10-15 kts and the effluent discharge rate was 6350 gpm.

On May 10th, the plume covered an area of 71 acres. The head of the plume formed a sharp point as can be seen near the left of figure 87. The plume extends to the right or south. The current velocity of 0.7 ft/sec was measured near the tail of the plume. Diffusion coefficients from the dye patch in the x and y directions were 2.8 and 0.1 ft<sup>2</sup>/sec, respectively. A few whitecaps are present near the outfall.

The long plume observed on May 13 extended nearly 9000 ft in a northeasterly direction and covered an area of 197 acres. The flow rate was 6050 gpm on this day. The plume can be seen in figure 89 as a light area with the head of the plume near the right. The photo was taken from 6000 ft at 14:10 and the tide at this time was 4.5 ft and rising toward a peak of 5.5 at 16:00. Numerous whitecaps can be seen in the sea with a finely mottled photo pattern.

The plume on May 14 extended from the outfall toward the west for approximately 2000 ft and then headed southward for a distance of 3500 ft. The area covered by the plume was 112 acres, and the velocity was 0.3 ft/sec in a southwestward direction. The flow rate of the effluent was 5800 gpm and diffusion coefficients were computed to be 2.4 ft<sup>2</sup>/sec in the x direction and 0.1 ft<sup>2</sup>/sec in the y direction. The photo in figure 91 was taken from 4000 ft at 14:48 and shows the plume as a large spot with light tone in the darker surrounding water. The tide at this time was at a stage of 5 ft and rising.

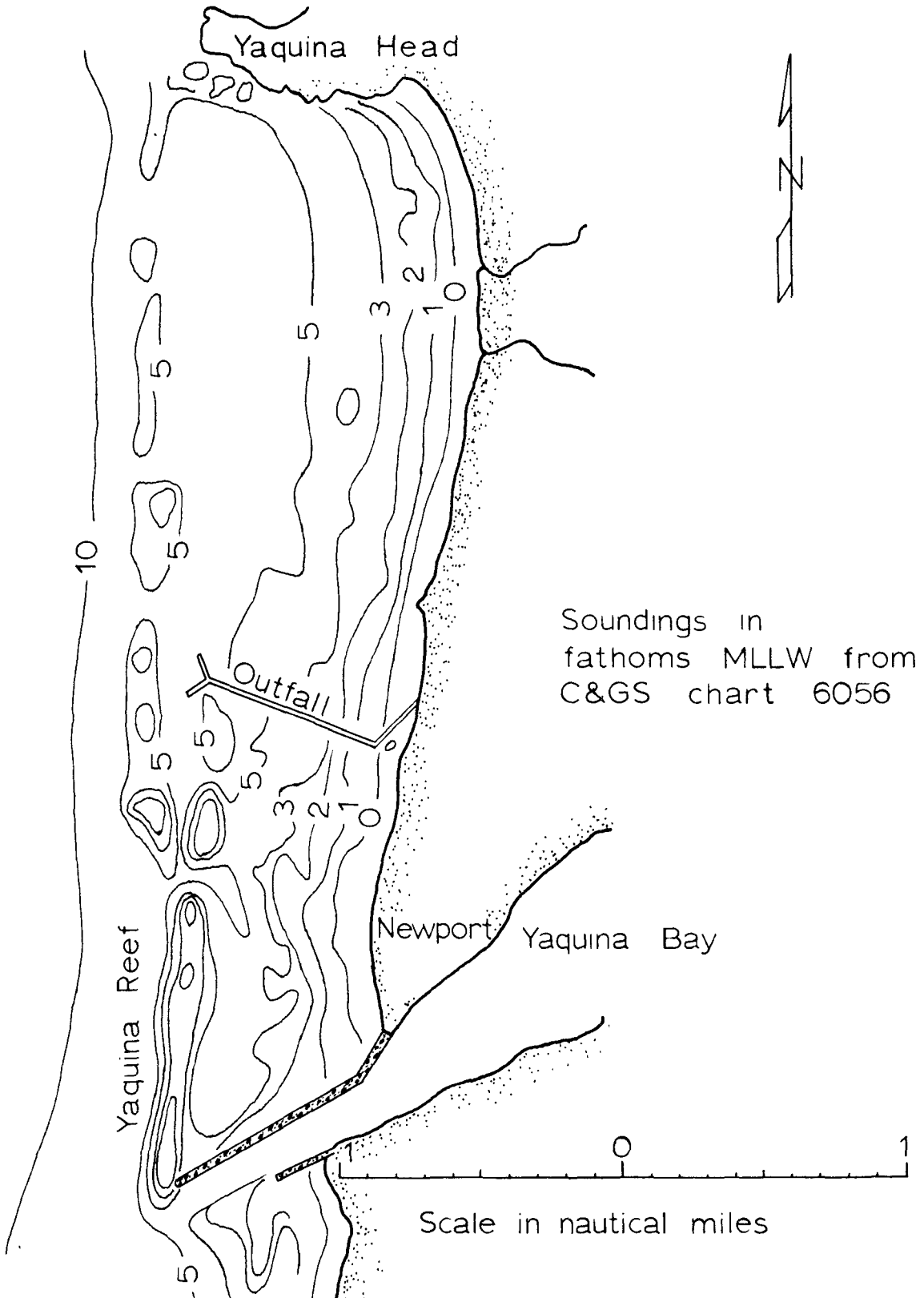


Figure 42. Chart of the outfall area at Newport, Oregon.



Figure 43. Aerial photo of outfall area on September 9, 1970 from 800 feet at 14:30.



Flow = 5850 gpm

$V_x = 0.3$  fps

Area = 275 Ac

$Dx = 12.9$  ft<sup>2</sup>/sec

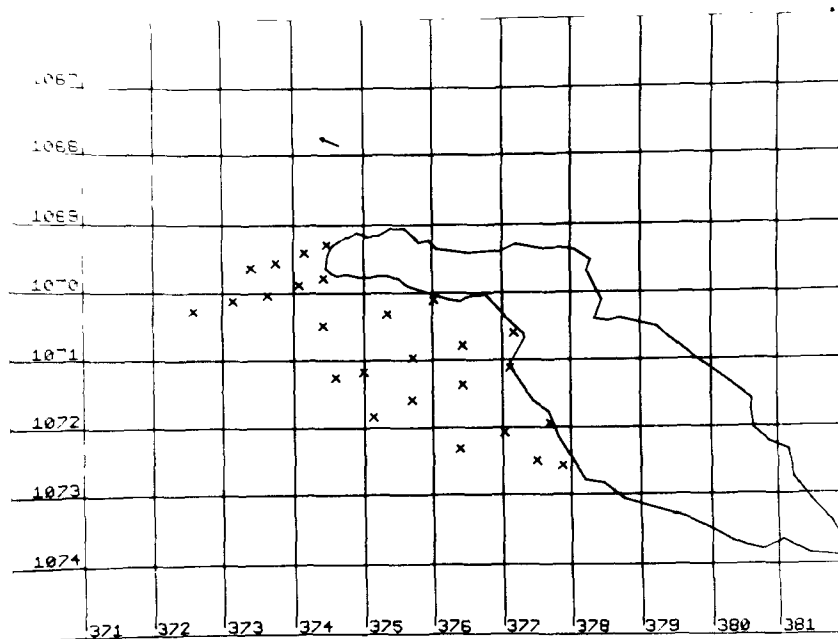
$Dy = 0.4$  ft<sup>2</sup>/sec

→ current vector

x foam

Δ outfall

1000-ft grid



TEK PLOT

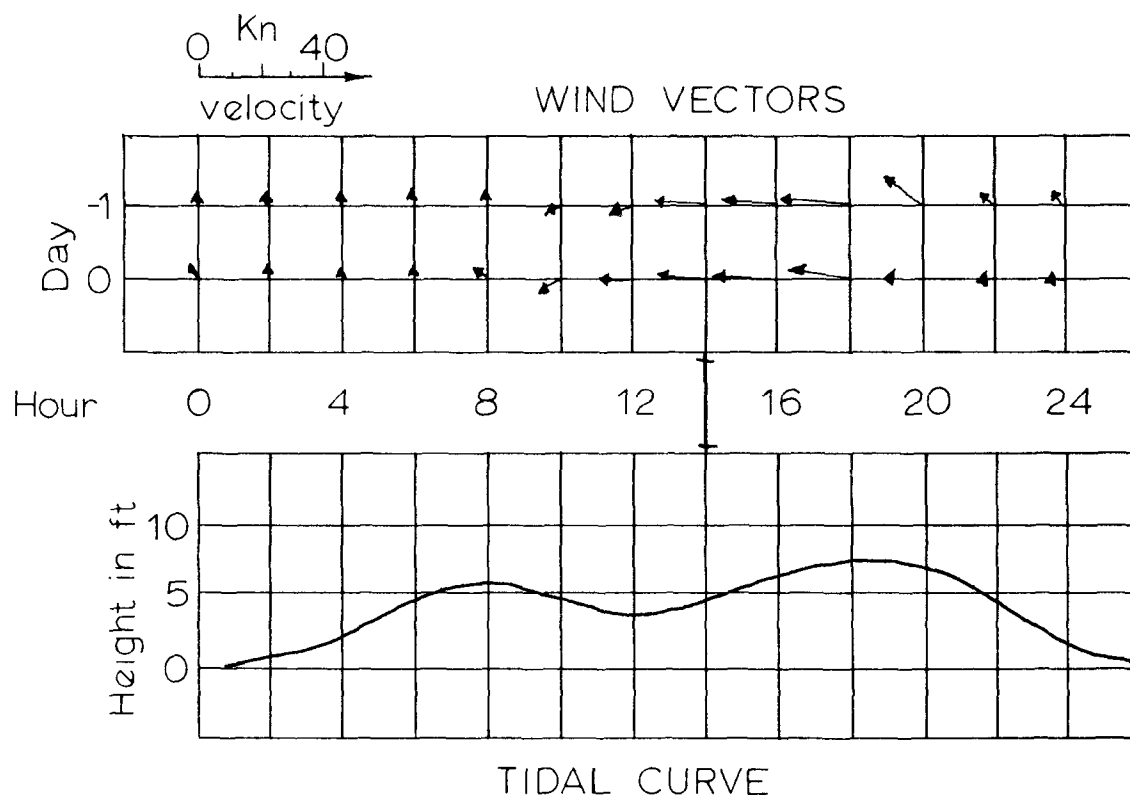


Figure 44. Data for September 9, 1970.



Figure 45. Aerial photo of outfall area on September 23, 1970 from 8000 feet at 15:30.

Flow = 5900 gpm

$V_x = 0.1$  fps

Area = 28 Ac

$D_x = 3.2$  ft<sup>2</sup>/sec

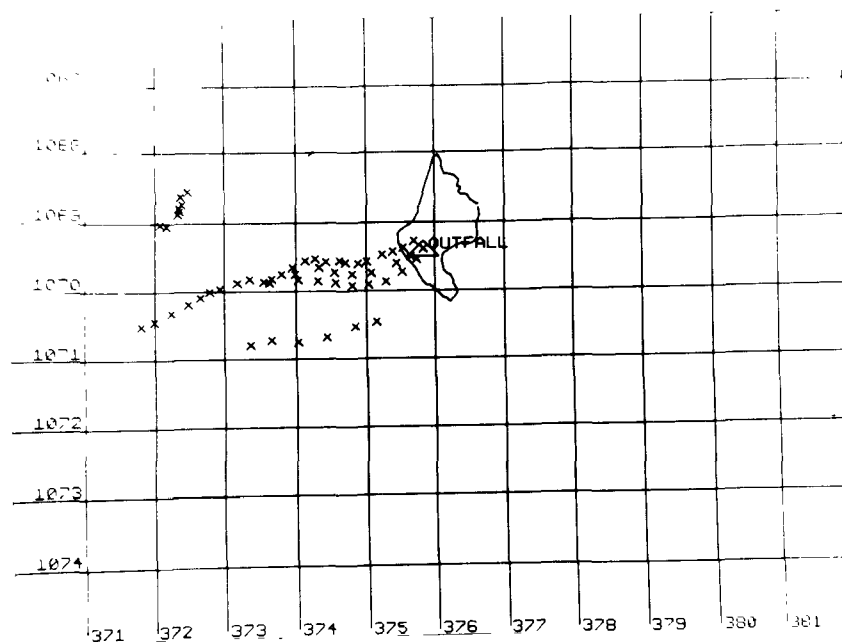
$D_y = 0.1$  ft<sup>2</sup>/sec

→ current vector

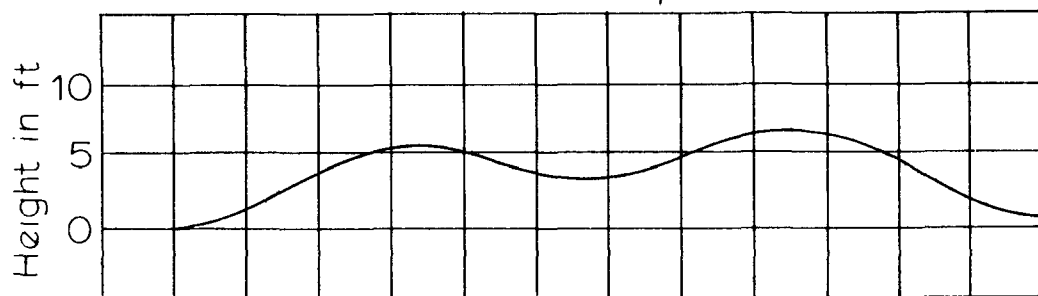
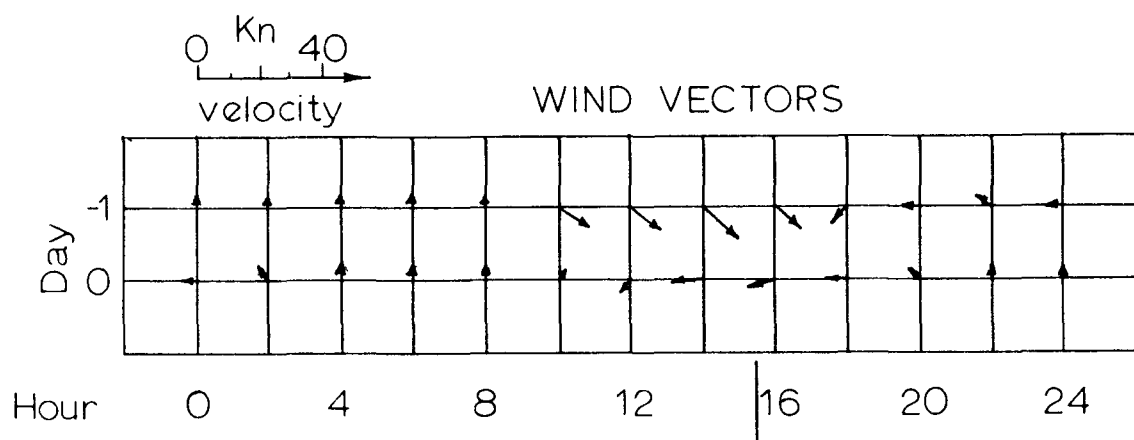
x foam

Δ outfall

1000-ft grid



TEK PLOT



TIDAL CURVE

Figure 46. Data for September 23, 1970.



Figure 47. Aerial photo of outfall area on September 30, 1970 from 5000 feet at 14:54.

Flow = 6950 gpm

$V_x = 0.74$  fps

Area = 128 Ac

$D_x = 7.5$  ft<sup>2</sup>/sec

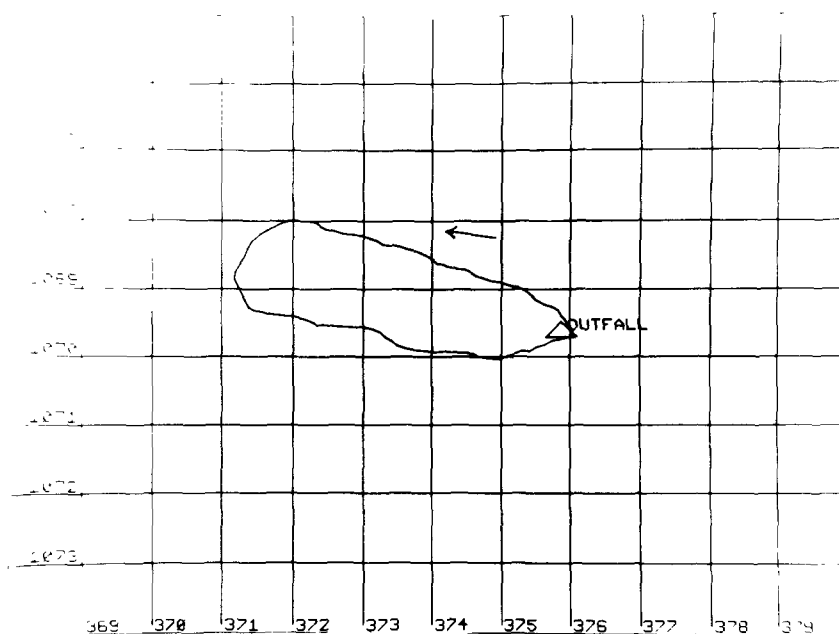
$D_y = 0.1$  ft<sup>2</sup>/sec

→ current vector

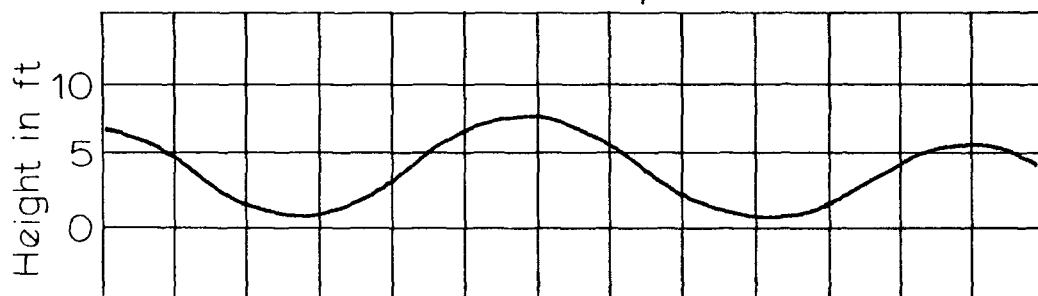
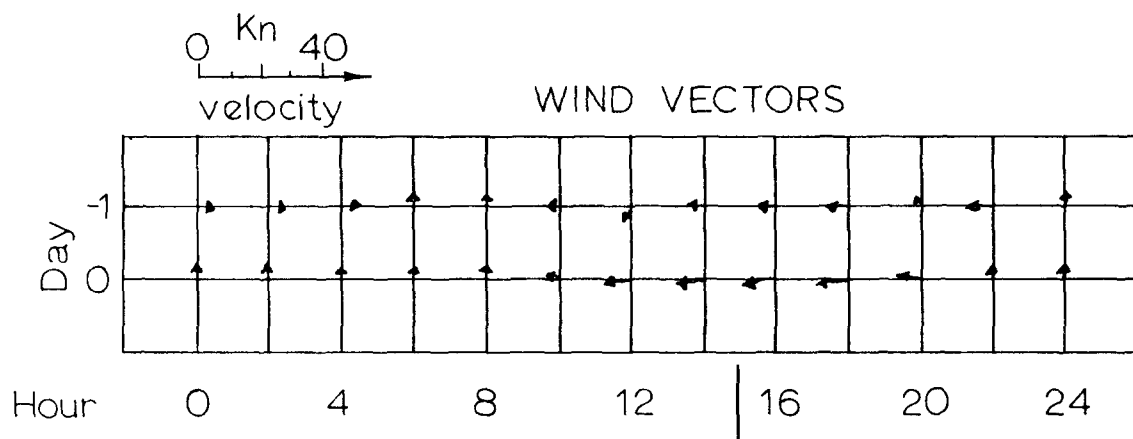
x foam

△ outfall

1000-ft grid



TEK PLOT



TIDAL CURVE

Figure 48. Data for September 30, 1970.

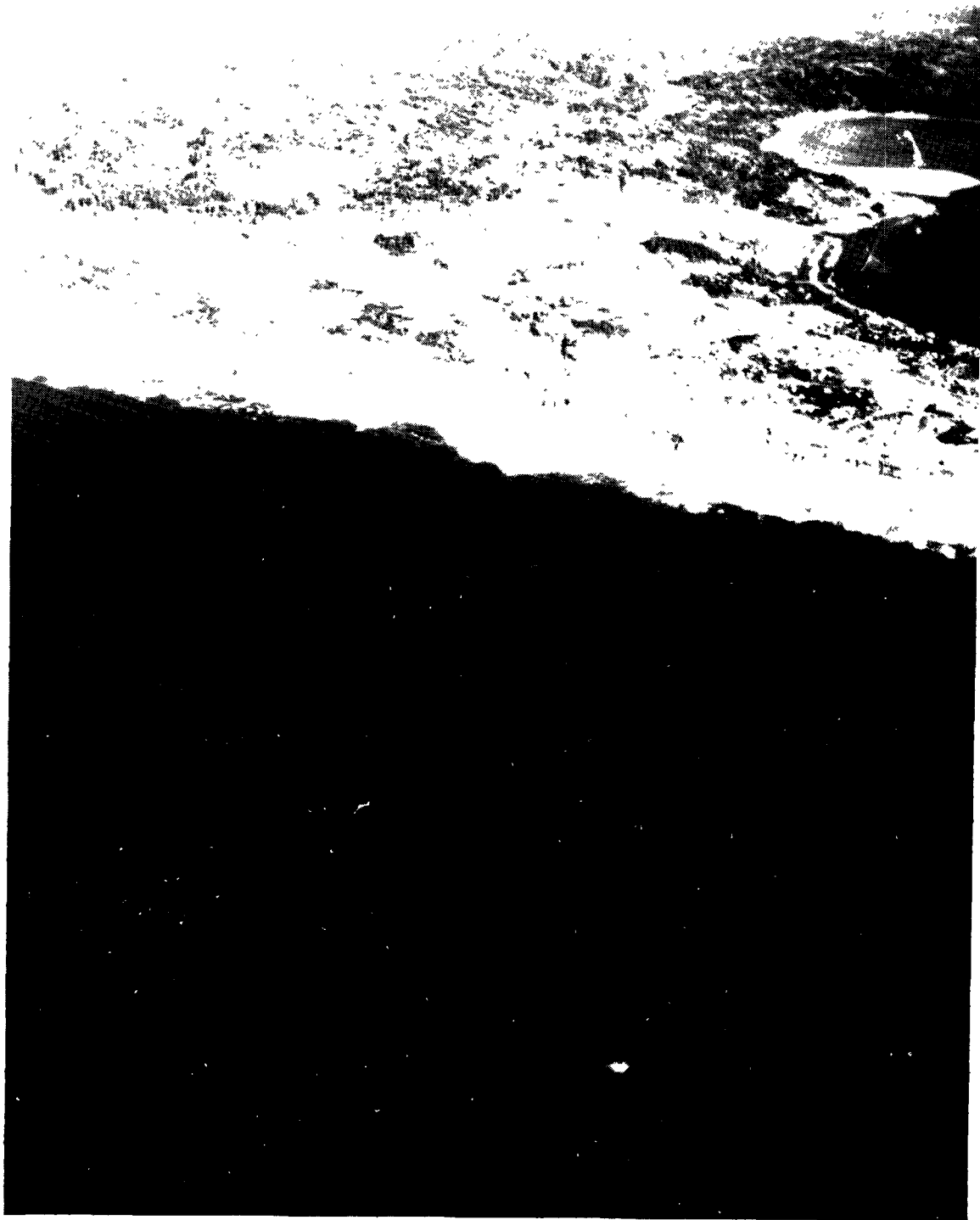


Figure 49. Aerial photo of outfall area on October 7, 1970  
from 3000 feet at 14:32.

Flow = 7450 gpm

$V_x =$         fps

Area = 9         $A_c$

$D_x =$          $\text{ft}^2/\text{sec}$

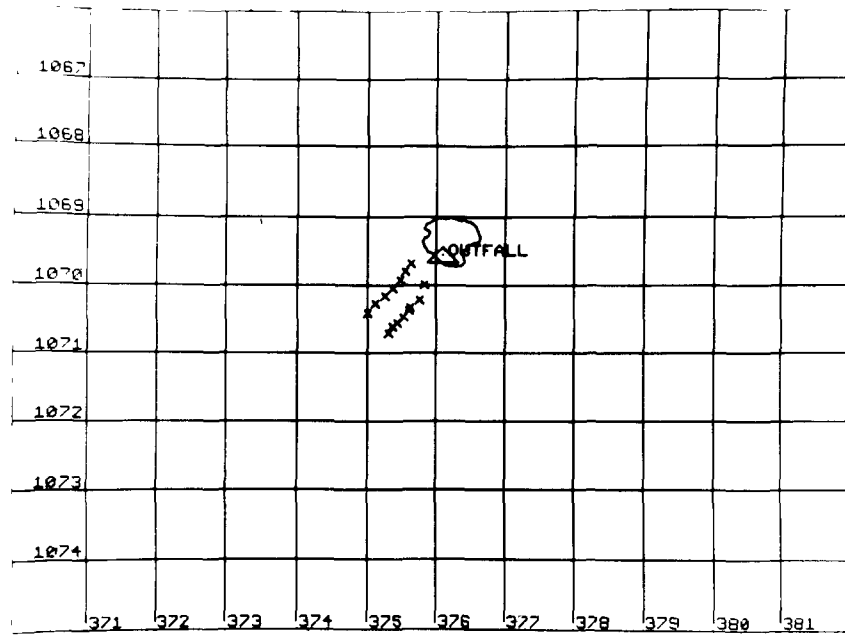
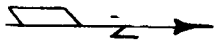
$D_y =$          $\text{ft}^2/\text{sec}$

→ current  
vector

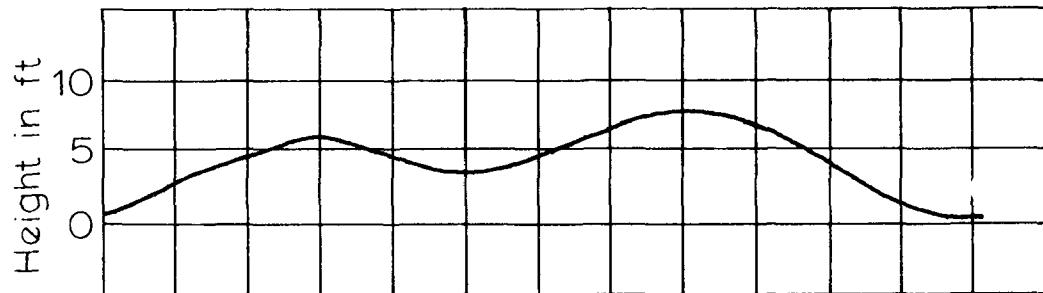
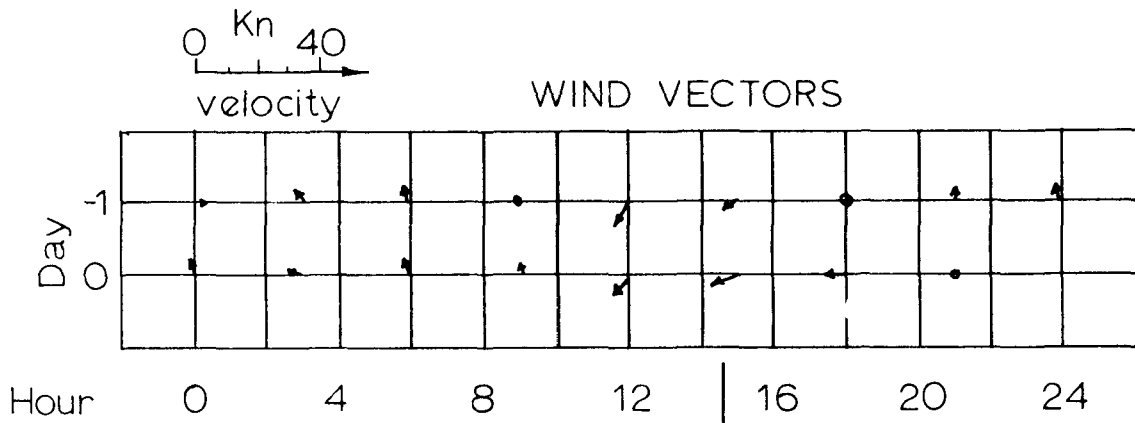
x foam

$\Delta$  outfall

1000-ft grid



TEK PLOT



TIDAL CURVE

Figure 50. Data for October 7, 1970.



Figure 51. Aerial photo of outfall area on October 12, 1970 from 4000 feet at 14:10.



Flow = 7650 gpm

$V_x =$             fps

Area = 89      Ac

$D_x =$             ft<sup>2</sup>/sec

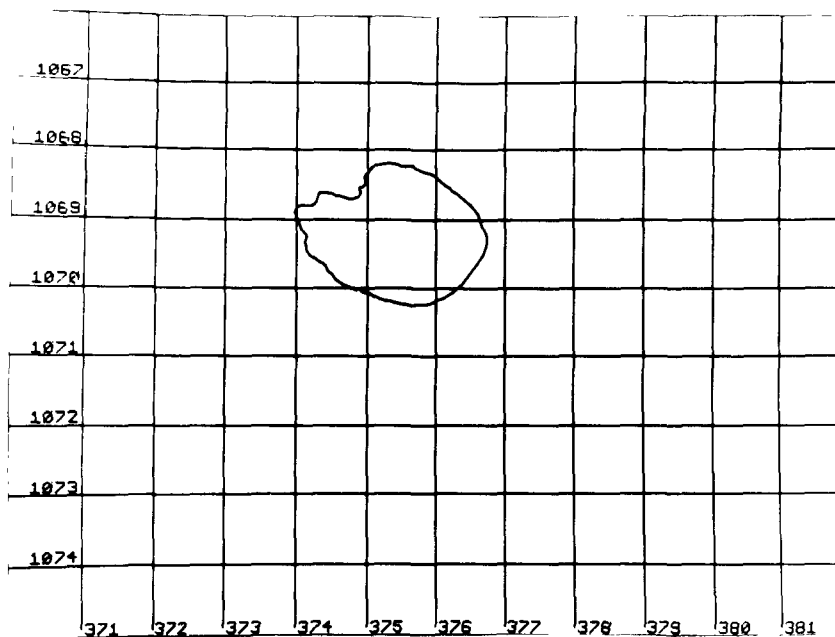
$D_y =$             ft<sup>2</sup>/sec

→ current  
vector

x foam

Δ outfall

1000-ft grid



TEK PLOT

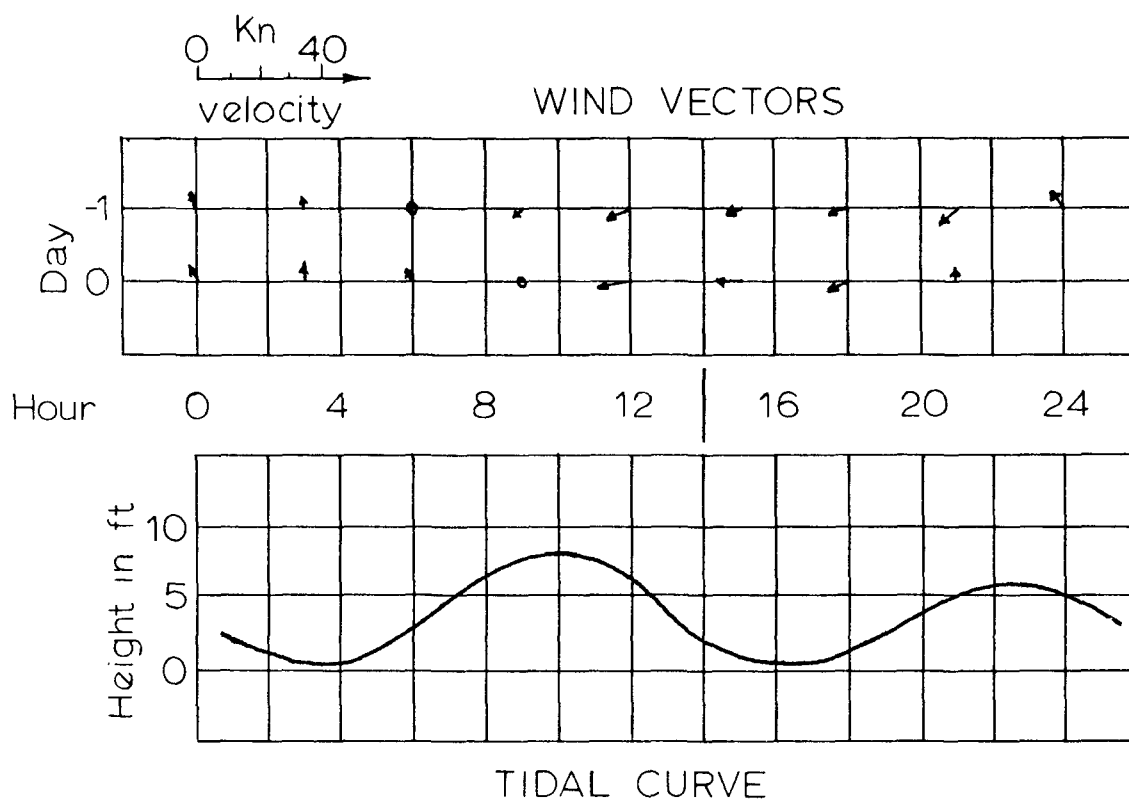


Figure 52. Data for October 12, 1970.

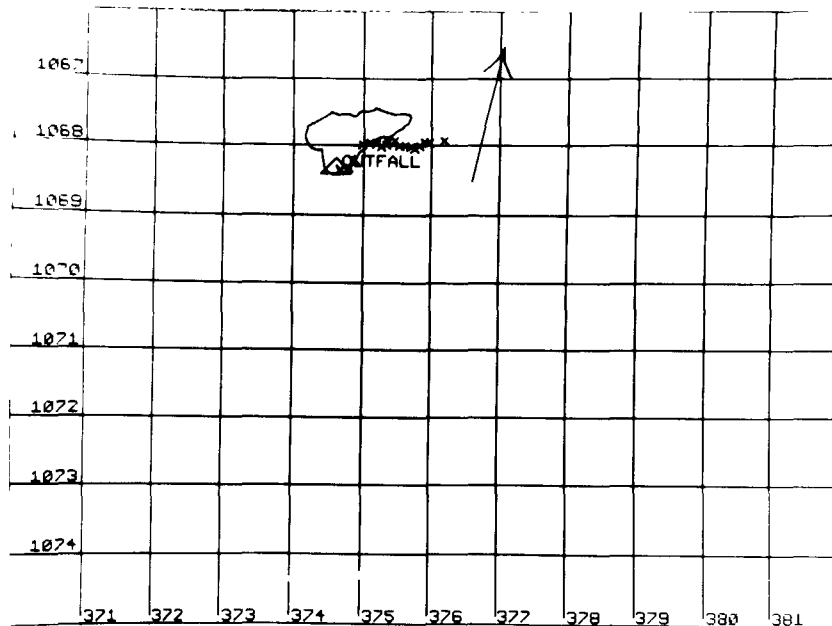
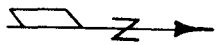


Figure 53. Aerial photo of outfall area December 21, 1970 from 6000 feet at 13:15.

Flow =            gpm  
 $V_x = 2.0$         fps  
 Area = 18        Ac  
 $D_x = 7.3$         ft<sup>2</sup>/sec  
 $D_y = 19$         ft<sup>2</sup>/sec

→ current  
       vector  
 x foam  
 Δ outfall

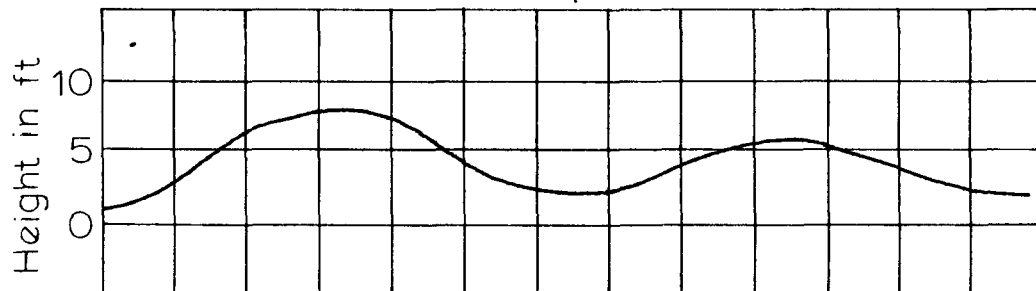
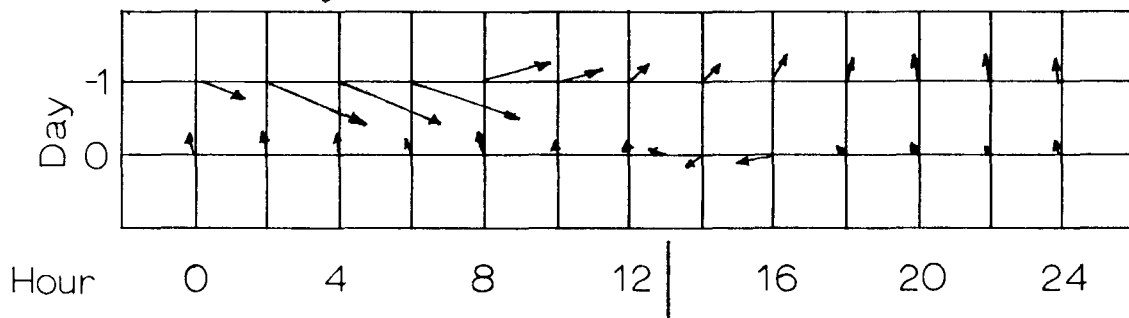
1000-ft grid



TEK PLOT

0 Kn 40  
 velocity

WIND VECTORS



TIDAL CURVE

Figure 54. Data for December 21, 1970.



Figure 55. Aerial photo of the outfall area on December 23, 1970 from 3000 feet at 11:25.

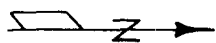
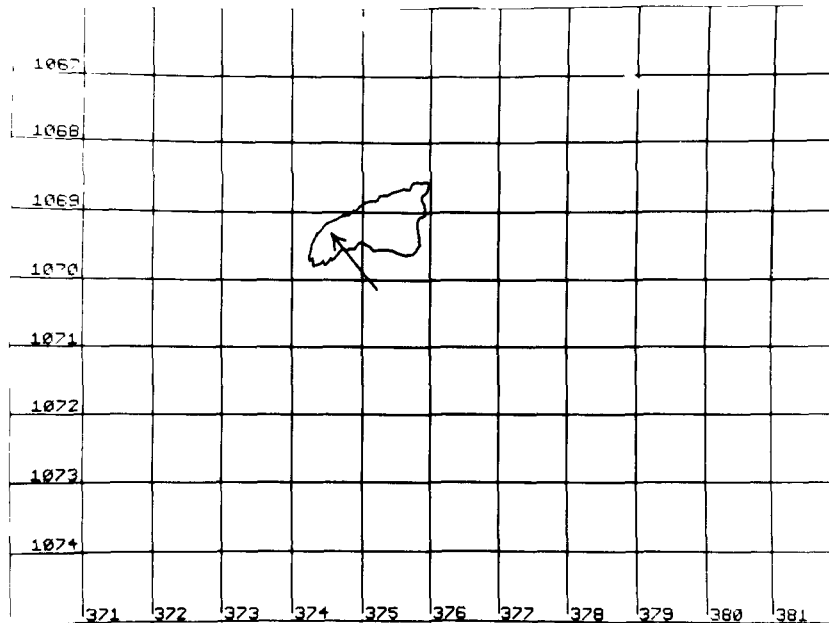
Flow =            gpm  
 $V_x = 1.1$         fps  
 Area = 26        Ac  
 $D_x = 5.1$         ft<sup>2</sup>/sec  
 $D_y = 0.7$         ft<sup>2</sup>/sec

→ current vector

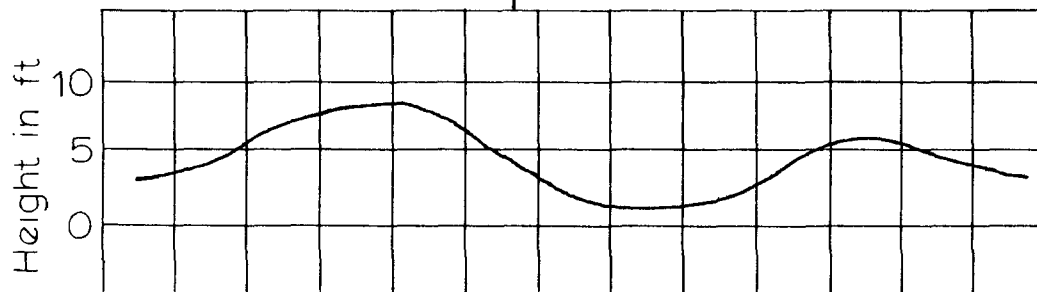
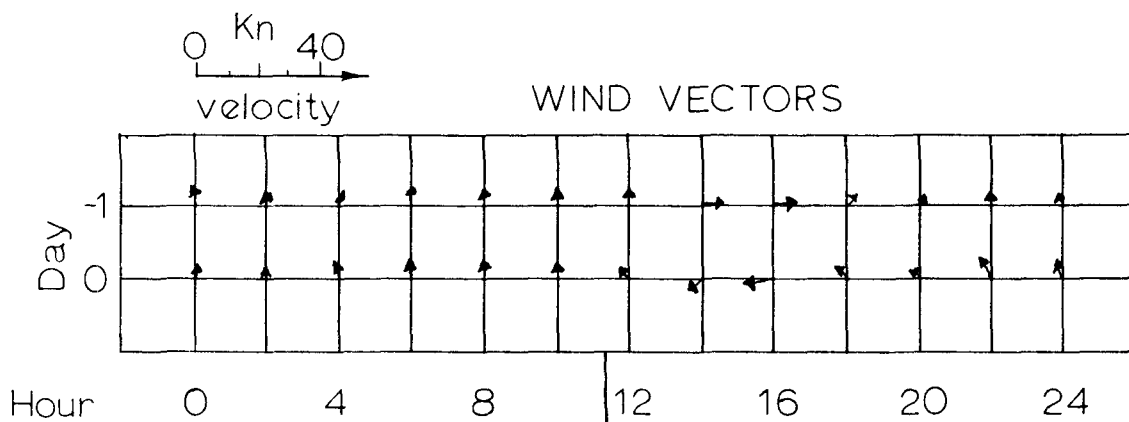
x foam

△ outfall

1000-ft grid



TEK PLOT



TIDAL CURVE

Figure 56. Data for December 23, 1970.



Figure 57. Aerial photo of outfall area on December 31, 1970 from 3000 feet at 12:10.

Flow = 8700 gpm

$V_x = 1.4$  fps

Area =  $A_c$

$D_x = 7.9$  ft<sup>2</sup>/sec

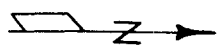
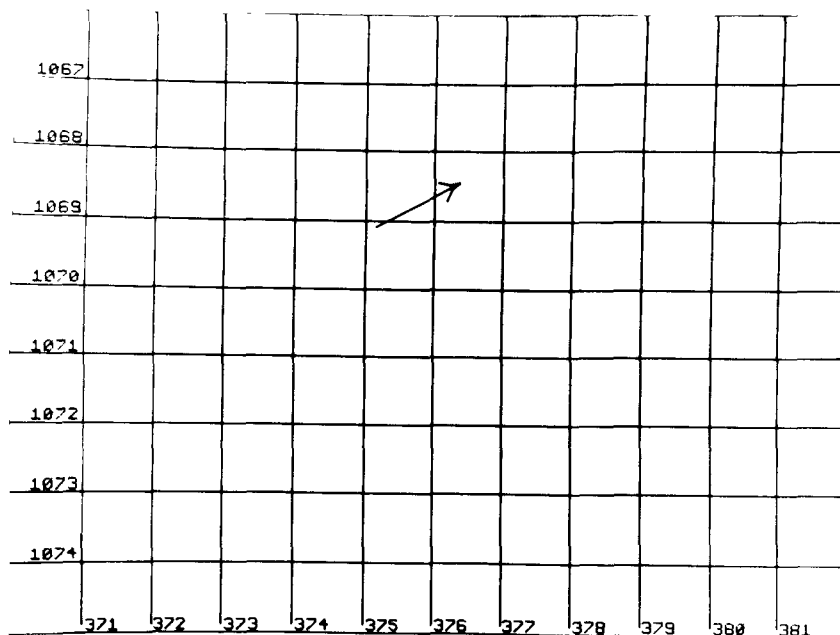
$D_y = 0.6$  ft<sup>2</sup>/sec

→ current vector

x foam

Δ outfall

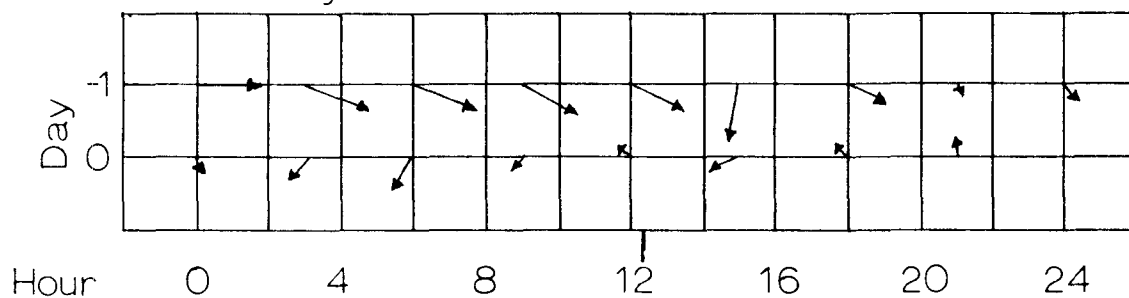
1000-ft grid



TEK PLOT

0 Kn 40  
velocity

WIND VECTORS



TIDAL CURVE

Figure 58. Data for December 31, 1970.

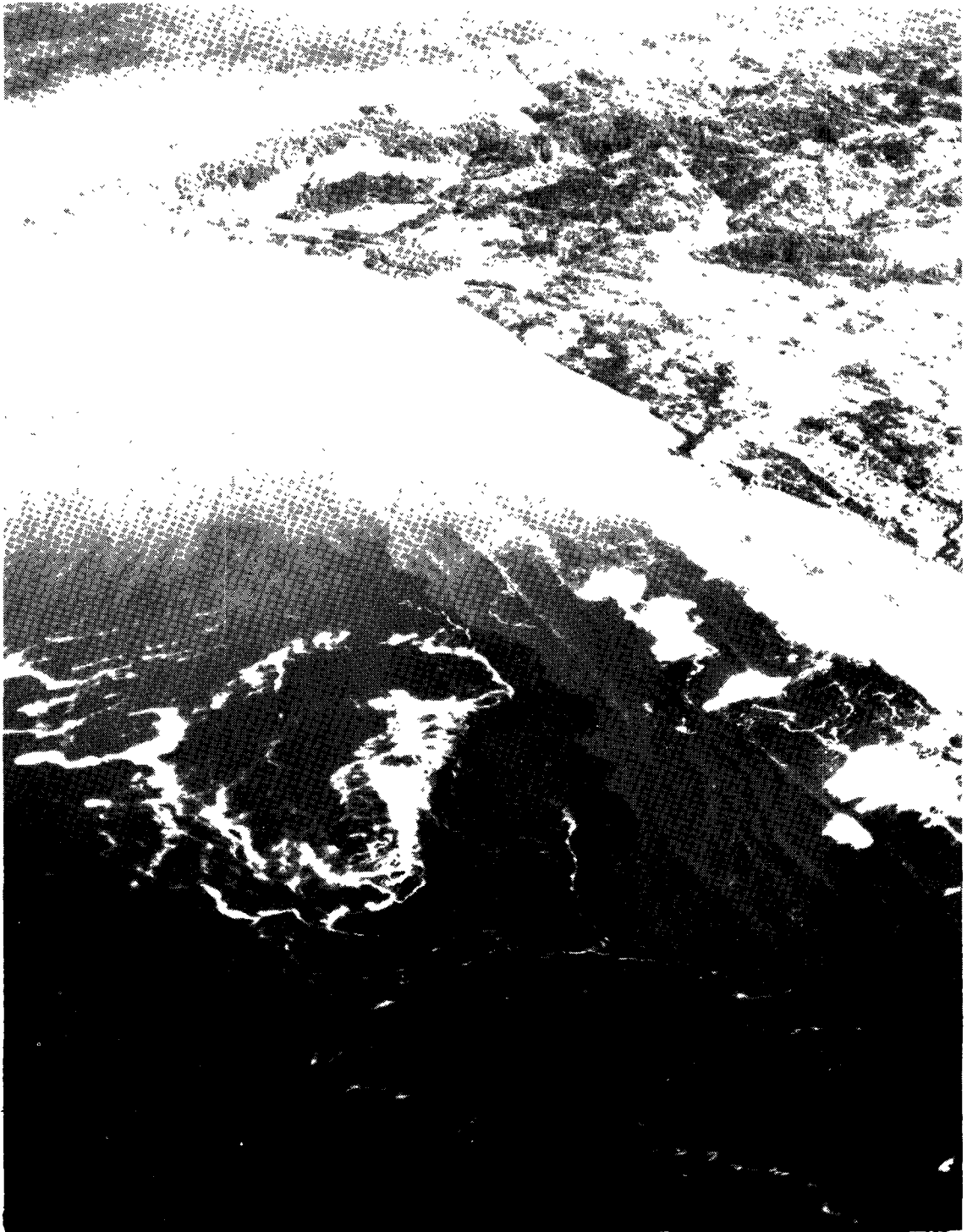


Figure 59. Aerial photo of outfall area on January 2, 1971 from 4000 feet at 11:40.



Flow = 6950 gpm

$V_x = 0.6$  fps

Area = 36 Ac

$Dx = 1.7$  ft<sup>2</sup>/sec

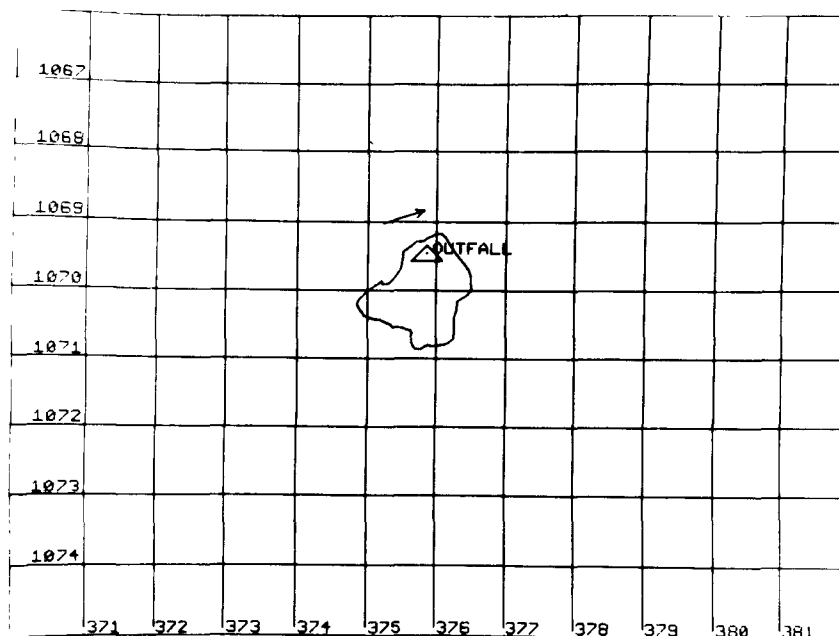
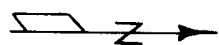
$Dy = 0.5$  ft<sup>2</sup>/sec

→ current vector

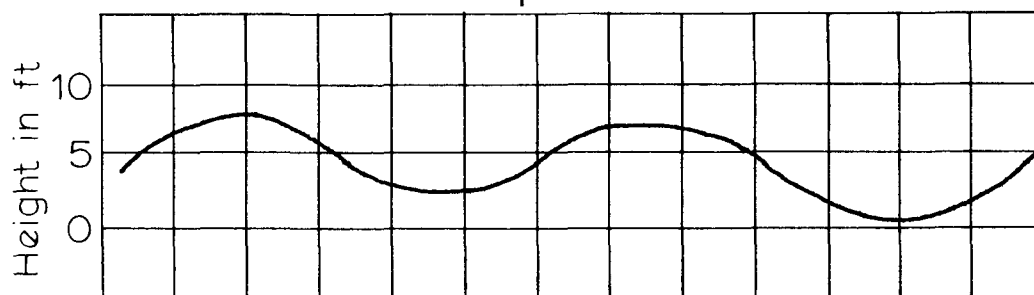
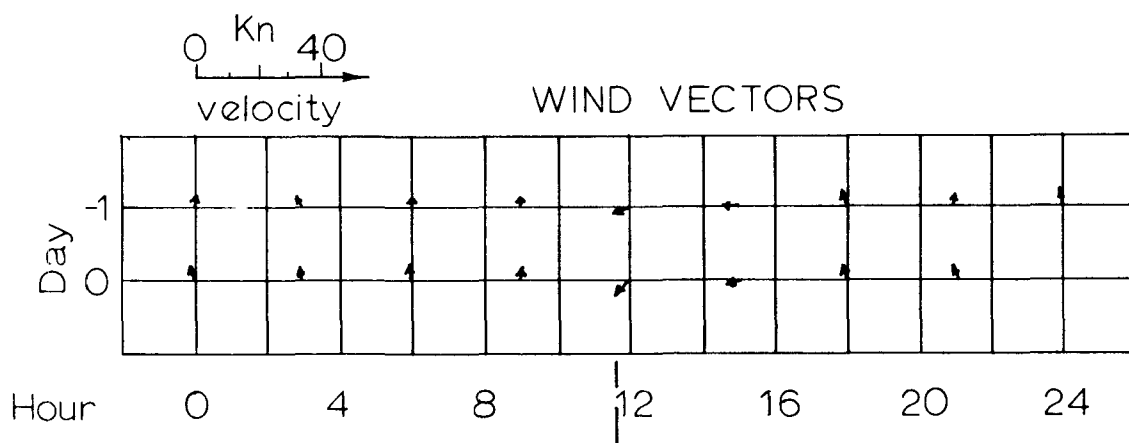
x foam

△ outfall

1000-ft grid



TEK PLOT



TIDAL CURVE

Figure 60. Data for January 2, 1971.



Figure 61. Aerial photo of outfall area on February 6, 1971  
from 6000 feet at 11:55.

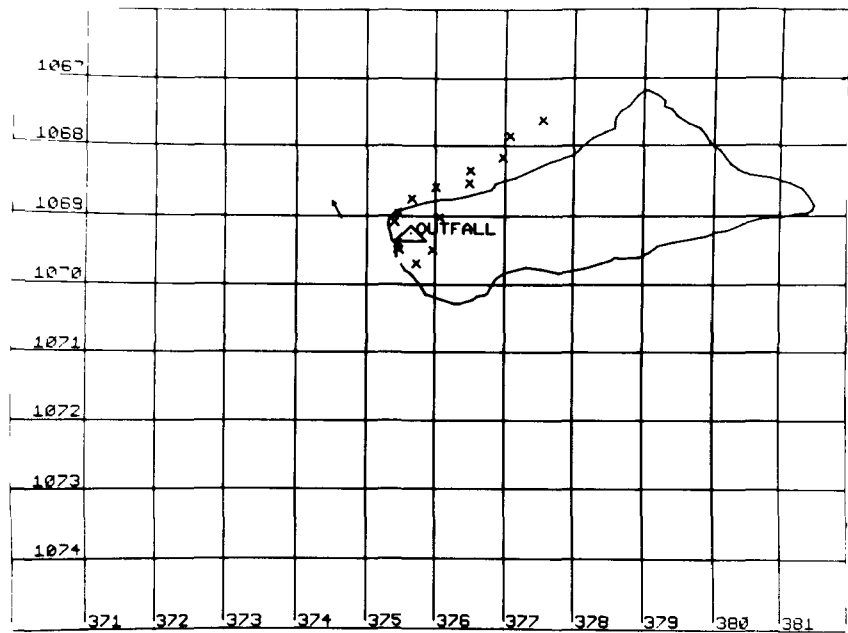
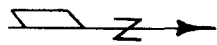
Flow = 6450 gpm  
 $V_x = 0.3$  fps  
 Area = 193 Ac  
 $D_x = 3.6$  ft<sup>2</sup>/sec  
 $D_y = 0.0$  ft<sup>2</sup>/sec

→ current vector

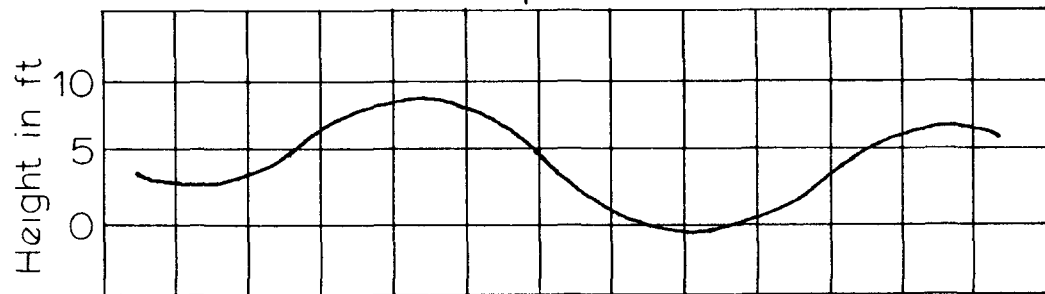
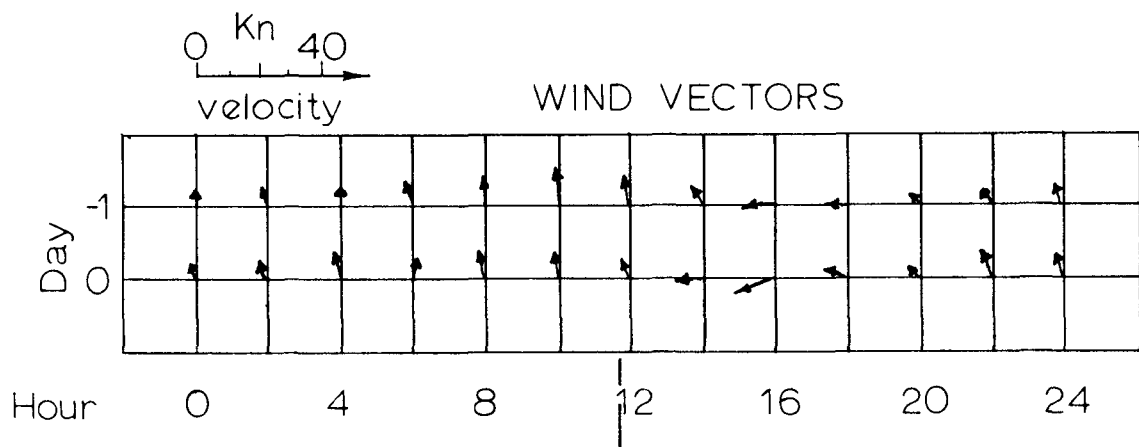
x foam

△ outfall

1000-ft grid



TEK PLOT



TIDAL CURVE

Figure 62. Data for February 6, 1971 AM.

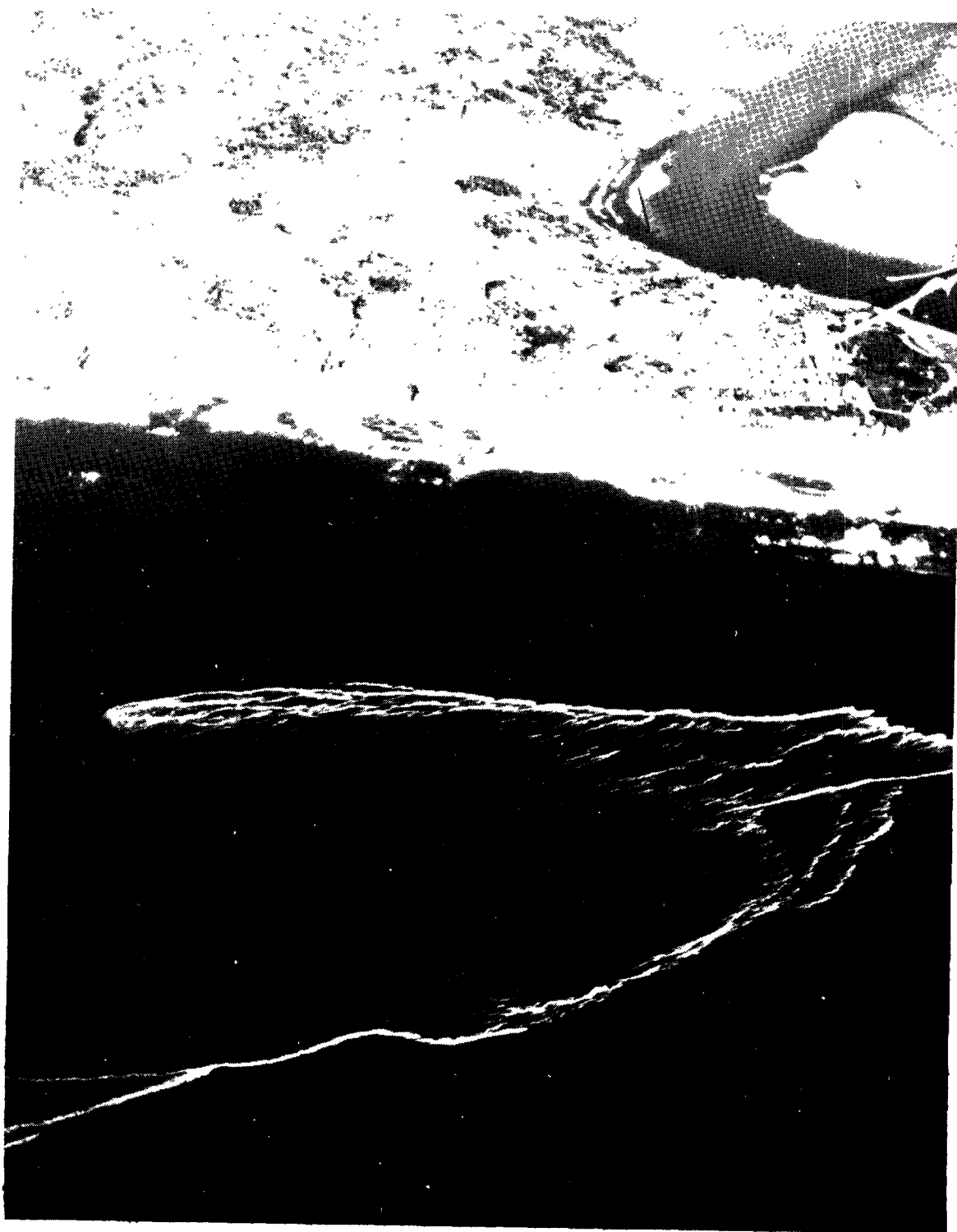


Figure 63. Aerial photo of outfall area on February 6, 1971 from 4000 feet at 14:18.

Flow = 6450 gpm

$V_x =$             fps

Area = 200    Ac

$D_x =$             ft<sup>2</sup>/sec

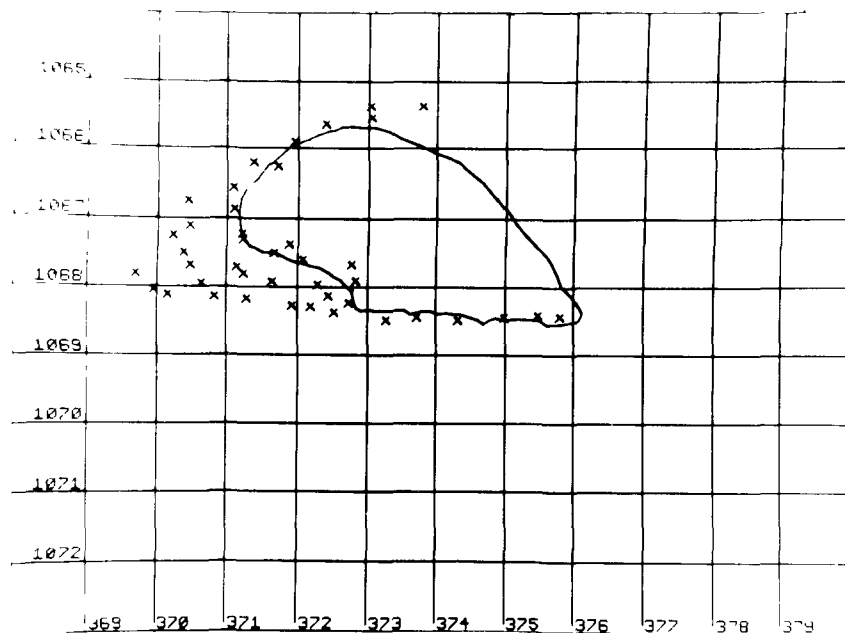
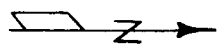
$D_y =$             ft<sup>2</sup>/sec

→    current  
      vector

x    foam

△    outfall

1000-ft grid



TEK PLOT

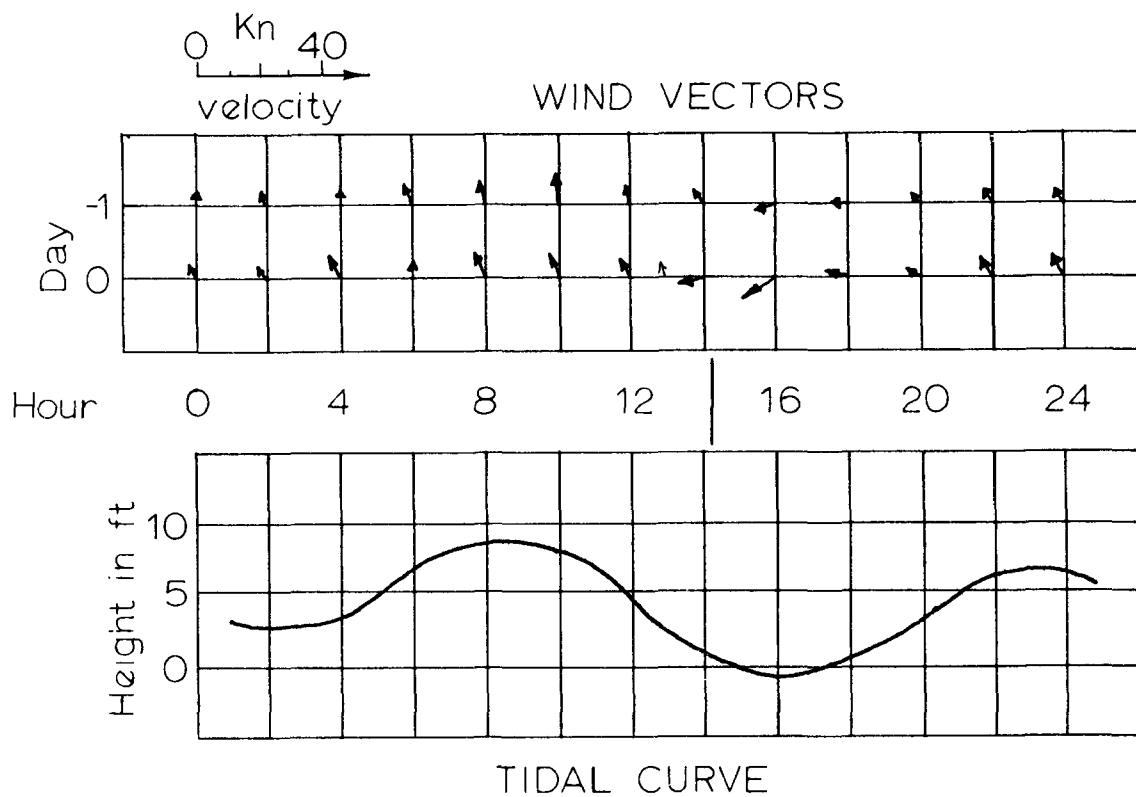


Figure 64. Data for February 6, 1971 PM.

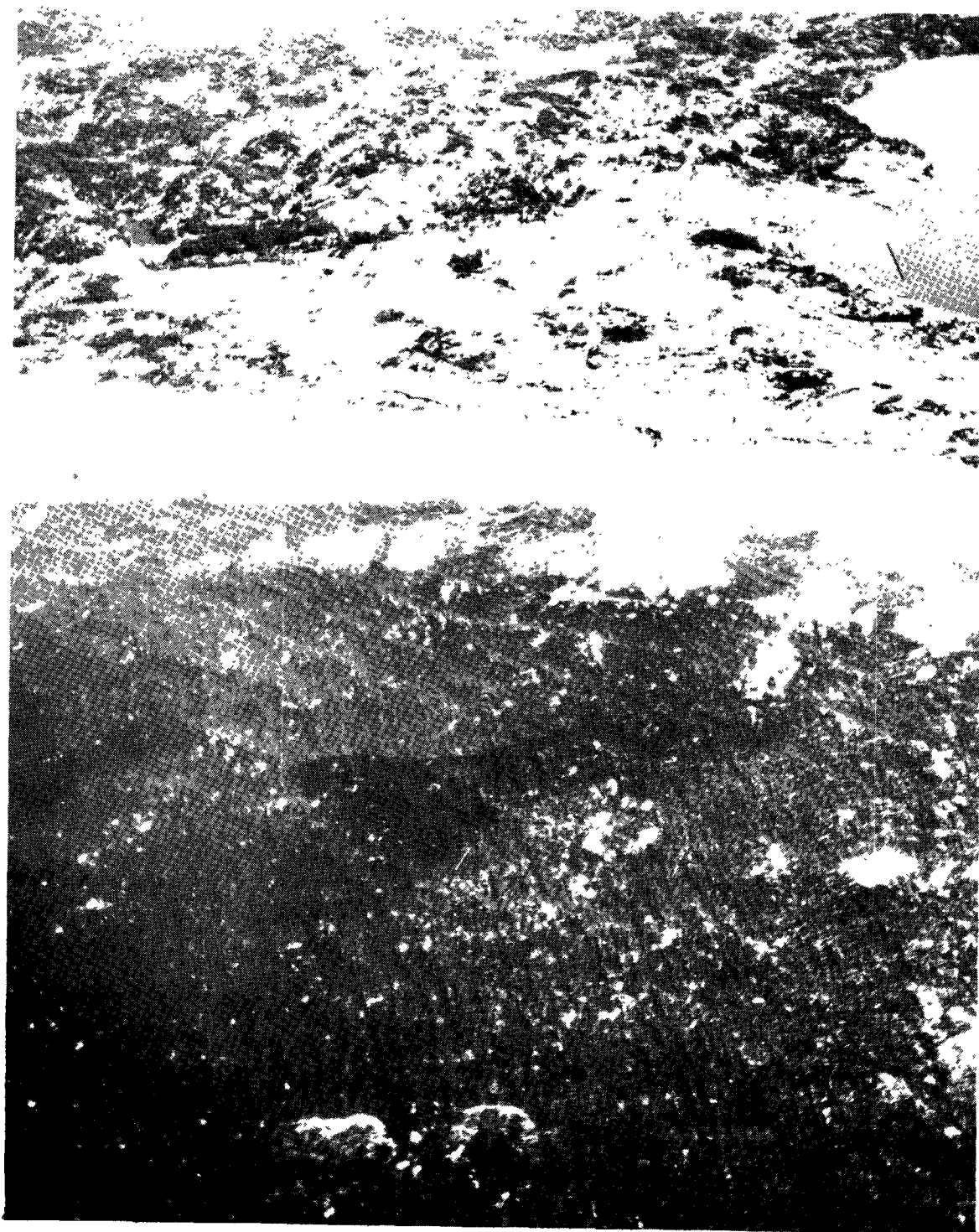


Figure 65. Aerial photo of outfall area on March 16, 1971  
from 4250 feet at 12:20.

Flow = 5750 gpm

$V_x =$             fps

Area = 22.     $A_c$

$D_x =$              $\text{ft}^2/\text{sec}$

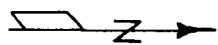
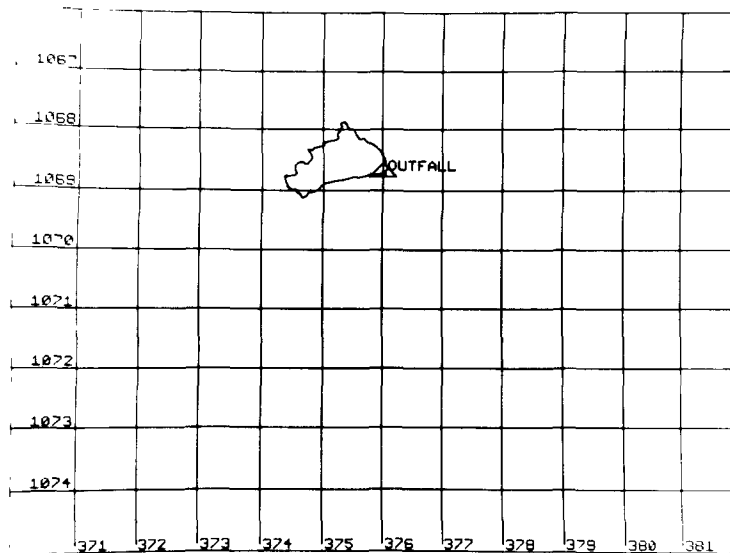
$D_y =$              $\text{ft}^2/\text{sec}$

→    current  
      vector

x    foam

△    outfall

1000-ft grid



TEK PLOT

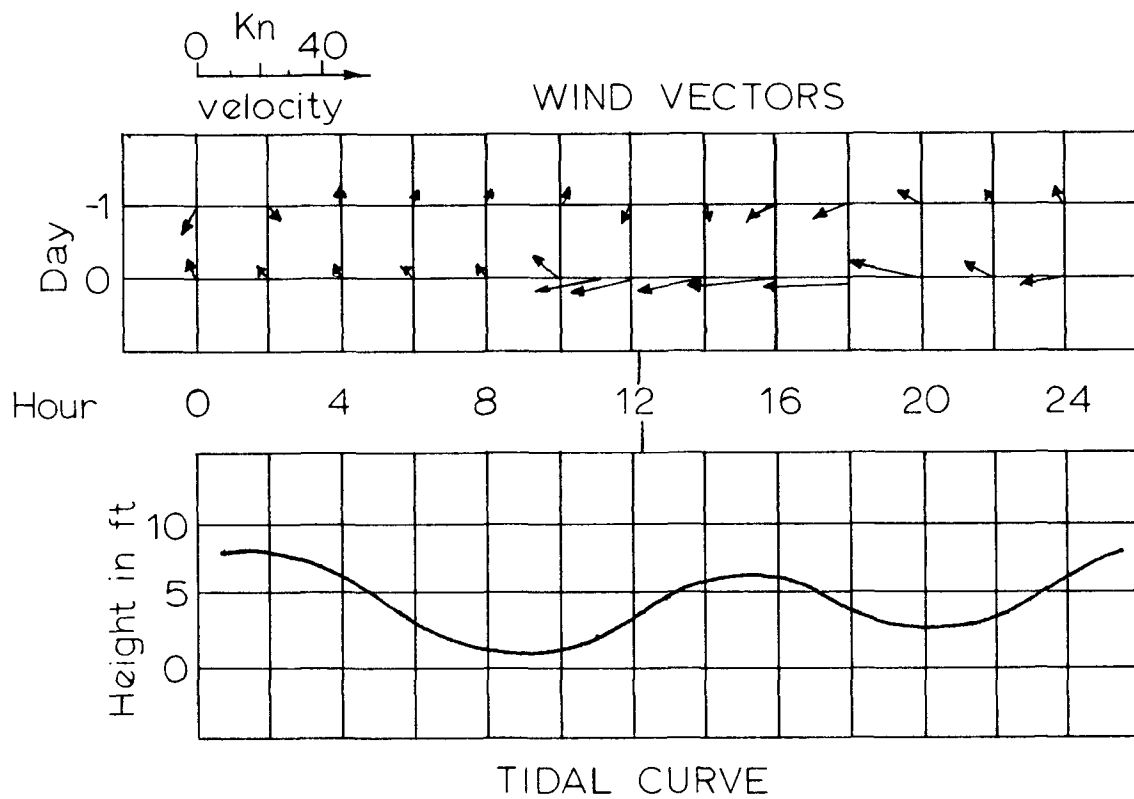


Figure 66. Data for March 16, 1971.



Figure 67. Aerial photo of outfall area on March 17, 1971  
from 4000 feet at 14:25.



Flow = 5600 gpm

$V_x = 0.3$  fps

Area = 126.  $A_c$

$D_x = 5.1$  ft<sup>2</sup>/sec

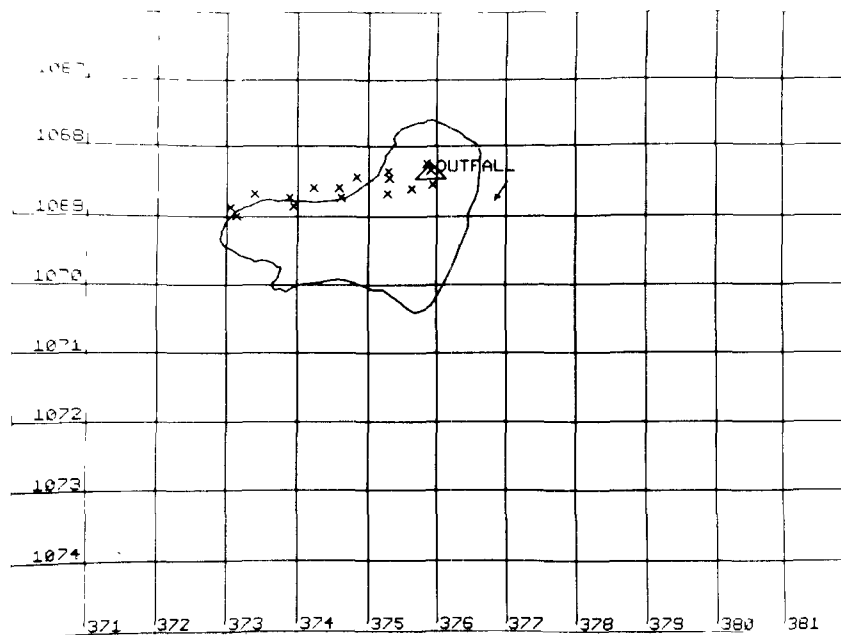
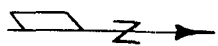
$D_y = 1.0$  ft<sup>2</sup>/sec

→ current  
vector

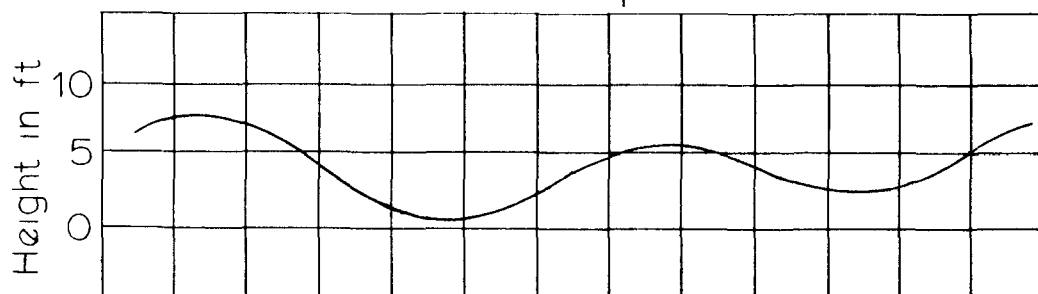
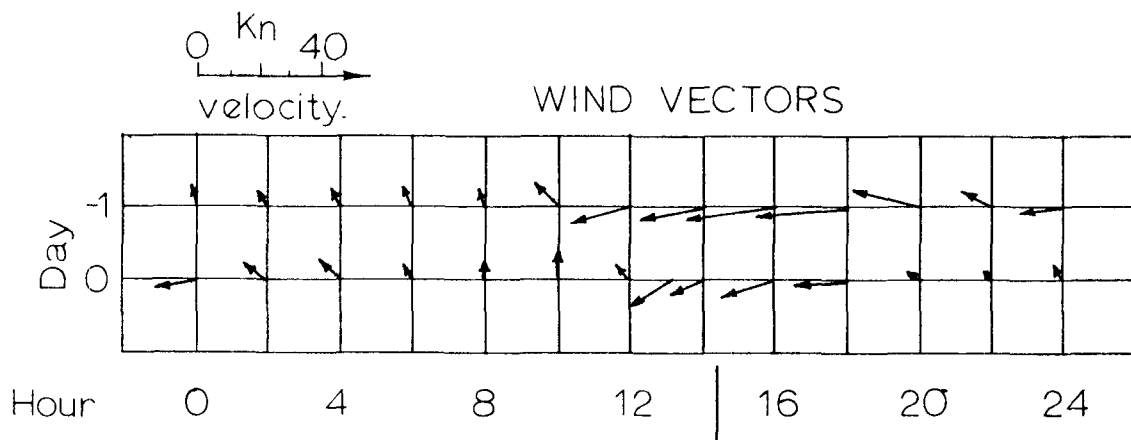
x foam

△ outfall

1000-ft grid



TEK PLOT



TIDAL CURVE

Figure 68. Data for March 17, 1971.



Figure 69. Aerial photo of outfall area on March 18, 1971  
from 8000 feet at 11:42.

Flow = 5950 gpm

$V_x = 0.7$  fps

Area = 111.  $A_c$

$D_x = 0.4$  ft<sup>2</sup>/sec

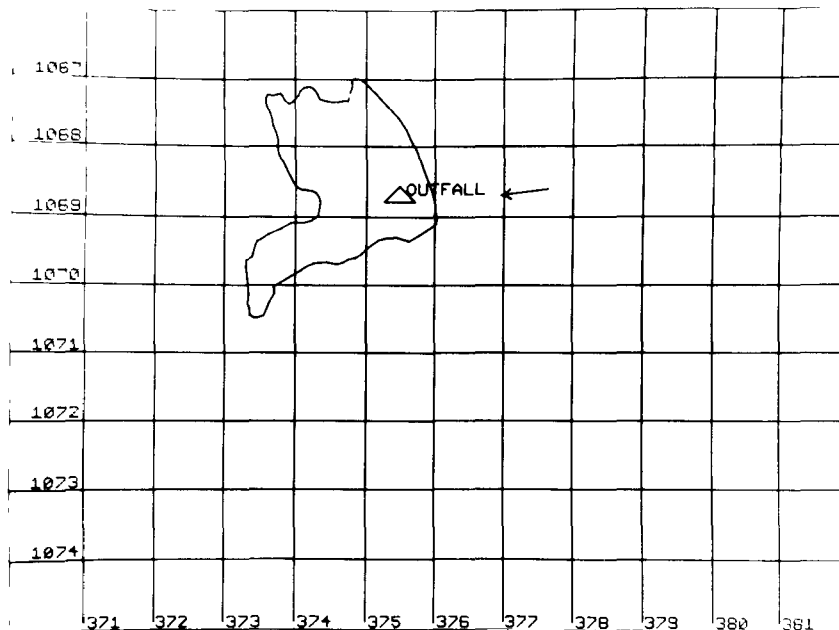
$D_y = 0.3$  ft<sup>2</sup>/sec

→ current vector

x foam

△ outfall

1000-ft grid



TEK PLOT

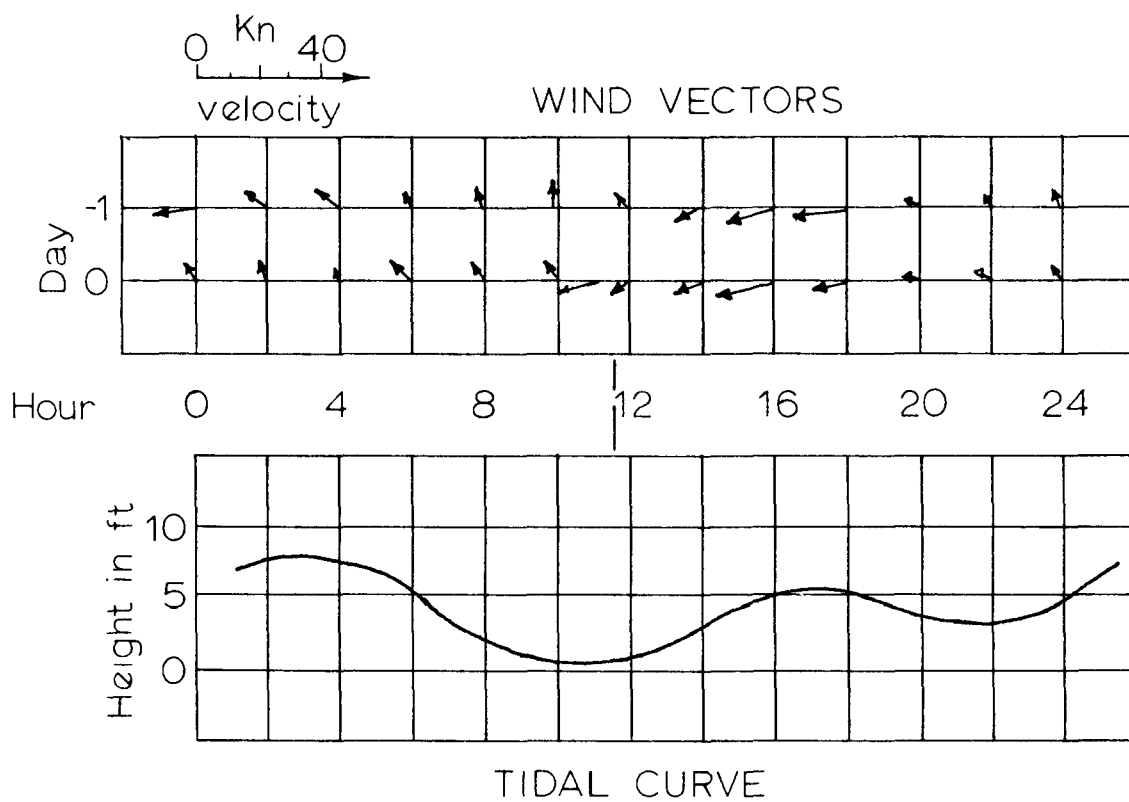


Figure 70. Data for March 18, 1971.

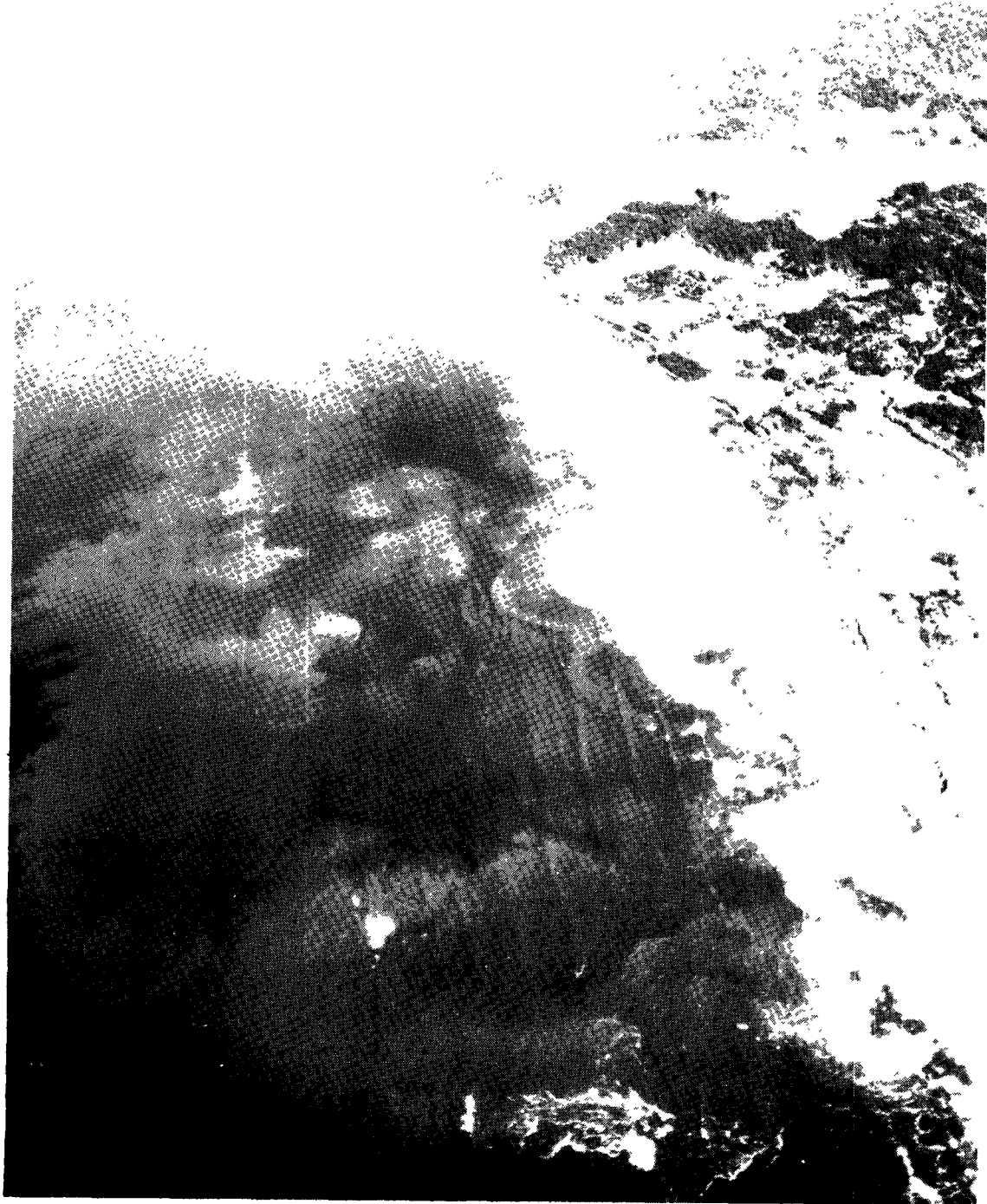


Figure 71. Aerial photo of outfall area on March 19, 1971  
from 8000 feet at 11:27.

Flow = 4500 gpm

$V_x = 0.3$  fps

Area = 73. Ac

$D_x = 1.2$  ft<sup>2</sup>/sec

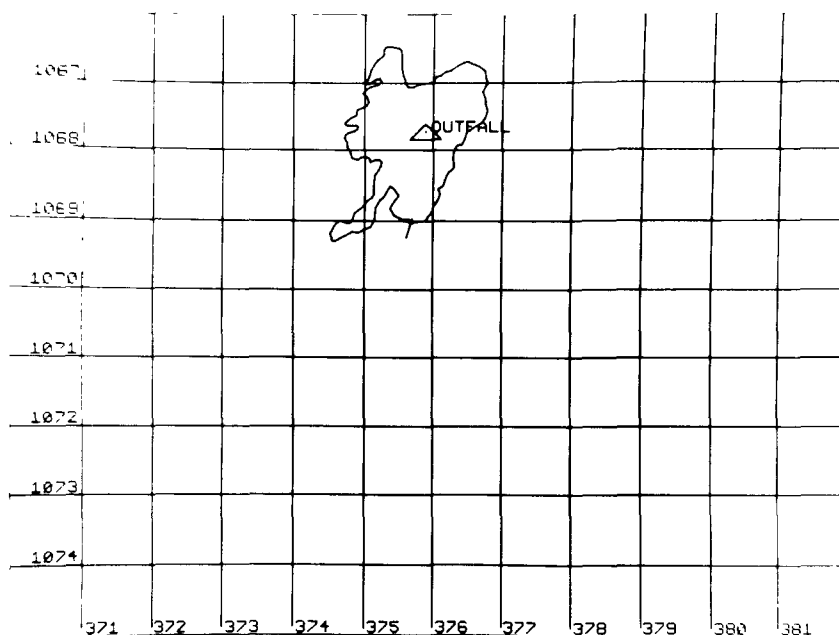
$D_y = 0.4$  ft<sup>2</sup>/sec

→ current vector

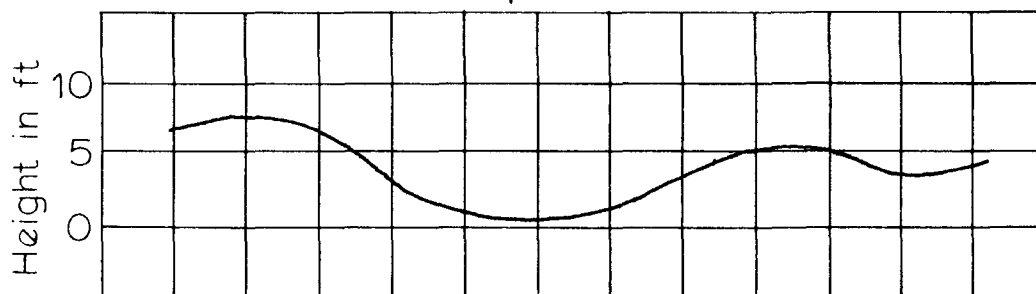
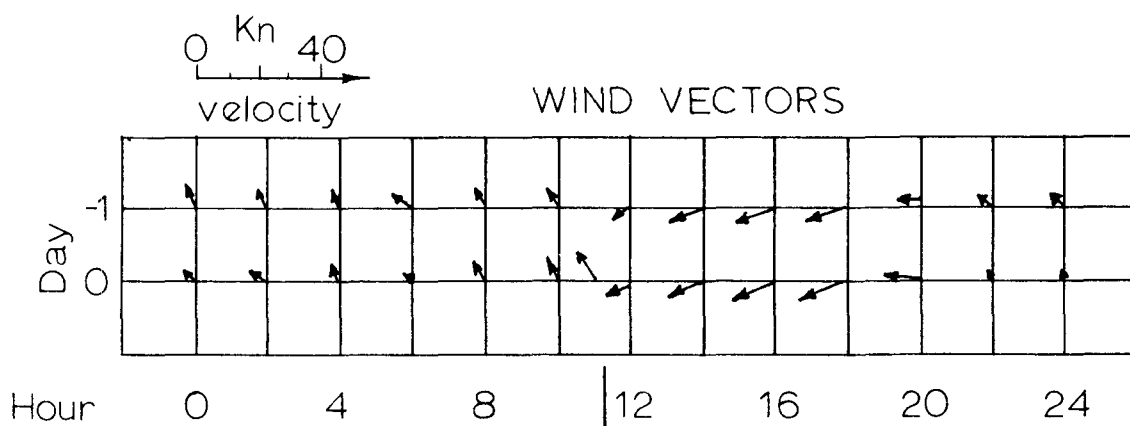
x foam

△ outfall

1000-ft grid



TEK PLOT



TIDAL CURVE

Figure 72. Data for March 19, 1971 AM.



Figure 73. Aerial photo of outfall area on March 19, 1971  
from 6000 feet at 13:50.

Flow = 4500gpm

$V_x =$         fps

Area = 83     $A_c$

$D_x =$          $\text{ft}^2/\text{sec}$

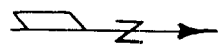
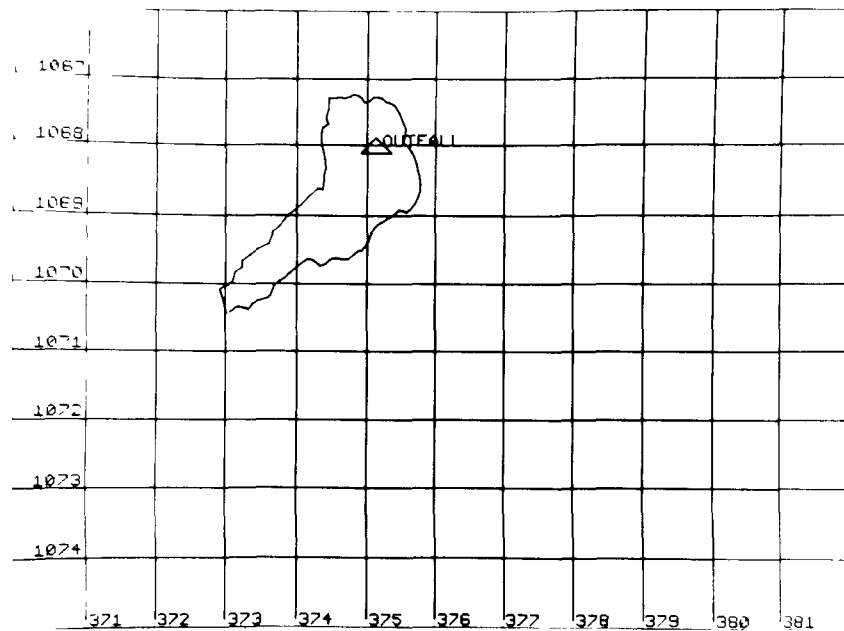
$D_y =$          $\text{ft}^2/\text{sec}$

→ current  
vector

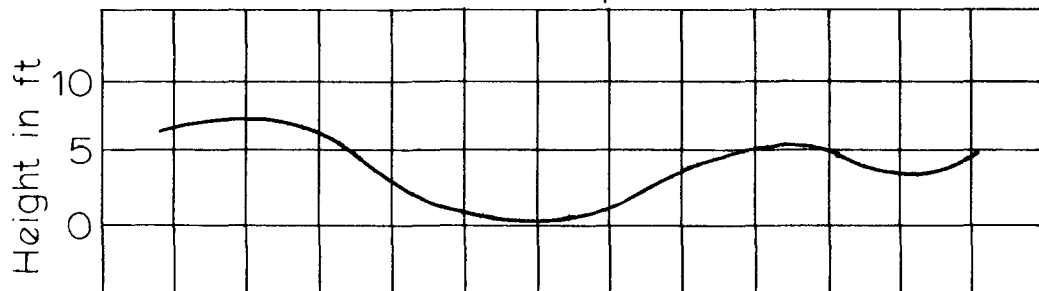
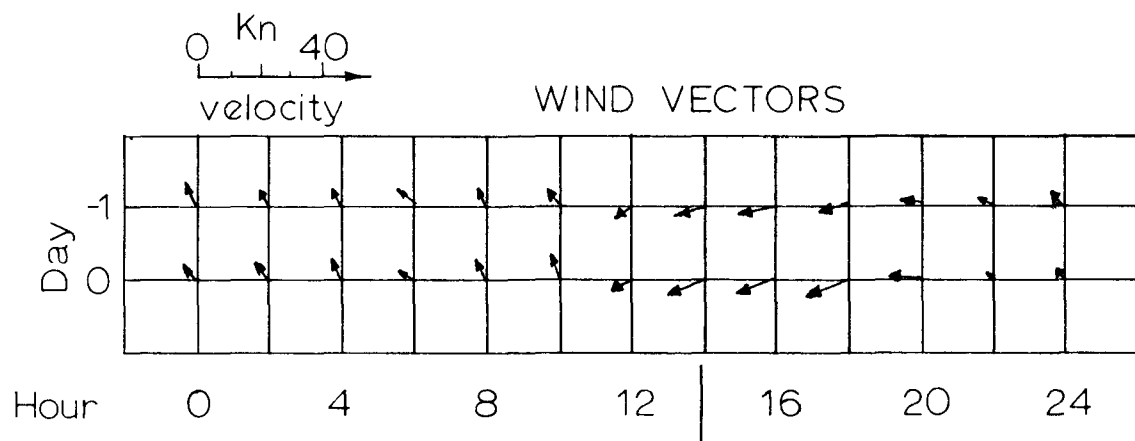
x foam

$\Delta$  outfall

1000-ft grid



TEK PLOT



TIDAL CURVE

Figure 74. Data for March 19, 1971 PM.

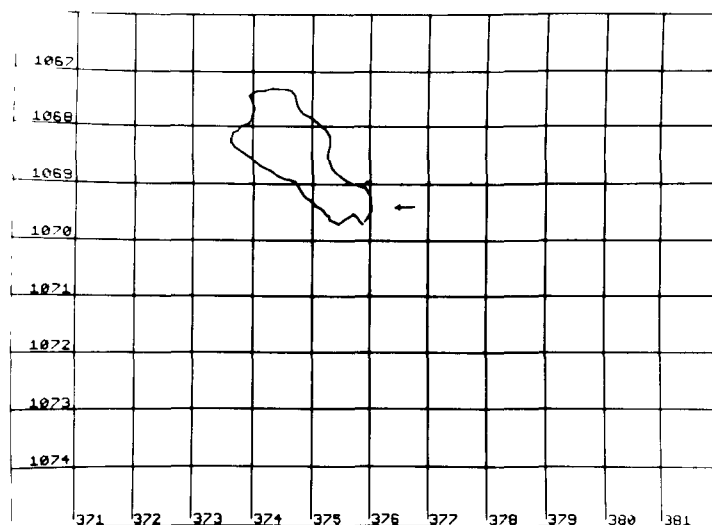


Figure 75. Aerial photo of outfall area on March 24, 1971 from 6000 feet at 16:00.

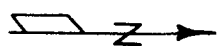


Flow = 7850 gpm  
 $V_x = 0.3$  fps  
 Area = 58 Ac  
 $Dx = 1.2$  ft<sup>2</sup>/sec  
 $Dy = 0.0$  ft<sup>2</sup>/sec

→ current vector  
 x foam  
 Δ outfall



1000-ft grid



TEK PLOT

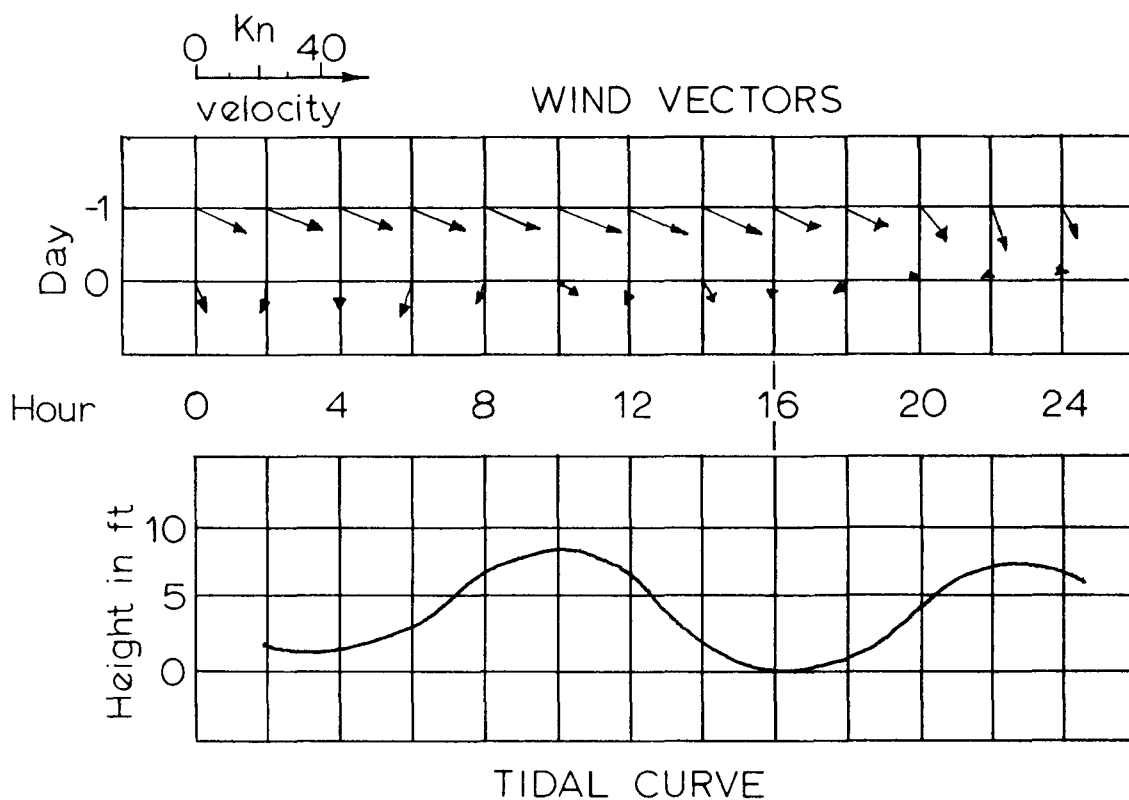


Figure 76. Data for March 24, 1971.



Figure 77. Aerial photo of outfall area on April 12, 1971  
from 6000 feet at 14:45.

Flow = 7700 gpm

$V_x = 0.4$  fps

Area = 7 Ac

$D_x = 8.07$  ft<sup>2</sup>/sec

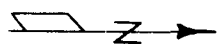
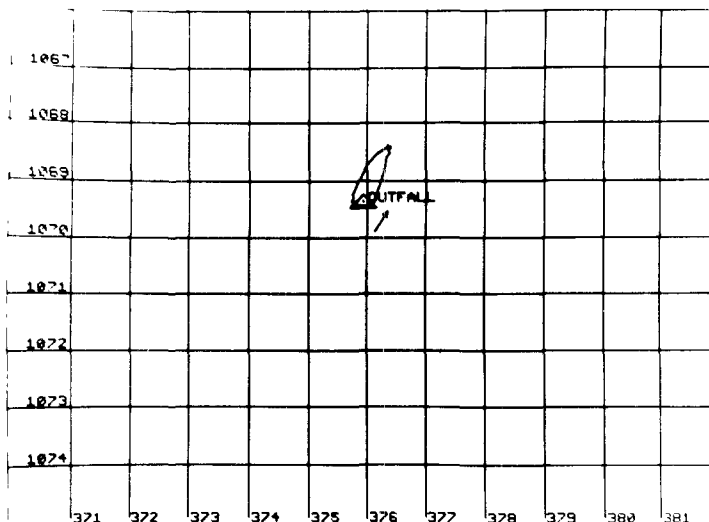
$D_y =$  ft<sup>2</sup>/sec

→ current vector

x foam

△ outfall

1000-ft grid



TEK PLOT

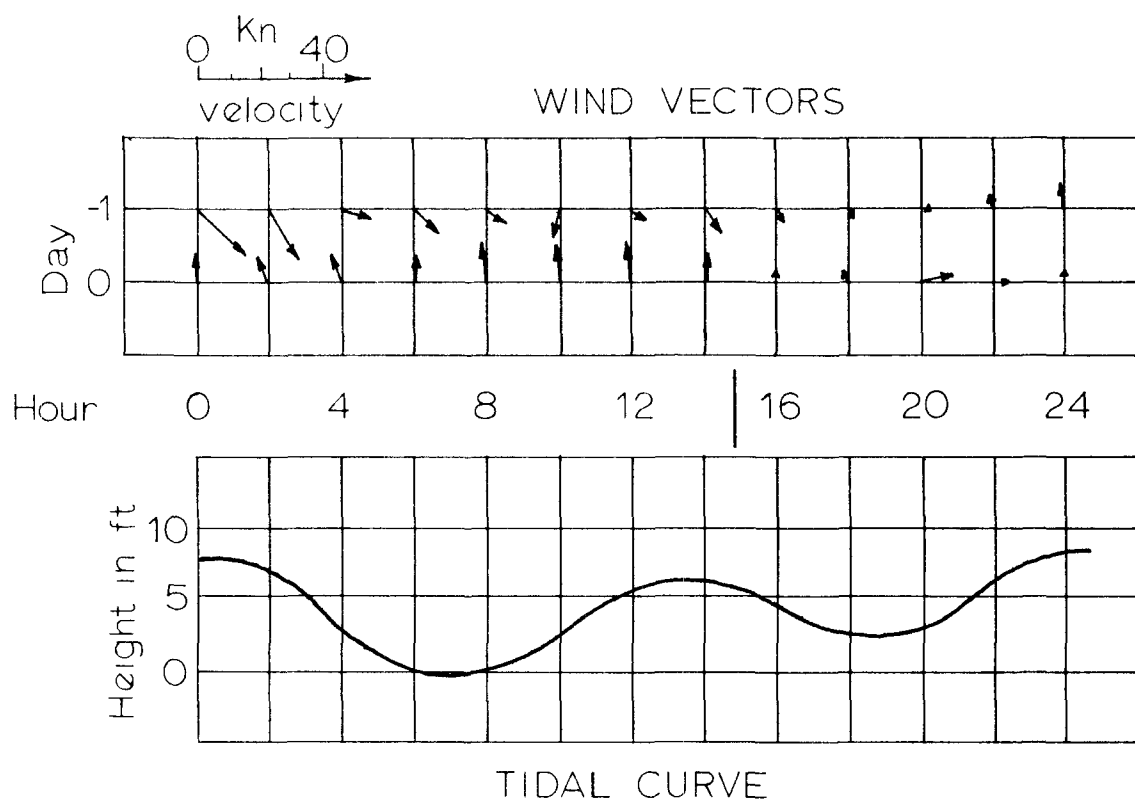


Figure 78. Data for April 12, 1971.



Figure 79. Aerial photo of outfall area on April 15, 1971 from 4000 feet at 14:07.

Flow = 7700 gpm

$V_x =$             fps

Area = 67.7    Ac

$D_x =$             ft<sup>2</sup>/sec

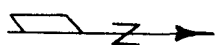
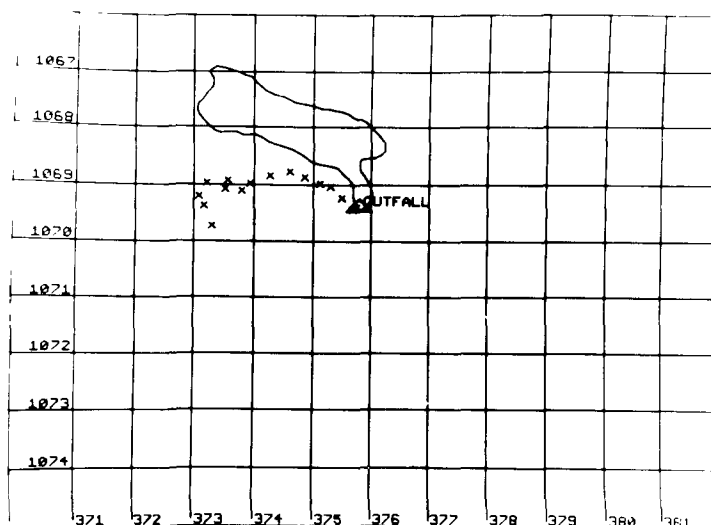
$D_y =$             ft<sup>2</sup>/sec

→    current  
         vector

x    foam

△    outfall

1000-ft grid



TEKPLOT

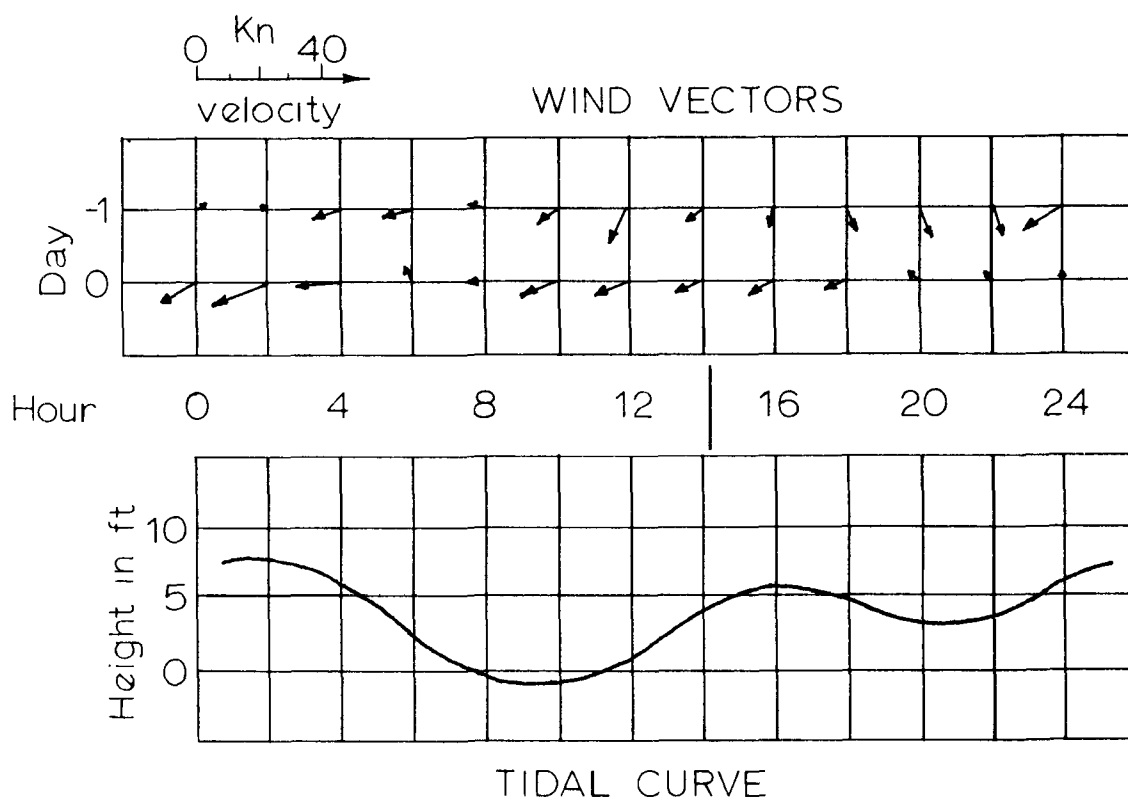


Figure 80. Data for April 15, 1971.



Figure 81. Aerial photo of outfall area on April 21, 1971 from 4000 feet at 13:46.

Flow = 5850 gpm

$V_x = 0.5$  fps

Area = 166 Ac

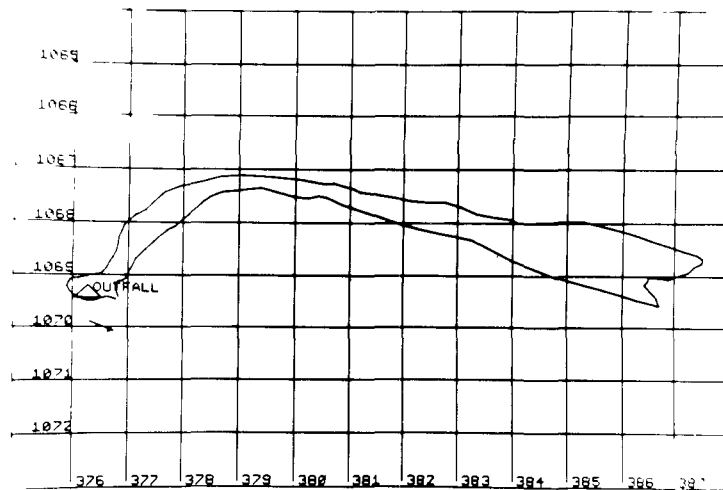
$D_x = 0.34$  ft<sup>2</sup>/sec

$D_y = 0.02$  ft<sup>2</sup>/sec

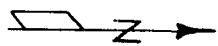
→ current  
vector

x foam

△ outfall



1000-ft grid



TEKPLOT

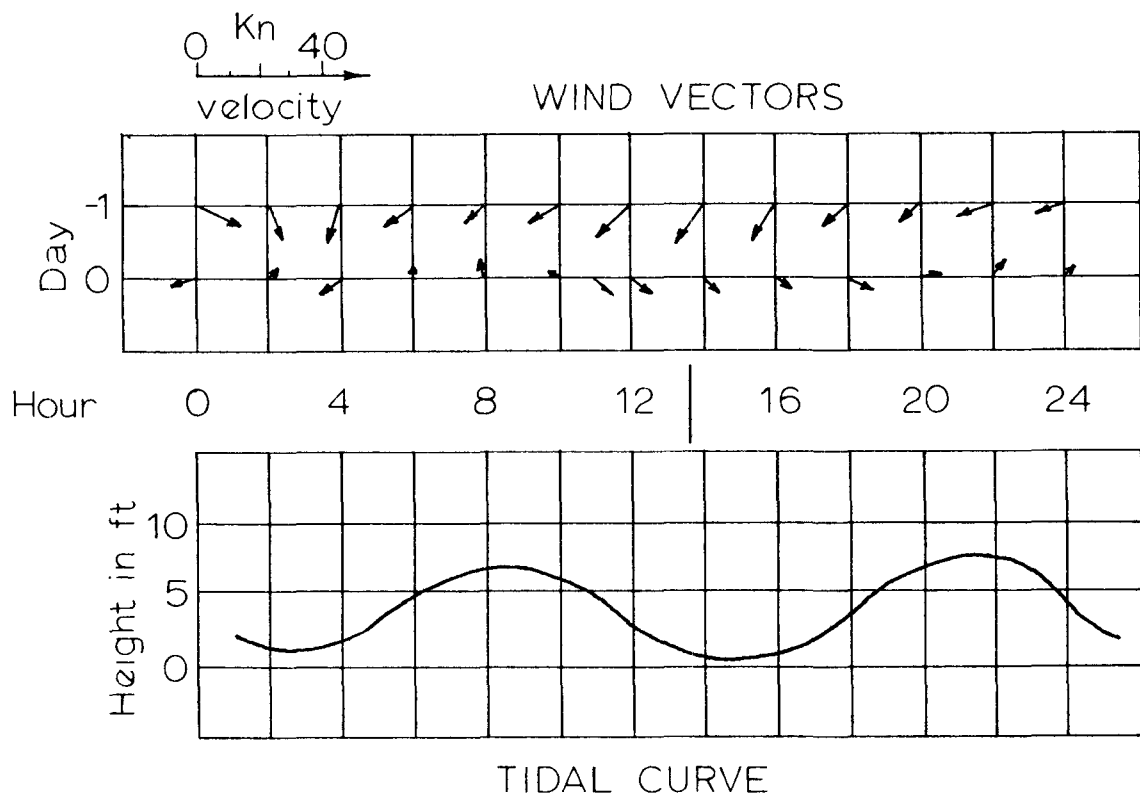


Figure 82. Data for April 21, 1971.



Figure 83. Aerial photo of outfall area on April 26, 1971 from 6000 feet at 14:20.



Flow = 5800 gpm

$V_x = 0.3$  fps

Area = 464 Ac

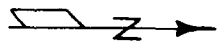
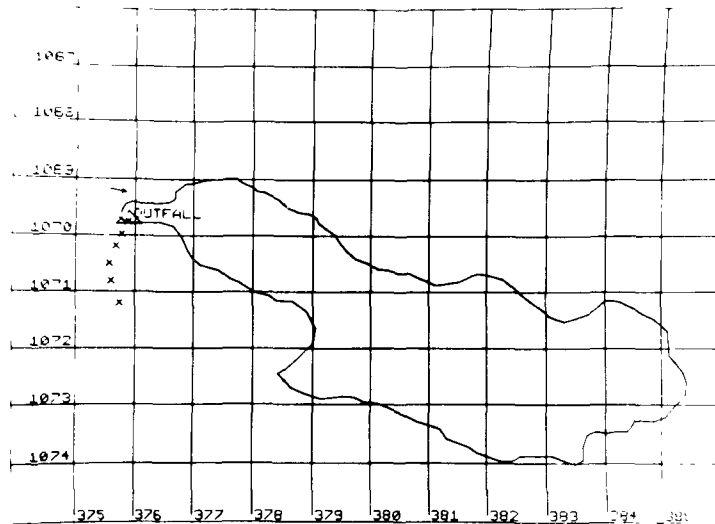
$Dx = 13.90$  ft<sup>2</sup>/sec

$Dy = 0.19$  ft<sup>2</sup>/sec

→ current vector

x foam

Δ outfall



TEKPLOT

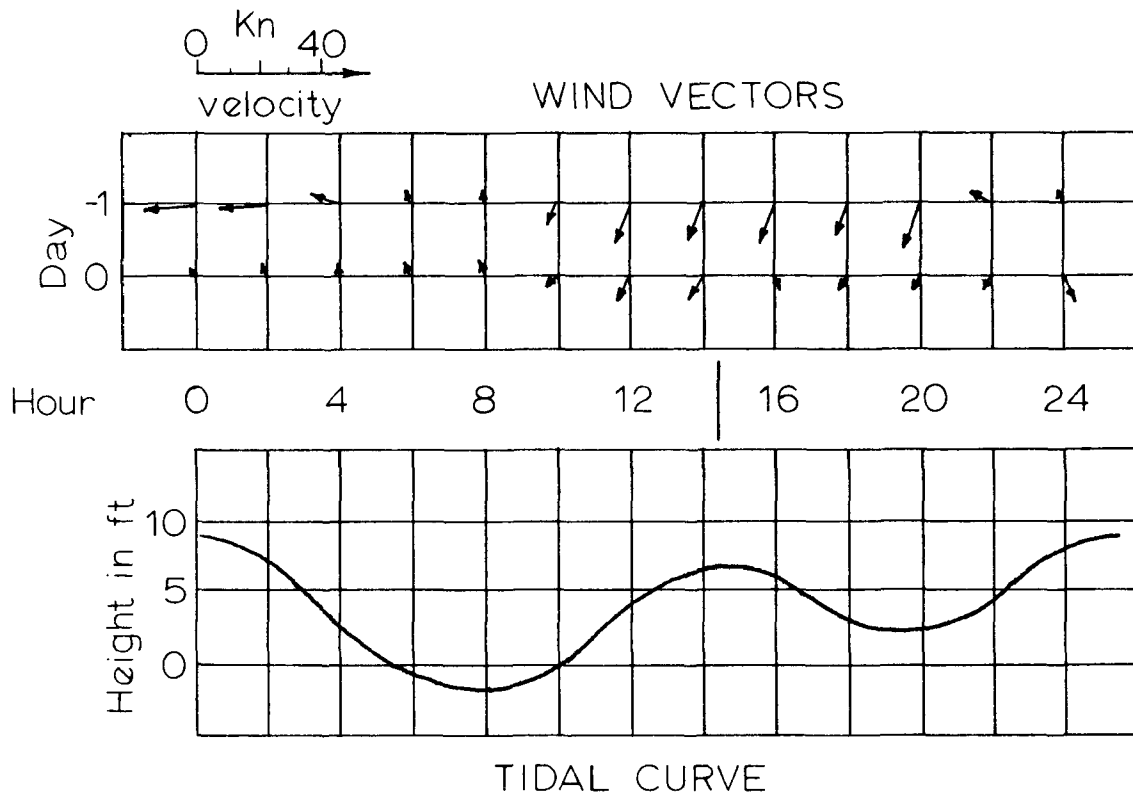


Figure 84. Data for April 26, 1971.



Figure 85. Aerial photo of outfall area on May 7, 1971  
from 4000 feet at 15:13.

Flow = 6350 gpm

$V_x =$             fps

Area = 34     $A_c$

$D_x =$              $\text{ft}^2/\text{sec}$

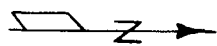
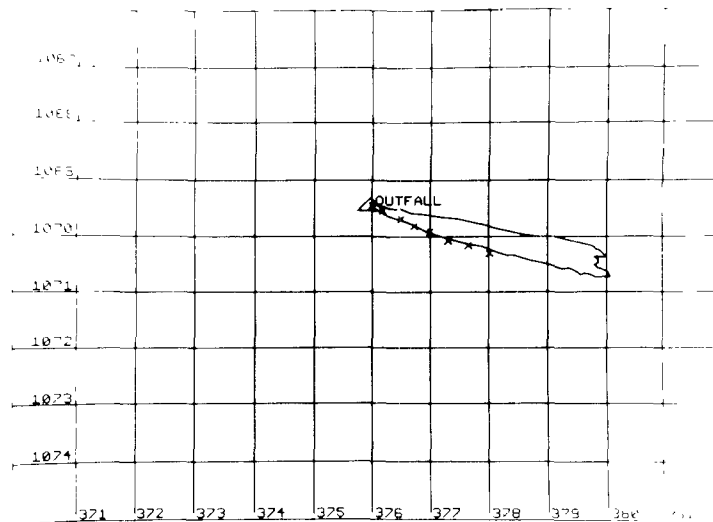
$D_y =$              $\text{ft}^2/\text{sec}$

→ current  
vector

x foam

Δ outfall

1000-ft grid



TEK PLOT

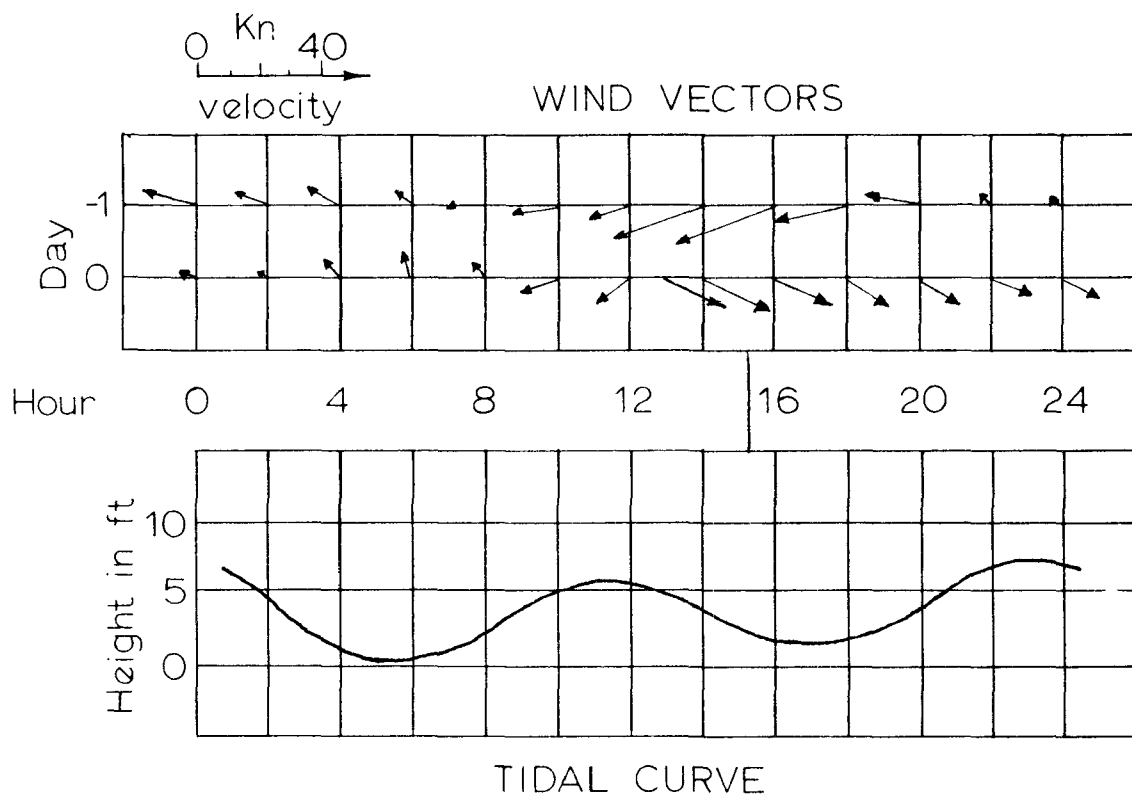


Figure 86. Data for May 7, 1971.



Figure 87. Aerial photo of outfall area on May 10, 1971 from 4000 feet at 16:10.

Flow = 5975 gpm

$V_x = 0.7$  fps

Area = 71 Ac

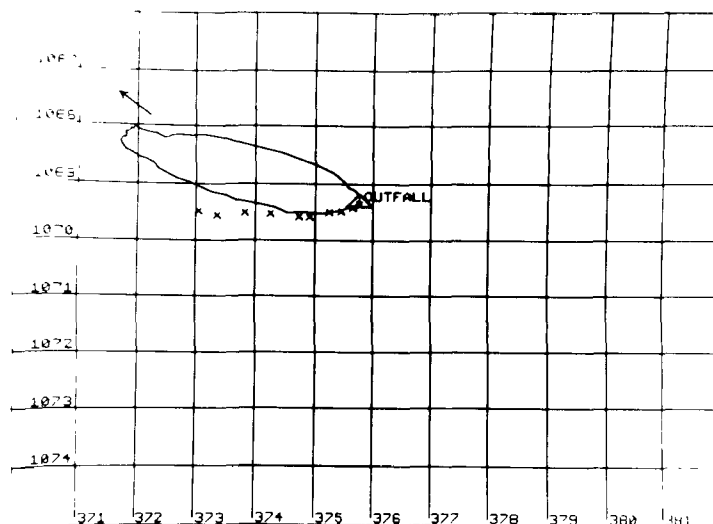
$D_x = 2.8$  ft<sup>2</sup>/sec

$D_y = 0.1$  ft<sup>2</sup>/sec

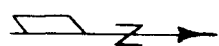
→ current vector

x foam

△ outfall



1000-ft grid



TEK PLOT

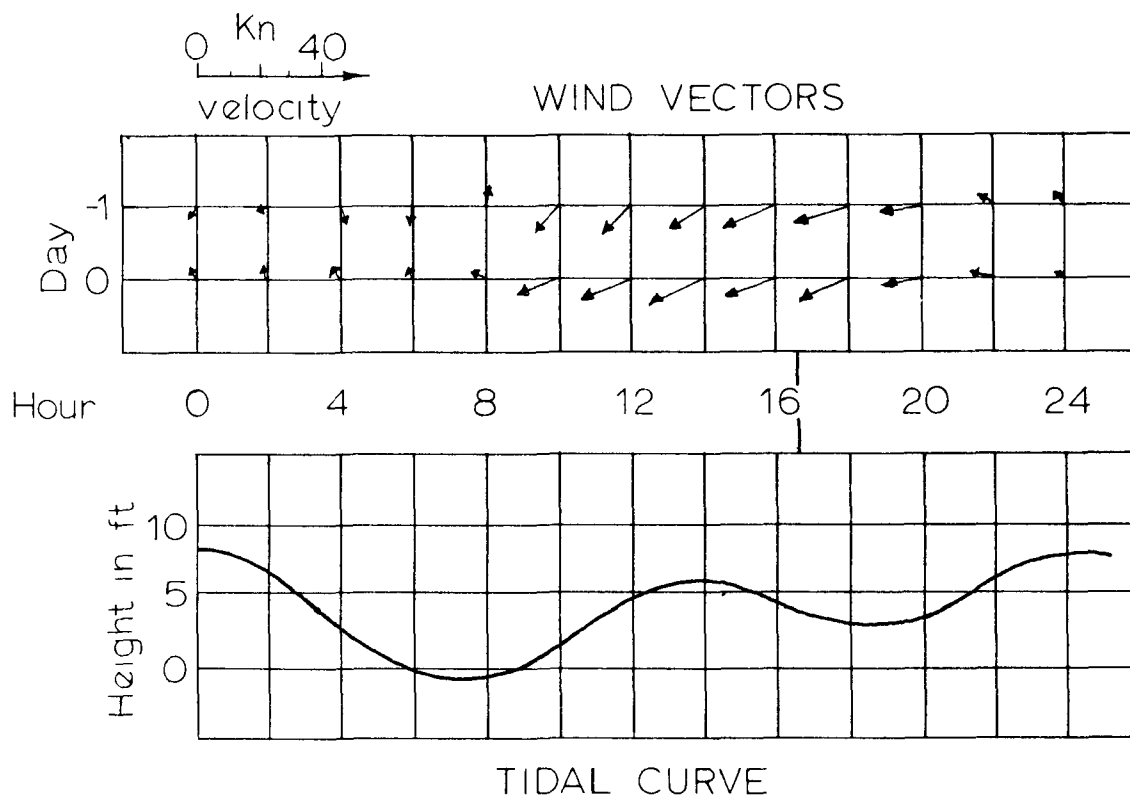


Figure 88. Data for May 10, 1971.



Figure 89. Aerial photo of outfall area on May 13, 1971 from 6000 feet at 14:10.

Flow = 6050 gpm

$V_x =$             fps

Area = 197    Ac

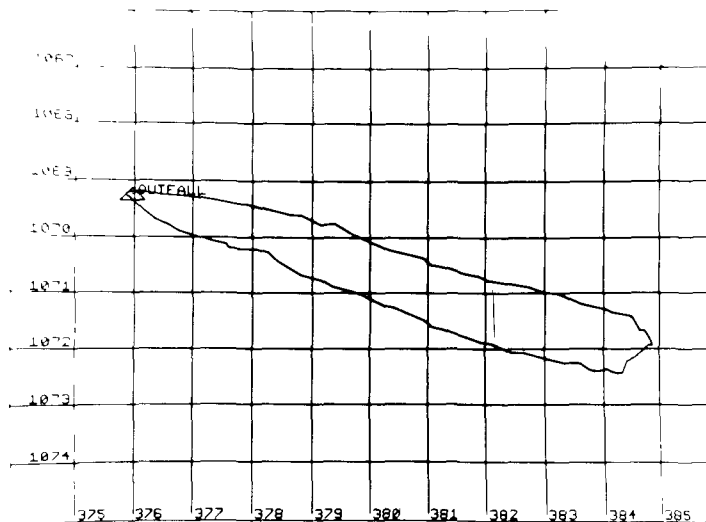
$D_x =$             ft<sup>2</sup>/sec

$D_y =$             ft<sup>2</sup>/sec

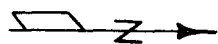
→ current  
vector

x foam

△ outfall



1000-ft grid



TEK PLOT

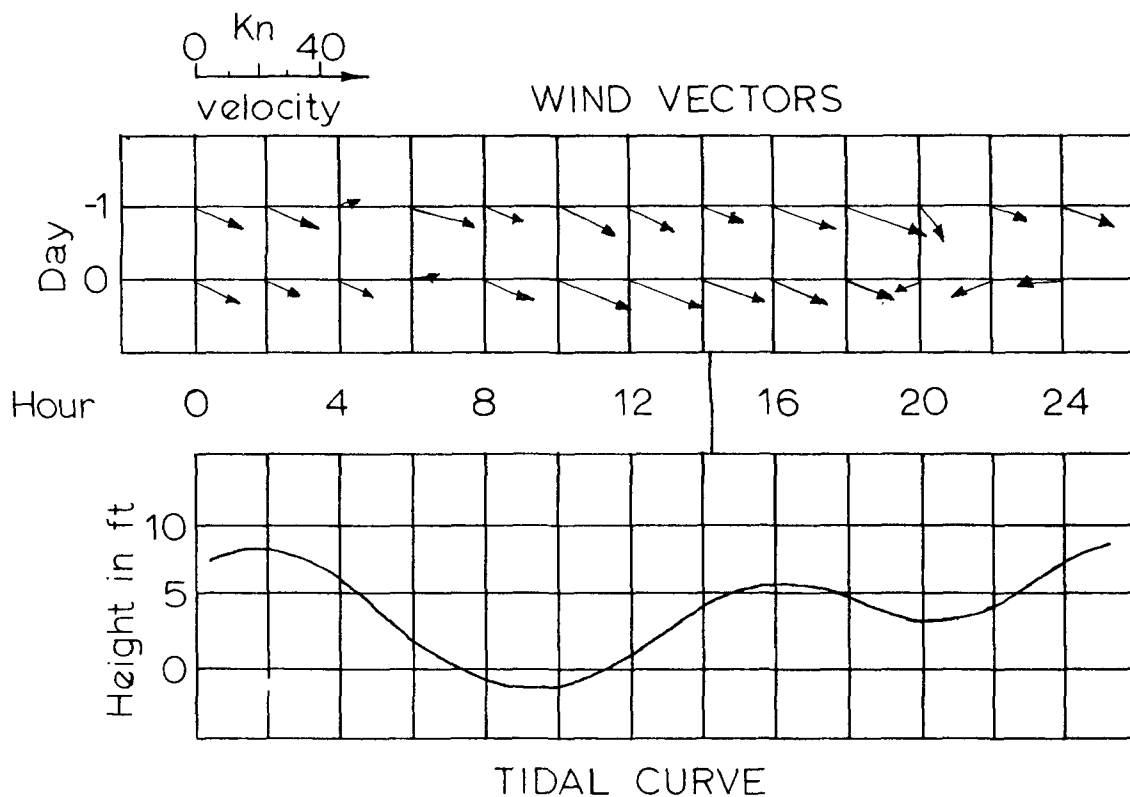


Figure 90. Data for May 13, 1971.



Figure 91. Aerial photo of outfall area on May 14, 1971  
from 4000 feet at 14:48.



Flow = 5800 gpm

$V_x = 0.3$  fps

Area = 112 Ac

$D_x = 24$  ft<sup>2</sup>/sec

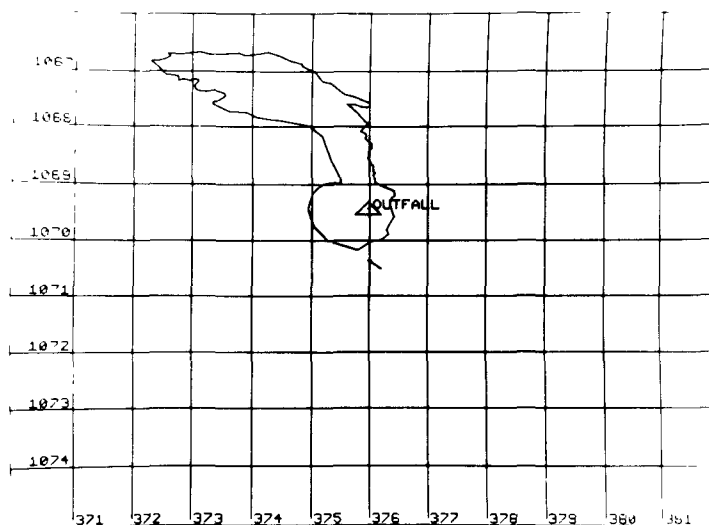
$D_y = 0.1$  ft<sup>2</sup>/sec

→ current  
vector

x foam

△ outfall

1000-ft grid



TEKPLOT

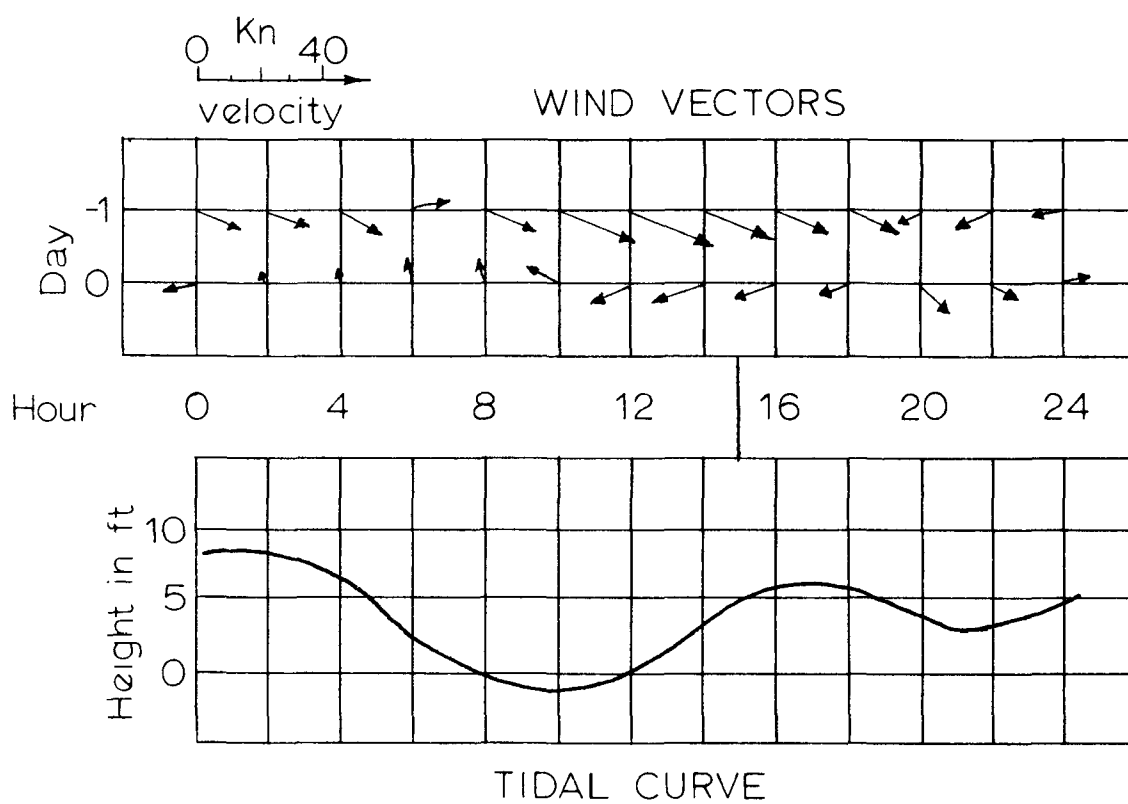
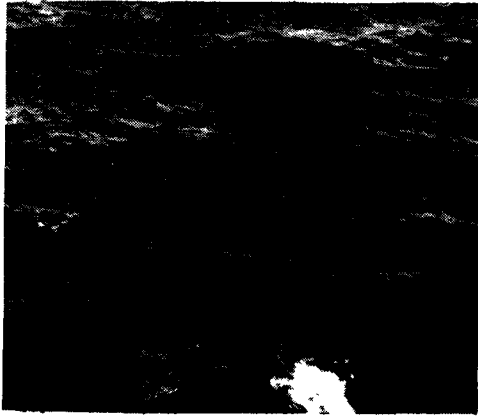
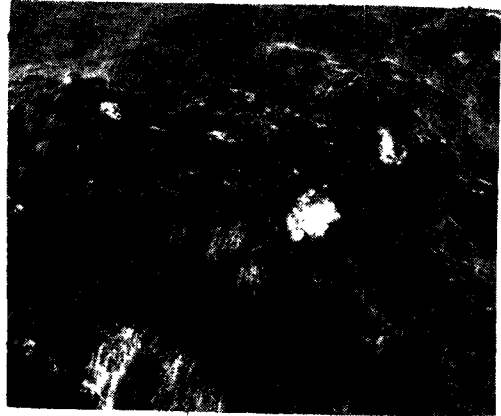


Figure 92. Data for May 14, 1971.



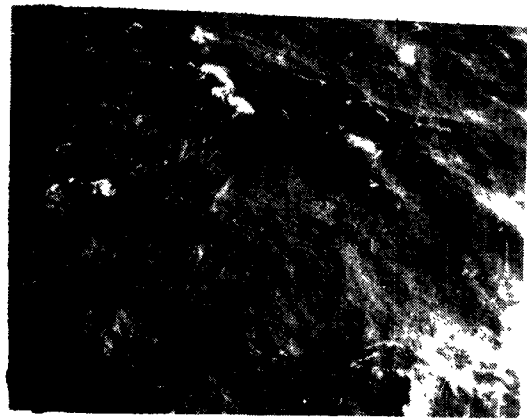
Wind 15 kts



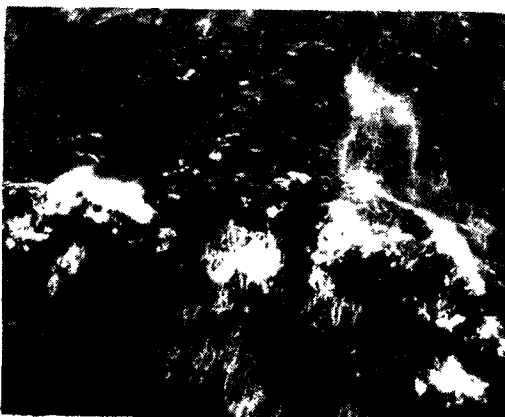
Wind 20 kts



Wind 25 kts



Wind 30 kts



Wind 40 kts



Wind 50 kts

Figure 93. Photos of sea conditions (from Neumann & Pierson, Jr., 1966).

Table 6. Wind scales and sea descriptions (after Bascom 1964).

Beaufort Scales	Wind Velocity Knots	Description	Wave Heights feet	State of Sea Code
1	1-3	Light air; ripples-no foam crests.	0	0
2	5	Light breeze; small wavelets, crests have glassy appearance and do not break.	0-1	1
3	10	Gentle breeze; large wavelets, crests begin to break. Scattered whitecaps.	1-2	2
4	15	Moderate breeze; small waves becoming longer. Frequent whitecaps.	2-4	3
5	20	Fresh breeze; moderate waves taking a more pronounced long form; mainly whitecaps, some spray.	4-8	4
6	25	Strong breeze; large waves begin to form extensive whitecaps everywhere, some spray.	8-13	5
7	30	Moderate gale; sea heaps up and white foam from breaking waves begins to be blown in streaks along the direction of the wind.	13-16	5-1/2
8	40	Fresh gale; edges of crests break into spindrift. The foam is blown in well-marked streaks along the direction of the wind.	16-20	6
10	50	Whole gale. The surface of the sea takes on a white appearance. The rolling of the sea becomes heavy.	20-30	7

Table 7. Summary of the 1970-71 data.

Date	Effluent Flow, gpm	Time Between Flights Seconds	Current Velocity, ft/sec	Plume Area, Acres	Diffusion	Coefficients	Tide ht - ft + flood - ebb	State of Sea Code
					$D_x$ ft <sup>2</sup> /sec	$D_y$ ft <sup>2</sup> /sec		
9-9-70	5850	1920	0.3	275	12.9	0.4	4 +	4
9-23-70	5900	1500	0.1	28	3.2	0.1	4 +	2
9-30-70	6950	780	0.74	128	7.5	0.1	4 -	3
10-7-70	7450	-----	-----	9	-----	-----	6.5+	2
10-12-70	7650	-----	-----	89	-----	-----	2.5-	3
12-21-70	-----	1200	2.0	18	7.3	1.9	2.5-	3
12-23-70	-----	540	1.1	26	5.1	0.7	4 -	2
12-31-70	8700	360	1.4	-----	7.9	0.6	7.5+	5
1-2-71	6950	600	0.6	36	1.7	0.5	3 +	2
2-6-71 am	6450	720	0.3	193	3.6	0.0	5 -	2
2-6-71 pm	6450	-----	-----	200	-----	-----	1.5-	2
3-16-71	5750	-----	-----	22	-----	-----	4 +	5
3-17-71	5600	2100	0.3	126	5.1	1.0	5 +	4
3-18-71	5950	1920	0.7	111	0.4	0.3	0.5+	2
3-19-71 am	4500	900	0.3	73	1.2	0.4	1 -	2
3-19-71 pm	4500	-----	-----	83	-----	-----	1 +	2
3-24-71	7850	1500	0.3	58	1.2	0.0	0 +	3
4-12-71	7700	2040	0.4	7	8.1	0.2	5.5-	2
4-15-71	7700	-----	-----	68	-----	-----	4.5+	3
4-21-71	5850	1020	0.5	166	0.3	0.0	0.5-	2
4-26-71	5800	1980	0.3	464	13.9	0.2	6.5-	3
5-7-71	6350	-----	-----	34	-----	-----	2.5-	3
5-10-71	5975	1680	0.7	71	2.8	0.1	4 -	3
5-13-71	6050	-----	-----	197	-----	-----	4.5+	4
5-14-71	5800	1980	0.3	112	2.4	0.1	5 +	3

## SECTION XI

### DISCUSSION OF RESULTS

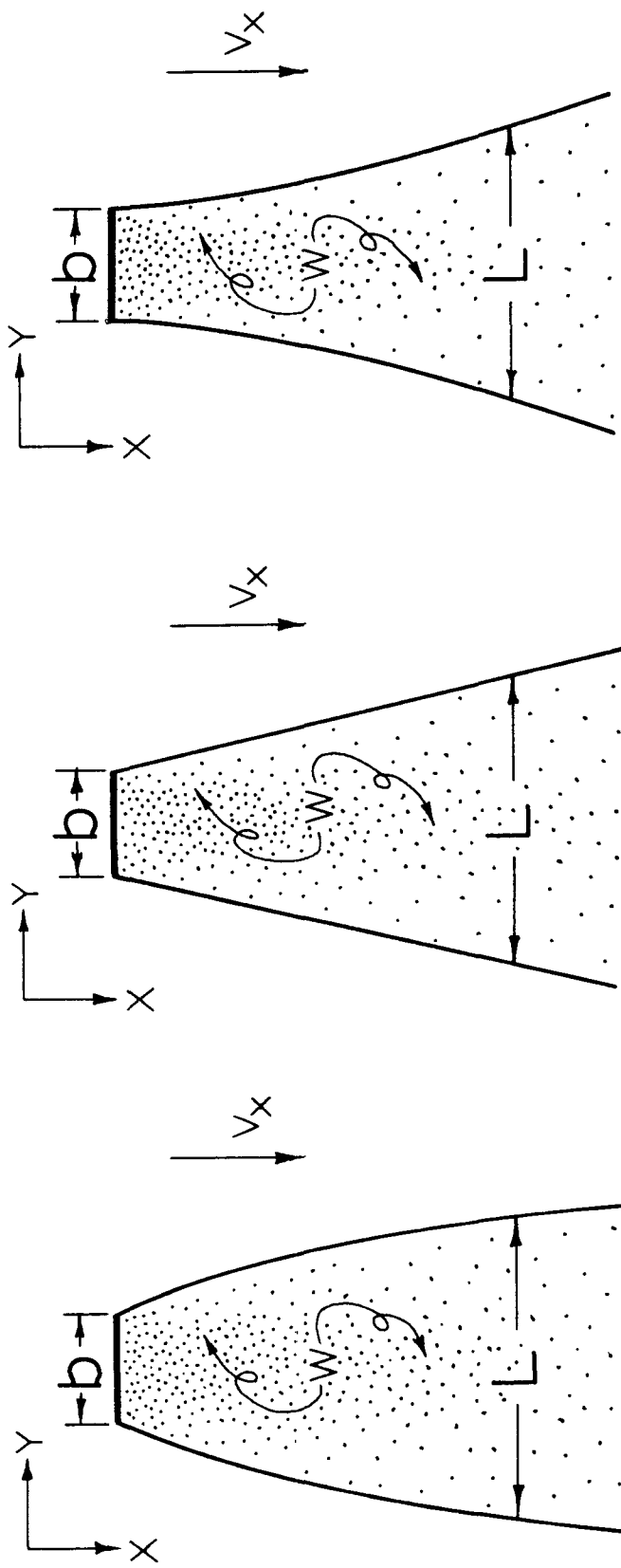
During the 1968 and 1969 field seasons, field work was conducted during the summer. Since boat work was required in the nearshore area, data acquisition was limited to periods of relatively calm seas when the swell seldom exceeded five ft and the current velocity was generally less than 0.5 ft/sec. Boat work was discontinued during the 1970-1971 season and field work was conducted during the fall, winter and spring when rough sea conditions prevailed and current velocities greater than 0.5 ft/sec were common.

#### One Dimensional Diffusion Model

As a result of the various plume patterns observed over the period of the project, the Fickian diffusion model with a unidirectional transport velocity appears to provide a reasonably accurate description of the surface transport and dilution process when the current velocity in the receiving water is high. A sketch showing the steady state plume patterns expected from a line source with a unidirectional velocity is given in figure 94. If the diffusion coefficient ( $D_y$ ) is constant, the widths of the plume should increase with the distance downstream from the outfall at a decreasing rate or the sides of the plume should be concaved inward. The center sketch in figure 94 shows the plume shape for a diffusion coefficient that increases linearly with the scale. For this model the sides of the plume are straight. If, however, the diffusion coefficient varies to a larger power of the scale such as the  $4/3$  power, the plume width should increase at an increasing rate or the sides of the plume should be concaved outward.

Sinusoidal oscillations along the length of the plume will cause the width to increase faster than normal. From the dye patch studies, the diffusion coefficient in the x-direction was generally several times greater than that in the y-direction or normal to the flow. In a steady state plume, the longitudinal diffusion coefficient is not effective in reducing the waste concentration because of the small change in concentration gradients in the x-direction. Oscillations along the length of the plume will cause the width of the plume to increase at a faster rate than would normally be expected from the magnitude of the lateral diffusion coefficient. A curved plume pattern will create large changes in the concentration gradient in the x-direction and the longitudinal diffusion coefficient will become effective in reducing the waste concentration.

A diffusion model with a unidirectional transport velocity is not applicable to the plume pattern when the current velocity in the receiving water is low. Figure 95 is an isoconcentration plot of the waste field on August 8, 1968. The outfall is located near the upper



$$D_y = \text{Constant} \qquad D_y = K \left( \frac{L}{b} \right) \qquad D_y = K \left( \frac{L}{b} \right)^{4/3}$$

$$D_y \frac{\partial^2 W}{\partial Y^2} - V_x \frac{\partial W}{\partial X} + aW = 0$$

Figure 94. Plume patterns for a unidirectional transport velocity.

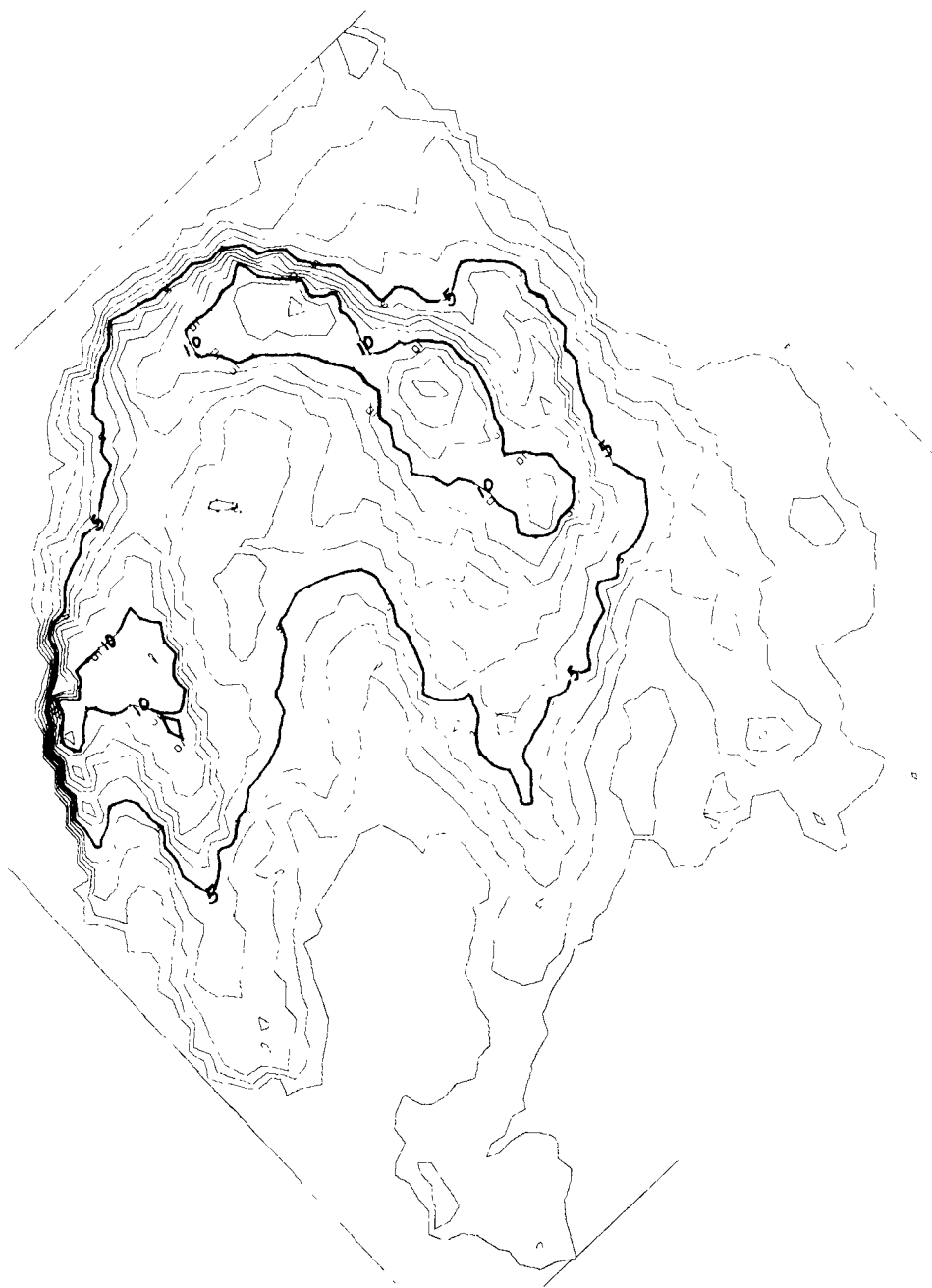


Figure 95. Isoconcentration plot, August 8, 1968.

center of the plot and the plume extends downward. The plume is 2400 ft wide and 3000 ft long. Concentrations shown on the plot are in ml/L. The diffusion coefficients computed from the one dimensional model are listed in table 8 for August 8, 1968. It can be seen that the diffusion coefficients computed from the change in variance between each fifth section along the axis of the plume are extremely high at the head of the plume with a few negative values toward the tail of the plume. While the sea was choppy, the initial spreading of the waste field was not due to diffusion but rather to the surface spreading of a source in a uniform stream. The average initial dilution over the outfall was about 1:100. The sea water, when combined with an effluent discharge rate of 12.4 cfs, would create a source with a strength of 1240 cfs over the outfall near the surface and a sink of nearly equal strength below the surface. The subsurface sink in general draws water upstream from the outfall similar to the draw down on a well in an aquifer, while the surface source discharges its water downstream. The vertical jet from the diffuser section of the outfall provides the connection for the transfer between the sink and source and supplies the energy necessary to lift the dense subsurface water from the bottom to the sea surface.

#### Potential Flow

Figure 96 shows a line source of strength  $\alpha$  in a uniform flowing stream. The velocity of the uniform flow is  $U$  and

$$\alpha = \frac{Q \text{ (DIL)}}{b \text{ (DEP)} 2\pi} \quad (108)$$

Where  $Q$  is the effluent discharge rate in cfs, DIL is the dilution over the outfall,  $b$  is the length of the diffuser section and DEP is the average depth of the waste field. The potential flow is given by

$$\begin{aligned} \Omega &= \phi + i \psi \\ &= -UZ + \int_{-b/2}^{b/2} \ln (iZ - y') dy' \end{aligned} \quad (109)$$

Where  $\phi$  is the potential function,  $\psi$  is the stream function and

$$Z = x + iy \quad (110)$$

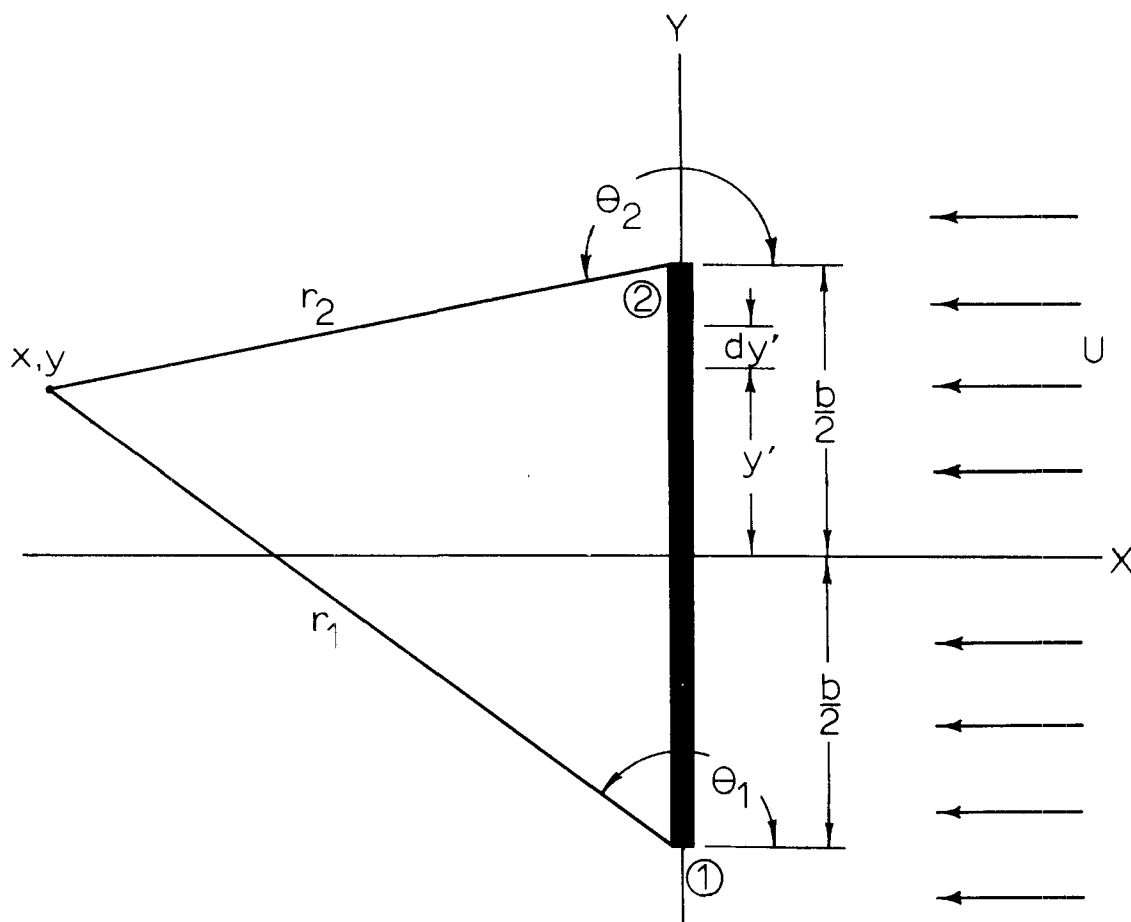
Equation 109 can be reduced to

$$\begin{aligned} \psi &= -UZ \\ &+ \alpha(iZ + b/2) \ln (iZ + b/2) \\ &- \alpha(iZ - b/2) \ln (iZ - b/2) \end{aligned} \quad (111)$$



Table 8. Preliminary diffusion coefficients, flight 2, August 8, 1968.

Section	Width Ft	Eff. Depth Ft	Sigma Y Ft	Coefficient PPT	State Plane Coordinates X Y	Diffusion Coefficient Ft <sup>2</sup> /sec Fifth Sec.	Diffusion Coefficient Ft <sup>2</sup> /sec Average
11	1007	9.6	3.160E 02	6.221E 00	1069767 375748	4.145E 01	4.145E 01
16	1429	3.5	4.215E 02	1.273E 01	1069428 375611	3.372E 01	3.758E 01
21	2059	3.3	5.252E 02	1.090E 01	1069277 375351	4.250E 01	3.922E 01
26	2475	3.3	6.169E 02	9.309E 00	1069136 375084	4.539E 01	4.076E 01
31	2613	3.5	7.055E 02	7.634E 00	1069031 374795	5.078E 01	4.277E 01
36	2784	4.4	7.147E 02	6.028E 00	1068938 374497	5.677E 00	3.659E 01
41	3091	6.5	6.748E 02	4.315E 00	1068904 374162	-2.406E 01	2.792E 01
46	3080	9.4	6.461E 02	3.104E 00	1068785 373881	-1.638E 01	2.238E 01
51	2207	14.2	6.958E 02	1.915E	1068407 373769	2.886E 01	2.310E 01
<div> <div>Flow Rate 12.4 CFS</div> <div>Sun Az. from S. 1.398 Rad.</div> <div>Current Velocity .26 FPS</div> <div>Sun Altitude .567 Rad.</div> </div> <div> <div>Area Within Each Concentration Range</div> <div>Range ml/l</div> <div>Area Sq Ft</div> <div>0- 2 2.477E 06</div> <div>2- 4 1.616E 06</div> <div>4- 6 9.036E 05</div> <div>6-10 1.613E 06</div> <div>10-15 2.376E 05</div> </div>							



### Line Source in a Uniform Stream

Figure 96. Geometry for a line source in a uniform stream.

from which the stream function is

$$\psi = -UY + \alpha \left[ \left( Y + \frac{b}{2} \right) \theta_1 - \left( Y - \frac{b}{2} \right) \theta_2 - X \ln \frac{r_1}{r_2} \right] \quad (112)$$

where

$$\tan \theta_1 = \frac{\left( Y + \frac{b}{2} \right)}{X} \quad (113)$$

$$\tan \theta_2 = \frac{Y - \frac{b}{2}}{X} \quad (114)$$

The value of the stream function along the axis of the plume ( $y = 0$ )

is

$$\psi = \alpha b \pi \quad (115)$$

While the value of  $y$  when  $\psi = 0$  and  $x$  approaches  $\infty$  is

$$y = \frac{\alpha b \pi}{U} \quad (116)$$

The values of the  $x$  and  $y$  velocity components are given by

$$V_x = \frac{\partial \psi}{\partial y} = -U + \alpha(\theta_1 - \theta_2) \quad (117)$$

$$V_y = \frac{-\partial \psi}{\partial x} = \alpha \ln \left( \frac{r_1}{r_2} \right) \quad (118)$$

Equation 112 was programmed to solve for the  $x$  and  $y$  coordinates of the streamlines. Two plots from the Tektronix plotter are shown in figure 97. The source strength for each plot is 300 cfs per ft of depth. A state plane coordinate grid is drawn and labeled at 1000-ft intervals. The outer streamline defines the plume boundary if the diffusion effluents were equal to zero. This plume can also be reproduced from the following modification of the diffusion model (equation 56).

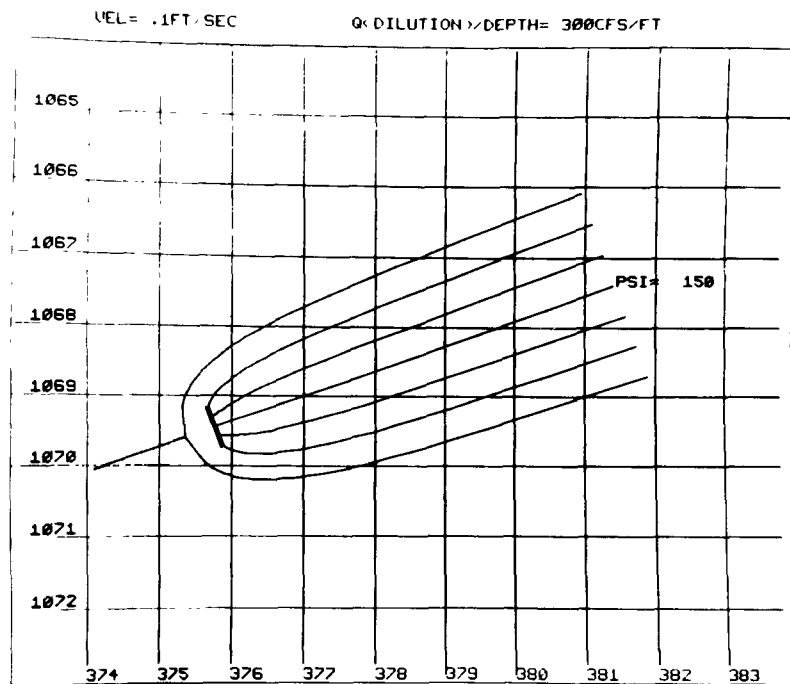
$$\frac{\partial W}{\partial t} = - \left[ \frac{\partial}{\partial Y} (V_y W) + \frac{\partial}{\partial X} (V_x W) \right] \quad (119)$$

where the  $x$  and  $y$  components of the velocity are determined from equations 117 and 118. The model given by equation 119 would be applicable when the sea is calm and the diffusion coefficients low.

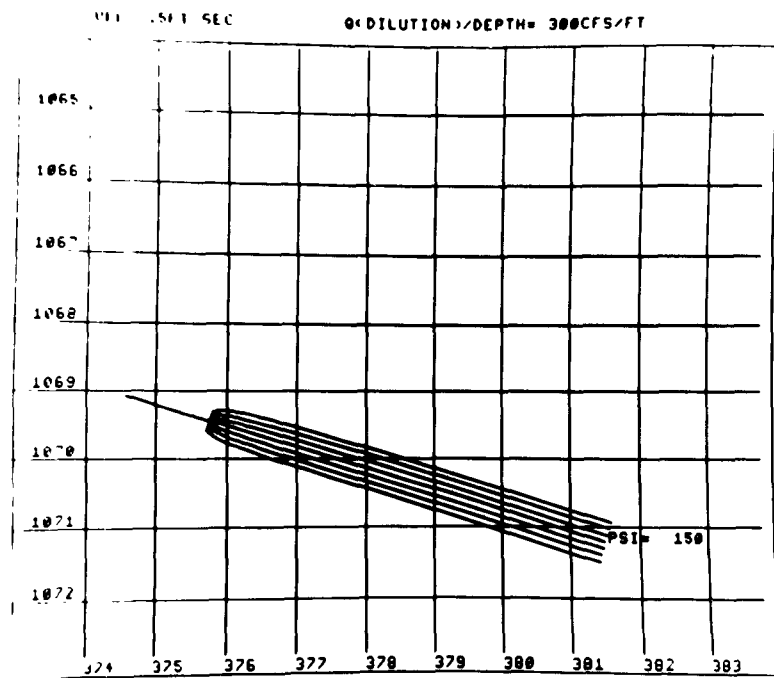
On each plot in figure 97 the outer streamline has a value of zero while the centerline has a value of 150 as given by equation 115. The two plots are for line sources oriented perpendicular to a uniform stream of 0.1 and 0.5 ft/sec, respectively.

The four streamline sketches in figure 98 are for a line source of strength 300 cfs per ft of depth in a uniform stream of 0.0, 0.1, 0.3 and 0.5 ft/sec, respectively. The streamlines were traced from Tektronix plots such as those shown in figure 97. At zero current velocity, the waste field lakes or ponds about the outfall area. As shown in figure 98, the potential flow solution would give a downstream plume width of 3000 ft in a uniform stream of 0.1 ft/sec. As the current velocity increases, the plume width decreases to 1000 ft at 0.3 ft/sec and 600 ft at 0.5 ft/sec. The minimum width of the plume would be the length of the diffuser section.

When a waste water stream discharged from a submerged outfall spreads at the surface, the resulting drift flow plume pattern is influenced



a



b

Figure 97. Plots of a source in a uniform stream.

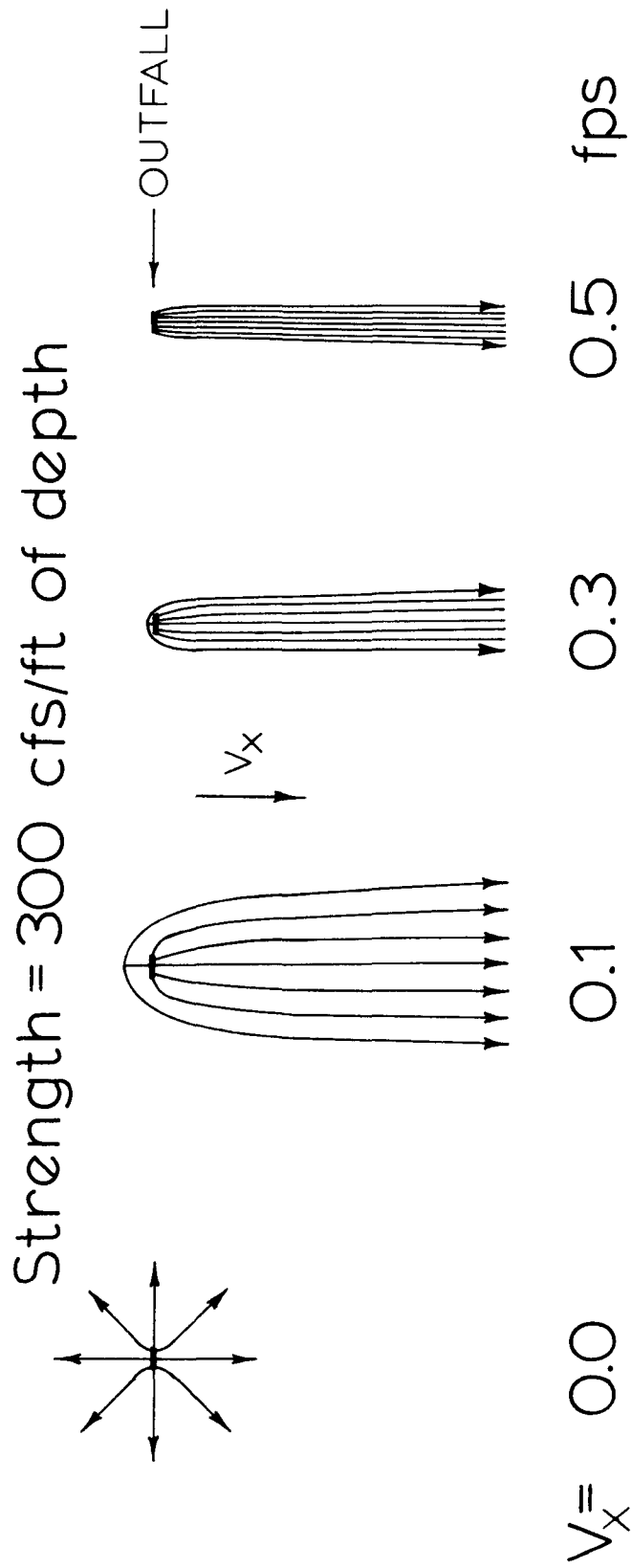


Figure 98. Potential flow solutions for a line source.

by the ambient current velocity and the amount of residual buoyancy and momentum (if any) in the waste stream (Baumgartner and Trent, 1970). Rather accurate methods are available to calculate dilutions in the buoyant jet, neglecting the influence of ambient currents in this region. When density stratification occurs in the region surrounding the outfall, a plume can form without residual buoyancy and these dilution models can be used to determine the depth at which the lens first forms, whether or not portions of the plume rise to the surface (Baumgartner, Trent and Byram). This model offers a means for estimating the initial concentration and depth of the drift flow plume. The initial width and curvature of the surface plume can be estimated using a potential flow solution for a source in a uniform stream. For a single outfall port a point source would be used and for a multiport diffuser, a line source over the diffuser length can be used. In this way the relative influence of the ambient current, diffuser length and orientation can be evaluated.

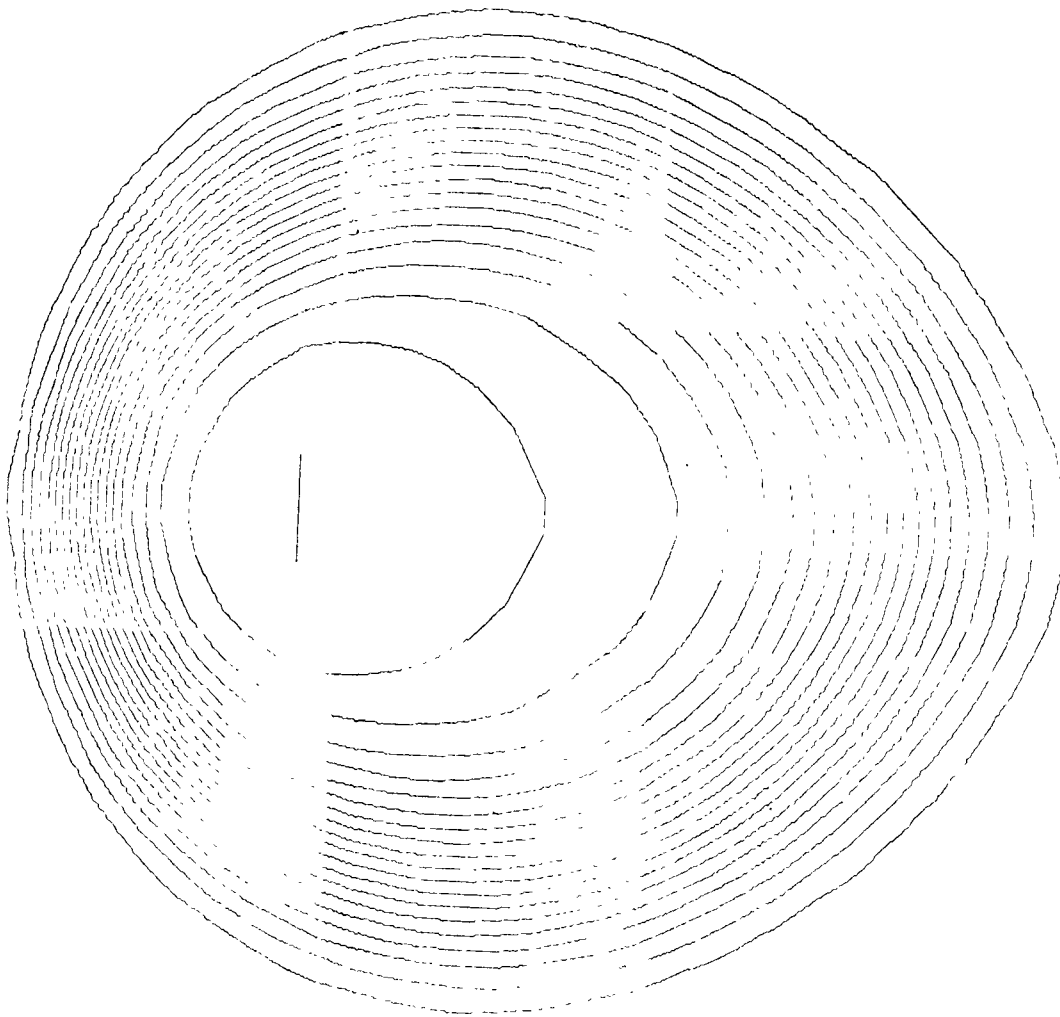
### Diffusion Model

In order to gain insight into the Fickian diffusion model and to determine the relative importance of the terms in the equation on the plume shape, a modified form of equation 56 was programmed so that the waste field could be simulated on the computer. For the computer model, the vertical diffusion coefficient ( $D_z$ ) and the velocity in the vertical direction ( $V_z$ ) in equation 56 were set equal to zero. In the resulting two-dimensional model the loss of waste to the lower layers due to vertical mixing was considered by substituting a decay term ( $-kW$ ) for the sink term in equation 56. The resulting two-dimensional diffusion equation is:

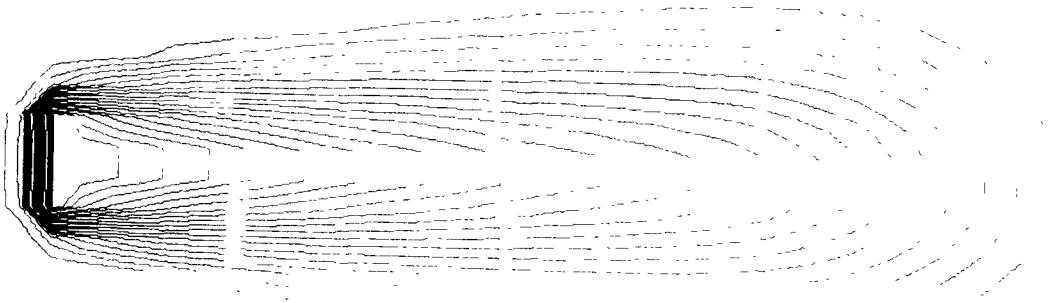
$$\begin{aligned} \frac{\partial W}{\partial T} = & \frac{\partial}{\partial Y} \left( D_y \frac{\partial W}{\partial Y} \right) + \frac{\partial}{\partial X} \left( D_x \frac{\partial W}{\partial X} \right) \\ & - \left[ \frac{\partial}{\partial Y} (V_y W) + \frac{\partial}{\partial X} (V_x W) \right] - kW \end{aligned} \quad (120)$$

The initial condition for the model was that the concentrations throughout the waste field were zero. At the start of each incremental time period, the waste concentration for the elements in the array at the outfall were set equal to the concentration that resulted from the initial jet dilution. During each incremental time period the waste field is moved or convected in the array, diffused and decayed according to the model.

Two isoconcentration plots from this model are shown in figure 99. The outfall is located at the top of each plot and the plume extends downward. Current velocities for the two plots were 0.1 ft/sec and 0.5 ft/sec, respectively, while the diffusion coefficients were  $D_y = D_x = 2 \text{ ft}^2/\text{sec}$ . A source strength of 300 cfs/ft of depth was used to determine the current velocity components. The print out time was 90 minutes from the start of the effluent discharge, and the decay



$U = 0.1 \text{ ft/sec}$



$U = 0.5 \text{ ft/sec}$

Figure 99. Isoconcentration plots from diffusion model.

coefficient was 0.1 per hour.

### Temperature

Vertical density stratification can cause the waste field to be formed below the sea surface. Of the 21 sampling runs conducted during the summers of 1968 and 1969, a surface plume was observed on eight days, the plume was submerged on six days and the waste field was not observed on seven days due to fog or rain. During these two summers a surface plume occurred for only 60% of the observations. Generally, the plume was not visible when the sea was calm. However, of the 25 observations conducted in the fall of 1970 and the winter and spring of 1971, the plume was not visible on only one day which was when the sea was extremely rough.

Changes in density can be caused by a variation in temperature and or salinity. Fresh water runoff from the coastal streams is at a minimum during the summer months and variations in temperature are generally the major cause of vertical density stratification in the nearshore area during the summer. Upwelling, which occurs during the summer, brings to the surface the more dense subsurface water rich in nutrients. Upon reaching the surface, plankton begin growing. This suspended material reduces the transparency of the water and increases the sunlight absorption coefficient. Under relatively calm sea conditions, a thin surface layer of dark green water warms rapidly and can become lighter than the less saline subsurface water. During periods of upwelling, there is generally a narrow band of clear water between the land and the dark green offshore water. In addition to the seasonal variation in temperature there is also a diurnal variation. The diurnal thermocline is especially prominent during calm summer days. The sketch in figure 100 shows the progressive variation in vertical temperature structure for various times of the day.

The absorption of solar radiation by the upper layers is readily apparent as the surface temperature increases to a late afternoon maximum and then decreases as the sun sets. Typical diurnal thermoclines may be as much as 30 feet deep and perhaps as much as 1° or 2° C in magnitude, though usually they are somewhat less. If a good breeze is blowing, the upper layers will become mixed, carrying the warm water to greater depths, having the effect of increasing the depth of the diurnal thermocline, but decreasing its magnitude, as the absorbed heat is spread out over a large volume of seawater.

### Wind

Water currents in the nearshore area can be caused by a combination of factors including wind, tide, waves, and the general ocean circulation patterns. The importance of each of the several factors vary with both time and location. The topographic configuration of the shore, bathymetry of the area, pressure gradients and Coriolis forces will tend to



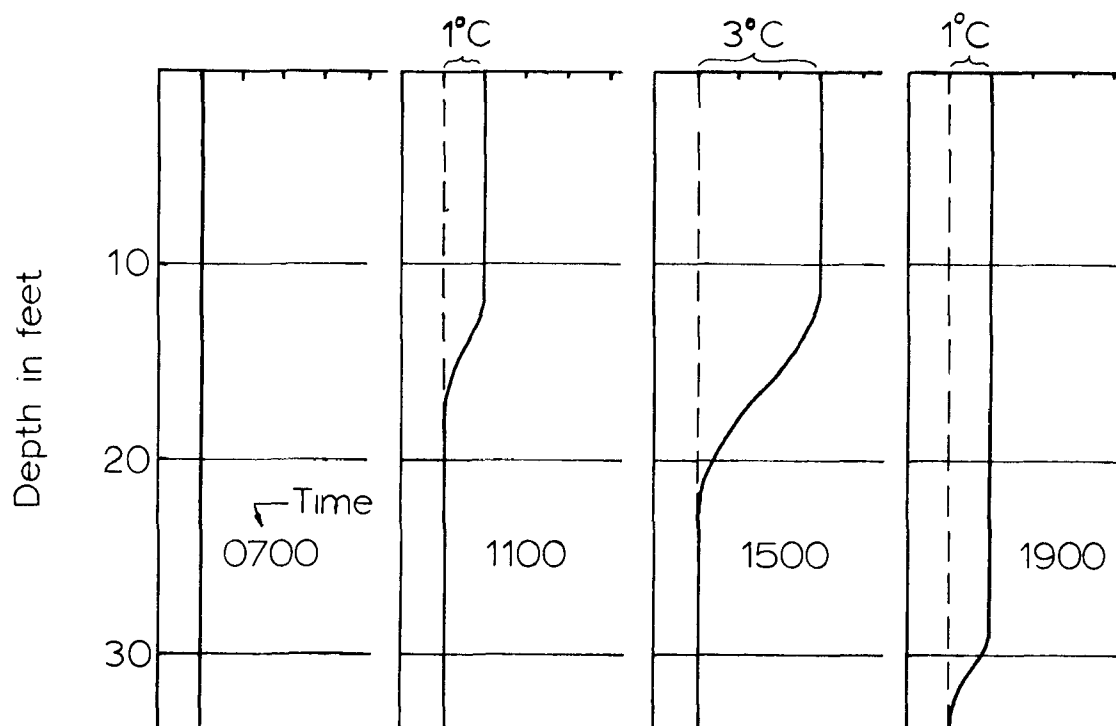


Figure 100. Typical diurnal thermoclines.  
(After Williams, Higginson & Rohrbough, 1968).

modify the flow pattern. Near the entrance to Yaquina Bay, there are large tidal currents while along the surf zone the wave height, beach slope and the angle the wave crests make with the beach are important considerations in estimating the longshore current. In the nearshore area of the outfall, wind appears to be the dominant factor in estimating water currents (Burgess and James, 1970 and Keene, 1971). The wind not only supplies energy for water transport but also energy in the form of turbulence.

The relationship between the wind and the water current velocity depends on the fetch, duration and magnitude of the wind as modified by the topography near the boundary of the sea. Diurnal variations in the coastal winds are common. An example of the effect of a shifting wind on the current velocity profile is given in figure 101. As the wind begins blowing, only the surface is affected. As the duration increases, the sea becomes turbulent and the energy is transferred deeper into the water. If the wind continues long enough in the same direction, the effect of the bottom drag may influence the velocity profile in the shallow areas. A reversal of the wind will affect the surface water first and will cause a change in the surface velocity vector. The surface waters can move in a direction opposite that of the subsurface water.

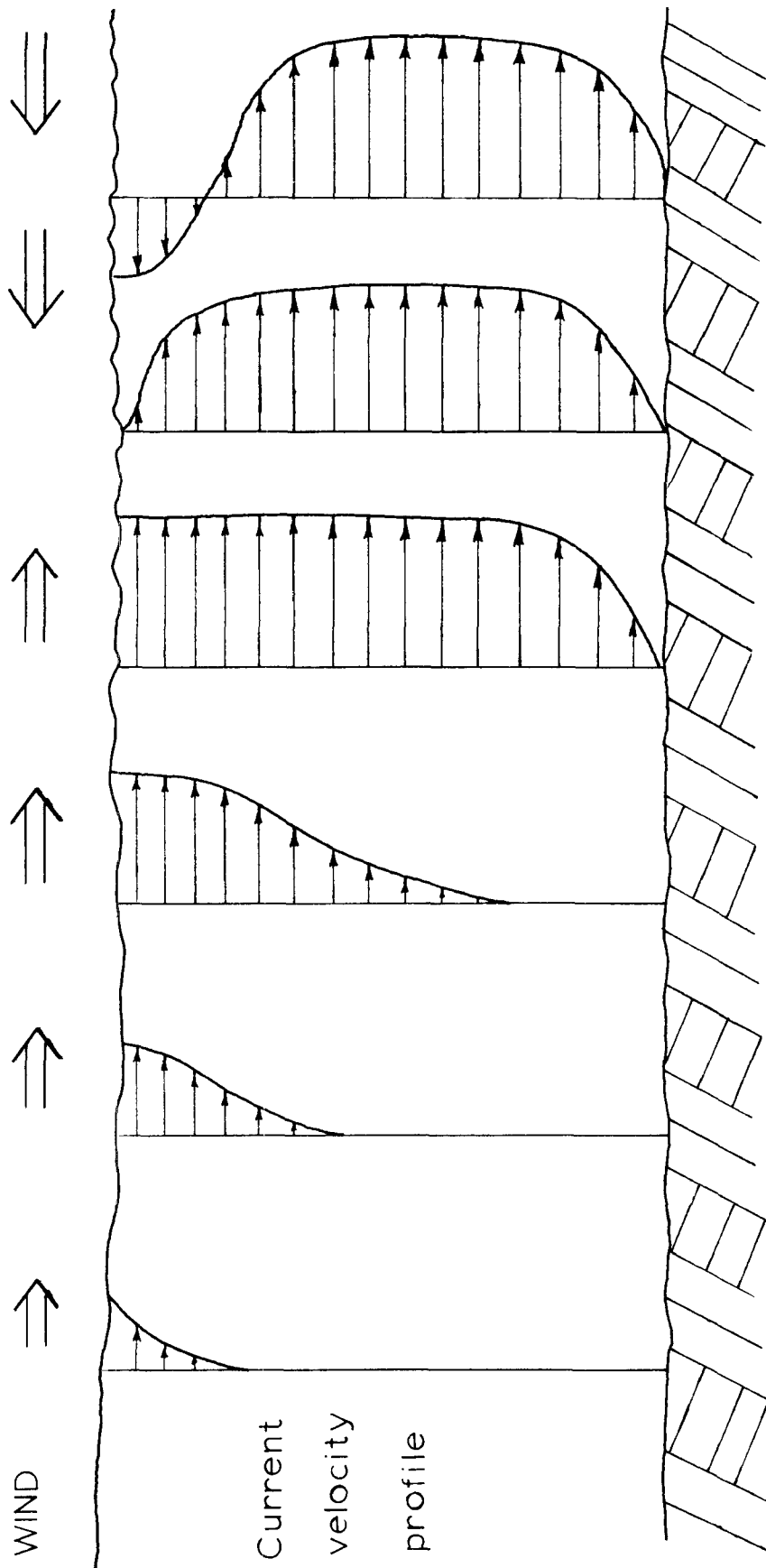


Figure 101. Development of current velocity profile.

### Sea State

Wind provides turbulent energy for mixing of wastes discharged into the ocean. When the horizontal velocity changes with depth, vertical turbulence will transfer mass between layers and will cause a slug discharge of waste to spread faster along the direction of motion than normal to the current direction. From the dye patch studies, large longitudinal diffusion coefficients can be expected when the wind first starts blowing or it changes direction.

The observations of the waste field during the 1970-71 field season were divided into three categories depending on the apparent dominant form of turbulent energy. These classes were: 1) sea surface roughness caused primarily by the wind, 2) sea roughness due to heavy swell, and 3) the sea state influenced by both the wind and breakers in the area.

Table 9 lists the observations for which wind was the main cause of the sea state. These dates are listed in order of increasing sea turbulence as determined by a visual interpretation of the photos. For all except two observations, the dye patch was elongated parallel to the wind. On April 26 the dye patch was oriented parallel to the water current while on September 9 the dye patch was v-shaped with one leg oriented parallel to the water current and the other leg oriented parallel to the wind.

Diffusion coefficients ranged from 3.0 to 14 ft<sup>2</sup>/sec in the longitudinal direction and 0.0 to 1.0 in the transverse direction. The diffusion coefficient determined for a one dimensional model from the 1968-1969 data were 11 ft<sup>2</sup>/sec and 14 ft<sup>2</sup>/sec on August 16, 1968, and July 8, 1969, respectively. The state of the sea code for both of these days was 3. The wind was 10-15 kts on August 16 with 6-ft swell and 15-kt wind on July 8 with a choppy sea.

Table 10 shows the sea state when the turbulence is due mainly to heavy swell. The diffusion coefficients ranged from 1.2 to 8 ft<sup>2</sup>/sec in the longitudinal direction and 0.0 to 1.9 in the transverse directions for a sea state code ranging from 3 to 5.

Table 11 lists the sea state for turbulence due to both wind and swell. Diffusion coefficients were not determined for rough sea condition but only for a sea state of 2. The values of the longitudinal and transverse diffusion coefficients were more nearly equal to each other for this condition than for either of the conditions represented in tables 9 or 10.

The waves normally observed at sea are composed of two types. The swell is a long and relatively symmetrical wave form having a period greater than 10 seconds, generated by winds at some distance from the area, and in the nearshore area is oriented nearly parallel to the

Table 9. Sea state due primarily to wind.

Date	Figure no.	Diffusion coef		State <sup>(1)</sup> of sea	Remarks
		$\frac{\text{ft}^2/\text{sec}}{\text{Dx}}$	$\text{Dy}$		
April 12	77	8.1	0.2	2	Strong east wind in oppo- site direction to swell.
Oct. 7	49	-	-	2	Very lightly mottled photo pattern.
Dec. 23	55	5.1	0.7	2	A curved dye patch. Wind changed from E to NE.
Feb. 6 am	61	3.6	0.0	2	Lightly mottled photo tone. A few scattered whitecaps.
Feb. 6 pm	63	-	-	2	Lightly mottled photo tone with a few scattered white- caps.
Sept. 23	45	3.2	0.1	2	Finely mottled photo tone with scattered whitecaps.
May 10	87	2.8	0.1	3	Wind from the northwest at 15 kts for six hours. Scattered whitecaps with a mottled photo tone.
May 7	85	-	-	3	Wind changed from NW to SW at 25 kts. Finely mottled photo tone with scattered whitecaps.
May 14	91	2.4	0.1	3	Finely mottled photo pat- tern with scattered white- caps.
April 26	84	13.9	0.2	3	Finely mottled photo pat- tern with scattered white- caps. Excessive longitudi- nal dispersion of dye patch ahead of main slug.
Sept. 30	47	7.5	0.1	3	Wind parallel to the x com- ponent for 4 hours. A mot- tled photo pattern with a linear trend normal to the wind direction and frequent whitecaps.

Table 9. Continued

Date	Figure no.	Diffusion coef		State <sup>(1)</sup> of Sea	Remarks
		$\frac{\text{ft}^2/\text{sec}}{\text{Dx}}$	$\frac{\text{ft}^2/\text{sec}}{\text{Dy}}$		
May 13	89	-	-	4	Wind 30 kts from the SW for 6 hours. Coarsely mottled pattern with same linear trend parallel to the wind.
Sept. 9	43	12.9	0.4	4	Mottled photo tone with numerous whitecaps. Dye patch is v-shaped.
Mar. 17	67	5.1	1.0	4	High turbidity near shore. Wind changed direction 2 hours before. Strong linear trend due to wind waves. Numerous whitecaps. Wind from the NW 15 kts.

<sup>(1)</sup> see table 6.

Table 10. Sea state due primarily to swell.

Date	Figure no.	Diffusion coef		State <sup>(1)</sup> of Sea	Remarks
		$\frac{\text{ft}^2/\text{sec}}{\text{Dx}}$	$\frac{\text{ft}^2/\text{sec}}{\text{Dy}}$		
March 21	75	1.2	0.0	3	Waves breaking on reef S of outfall. Lightly mottled photo pattern with scattered whitecaps.
Dec. 21	53	7.3	1.9	3	Waves breaking along reef. Mottled photo pattern with a few scattered whitecaps.
Dec. 31	57	7.9	0.6	5	Waves breaking everywhere.

<sup>(1)</sup> see table 6.

Table 11. Sea state due to wind and swell.

Date	Figure no.	Diffusion coef		State <sup>(1)</sup> of Sea	Remarks
		$\frac{\text{ft}^2}{\text{sec}}$ Dx	Dy		
Mar. 18	69	0.4	0.3	2	Turbid nearshore water. Finely mottled photo tone a few whitecaps.
Mar. 19 am	71	1.2	0.4	2	Turbid nearshore water mottled photo tone.
Mar. 19 pm	73	-	-	2	Wind 15 kts from NW. Mottled photo tone with scattered whitecaps.
Jan. 2	59	1.7	0.5	2	Low wind velocity. Dye patch oriented normal to wind and parallel to direction of swell.
April 21	81	0.3	0.0	2	Wind 10 kts from the SW. Wind wave from both the NW and SW.
April 15	79	-	-	3	Frequent whitecaps. Finely mottled photo pattern. Wind 15 kts from NW.
Oct. 12	51	-	-	3	Finely mottled photo pattern with frequent whitecaps. Wind 15 kts from NW.
Mar. 16	65	-	-	5	Wind 20 kts NW for two hours. Linear trend normal to wind. Coarsely mottled photo tone with whitecaps everywhere.

<sup>(1)</sup> see table 6.

coast. The second wave type is the sea which is generated by the local winds, has a short wave period and a steep, unsymmetrical wave form.

As the wind begins flowing over the water surface, the sea changes from a mirror lake surface to a surface that includes a number of wave trains superimposed on each other. The length of each crest is short and both the wave length and height are irregular. If fetch is large enough and the wind continues long enough as listed in table 12, the significant wave height and peak energy period would be as listed in this table.

The wave forms appear on the aerial photography as a mottled pattern. The curved surfaces of the wave tend to concentrate the sunlight under the wave crest as shown in figure 102. The wave crests appear light while the trough appears dark on the photo, since the wind generated waves are unsymmetrical, the sea in general will appear rougher when viewed looking into the wind than when viewed down wind. This is also true of the oblique aerial photography.

As the wind velocity increases, the average wave length also becomes larger. On the aerial photos the photo pattern changes from a finely mottled tone to a coarse pattern. For a steady wind the mottling will generally show a linear trend normal to the wind direction. When the wind is blowing at 10 kts a few scattered whitecaps will begin appearing; as the wind increases to 15 kts there are frequent whitecaps and at 25 kts whitecaps are everywhere. When the wind exceeds about 25 kts, streaks parallel to the wind direction begin appearing.

#### Photographic Limitations

The photographic method of studying waste dispersion is subjected to interferences from several sources. Clear sky with the sun altitude above 25 degrees has given the best results. Clouds in the sky increase the water surface brightness and reduce the subsurface contrast. With the oblique camera mounting, the photography is taken to avoid the direct sunlight reflection. Polarizing filters reduce but do not eliminate the skylight reflection. Shadows from scattered clouds cause uneven lighting and will interfere with the quantitative data processing.

Kraft pulp mill effluent under certain conditions will foam when discharged into the sea. The white foam can cover areas of the plume and, where present, will prevent any photographic measurement of the waste concentration. Whitecaps and spray generated when wind velocities exceed about 15 kts can also interfere with the photographic techniques.

The natural color of the sea varies, with color gradients generally greatest perpendicular to the beach. Near the shore, turbulence in the surf zone entrains and suspends sand and silt particles. The width of this discoloration zone depends on the sea roughness and may extend

Table 12. Conditions in fully developed seas (from Bascom, 1964).

Wind velocity (kts)	Fetch (miles)	Duration (hours)	Wave <sup>(1)</sup> height (ft)	Wave <sup>(2)</sup> period (sec)
10	10	2.4	1.4	4
15	34	6.0	3.5	6
20	75	10.0	8.0	8
25	160	16.0	14.0	10
30	280	23.0	22.0	12
40	710	42.0	44.0	16
50	1420	69.0	78.0	20

(1) Average of highest 1/3

(2) Period where most of the energy is concentrated.

several thousand feet offshore. During the summer months, dark green upwelled water may appear offshore. If the plume is completely surrounded by the green water, the upwelling does not interfere with the processing; however, often due to horizontal density stratification, the dark upwelled water will form the offshore boundary of the effluent plume. Computer processing of the photographic film requires that film densities be measured throughout the photographs. This processing step can either be done automatically or semi-automatically. When the photograph is digitized automatically, film densities and photo coordinates are measured on a selected grid pattern and a large volume of data is generated. The effect of the interferences listed above can be reduced but not eliminated by computer programming techniques. In the semi-automatic digitizing procedure, the location of points for digitizing is selected manually. This method results in fewer but better data points as areas on the photograph with interferences can be avoided in this step.

#### Aerial Photography

Aerial photography provides a comprehensive method of analyzing the dispersion of wastes from existing or proposed outfall sites and is not restricted to periods of calm seas. Field data for measuring concen-



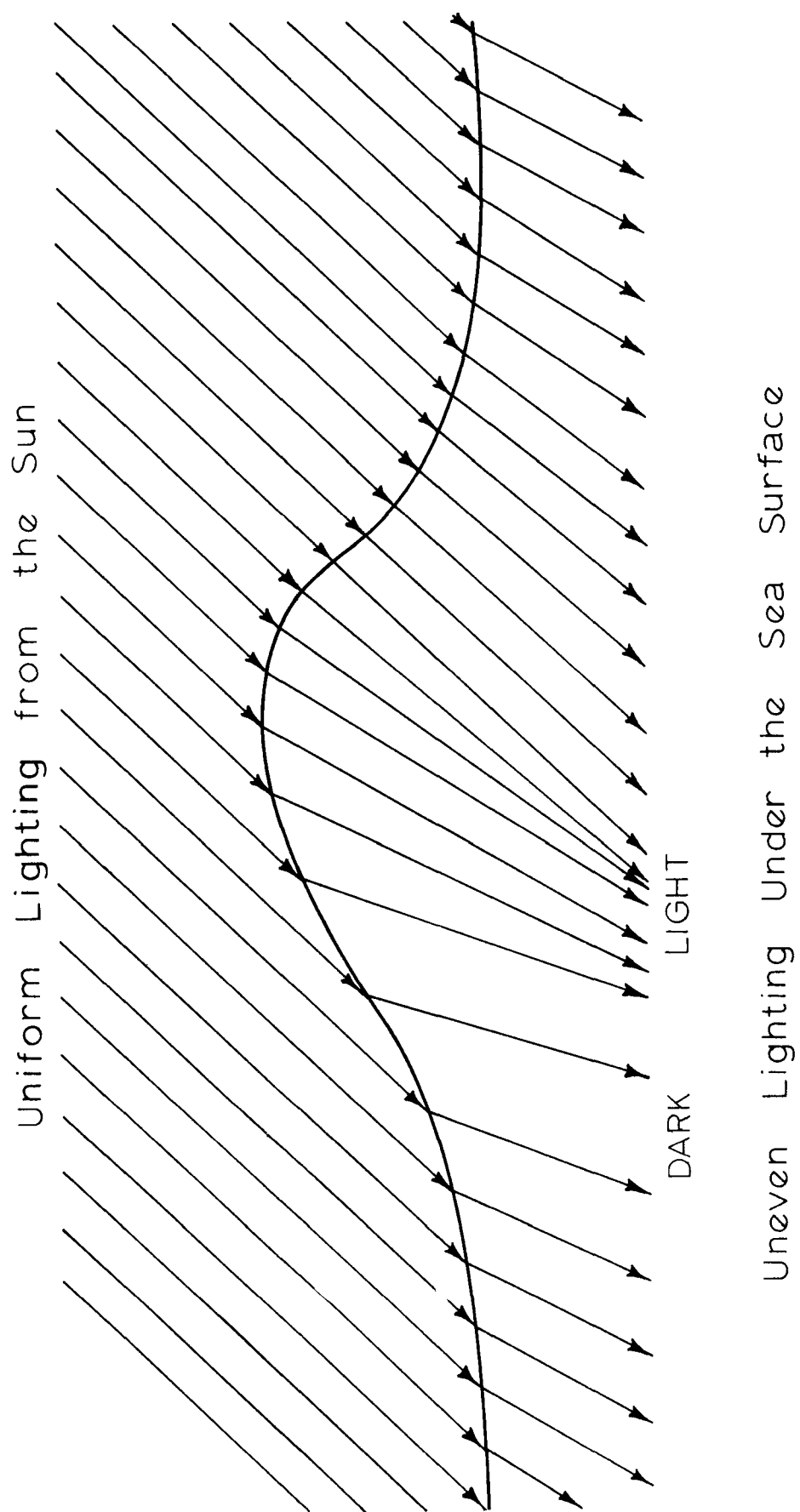


Figure 102. Mottled photo pattern from surface waves.

trations throughout the waste disposal area can be collected in a fraction of a second.

While the time required for gathering concentration data photogrammetrically is short, the computation of current velocities and diffusion coefficients require a minimum of two flights over the area. Generally photographic flights were made at 15-minute intervals. The time between flights need not be lost if several neighboring locations can be studied at the same time.

Boat sampling is hazardous in the nearshore area and is impossible during heavy seas. In order to adequately define a waste ordye field, a boat survey is conducted over an extended period of time. Since the tide, wind and currents are continuously changing, the survey does not represent a pattern at any one instant but is a composite pattern during the sampling period.

During the summer of 1969, aerial photographic surveys and conventional boat sampling surveys were conducted at the same time. The conventional survey was conducted over an eight to twelve hour period including travel time from the dock and required in addition to the boat operator, three people on the vessel to run equipment and two people on shore to locate the boat. The aerial survey team consisted of a pilot and photographer. Two 2-hour photographic flights were made, one in the morning and the second in the afternoon.

The cost of the aerial survey was essentially the same as the conventional survey. The fluorometer aboard the survey vessel cost the same as the three cameras aboard the airplane. The oblique camera mounting eliminated the need for establishing horizontal control markers in the water. A seaworthy boat and experienced operator cost about \$200 per day while an airplane and pilot cost about \$120 for four hours. The cost of the film and photographic processing range from \$30 to \$100 per day depending on the type of film.

Computerized techniques were developed for data processing of both the boat records and the aerial photography. Strip chart records from the boat instruments were digitized with the same equipment that was used to measure photographic coordinates. A densitometer would not be required for processing aerial photos from a dye patch study conducted for the purpose of acquiring design information at proposed outfall sites. The computer time for data processing would be nearly the same for the two survey methods.

The aerial survey is not limited by sea conditions, provides comprehensive information on the diffusion process and can be conducted fast with a minimum of personnel. It is a technically and economically feasible method for acquiring ocean outfall design data.

## SECTION XII

### SUMMARY

The objective of this research was to develop a remote sensing tool for the evaluation of dispersion of wastes from existing or proposed ocean outfalls. Photogrammetric and photo interpretation methods are used to determine dispersion patterns, diffusion coefficients, waste concentrations and nearshore currents. This study is unique in that the aerial photography is not only used to determine the position of points and the size of objects as in normal photogrammetry, but the photograph is also used as an energy sensor. The amount of light reflected from an object is recorded by the photograph as the film density of the image. The light scattered from within the sea is measured from the film with a photo densitometer and can be related to certain water quality parameters.

Ocean outfall sewers for the disposal of waste along the Pacific Northwest coastline are, in general, located on the relatively shallow coastal shelf which is subjected to heavy seas. Sampling from a boat in these areas is dangerous at all times and impossible much of the time due to rough water. The use of aerial photography and photogrammetric methods presents a possible method for overcoming this difficulty. From two to eight hours of continuous sampling from a boat is required to adequately define the waste field in the vicinity of an ocean outfall. The waste field is usually shifting thus making a comprehensive study nearly impossible by conventional methods. The aerial photographic technique presents a method where concentrations throughout the waste field can be measured in one instant. Consideration of these factors suggest that photogrammetry can be a most useful tool for water quality investigations. Prior to this time the use of aerial photography for water quality studies has been limited to identifying pollution sources but has not been used for making quantitative measurements from the photographs.

In order to obtain design information at proposed outfall locations, aerial photography is taken of dye patches. The dye markers are dropped from the aircraft at selected locations in the waste disposal area. Current velocities and diffusion coefficients are determined from the change in position and size of the dye patches between two photographic flights over the proposed site.

The field work was conducted at the Georgia-Pacific Kraft pulp mill outfall at Newport because of its convenient location. This site provided an additional advantage since the natural color of the waste effluent was visible on aerial photography. However, the results of this study are not limited to Kraft pulp mill outfalls. If the effluent from an outfall has the same light scattering and light absorption properties as the receiving water, dye can be added to the effluent to distinguish the waste field from the receiving body of

water. The natural color characteristics of the Kraft pulp waste will vary with time while the addition of dye to a colorless waste will give greater control over the test.

Three different field procedures were used on the project. During the 1968 and 1969 field seasons, work was carried out by conducting simultaneous studies of the waste plumes by aerial photographic methods and by conventional boat sampling. Concentrations in the plume were determined by metering rhodamine WT tracer into the pipeline and measuring the tracer concentration in the waste field with a fluorometer aboard the survey boat.

During the first field season, two fluorometers were used to sample from one foot and five feet below the water surface. Since there was no significant difference in the concentration at these two depths, only one fluorometer was used during the following field season. A ten-foot sampling probe for the fluorometer intake was constructed for the 1969 field season. Boat sampling was discontinued during the 1970-71 field season and field work continued throughout the fall, winter, and spring when boat operations were impossible due to rough sea conditions most of the time.

Vertical color aerial photography was taken with a single camera by a commercial aerial photography firm during the 1968 field season. As the firm was located approximately 100 miles from the study area, scheduling of the photography was difficult. Photography was taken at scales of 1:6,000 and 1:12,000 using precise mapping cameras. The small scale photography was intended to be used for buoy location by analytical strip bridging. However, it was found more convenient to triangulate the position of the buoys from the shore stations.

As listed in the original proposal, the first year of the study was divided into two phases: 1) Photographing the plume and current floats and 2) Photographing dye slugs introduced into the pipeline. Aerial photography of the dye slugs was difficult to process. Considering a nonsteady state dye patch within a nearly steady state waste field, the amount of dye, waste and sea water could occur in various combinations which would be impossible to distinguish by measuring the light return with the three broad bands of color photography. At a minimum, four individual narrow pass bands would have been required to obtain meaningful results. This phase of the study was later replaced by dye slugs dropped from the airplane away from the waste field.

One of the primary problems encountered in processing the 1968 vertical photography was the direct sunlight reflection from the water surface. Photography after 1968 was taken with an oblique camera mounting to avoid the sun spot. Three cameras were purchased and mounted in the baggage compartment of a small high wing aircraft. The oblique camera mounting reduced the requirement for horizontal control in the water. The large camera photographs included the horizon and two horizontal

control points could be identified on shore. The mapping camera, because of its large angular coverage, permitted photographic orientation of the two smaller cameras. Films from the two 70 mm cameras were used for detailed analyses and measurements of the waste field. Polarizing filters on the 70 mm cameras reduced the skylight reflection from the water surface.

During the 1968-1969 field seasons, work was conducted in late June, July, August and early September. Fourteen sampling runs were made during this period. For eight of the fourteen sampling runs, the waste field from the ocean outfall was at the sea surface. A submerged plume occurred during the remaining six sampling runs. When the plume was submerged both the swell height and the wind velocity were significantly less at a 90 percent confidence level than when the plume formed at the surface. Both steady state and nonsteady state diffusion coefficients were computed when possible for each sampling run. Of the eight days that a surface plume occurred, a one dimensional diffusion model was applicable to the plume pattern on only three days. A two dimensional model was necessary to describe the plume when the current velocity was low. When the velocity was greater than 0.4 ft/sec, a one dimensional diffusion model was adequate.

For each day that waste concentrations were computed from both the densitometer measurements taken on the aerial photography and the fluorometer records from the boat sampling, a comparison was made of the concentrations determined by the two methods by matching the ground coordinates. The correlation coefficients for these comparisons ranged from 0.85 to 0.95. When the boat sampling was conducted, there were several locations where the sampling lines crossed and the concentrations were measured twice at one point. The mean square residual determined at these points was significantly greater than the mean square residual between the concentrations determined by boat sampling and aerial photography (generally at a 95% confidence level).

During the final year of the project, 25 field observations were conducted starting in September of 1970 and ending in May of 1971. Diffusion coefficients and water current velocities were computed from the transport and spread of a dye slug dropped from the airplane. Continuous wind records were available from anemometers located on the south jetty. Longitudinal diffusion coefficients determined from the dye patch study ranged from 0.3 to 13.9 while the transverse diffusion coefficients range from 0.0 to 1.9 ft<sup>2</sup>/sec. The dye patch was nearly always oriented parallel to the wind. When the wind velocity was low, the major axis of the elliptical dye patch would usually be oriented perpendicular to the swell crest.

Of the 25 observations conducted during the fall, winter and spring, the plume was not visible on only one day, covered less than 30 acres on seven days and less than 100 acres on 15 days. The size of the plume was not directly related to the state of the sea code, diffusion coefficients nor related to the effluent discharge rate within the

range covered by the study.

The water current velocities ranged from 0.1 to 2.0 ft/sec. The surface water current was found to be the dominant factor in the resulting plume pattern. By a visual comparison, the general direction of the current could be explained by the wind record for 12 of the 17 days that the current velocity was measured.

The Fickian diffusion equation with a unidirectional transport velocity was not applicable to the majority of the observations. A two dimensional model with losses of waste to the lower layers considered by using a decay coefficient was able to better explain the observed plume patterns. The x and y velocity components for this model were determined from the equation as for a line source in a uniform stream.

The characteristic airphoto pattern elements can be used to estimate state of the sea, wind velocity and diffusion coefficients. As the sea becomes rough, the finely mottled tone changes to a coarsely mottled pattern. The density of whitecaps increases with the wind speed and when the wind velocity exceeds 25 kts, streaks parallel to the direction of the wind begin appearing. Within the generating area of the wind curves, the waves are irregular and confused, they appear to have no particular period or common wave height, giving rise to a randomly mottled photo tone. As a dominant wave train develops, the photo pattern has a linear trend normal to the wave movement. With the wave length measured from the photos, the wave period and speed can be estimated using wave formulas.

## SECTION XIII

### ACKNOWLEDGMENTS

The writers wish to express their gratitude to the following: Messrs. T. Fenwick and P. O'Hara of the Georgia Pacific Corporation at Toledo, Oregon.

To members of the Pacific Northwest Water Laboratory, especially Messrs. D. Baumgartner, L. Bentsen, R. Callaway, W. Clotheir, W. DeBen, G. Dittsworth, R. Scott, and D. Trent for their guidance and assistance in collection of the data;

Captain R. Redmond and Messrs. D. McKeel, B. Danby and R. Ervin of Marine Science Center at Newport, Oregon, for their help with the boat operations;

Professors R. Schultz, M. Northcraft, D. Phillips and D. Bella of Oregon State University for their advice and assistance on the project;

Students J. Graham, L. Doester, B. Valentine, R. Spaw, D. Monroe, R. Scholl, W. Hart, T. Basgen, Ching-Lin Chang, M. Soderquist, R. Collier, R. Mann, P. Klampe, B. Barnes, G. Carman, J. Plasker, W. Halverson, A. Langdon, K. Cerotsky and W. Gilbert for their assistance in collection of data, construction of equipment and processing data; and

the Federal Water Quality Office for financial support of the project.

## SECTION XIV

### REFERENCES

- Allen Hancock Foundation. 1964. An investigation on the fate of organic and inorganic wastes discharged into the marine environment and their effects on biological productivity. Los Angeles, University of Southern California. 118 p. (California State Water Quality Control Board Publication 29).
- American Society of Photogrammetry. 1968. Manual of color aerial photography. Menasha, George Banta Company. 550 p.
- American Society of Photogrammetry. 1960. Manual of photographic interpretation. Menasha, George Banta Company. 868 p.
- Bascom, Willard. 1964. Waves and beaches. Garden City, Doubleday & Co. 267 p.
- Baumgartner, D. J., W. P. James and G. L. O'Neal. 1969. A study of two ocean outfalls. National Council for Air and Stream Improvement Technical Bulletin No. 231. p 27-53.
- Baumgartner, D. J. and D. S. Trent. 1970. Ocean outfall design, part I, literature review and theoretical development. USDI, FWQA, Pacific Northwest Water Laboratory, Corvallis, Oregon. April. 129 p.
- Baumgartner, D. J., D. S. Trent and K. V. Byram. 1971. User's guide and documentation for outfall plume model. EPA, WQO, Pacific Northwest Water Laboratory, Corvallis, Oregon. Working Paper No. 80, May.
- Brooks, Norman H. 1960. Diffusion of sewage effluent in an ocean current. Proceedings of the First International Conference on Waste Disposal in Marine Environment, London, Pergamon Press. p. 246-267.
- Burgess, F. J. and W. P. James. 1970. An aerial photographic tracing of pulp mill effluent in marine waters. Federal Water Quality Office, EPA, Water Pollution Control Research Series 12040EBY, Grant WP-00524. 152 p.
- Burt, Wayne V. 1953. A note on the reflection of diffusion radiation by the sea surface. Transactions, American Geophysical Union 34(2): 199-200.
- Cox, C. and W. Munk. 1954. Measurement of the roughness of the sea surface from photographs of the sun's glitter. Journal of the Optical Society of America 44:838-850.
- Cox, Charles and Walter Munk. 1955. Some problems in optical oceanography. Journal of Marine Research 14(1):63-78.



- Elterman, Louis and Robert B. Toolin. 1965. Atmospheric optics. In: Handbook of Geophysics and Space Environment, ed. by Shea L. Valley, Cambridge, Air Force Cambridge Research Laboratories. p 7.1-7.36.
- Faas, V. A. 1960. The procurement of aerial photography of underwater objects. In: Manual of photographic Interpretation, American Society of Photogrammetry, Menasha, George Banta Company. p. 96.
- Fisher, Davis, and Sousa. 1966. Fresh-water springs of Hawaii from infrared images. U.S. Geological Survey Hydrologic Investigations Atlas HA-218. Washington, D. C.
- Fritz, N. L. 1967. Optimum methods for using infrared-sensitive color films. Photogrammetric Engineering 33:1128-1138.
- Holter, Marvin R. 1967. Infrared and multispectral sensing. Bio-Science June. p. 376-383.
- Hutchinson, G. E. 1957. A treatise on limnology. Vol. 1. New York, John Wiley and Sons, Inc. 1015 p.
- Ichiye, T. and N. B. Plutchak. 1966. Photodensitometric measurements of dye concentration in the ocean. Limnology and Oceanography 2:364-370.
- Jensen, Niels. 1968. Optical and photographic reconnaissance systems. New York, John Wiley and Sons, Inc., 211 p.
- Jerlov, N. G. 1964. Optical classification of ocean water. In: Symposium on Physical Aspects of Light in the Sea, ed. J. E. Typer, Honolulu, University of Hawaii Press. p. 45-49.
- Jerlov, N. G. 1968. Optical oceanography. Amsterdam, Elsevier Publishing Company. 194 p.
- Jones, L. A. and H. R. Condit. 1948. Sunlight and skylight as determinants of photographic exposure. Optical Society of America 38:123-178.
- Keller, Morton. 1963. Tidal current surveys by photogrammetric methods. U.S. Coast and Geodetic Survey, Technical Bulletin 22. 20 p.
- Keller, M. and G. C. Tewinkel. 1966. Space resection in photogrammetry. U.S. Coast and Geodetic Survey Technical Bulletin 32. 10 p.
- Keene, D. F. 1971. A physical oceanographic study of the nearshore zone at Newport, Oregon. M.S. thesis. Corvallis, Oregon State University.

- Masch, F. D. 1961. Mixing and dispersive action of wind waves. Berkeley, University of California, IER Technical Report 138-6.
- Molineux, C. E. 1965. Multiband spectral system for reconnaissance. Photogrammetric Engineering 31:131-143.
- Neumann, G. and W. J. Pierson, Jr. 1966. Principles of physical oceanography. Prentice-Hall, Englewood Cliffs, N. J. 545 p.
- Neumaier, G., F. Silvestro, H. Thung, and R. Frank. 1967. Project aqua-map development of aerial photography as an aid to water quality management. Buffalo, Cornell Aeronautical Laboratory, Inc. (Contract No. HC-9768 of the State of New York Conservation Department).
- Ory, T. R. 1965. Line scanning reconnaissance systems in land utilization and terrain studies. In: Third symposium on remote sensing of environment. Ann Arbor, University of Michigan. p. 393-398.
- Pearson, E. A. 1955. An investigation of the efficacy of submarine outfall disposal of sewage and sludge. California Waste Pollution Control Board Publication 14. 154 p.
- Pearson, E. A., P. N. Storrs and R. E. Selleck. 1967. Some physical parameters and their significance in marine waste disposal. In: Pollution and Marine Ecology, ed. by F. J. Burgess and T. A. Olson, New York, Interscience. p. 297-315.
- Romanovsky, V. 1966. Coastal currents. In: Proceedings of the Third International Conference on Advances in Water Pollution Research, Munich. Baltimore, Port City Press, Inc. Vol. 3, p. 290-292.
- Scherz, James P. 1967. Aerial photographic techniques in pollution detection. Doctoral dissertation. Madison, University of Wisconsin. 82 numb. leaves. (Microfilm)
- Strandberg, C. H. 1966. Water quality analysis. Photogrammetric Engineering 32 (2):234-248.
- Strandberg, C. H. 1967. Aerial discovery manual. New York, John Wiley and Sons. 249 p.
- Sverdrup, H. V., M. W. Johnson and R. H. Fleming. 1942. The oceans. New York, Prentice-Hall. 1087 p.
- Swanson, L. W. 1964. Aerial photography and photogrammetry in the Coast and Geodetic Survey. Photogrammetric Engineering, 30(5):699-726.
- Tarkington, Raife G. 1966. The photographic process. In: Manual of photogrammetry, 3d ed., Menasha, George Banta Company. p. 243-293.

Tyler, J. E. and W. H. Richardson. 1958. Nephelometer for volume scattering function in situ. Journal of the Optical Society of America 48(5):354-357.

Waldichuk, Michael. 1966. Currents from aerial photography in coastal pollution studies. Proceedings of the Third International Conference on Advances in Water Pollution Research, Munich. Baltimore, Port City Press, Inc. Vol. 3, p. 263-284.

Water Pollution Research Board. 1964. Coastal pollution. Report of the Director, Department of Scientific and Industrial Research, London. p. 136-142.

Wiegel, R. L. 1964. Oceanographical engineering. London, Prentice Hall International. 532 p.

Williams, J., J. J. Higginson and J. D. Rohdbough. 1968. Air and sea-the naval environment. Menasha, George Banta Company. 338 p.

Wilson, James F., Jr. 1968. Fluorometric procedures for dye tracing. U.S. Geological Survey, Chapter A12 of Book 3 (Applications of Hydraulics). 31 p.

Yost, E. F. and S. Wenderoth. 1967. Multispectral color aerial photography. Photogrammetric Engineering 33:1020-1033.

## SECTION XV

### PUBLICATIONS

1. Burgess, F. J. and W. P. James. 1970. Pulp mills take to the air to monitor ocean outfalls. Pulp and Paper, September.
2. James, W. P. and F. J. Burgess. 1969. The use of photogrammetry in predicting outfall diffusion. National Council for Air and Stream Improvement Technical Bulletin No. 231. p. 2-26.
3. James, W. P. and F. J. Burgess. 1970. Ocean outfall dispersion. Photogrammetric Engineering Journal 36(12):1241-1250.
4. James, W. P. and F. J. Burgess. 1971. Pulp mill outfall analysis by remote sensing techniques. Journal of the Technical Association of the Pulp and Paper Industry. 54(3):414-418.
5. James, W. P., F. J. Burgess and D. Baumgartner. 1971. An aerial photographic study of waste fields from three ocean outfalls. Offshore Technology Conference Proceedings, Houston, Texas; April 19-21. OTC paper 1374, PPI 483-I498.

## SECTION XVI

### APPENDICES

	<u>Page</u>
A. Definition of Terms. . . . .	189
B. Computer Program for Processing Vertical Photography . . . .	193
Figure	
B-1 Flow diagram for computer program DIFFUSION . . . .	200
B-2 Listing of program. . . . .	204
B-3 Listing of subroutines. . . . .	216
B-4 Sample input, LUN 1 . . . . .	222
B-5 Sample input LUNS 3 and 19. . . . .	223
C. Processing 1969 Photographic Data. . . . .	224
Figure	
C-1 Flow diagram for computer program EDIT. . . . .	<b>231</b>
C-2 Listing of program EDIT . . . . .	233
C-3 Sample input for program EDIT . . . . .	241
C-4 Sample output from program EDIT . . . . .	242
C-5 Flow diagram of program REMOTE. . . . .	243
C-6 Flow diagram of subroutine PROCESS. . . . .	245
C-7 Program listing for REMOTE. . . . .	247
C-8 Subroutines used with program REMOTE. . . . .	260
C-9 Sample input data for REMOTE. . . . .	271
D. Processing of 1970-71 Photographic Data. . . . .	272
Figure	
D-1 Flow diagram for computer program INSHORE . . . . .	275
D-2 Listing of program INSHORE. . . . .	277
E. Streamlines for a Source in a Uniform Flow . . . . .	284
Figure	
E-1 Flow diagram of program FLOWNET . . . . .	285
E-2 Listing of program FLOWNET. . . . .	286

## APPENDIX A

### DEFINITION OF TERMS

The following terms that were used in The Rationale are defined as follows:

A	is the extinction optical thickness for a standard atmosphere. When subscripted the subscripts b, g and r refer to the blue, green and red bands of the color photograph, respectively.
a	is the sea water attenuation coefficient per meter.
Az	is the azimuth of the sun from true north.
AZ	is the azimuth of the sun from grid north.
$\alpha$	is the angle at the incremental scattering volume between incident and scattered beams.
b	is the waste absorption coefficient in (Meter-ml/liter) <sup>-1</sup> .
$\beta(\alpha)$	is the volume scattering function per meter.
C	is the attenuation coefficient for the sea water and waste per meter.
c	is the angle between the ray to the camera and the camera axis.
$D_b(x,y)$ , $D_g(x,y)$	and $D_r(x,y)$ are the film densities measured at photo coordinates x and y for the blue, green and red bands, respectively.
dJ	is the scattered light intensity from the incremental scattering volume.
d $\Omega$	is the solid angle in steradians.
dV	is the incremental scattering volume.
E	is the extinction optical thickness for the atmosphere from the sea surface to the camera. When subscripted the subscripts b, g and r refer to the blue, green and red bands of color photograph, respectively.
EX	is the photographic exposure.

$f$	is the cameras focal length.
$FNO$	is the relative aperture of the lens.
$G$	is a constant representing film contrast.
$H$	is the irradiance in watts per square centimeter.
$H_o$	is the irradiance from the sun at the outer atmosphere normal to the ray.
$H_s$	is the irradiance on a horizontal plane from the sun at the sea surface.
$H_{sky}$	is the irradiance from skylight at the sea surface.
$H_a$	is the irradiance at the sea surface from the scattering volume.
$H_w$	is the irradiance from the sun on a plane normal to the ray below the water surface.
$H_z$	is the irradiance from the sun at a depth $z$ below the water surface.
$H'$	is the irradiance of the film image.
$i$	is the angle of incidence of the direct sunlight at the water surface.
$i_2$	is the angle of incidence of the scattered light at the water surface.
$j$	is the angle of refraction of the direct sunlight at the water surface.
$j_2$	is the angle between the vertical and the object ray.
$K$	is a constant.
$Ka$	is the rotation angle about the $Z$ camera axis.
$M$	is a constant representing film speed.
$n$	is the refractive index of water.
$N$	is the total radiance from the sea in watts per square centimeter-steradian.
$N_a$	is the radiance from the scattering volume above the

	sea surface.
$N_b$ , $N_g$ and $N_r$	are the total radiance at the sea surface including reflected skylight, reflected direct sunlight and scattered light from within the sea for the blue, green and red bands of the photograph, respectively.
$N_c$	is radiance from the sea measured at the camera station.
$N_d$	is the radiance of direct sunlight reflection from the water surface.
$N_{sky}$	is the skylight radiance reflected from the water surface.
$N_w$	is the radiance from the scattering volume under the sea surface.
$P_a$	is the reflectivity of direct sunlight from the sea surface.
$P_s$	is the reflectivity of skylight from the water surface.
$P_w$	is the reflectivity of uplighting from the sea at the surface.
RA	is the variation in the ratio of red to green light returned from within the sea due to the waste.
RM	is photographic orientation matrix.
$R_p$	is the ratio of red to green radiance at the camera station.
$R_{ph}$	is the ratio of red to green radiance at the sea surface.
$R_{pho}$	is the estimated ratio of red to green radiance at the sea surface if there was no waste present.
SUNR	is the angle between the object ray and the direct sunlight reflection from a horizontal plane.
TIM	is the photographic exposure time in seconds.
TR	is the lens transmittance. When it is subscripted the subscripts b, g and r refer to the blue, green and red bands, respectively.



$W$	is the waste concentration in milliliters per liter.
$W_o$	is the rotation angle about the X axis of the camera.
$Z$	is the flying height in feet.
$z$	is the distance in meters below the water surface.
$\phi$	is the rotation angle about the Y axis of the camera.

APPENDIX B  
COMPUTER PROGRAM  
FOR  
PROCESSING VERTICAL PHOTOGRAPHY

Introduction

Included in this appendix are the program and subprogram listings and sample input data for processing of vertical photography. The program determines diffusion coefficients from two flights of aerial color photographs and was written for the CDC 3300 system in Fortran IV computer language. The unique feature of this system is the remote access to the computer by teletypes on a time sharing basis.

Input data for the program is either from a logical unit number (LUN) or from the teletype keyboard. The input statements include the standard READ statement, FFIN (1), or TTYIN(4H X = ). The free form input (FFIN) will accept data in any format in columns 1 to 72 as long as the words are separated by at least one space. The number in parentheses with the call command is the input LUN. The teletype free form input command (TTYIN) allows the user to enter data from the teletype. The parameter in the TTYIN function must be a hollerith constant containing four characters. When the fortran statement is executed, the hollerith message is printed on the user's teletype. Only a single variable can be entered each time the function is executed.

Program Listing

Flow diagram for the program used to process the 1968 photographic data is shown in figure B-1. The numbers in parentheses on the diagram refer to the line numbers on the program listing shown in figure B-2. The main array was declared an integer to save storage space and is dimensioned 2, 120, 60. If the size of this array is changed, only lines 3, 30, 31, 539 and 540 in the main program will require modification.

All except two of the subroutines called in the main program are listed in figure B-3. These subroutines, date and time, return the time and date of computer processing. If they are not available, lines 26 through 29 of the main program should be erased. The following subroutines are included in the listing:

- |         |   |
|---------|---|
| Rotate  | - Converts state plane coordinates to coordinates based on system oriented about waste field. |
| Sunlite | - Determines sun altitude and azimuth.  |
| Resect  | - Determines the orientation of near vertical photographs and was modified from USC & GS      |

program resection. Each time the subroutine is called, the camera station coordinates and orientation matrix are printed on LUN 2.

- Leastfit        - Determines the least squares solution of the regression coefficients for a linear model to data with one independent and up to nine dependent variables. Each time the subroutine is executed, values of the regression coefficients, standard deviation, variance-covariance matrix, and  $\bar{Y}$ ,  $\bar{Y}$ , and  $e$  for each observation are written on LUN 2.
- Matinv         - Determines the inverse of a square matrix.
- Trncoord       - Converts the photographic vector to a unit vector oriented with the state plane coordinate system.
- Grdcoord       - Determines the ground coordinates of the unit vector.
- Angles         - Determines the angles between the object ray and the vertical in air and under the water. Determines the angles between the sun ray and the object ray above and below the water surface.

#### Input Data

Input data for the program are from five sources. These are the teletype, photo coordinates and film densities from LUN 1, ground control coordinates from LUN 3, general information from LUN 5 and waste concentration as measured by fluorometers with ground coordinates from LUN 19.

#### Teletype

The following information is to be typed on the teletype after the hollerith constant is printed during program execution.

No.	Hollerith Constant	Remarks
1.	IG0	Type in 1 if the photo values in the array are to be averaged and the maximum value printed on the teletype for each section across the waste field or 2 if this is not required.
2.	B1=	Coefficient for the linear term relating the photo value to waste concentration.
3.	B2=	Coefficient for the squared term relating the photo value to waste concentration.

No.	Hollerith Constant	Remarks
4.	VEL=	Estimated velocity if there were no current floats.
5.		Repeat above items 1-3 for second flight.

#### LUN 1

Sample input from LUN 1 is shown in figure B-4. As the input on this LUN is mostly from the digitizer the Z value (densitometer voltage) is always recorded but is not always used in the computations. In the sample input there were two photos in the first flight (lines 1 through 359) and three in the second flight (lines 360 through 1336). In figure B-4, lines 1 through 33 and lines 360 through 398 are read with free form input while the other lines are read on a fixed format.

Description of the input data one LUN 1 follows

Item	Line No.	Remarks
1.	1	Camera focal length in mm for photo 1 of flight 1.
2.	2	Photo number in flight (00001), number of photo control points on the photograph (0006) and the X, Y, Z photo coordinates of the principal point.
3.	3-4	Point identification number and the X, Y, Z values of control points. This series is repeated six times to input photo coordinates.
4.	5	0.0 to indicate end of current float coordinates (none in this example).
5.	6	Identification number and the X, Y, Z photo coordinates at the head of the plume and at a point along the plume. These points are used to orient the array about the plume.
6.	8-9	Eighteen film densities on the standard grey scale.
7.	10-15	Identification number and the X, Y, Z values

Item	Line No.	Remarks
		measured on the grey scale with the red filter in the densitometer. Only the voltage in the Z coordinate is used in computations.
8.	16-21	Same as lines 10-15 except readings are with the green filter.
9.	22-27	Same as lines 10-15 except readings are with the blue filter.
10.	28	Focal length in mm for photo number two of the first flight.
11.	29	Photo number, number of control points and X, Y, Z photo coordinates.
12.	30-31	Same as lines 2-4.
13.	33	0.0 to indicate end of current float coordinates (none in this case).
14.	34-70	Film densities for points outside the plume with one line being required for each point. The first number on each line is the photo number followed by the point number which is less than 200. The point number with the X, Y, Z values are repeated three times to input the red, green and blue film density voltages. The green film density voltage is the Z value of the center group while the blue or red can be in either the first or third group. The red film density voltage is always larger than the blue value.
15.	71-358	Same as lines 34-70 except the points are in the waste field and are numbered between 300 and 399.
16.	359	Blank card to indicate end of flight 1.
17.	360	Same as item 1 except for photo 1 of flight 2.
18.	361	Same as item 2.
19.	362-363	Same as item 3.

Item	Line No.	Remarks
20.	364	Same as item 4.
21.	366-367	Same as item 7.
22.	368-385	Same as items 8, 9 and 10.
23.	386	Same as item 1 except for photo 2 of flight 2.
24.	387	Same as item 2.
25.	388	Same as item 3.
26.	389-390	Point identification number (900 or greater) and X, Y, Z photo coordinates of current floats.
27.	392	Same as item 4.
28.	393	Same as item 1 except for photo 3 of flight 2.
29.	394	Same as item 2.
30.	395-396	Same as item 3.
31.	398	Same as item 4.
32.	399-458	Same as item 15.
33.	459-1335	Same as item 16.
34.	1336	Blank card to indicate end of input data.

### LUN 3

Sample input from LUN 3 is shown in figure B-5. This LUN contains the ground coordinates of the photo control stations and some initial orientation parameters for the five photographs. On the lines containing four numbers, the numbers are the point identification number, and the X, Y, Z state plane coordinates for the photo control. The control data must be listed in the same sequence as the photo coordinates were listed on LUN 1. Lines in figure B-5 containing three numbers list the initial approximation of the camera station coordinates (X, Y, Z). The lines containing 0.0 and 1.0 list the sine and cosine values of the initial approximation of the photo azimuth.

## LUN 5

LUN 5 contains the general information required for the program. The information is read with free form input and is described as follows:

No.	Description
1.	Number of flights to be processed.
2.	Time difference between flights in seconds.
3.	Effluent flow rate in gpm.
4.	Number of photos in flight 1.
5.	Time of day of first flight in hours.
6.	Time of day - minutes past even hour.
7.	Declination in degrees at 0 hr GCT.
8.	Declination - minutes over even degree.
9.	Change in declination in minutes per hour.
10.	Equation of time in minutes.
11.	Equation of time - seconds over even minute.
12.	Change in equation of time in seconds per hour.
13.	Longitude of exposure station in degrees.
14.	Latitude of exposure station in degrees.
15.	Reciprocal of exposure time.
16.	F - number of lens setting.
17.	Film gamma to base 10.
18.	Photo identification for symbolic plot.
19.	Day for heading on symbolic plot.
20.	Month for heading of symbolic plot.

If two flights are being processed, the following information is required:

No.	Description
21.	Number of photos in second flight.
22.	F - number of lens setting.
23.	Film gamma to base 10.
24.	Photo identification for symbolic plot.
25.	Day for heading on symbolic plot.
26.	Month for heading on symbolic plot.

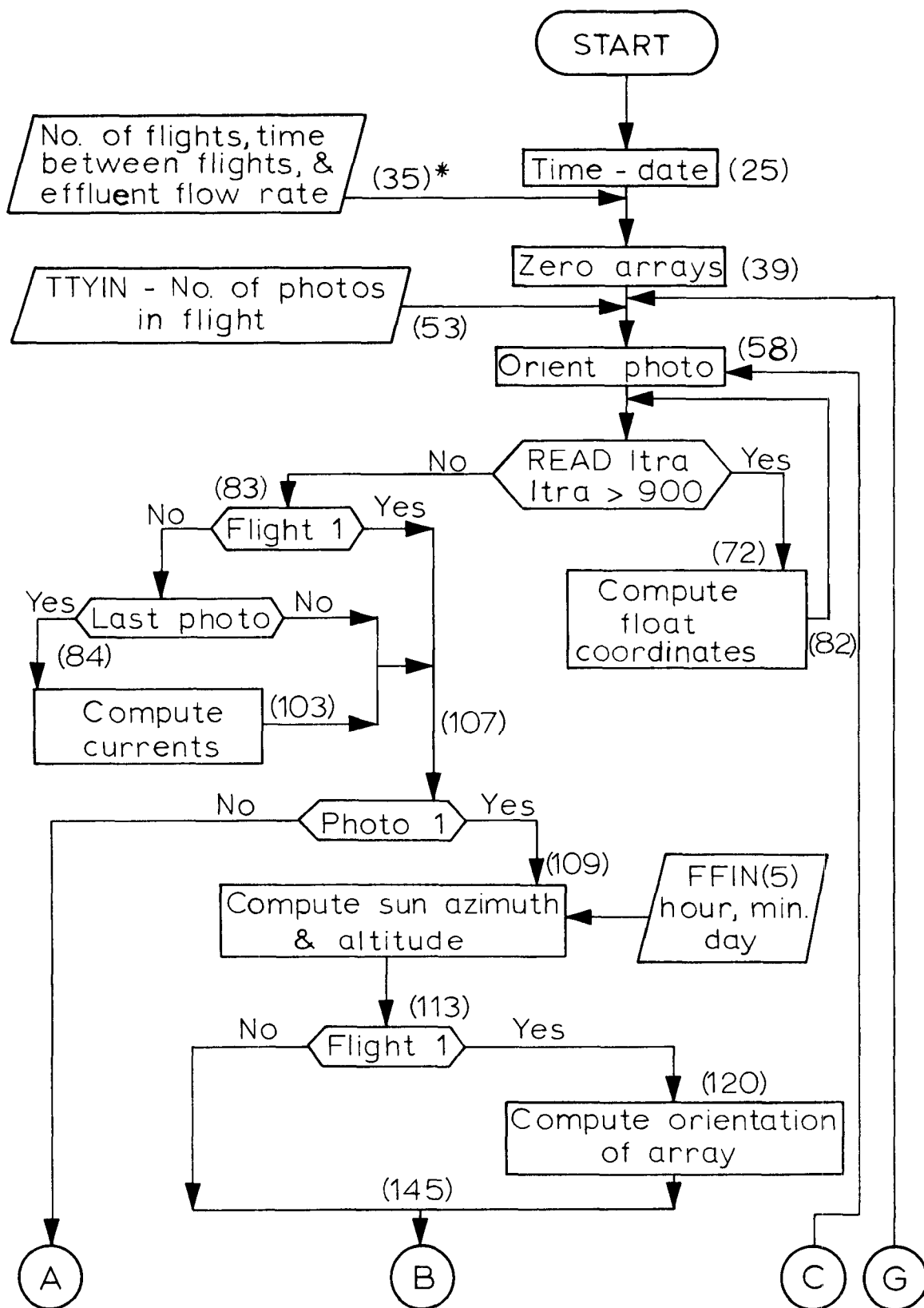
#### LUN 19

A partial listing of data on LUN 19 is also shown in figure B-5. Each line contains the position number, X, Y state plane coordinates of the boat, waste concentration in milliliters per liter and the sampling depth. A blank line is inserted after the data to indicate end of data.

#### Output from Program

Output from program DIFFUSION is on LUNS 2, 4 and 20. The output on LUN 2 includes the photo orientation matrix, current float coordinates, statistical information from subroutine LEASTFIT, symbolic plots, a plot of difference in concentration between flights and diffusion coefficients. The output on LUN 4 is used for more detailed statistical analyses of photo values ( $R_{ph} - R_{pho}$ ) and boat concentrations and ground coordinates are read out on LUN 20.





\* ( ) Program line number

Figure B-1. Flow diagram for computer program DIFFUSION.

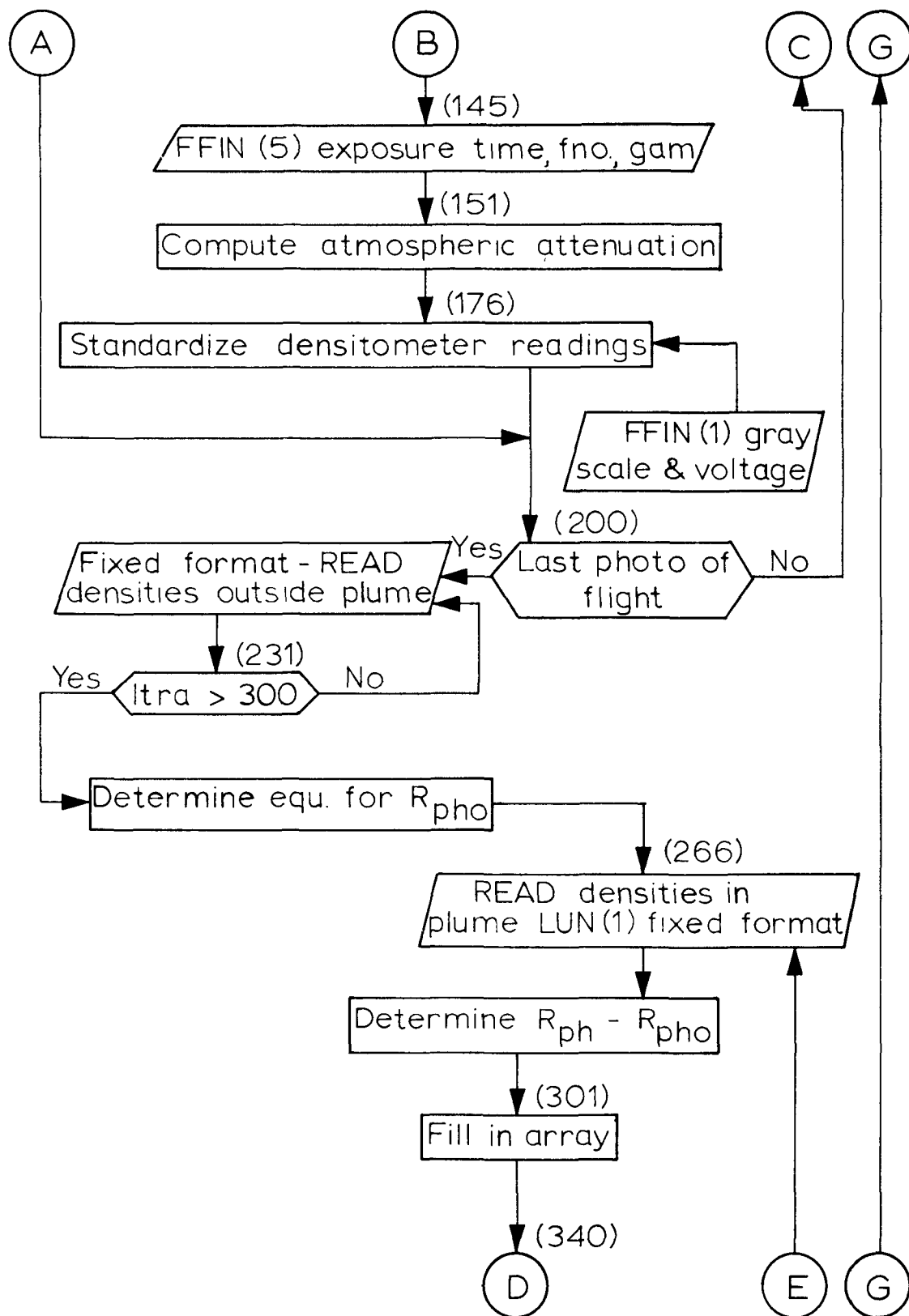


Figure B-1. Flow diagram for computer program DIFFUSION.

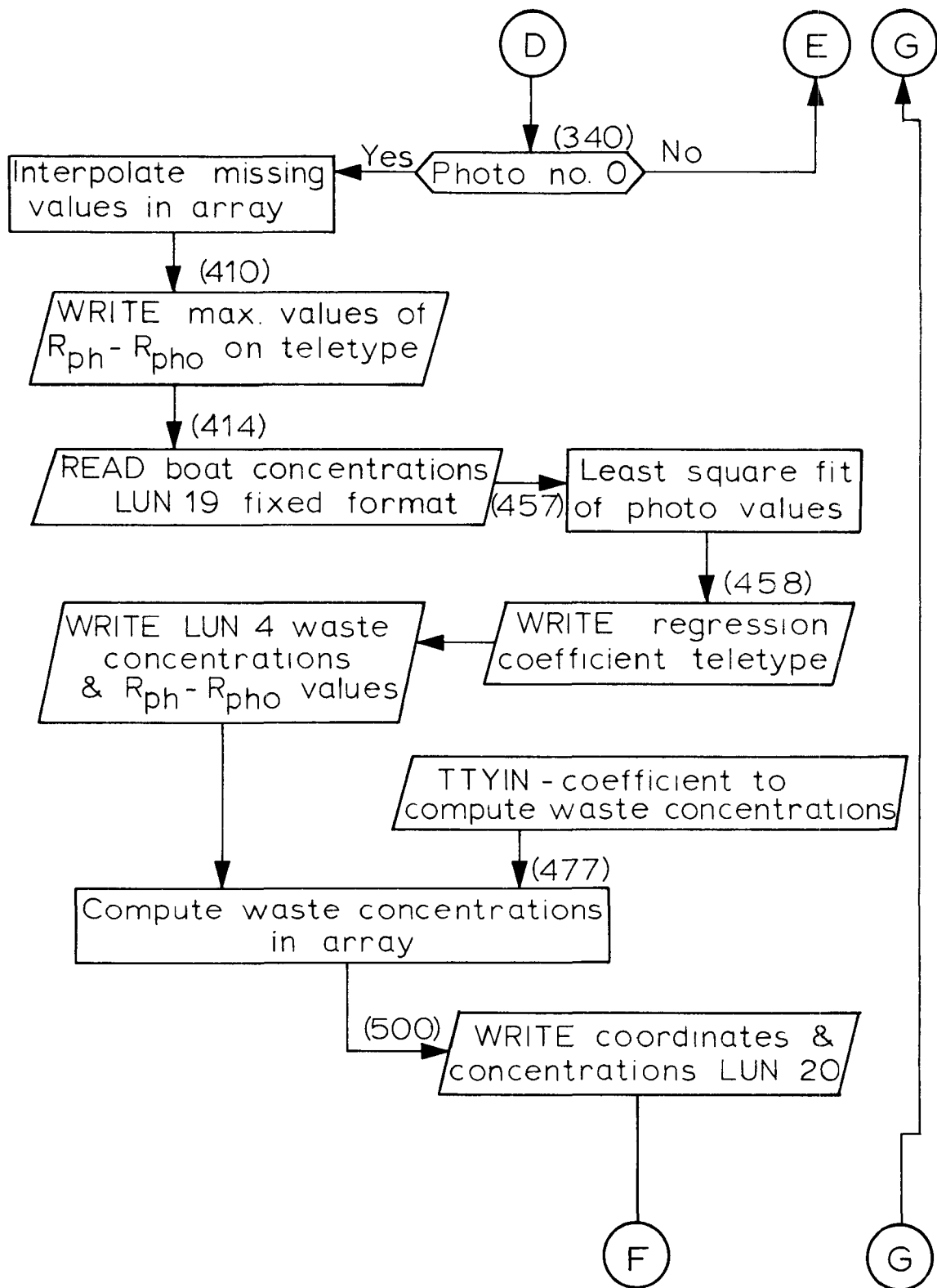


Figure B-1. Flow diagram for computer program DIFFUSION.

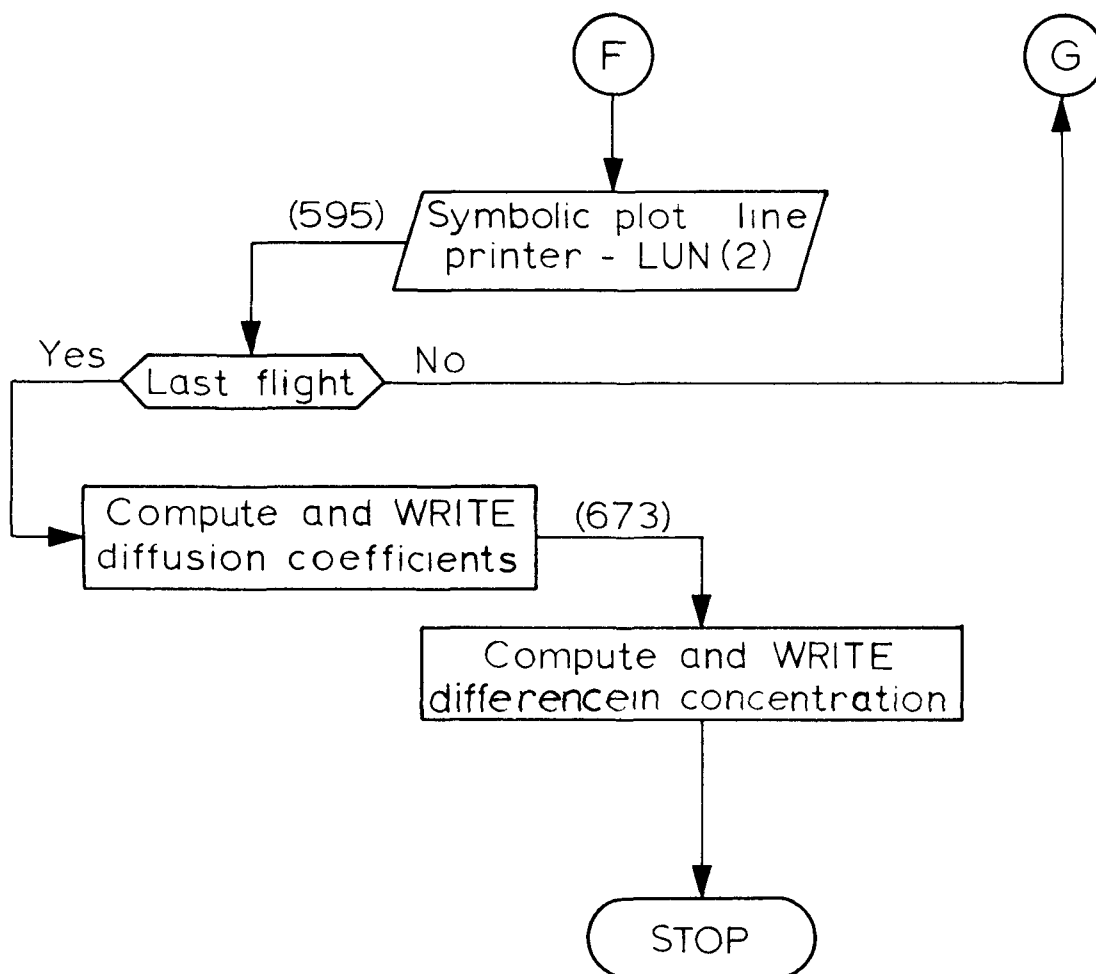


Figure B-1. Flow diagram for computer program DIFFUSION.

PROGRAM DIFFUSION	00001
DIMENSION C(20,2),XFTS(2,10,2),XT(3),XS(9),DEN(3),THI(3),B(9),	00002
1 RATIO(2,120,60),XPG(2),CAMO(3,5,3),RAD(3),XAR(2,8),	00003
2 DB(4,3)	00004
COMMON X(10,200)	00005
INTEGER RATIO,HARDWARE	00006
IF (HARDWARE(2) .EQ. 1) GO TO 62	00007
CALL EQUIP(2,5HFILE )	00008
GO TO 63	00009
62 REWIND 2	00010
63 IF (HARDWARE(4) .EQ. 1) GO TO 64	00011
CALL EQUIP(4,5HFILE )	00012
GO TO 65	00013
64 REWIND 4	00014
65 IF (HARDWARE(20) .EQ. 1) GO TO 66	00015
CALL EQUIP(20,5HFILE )	00016
GO TO 67	00017
66 REWIND 20	00018
67 IF (HARDWARE(19) .EQ. 1) 68,1000	00019
68 IF (HARDWARE(3) .EQ. 1) 69,1000	00020
69 REWIND 3	00021
IF (HARDWARE(1) .EQ. 1) 70,1000	00022
70 REWIND 1	00023
IF (HARDWARE(5) .EQ. 1) 71,1000	00024
71 REWIND 5	00025
CALL TIME(ETIME)	00026
CALL DATE(EDATE)	00027
WRITE(02,56) EDATE,ETIME	00028
56 FORMAT(////////10X,A8,30X,A8////////)	00029
NNXS=120	00030
NNYS=60	00031
YMIDY=30*NNYS	00032
C NO. OF FLIGHTS OVER AREA, TIME DIFFERENCE BETWEEN	00033
C FLIGHTS IN SECONDS, AND FLOW RATE OF EFFLUENT IN GPM	00034
IRUN=FFIN(5)	00035
DTIM=FFIN(5)	00036
RATE=FFIN(5)	00037
RATE=RATE/(7.48*60.)	00038
C ZERO ARRAY	00039
DO 50 LX=1,NNXS	00040
DO 50 LY=1,NNYS	00041
DO 50 K=1,2	00042
RATIO(K,LX,LY)=0	00043
50 CONTINUE	00044
DO 55 I=1,2	00045
DO 55 J=1,10	00046
DO 55 K=1,2	00047
XFTS(I,J,K)=0.	00048
55 CONTINUE	00049
IRUN=1	00050
54 REWIND 19	00051
C NO OF PHOTOS IN THIS FLIGHT	00052
IPMX=FFIN(5)	00053
IPHOT=1	00054
WRITE (02,31)	00055
KFTS=1	00056
C ORIENT PHOTO	00057
100 CALL RESECT (FL,XP,YP,C)	00058
CAMO(IPHOT,5,1)=XP/1000.	00059
CAMO(IPHOT,5,2)=YP/1000.	00060
DO 105 J=1,3	00061
CAMO(IPHOT,!,J)=C(1,J)	00062
105 CONTINUE	00063

Figure B-2. Listing of program.

DO 106 J=2,4	00064
K=J+2	00065
DO 106 I=1,3	00066
CAMO(IPHOT,J,I)=C(K,I)	00067
106 CONTINUE	00068
J=1	00069
104 ITRA=FFIN(1)	00070
IF (ITRA-900) 108,107,107	00071
107 X(2,J)=(FFIN(1)-XP)/1000.	00072
X(1,J)=(FFIN(1)-YP)/1000.	00073
BB=FFIN(1)	00074
CALL TRNCOORD (CAMO,XT,J,FL,IPHOT)	00075
CALL GRDCOORD(CAMO,XT,XPG,J,IPHOT)	00076
WRITE (02,34) ITRA,XPG(1),XPG(2)	00077
34 FORMAT (' FLOAT ',I5,2F10.0)	00078
XFTS(IRUN,KFTS,1)=XPG(1)	00079
XFTS(IRUN,KFTS,2)=XPG(2)	00080
KFTS=KFTS+1	00081
GO TO 104	00082
108 GO TO (109,130),IRUN	00083
130 IF(IPMX-IPHOT) 131,131,109	00084
131 J=0	00085
DO 135 K=1,10	00086
DX=XFTS(1,K,1)-XFTS(2,K,1)	00087
DY=XFTS(1,K,2)-XFTS(2,K,2)	00088
DX=SQRT(DX*DX+DY*DY)	00089
IF (DX .LE. 100. .OR. DX .GT. 3000.) 135,133	00090
133 J=J+1	00091
X(1,J)=DX/DTIM	00092
WRITE (02,16) J,X(1,J)	00093
16 FORMAT (' VELOCITY ',I5,10X,F10.2,' FT PER SEC')	00094
135 CONTINUE	00095
K=J+1	00096
VFL=0.0	00097
GO TO (111,132),K	00098
132 DX=J	00099
DO 140 K=1,J	00100
VEL=VEL+X(1,K)	00101
140 CONTINUE	00102
VEL=VEL/DX	00103
111 IF (VEL-0.001) 142,142,143	00104
142 VEL=TTYIN(4HVEL=)	00105
143 LDFX=VEL*DTIM/60.+0.5	00106
109 GO TO (110,219),IPHOT	00107
C COMPUTE ALTITUDE AND AZIMUTH OF THE SUN	00108
110 CALL SUNLITE (H,AZ,IRUN,DTIM)	00109
SAZ=AZ+3.14159	00110
IF (SAZ-6.28318) 114,114,112	00111
112 SAZ=SAZ-6.28318	00112
114 GO TO(115,116),IRUN	00113
116 ROT=-ROT	00114
XLOW=XORG	00115
Y MID=YORG	00116
GO TO 211	00117
C READ IN THE DIRECTION OF THE PLUME AND ORIENT RATIO ARRAY	00118
C FIRST POINT DEFINES ZERO O. GRID FOR PLUME	00119
115 DO 200 J=1,2	00120
ITRA=FFIN(1)	00121
X(2,J)=(FFIN(1)-XP)/1000.	00122
X(1,J)=(FFIN(1)-YP)/1000.	00123
BB=FFIN(1)	00124
CALL TRNCOORD(CAMO,XT,J,FL,IPHOT)	00125
CALL GRDCOORD(CAMO,XT,XPG,J,IPHOT)	00126

Figure B-2. Listing of program (continued).

	IF (J-1) 196,196,198	00127
196	XLOW=XPG(1)	00128
	YMID=XPG(2)	00129
198	X(3,J)=XT(1)	00130
	X(4,J)=XT(2)	00131
200	CONTINUE	00132
	BOT=X(3,2)-X(3,1)	00133
	TOP=X(4,2)-X(4,1)	00134
	DIV=BOT/TOP	00135
	ROT=ATANF(DIV)	00136
	IF (TOP) 206,211,211	00137
206	ROT=ROT+3.14159	00138
211	SRUT=SINF(ROT)	00139
	CROT=COSF(ROT)	00140
	WRITE(02,2) RCT,XLOW,YMID	00141
2	FORMAT(' ROT ANGLE = ',F10.5,5X,'XLOW',F10.0,5X,'YMID',F10.0)	00142
	SXF=-SINF(AZ)	00143
	SYF=-COSF(AZ)	00144
C	EXPOSURE TIME ,F/D, AND FILM GAMMA TO BASE 10	00145
	ETIME=FFIN(5)	00146
	FNUM=FFIN(5)	00147
	GAM=FFIN(5)/2.30	00148
	CEXP=ETIME*FNUM**2	00149
C	OPTICAL THICKNESS 3000 TO 10,000 FT	00150
	THI(1)=0.108+0.069*LOGF(C(1,3)/3280.)	00151
	THI(2)=THI(1)*1.15	00152
	THI(3)=THI(1)*1.4	00153
	RAD(1)=EXPF(-0.252/SINF(H))	00154
	RAD(2)=EXPF(-0.331/SINF(H))	00155
	DTHI=-0.024*LOGF(C(1,3)/3280.+1)	00156
	TENR=RAD(1)/RAD(2)	00157
	RAD(3)=EXPF(-0.45/SINF(H))	00158
	HI=3.14159/2.-H	00159
	SINH=0.75*SINF(HI)	00160
	COSH=SQRT(1.0-SINH**2)	00161
	TANH=SINH/COSH	00162
C	ANGLE BETWEEN SUN RAY AND VERTICAL UNDER WATER	00163
	HW=ATANF(TANH)	00164
	WRITE (02,3) HW	00165
3	FORMAT(' UNDERWATER SUN ANGLE = ',F10.5)	00166
	XS(1)=SINF(HW)*(-SXF)	00167
	XS(2)=SINF(HW)*(-SYF)	00168
	XS(3)=-COSF(HW)	00169
	XS(4)=COSF(H)*(-SXF)	00170
	XS(5)=COSF(H)*(-SYF)	00171
	XS(6)=-SINF(H)	00172
	XS(7)=-COSF(H)	00173
	XS(8)=SINF(SAZ)	00174
	XS(9)=COSF(SAZ)	00175
C	READ IN FILM DENSITIES FROM GREY SCALE	00176
	DO 215 J=1,18	00177
	X(5,J)=FFIN(1)	00178
	X(1,J)=1.0	00179
215	CONTINUE	00180
C	READ IN VOLTAGES RED GREEN AND BLUE	00181
	DO 217 I=1,3	00182
	DO 216 J=1,18	00183
	ITRA=FFIN(1)	00184
	ITRA=FFIN(1)	00185
	ITRA=FFIN(1)	00186
	X(2,J)=FFIN(1)/10.	00187
	X(3,J)=X(2,J)*X(2,J)	00188
	X(4,J)=X(3,J)*X(2,J)	00189

Figure B-2. Listing of program (continued).

216	CONTINUE	00190
	N=5	00191
	NO=18	00192
	CALL LEASTFIT(N,NO,B)	00193
	DB(1,I)=B(1)	00194
	DB(2,I)=B(2)	00195
	DB(3,I)=B(3)	00196
	DB(4,I)=B(4)	00197
217	CONTINUE	00198
219	IPHOT=IPHOT+1	00199
	IF (IPHOT-IPMX) 100,100,218	00200
218	J=1	00201
220	READ(01,35) IPHOT,ITRA,X(2,J),X(1,J),DEN1,DEN(2),DEN3	00202
	IF (DEN1-DEN3) 222,222,224	00203
222	DEN(3)=DEN1	00204
	DFN(1)=DEN3	00205
	GO TO 225	00206
224	DEN(1)=DEN1	00207
	DEN(3)=DEN3	00208
225	DO 227 I=1,3	00209
	DEN(I)=DB(1,I)+DB(2,I)*DEN(I)+DB(3,I)*DEN(I)*DEN(I)	00210
	1 +DB(4,I)*DEN(I)**3	00211
227	CONTINUE	00212
	IF (DEN(1) .LE. 0.9 .OR. DEN(1) .GT. 3.25) 220,228	00213
228	IF (DEN(2) .LE. 0.7 .OR. DEN(2) .GT. 3.25) 220,229	00214
229	IF (DEN(3) .LE. 0.4 .OR. DEN(3) .GT. 3.25) 220,231	00215
35	FORMAT (I5,I4,2F6.3,F5.1,17X,F5.1,17X,F5.1)	00216
231	X(1,J)=X(1,J)-CAMO(IPHOT,5,2)	00217
	X(2,J)=X(2,J)-CAMO(IPHOT,5,1)	00218
C	ANGLE BETWEEN CAMERA AXIS AND RAY	00219
	R=SQRT(X(1,J)**2+X(2,J)**2)	00220
	CAM=ATANF(R/FL)	00221
	CALL TRNCOORD(CAMO,XT,J,FL,IPHOT)	00222
	CALL ANGLES(XT,XS,FL,J,CAN,CCA,TAB,SUNR)	00223
	X(10,J)=SUNR	00224
	X(5,J)=COSF(CAN)	00225
	X(6,J)=DEN(1)-DEN(2)	00226
	X(6,J)=EXPF(X(6,J)/GAM+(DTHI)/X(5,J))/TENR	00227
	X(7,J)=EXPF(DEN(3)/GAM)*CEXP/COSF(CAM)**4	00228
	X(8,J)=CAN	00229
	J=J+1	00230
	IF (ITRA-300) 220,230,230	00231
230	INO=J-2	00232
	K=1	00233
	DO 238 J=1,INO	00234
	X(1,K)=1.0	00235
	X(2,K)=X(8,J)	00236
	X(3,K)=X(2,K)*X(2,K)	00237
	X(4,K)=1.0/X(7,J)	00238
	WRITE (02,44) X(1,K),X(2,K),X(3,K),X(4,K)	00239
44	FORMAT (4E11.3)	00240
	K=K+1	00241
238	CONTINUE	00242
	NO=K-1	00243
	N=4	00244
	CALL LEASTFIT(N,NO,B)	00245
	A1=B(1)	00246
	A2=B(2)	00247
	A3=B(3)	00248
	DO 243 J=1,INO	00249
	TRB=A1+A2*X(8,J)+A3*X(8,J)*X(8,J)	00250
	X(1,J)=1.	00251
	X(2,J)=X(10,J)	00252

Figure B-2. Listing of program (continued).



```

      X(3,J)=X(7,J)*TRB
      X(4,J)=X(6,J)
      WRITE (02,43) X(1,J),X(2,J),X(3,J),X(4,J)
43  FORMAT (4E11.3)
243 CONTINUE
      N=4
      NO=INO
      CALL LEASTFIT (N,NO,B)
      B1=B(1)
      B2=B(2)
      B3=B(3)
      XLAST=0.0
      J=1
245 XFAD (01,35) IPHOT,ITRA, X(2,J),X(1,J),DEN1,DEN(2),DEN3
      IF (IPHOT) 260,260,244
244 IF (DEN1-DEN3) 322,322,324
222 DEN(1)=DEN3
      DEN(3)=DEN1
      GO TO 325
224 DEN(1)=DEN1
      DEN(3)=DEN3
225 DO 327 I=1,3
      DEN(I)=DB(1,1)+DB(2,1)*DEN(1)+DB(3,1)*DEN(1)*DEN(1)
      +DB(4,1)*DEN(1)**3
227 CONTINUE
      IF (DEN(1) .LE. 0.9 .OR. DEN(1) .GT. 3.25) 245,328
228 IF (DEN(2) .LE. 0.7 .OR. DEN(2) .GT. 3.25) 245,329
229 IF (DEN(3) .LE. 0.4 .OR. DEN(3) .GT. 3.25) 245,246
246 IF(X(1,J)-XLAST) 260,260,247
247 XLAST=X(1,J)
      X(1,J)=X(1,J)-CAMO(IPHOT,5,2)
      X(2,J)=X(2,J)-CAMO(IPHOT,5,1)
      R=SQRT(X(1,J)**2+X(2,J)**2)
      CAM=ATANF(R/FL)
      CALL TRNCOORD(CAMO,XT,J,FL,IPHOT)
      CALL GRDCOORD(CAMO,XT,XPG,J,IPHOT)
      CALL ANGLES(XT,XS,FL,J,CAN,CCA,TAB,SUNR)
      CALL ROTATE(XPG,XLGN,YMID,CROT,SRGT,J)
      COSC=COSF(CAN)
      YRRA=CEXP/COSF(CAM)**4
      DEN(1)=EXPF((DEN(1)-DEN(2))/GAM+DTHI/COSC)
      1 /TENR
      DEN(3)=EXPF(DEN(3)/GAM)*YRRA
      TRB=A1+A2*CAN+A3*CAN*CAN
      BLUE=DEN(3)*TRB
      X(10,J)=DEN(1)-B1-B2*SUNR-B3*BLUE
      J=J+1
      IF (J-200) 245,245,260
C  FILL IN ARRAY WITH PHOTO VALUES
C  X AXIS ALONG THE CENTER LINE OF PLUME
260 KK=J-1
      DO 285 J=1,KK
      LX=X(1,J)/60.+0.5
      IF (LX .LE. 0 .OR. LX .GT. NNXS) 285,262
262 LY=(X(2,J)+YMIDY)/60.+0.5
      IF (LY .LE. 0 .OR. LY .GT. NNYS) 285,264
264 RATIO(IRUN,LX,LY)=X(10,J)*1000.
      IF (J-1) 280,280,267
267 DDEN=X(10,J)-X(10,J-1)
      DKX=LX-LLX
      DKY=LY-LLY
      XKX=ABSF(DKX)
      YKY=ABSF(DKY)

```

Figure B-2. Listing of program (continued).

IF (XKX-YKY) 268,269,269	00316
268 KY=YKY-1.	00317
DIV=YKY	00318
GO TO 270	00319
269 KY=XKX-1.	00320
DIV=XKX	00321
270 IF (DIV-0.) 272,272,280	00322
272 DO 275 K=1,KY	00323
YYK=K	00324
DE=X(10,J-1)+DDEN*YYK/DIV	00325
KKX=LLX+YYK*DKX/DIV+0.5	00326
KKY=LLY+YYK*DKY/DIV+0.5	00327
RATIO(IRUN,KKX,KKY)=DE*1000.	00328
275 CONTINUE	00329
280 LLX=LX	00330
LLY=LY	00331
285 CONTINUE	00332
J=1	00333
KK=KK+1	00334
IF (KK-200) 284,283,283	00335
283 XLAST=0.0	00336
IF (IPHOT) 300,300,245	00337
284 X(1,J)=X(1,KK)	00338
X(2,J)=X(2,KK)	00339
IF (IPHOT) 300,300,247	00340
C INTERPOLATE MISSING VALUES IN ARRAY	00341
300 KND=7	00342
KDN=5	00343
301 NXS=NNXS-2	00344
NYS=NNYS-2	00345
DO 340 I=1,NNYS	00346
DO 340 J=1,NXS	00347
IF (RATIO(IRUN,J,I)) 330,340,330	00348
330 IF (RATIO(IRUN,J+1,I)) 340,332,340	00349
332 DO 334 K=2,KND	00350
KJ=J+K	00351
IF (KJ-NNXS) 333,333,340	00352
333 IF (RATIO(IRUN,KJ,I)) 336,334,336	00353
334 CONTINUE	00354
GO TO 340	00355
336 LJ=KJ-J-1	00356
DJ=KJ-J	00357
DIF=RATIO(IRUN,J,I)-RATIO(IRUN,KJ,I)	00358
DO 338 K=1,LJ	00359
AJ=K	00360
LLJ=J+K	00361
RATIO(IRUN,LLJ,I)=RATIO(IRUN,J,I)-DIF*AJ/DJ	00362
338 CONTINUE	00363
340 CONTINUE	00364
DO 320 I=1,NNXS	00365
DO 320 J=1,NYS	00366
IF (RATIO(IRUN,I,J)) 310,320,310	00367
310 IF (RATIO(IRUN,I,J+1)) 320,312,320	00368
312 DO 314 K=2,KDN	00369
KJ=J+K	00370
IF (KJ-NNYS) 313,313,320	00371
313 IF (RATIO(IRUN,I,KJ)) 316,314,316	00372
314 CONTINUE	00373
GO TO 320	00374
316 LJ=KJ-J-1	00375
DJ=KJ-J	00376
DIF=RATIO(IRUN,I,J)-RATIO(IRUN,I,KJ)	00377
DO 318 K=1,LJ	00378

Figure B-2. Listing of program (continued).

AJ=K	00379
LLJ=J+K	00380
RATIO(IRUN,I,LLJ)=RATIO(IRUN,I,J)-DIF*AJ/DJ	00381
318 CONTINUE	00382
320 CONTINUE	00383
IF (KND=6) 302,302,303	00384
302 KND=10	00385
KDN=6	00386
GO TO 301	00387
C AVERAGE VALUES IN ARRAY	00388
303 WRITE(61,1)	00389
1 FORMAT ( ' TYPE IN 1 TO AVERAGE VALUES OR 2 IF NOT ' )	00390
IGO=TTYIN(4HIGO=)	00391
GO TO (304,380) IGO	00392
304 ITEST=1	00393
DO 370 I=1,NXS	00394
DO 360 J=2,NYS	00395
GO TO (362,364),ITEST	00396
362 X(1,J)=(RATIO(IRUN,I,J)+RATIO(IRUN,I,J-1)+RATIO(IRUN,I,J+1)+	00397
1 RATIO(IRUN,I+1,J))/4	00398
364 X(2,J)=(RATIO(IRUN,I,J)+RATIO(IRUN,I+1,J)+RATIO(IRUN,I+2,J)+	00399
1 RATIO(IRUN,I+1,J+1)+RATIO(IRUN,I+1,J-1))/5	00400
360 CONTINUE	00401
ITEST=2	00402
XMAX=0.0	00403
DO 365 J=2,NYS	00404
RATIO(IRUN,I,J)=X(1,J)	00405
IF (XMAX-X(1,J)) 361,363,363	00406
361 XMAX=X(1,J)	00407
363 X(1,J)=X(2,J)	00408
365 CONTINUE	00409
WRITE (61,39) XMAX	00410
39 FORMAT (E11.3)	00411
370 CONTINUE	00412
380 J=1	00413
READ (19,12) FIX,XL,YL,CONL	00414
500 READ (19,12) FIX,XF,YF,CONF	00415
IF (FIX) 520,520,505	00416
505 DDEN=CONF-CONL	00417
DKX=(XF-XL)	00418
DKY=(YF-YL)	00419
XKX=ABSF(DKX)/50.	00420
YKY=ABSF(DKY)/50.	00421
IF (XKX-YKY) 450,460,460	00422
450 KY=YKY	00423
DIV=YKY	00424
GO TO 470	00425
460 KY=XKX	00426
DIV=XKX	00427
470 IF (DIV=8.) 472,472,490	00428
472 DO 485 K=1,KY	00429
YYK=K	00430
CONC=CONL+DDEN*YYK/DIV	00431
IF (CONC=0.5) 490,490,475	00432
475 XPG(1)=XL+DKX*YYK/DIV	00433
XPG(2)=YL+DKY*YYK/DIV	00434
12 FORMAT (F7.1,2F14.0,F10.1)	00435
CALL ROTATE(XPG,XLOW,YMID,CROT,SROT,J)	00436
LX=X(1,J)/60.+0.5	00437
IF (LX.LE. 0 .OR. LX.GT. NNXS) 490,512	00438
512 LY=(X(2,J)+YMIDY)/60.+0.5	00439
IF (LY.LE. 0 .OR. LY.GT. NNYS) 490,514	00440
514 IF (RATIO(IRUN,LX,LY)) 516,490,516	00441

Figure B-2. Listing of program (continued).

516	CONTINUE	00442
	X(1,J)=RATIO(IRUN,LX,LY)	00443
	X(2,J)=X(1,J)*X(1,J)	00444
	X(3,J)=CONC	00445
	WRITE (04,13) (X(1,J),I=1,3)	00446
13	FORMAT (7E11.3)	00447
	J=J+1	00448
	IF (J-200) 485,485,520	00449
485	CONTINUE	00450
490	XL=XF	00451
	YL=YF	00452
	CONL=CONF	00453
	GO TO 500	00454
520	NO=J-1	00455
	N=3	00456
	CALL LEASTFIT(N,NO,B)	00457
	WRITE (61,37) B(1),B(2)	00458
37	FORMAT ( ' B1',E11.3,'B2',E11.3)	00459
	WRITE (02,42) XLOW,YMID,ROT	00460
42	FORMAT(1H1,'XORG=',F8.0,' YORG=',F7.0,' ROTATION ANGLE=',F5.3)	00461
	DO 540 I=1,NNXS,20	00462
	WRITE (02,31)	00463
31	FORMAT (1H1)	00464
	DO 540 J=1,NNYS	00465
	KK=I+19	00466
	WRITE (02,30) (RATIO(IRUN,K,J),K=I,KK)	00467
30	FORMAT (20I5)	00468
540	CONTINUE	00469
	ROT=-ROT	00470
	SROT=-SINF(ROT)	00471
	CROT=-COSF(ROT)	00472
	XORG=XLOW	00473
	YORG=YMID	00474
	XLOW=0.0	00475
	YMID=YMIDY	00476
	CB=TTYIN(4HB1= )	00477
	CA=TTYIN(4HB2= )	00478
	XSUM=0.	00479
	DO 522 J=1,NO	00480
	XSUM=XSUM+(CB*X(1,J)+CA*X(2,J)-X(3,J))*2	00481
522	CONTINUE	00482
	XNO=NO	00483
	XSUM=XSUM/XNO	00484
	WRITE (61,38) XSUM,NO	00485
38	FORMAT(' MEAN SQUARE ',E11.3,' DF',I5)	00486
	DO 530 I=1,NNXS	00487
	DO 530 J=1,NNYS	00488
	IF (RATIO(IRUN,I,J)) 524,530,524	00489
524	AJ=J	00490
	AI=I	00491
	XPG(1)=AI*60.	00492
	XPG(2)=AJ*60.	00493
	CALL ROTATE(XPG,XLOW,YMID,CROT,SROT,J)	00494
	XPG(1)=X(1,J)+XORG	00495
	XPG(2)=X(2,J)+YORG	00496
	AXZ=RATIO(IRUN,I,J)	00497
	AXZ=CB*AXZ+CA*AXZ*AXZ	00498
	IF (AXZ-C.6) 530,537,537	00499
537	WRITE(20,10) I,XPG(1),XPG(2),AXZ	00500
10	FORMAT(I3,3F15.2)	00501
	RATIO(IRUN,I,J)=AXZ*10.	00502
530	CONTINUE	00503
	J=1	00504

Figure B-2. Listing of program (continued).

	WRITE (20,14) J	00505
14	FORMAT (55X,I3)	00506
	END FILE 20	00507
	WRITE (02,42) XORG,YORG,ROT	00508
	DO 542 I=1,NNXS,20	00509
	WRITE (02,31)	00510
	DO 542 J=1,NNYS	00511
	KK=1+19	00512
	WRITE (02,30) (RATIO(IRUN,K,J),K=1,KK)	00513
542	CONTINUE	00514
	SUM=-ROT	00515
C	IDENTIFICATION FOR SYMBOLIC PLOT. PHOTO NOS, DAY MONTH	00516
	DIF=FFIN(5)	00517
	EDATE=FFIN(5)	00518
	ETIME=FFIN(5)	00519
	DO 602 J=1,8	00520
	X(3,J)=0.0	00521
602	CONTINUE	00522
	WRITE (02,15) SUM,DIF,EDATE,ETIME	00523
15	FORMAT(1H1,///42X,AIRPHOTO ANALYSIS OF OCEAN OUTFALL DISPERSION,	00524
	1 ///,45X,VOLUMETRIC WASTE CONCENTRATION ML PER L'///,55X,	00525
	2'SKETCH ON 60 - FT GRID'//,49X,DIRECTION OF PLUME ' ,F5.2,	00526
	3 ' RADIANS'//,35X,PHOTO NO. ,F4.0,30X,DATE ' ,F3.0, '- ,F3.0,	00527
	4'-68'//)	00528
	WRITE (02,23)	00529
23	FORMAT( 35X, ' CONCENTRATION CODE IN ML/L'//,45X,	00530
	1' ) 0 - 2',15X, ' 1 2 - 4'//,71X, '1'//,45X,	00531
	2'II 4 - 6',15X, 'LL 6 - 10'//,45X, '1',25X, 'LL'//,45X,	00532
	3'PP 10 - 15',14X, 'RR 15 - 20'//,45X, 'PP',24X, 'RR'//,45X,	00533
	4'MM' 20 - 25',14X, '** GT 25 '//,45X, 'MM',24X, '**'/////)	00534
	WRITE (02,45) XORG,YORG	00535
45	FORMAT(60X,'+ X=' ,F8.0, 'E, Y=' ,F7.0, 'N')	00536
	NNYS=NNYS-10	00537
	IKS=NNYS/2	00538
	IEKS=IKS+29	00539
	IKS=IKS-29	00540
	DO 700 LX=2,NNXS	00541
	DO 690 LY=1,NNYS	00542
	AXZ=RATIO(IRUN,LX,LY)	00543
	AXZ=AXZ/10.	00544
	IF (AXZ-0.5) 510,610,605	00545
605	XL=AXZ/2.+1.	00546
	IDO=XL	00547
	GO TO (620,630,640,660),IDO	00548
610	X(1,LY)=8H	00549
	X(2,LY)=8H	00550
	GO TO 690	00551
620	X(1,LY)=8H I	00552
	X(2,LY)=8H	00553
	X(3,1)=X(3,1)+1.	00554
	GO TO 690	00555
630	X(1,LY)=8HI	00556
	X(2,LY)=8HI	00557
	X(3,2)=X(3,2)+1.	00558
	GO TO 690	00559
640	X(1,LY)=8HII	00560
	X(2,LY)=8HI	00561
	X(3,3)=X(3,3)+1.	00562
	GO TO 690	00563
650	X(1,LY)=8HLL	00564
	X(2,LY)=8HLL	00565
	X(3,4)=X(3,4)+1.	00566
	GO TO 690	00567

Figure B-2. Listing of program (continued).

660	IF (AXZ-10.) 650,650,670	00568
670	XL=AXZ/5.-1.	00569
	IDC=XL	00570
	GO TO (675,680,685,688),IDC	00571
675	X(1,LY)=8HOP	00572
	X(2,LY)=8HPP	00573
	X(3,5)=X(3,5)+1.	00574
	GO TO 690	00575
680	X(1,LY)=8HRR	00576
	X(2,LY)=8HRR	00577
	X(3,6)=X(3,6)+1.	00578
	GO TO 690	00579
685	X(1,LY)=8HMM	00580
	X(2,LY)=8HMM	00581
	X(3,7)=X(3,7)+1.	00582
	GO TO 690	00583
688	X(1,LY)=8H**	00584
	X(2,LY)=8H**	00585
	X(3,8)=X(3,8)+1.	00586
690	CONTINUE	00587
	WRITE (02,24) (X(1,J),J=IKS,IEKS)	00588
	WRITE (02,24) (X(2,J),J=IKS,IEKS)	00589
24	FORMAT (70A2)	00590
700	CONTINUE	00591
	DO 603 J=1,8	00592
	XAR(IRUN,J)=X(3,J)*3600.	00593
603	CONTINUE	00594
	IRUN=IRUN+1	00595
	IF (IRUN-IRUNM) 54,54,593	00596
593	AMASS=RATE*60./ABSF(VEL)	00597
	DO 594 IRUN=1,IRUNM	00598
	WRITE(02,18) IRUN	00599
18	FORMAT(1H1,47X,'PRELIMINARY DIFFUSION COMPUTATIONS'//,	00600
1	58X,'FLIGHT NO.',I3, '//19X,	00601
2	' SECTION WIDTH EFF DEPTH SIGMA Y'	00602
3	' COEFFICIENT GROUND X GROUND Y DIFFUSION COEF'//	00603
4	,29X,'FT',7X,'FT',14X,'FT',9X,'PPT',7X,'STATE PLANE '	00604
5	, ' COORDINATES',3X,'FT SQ PER SEC'//)	00605
	L=1	00606
	GO TO (550,552),IRUN	00607
550	LDF=9	00608
	LDD=7	00609
	LDST=3	00610
	GO TO 554	00611
552	LDF=10	00612
	LDD=8	00613
	LDST=LDFX+3	00614
554	NXS=NNXS-2	00615
	DO 600 I=LDST,NXS,5	00616
	DO 560 J=1,NNYS	00617
	IF (RATIO(IRUN,I,J)) 560,560,570	00618
560	CONTINUE	00619
	GO TO 600	00620
570	JST=J	00621
	LNJ=0	00622
	DIV=0.0	00623
	SUM=0.0	00624
	DIF=0.0	00625
	DO 580 J=1,NNYS	00626
	AJ=J*60	00627
	ACD=(RATIO(IRUN,I,J)+RATIO(IRUN,I-1,J)+RATIO(IRUN,I+1,J)+	00628
1	RATIO(IRUN,I-2,J)+RATIO(IRUN,I+2,J))/50	00629
	SUM=SUM+ACD*AJ	00630

Figure B-2. Listing of program (continued).

DI = DIV + ACD	00631
DI = DIV + ACD * AJ * AJ	00632
IF (RATIO (IRUN, I, J)) 580, 580, 575	00633
475 LNY = LNY + 1	00634
580 CONTINUE	00635
XMEAN = SUM / DIF	00636
X(10, L) = DIV / DIF - XMEAN * XMEAN	00637
X(4, L) = LNY * 60	00638
X(5, L) = AMASS / (DIF * 3.6)	00639
X(6, L) = SQRT (X(10, L))	00640
X(7, L) = DIF * 60. / (2.51 * X(6, L))	00641
XPG(1) = 1 * 60	00642
XPG(2) = XMEAN	00643
J = 1	00644
CALL ROTATE (XPG, XLOW, YMID, CROT, SROT, J)	00645
X(8, L) = X(1, J) + XORG	00646
X(9, L) = X(2, J) + YORG	00647
IF (L - 1) 585, 585, 590	00648
585 DJ = 0.	00649
GO TO 595	00650
590 DJ = ABSF (VEL) * (X(10, L) - X(10, L - 1)) / 600.	00651
595 LI = L + 150	00652
X(LDF, LL) = X(10, L)	00653
X(LDD, LL) = X(4, L)	00654
WRITE (02, 17) 1, X(4, L), X(5, L), X(6, L), X(7, L), X(8, L), X(9, L), DJ	00655
17 FORMAT (19X, I6, F9.0, F9.1, 8X, 2E11.3, 2F13.0, E14.3)	00656
L = L + 1	00657
600 CONTINUE	00658
WRITE (02, 26) RATE, VEL	00659
26 FORMAT (177/35X, ' FLOW RATE', F5.1, ' CFS', 17X,	00660
1 'CURRENT VELOCITY', F4.2, ' FPS'//)	00661
WRITE (02, 27) AZ, H	00662
27 FORMAT (35X, ' SUN AZ FM S.', F6.3, ' RAD'	00663
1, 17X, ' SUN ALTITUDE', F6.3, ' RAD')	00664
WRITE (02, 40)	00665
40 FORMAT (47X, 'AREA WITHIN EACH CONCENTRATION RANGE',	00666
1 55X, 'RANGE', 13X, 'AREA', 55X, 'ML/L', 13X, 'SQ FT')	00667
WRITE (02, 41) (XAR (IRUN, J), J = 1, 8)	00668
41 FORMAT (55X, '0 - 2', 8X, E11.3/, 55X, '2 - 4', 8X, E11.3/,	00669
1 55X, '4 - 6', 8X, E11.3/, 55X, '6 - 10', 8X, E11.3/,	00670
2 55X, '10 - 15', 8X, E11.3/, 55X, '15 - 20', 8X, E11.3/,	00671
3 55X, '20 - 25', 8X, E11.3/, 55X, 'GT 25', 8X, E11.3)	00672
594 CONTINUE	00673
AJ = 0.0	00674
DIV = 0.0	00675
SUM = 0.0	00676
AXZ = 0.0	00677
WRITE (02, 31)	00678
NNXS = NNXS - 1	00679
DO 728 I = 1, NNXS	00680
DO 725 J = 1, NNYS	00681
DKX = RATIO (2, I, J) - RATIO (1, I, J)	00682
IF (DKX) 722, 724, 722	00683
722 DKX = DKX / 10.	00684
AJ = AJ + 1.	00685
DIV = DIV + DKX	00686
SUM = SUM + DKX * DKX	00687
AXZ = AXZ + ABSF (DKX)	00688
724 RATIO (2, NNXS, J) = DKX	00689
725 CONTINUE	00690
WRITE (02, 49) (RATIO (2, NNXS, J), J = 1, NNYS)	00691
49 FORMAT (5X, 60I2/)	00692
728 CONTINUE	00693

Figure B-2. Listing of program (continued).

DKX=DIV/AJ	00694
DKY=SUM-DIV*DIV/AJ	00695
DKY=SQRT(DKY/(AJ-1.))	00696
AXZ=AXZ/AJ	00697
AJ=AJ-1.0	00698
WRITE (02,48) DKX,AXZ,DKY,AJ	00699
48 FORMAT(1H1,////,' MEAN DIFFERENCE IN CONCENTRATION',F6.2,	00700
1/' ABSOLUTE MEAN DIFFERENCE ',F6.2,/'	00701
2' STANDARD DEVIATION OF THE MEAN',F6.2,/' DEGREES OF '	00702
3'FREEDOM',F6.0)	00703
L=3	00704
WRITE (02,53)	00705
53 FORMAT (1H1,///20X,'NON STEADY STATE'	00706
1' DIFFUSION COEFFICIENTS'//	00707
2 ,23X,'SECTION',12X,'WIDTH 1',12X,'WIDTH 2',8X,	00708
2 'COEFFICIENTS'//)	00709
DIV=0.	00710
SUM=0.	00711
DTIM=DTIM*2.	00712
LXF=150	00713
LXL=150	00714
730 DJ=(X(10,LXF)-X(9,LXL))/DTIM	00715
WRITE (02,52) L,X(7,LXL),X(8,LXF),DJ	00716
52 FORMAT (23X,15,14X,F6.0,12X,F6.0,10X,F8.2)	00717
L=L+5	00718
SUM=SUM+DJ	00719
DIV=DIV+1.	00720
LXF=LXF+1	00721
LXL=LXL+1	00722
IF(LXF-LL) 730,730,740	00723
740 DIV=SUM/DIV	00724
WRITE (02,60) DIV	00725
60 FORMAT(23X,' MEAN DIFFUSION COEFFICIENT',F10.2)	00726
STOP	00727
END	00728
..	
..	

Figure B-2. Listing of program (continued).



SUBROUTINE ROTATE(XPG,XLOW,YMID,CROT,SROT,J)	00001
DIMENSION XPG(2)	00002
COMMON X(10,200)	00003
RGX=XPG(1)-XLOW	00004
RGY=XPG(2)-YMID	00005
X(1,J)=RGX*SROT+RGY*CROT	00006
X(2,J)=-RGX*CROT+RGY*SROT	00007
RETURN	00008
END	00009
SUBROUTINE SUNLITE (H,AZ,IRUN,DTIM)	00010
C     COMPUTE THE ALTITUDE AND AZIMUTH OF THE SUN	00011
C     TIME IS PACIFIC DAYLIGHT TIME	00012
GO TO (10,20),IRUN	00013
C     READ IN TIME OF DAY IN HRS AND MIN FOR FIRST FLIGHT	00014
10 DPT=FFIN(5)	00015
DP=FFIN(5)	00016
DPT=DPT+DP/60.	00017
C     READ IN DECLINATION OF SUN IN DEGREES (AA),AND MIN (B)	00018
C     AND CHANGE IN MIN PER HOUR (CC). EQUATION OF TIME	00019
C     IN MINUTES (DD), SECONDS (E), AND CHANGE PER HOUR (F)	00020
C     LONGITUDE (WLOX) AND LATITUDE (ALAT).	00021
AA=FFIN(5)	00022
B=FFIN(5)	00023
CC=FFIN(5)	00024
DD=FFIN(5)	00025
E=FFIN(5)	00026
F=FFIN(5)	00027
WLOX=FFIN(5)	00028
ALAT=FFIN(5)	00029
GO TO 30	00030
20 DPT=DPT+DTIM/3600.	00031
30 GCT=DPT+7.	00032
DEC=(AA+(B+CC*GCT)/60.)*3.14159/180.	00033
EQT=(DD+(E+F*GCT)/60.)/60.	00034
GHA=(GCT+EQT)*15.0-180.	00035
TT=GHA-WLOX	00036
TT=TT*3.14159/180.	00037
T=ABS(TT)	00038
ALAT=ALAT*3.14159/180.	00039
Z=SINF(T)/(COSF(ALAT)*TANF(DEC)-SINF(ALAT)*COSF(T))	00040
AZ=ATANF(Z)	00041
IF (TT) 120,120,123	00042
120 IF (AZ) 121,121,122	00043
121 AZ=2.*3.14159+AZ	00044
GO TO 126	00045
122 AZ=3.1359+AZ	00046
GO TO 126	00047
123 IF (AZ) 124,124,125	00048
124 AZ=-AZ	00049
GO TO 126	00050
125 AZ=3.14159-AZ	00051
126 CONTINUE	00052
SINH=SINF(ALAT)*SINF(DEC)+COSF(ALAT)*COSF(DEC)*COSF(T)	00053
COSH=SINF(T)*COSF(DEC)/SINF(AZ)	00054
ALT=ABS(SINH/COSH)	00055
HH=ATANF(ALT)	00056
REF=((1.+25./60.)/60.)*3.14159/180.	00057
H=HH+REF	00058
WRITE (02,1) H,REF,AZ	00059
1 FORMAT(11H SUN'S ALT. ,F10.6,12H REFRACTION ,F10.6,	00060
1/16H AZIMUTH OF SUN ,F10.6)	00061
RETURN	00062
END	00063

Figure B-3. Listing of subroutines.

	SUBROUTINE RESECT (FL,XP,YP,C)	00064
	DIMENSION B(15,6),C(20,3),P(2,8),D(6,7)	00065
C	PHOTO RESECTION PHASE	00066
C	READ IN REFINED PLATE AND GROUND COORDS OF RESECTION POINTS	00067
	IGO=1	00068
	FL=FFIN(1)/25.4	00069
C	FL IS FOCAL LENGTH	00070
	IPLATE=FFIN(1)	00071
	IMAGE=FFIN(1)	00072
	XP=FFIN(1)	00073
	YP=FFIN(1)	00074
	BB=FFIN(1)	00075
	DO 10 I=1,IMAGE	00076
	B(I,1)=FFIN(1)	00077
	B(I,3)=(FFIN(1)-XP)/1000.	00078
	B(I,2)=(FFIN(1)-YP)/1000.	00079
	BB=FFIN(1)	00080
10	CONTINUE	00081
	DO 15 I=1,IMAGE	00082
	BB=FFIN(3)	00083
	B(I,4)=FFIN(3)	00084
	B(I,5)=FFIN(3)	00085
	B(I,6)=FFIN(3)	00086
15	CONTINUE	00087
C	INITIAL APPROXIMATION OF CAMERA PARAMETERS	00088
	C(1,1)=FFIN(3)	00089
	C(1,2)=FFIN(3)	00090
	C(1,3)=FFIN(3)	00091
	C(2,1)=FFIN(3)/57.2928	00092
	C(3,1)=COSF(C(2,1))	00093
	C(2,1)=SINF(C(2,1))	00094
	C(2,2)=FFIN(3)/57.2928	00095
	C(3,2)=COSF(C(2,2))	00096
	C(2,2)=SINF(C(2,2))	00097
	C(2,3)=FFIN(3)/57.2928	00098
	C(3,3)=COSF(C(2,3))	00099
	C(2,3)=SINF(C(2,3))	00100
C	ORIENTATION FACTORS IN C ARRAY	00101
610	C(4,1)=C(3,2)*C(3,3)	00102
	C(5,1)=-C(3,2)*C(2,3)	00103
	C(6,1)=C(2,2)	00104
	C(10,1)=-C(2,2)*C(3,3)	00105
	C(11,1)=C(2,2)*C(2,3)	00106
	C(12,1)=C(3,2)	00107
	C(10,2)=C(4,1)*C(2,1)	00108
	C(11,2)=C(5,1)*C(2,1)	00109
	C(12,2)=C(2,1)*C(2,2)	00110
	C(10,3)=-C(4,1)*C(3,1)	00111
	C(11,3)=-C(5,1)*C(3,1)	00112
	C(12,3)=-C(3,1)*C(2,2)	00113
	C(4,2)=C(3,1)*C(2,3)+C(12,2)*C(3,3)	00114
	C(5,2)=C(3,1)*C(3,3)-C(12,2)*C(2,3)	00115
	C(6,2)=-C(2,1)*C(3,2)	00116
	C(4,3)=C(2,1)*C(2,3)+C(10,1)*C(3,1)	00117
	C(5,3)=C(2,1)*C(3,3)+C(11,1)*C(3,1)	00118
	C(6,3)=C(3,1)*C(3,2)	00119
	DO 612 I=7,9	00120
	C(I,1)=0.	00121
	C(I,2)=-C(I-3,3)	00122
	C(I,3)=C(I-3,2)	00123
	C(13,I-6)=C(5,I-6)	00124
	C(14,I-6)=-C(4,I-6)	00125
612	C(15,I-6)=0.	00126

Figure B-3. Listing of subroutines (continued).

	GO TO (613,763),IGO	00127
C	CLEAR NORMAL EQUATION D ARRAY TO ZERO	00128
613	DO 614 I=1,6	00129
	DO 614 J=I,7	00130
614	D(I,J)=0.	00131
C	COMPUTE P TERMS FOR RESECTION PASS POINTS	00132
	DO 618 NU=1,IMAGE	00133
	DO 619 K=1,3	00134
619	C(16,K)=B(NU,K+3)-C(1,K)	00135
	K=4	00136
	DO 620 L=17,20	00137
	DO 620 I=1,3	00138
	C(L,I)=C(K,1)*C(16,1)+C(K,2)*C(16,2)+C(K,3)*C(16,3)	00139
620	K=K+1	00140
	DO 621 I=1,2	00141
	DO 622 L=1,4	00142
622	P(I,L)=(B(NU,I+1)*C(L+16,3)-(-FL)*C(L+16,I))/C(17,3)	00143
	DO 623 L=5,7	00144
623	P(I,L)=(-B(NU,I+1)*C(6,L-4)+(-FL)*C(I+3,L-4))*C(1,3)/C(17,3)	00145
621	P(I,8)=-P(I,1)	00146
C	CONTRIBUTION TO NORMAL EQUATIONS	00147
	DO 618 I=1,6	00148
	DO 618 J=I,7	00149
	DO 618 K=1,2	00150
618	D(I,J)=D(I,J)+P(K,I+1)*P(K,J+1)	00151
C	FOREWARD SOLUTION	00152
	DO 699 I=1,6	00153
	SQR=SQRT(D(1,1))	00154
	DO 698 J=I,7	00155
698	D(I,J)=D(I,J)/SQR	00156
	IF (I-6)697,696,696	00157
697	IP1=I+1	00158
	DO 699 L=IP1,6	00159
	DO 699 J=L,7	00160
699	D(L,J)=D(L,J)-D(I,L)*D(I,J)	00161
C	BACK SOLUTION	00162
696	D(6,7)=D(6,7)/D(6,6)	00163
	DO 691 I=1,5	00164
	NMI=6-I	00165
	NMIP1=NMI+1	00166
	DO 690 J=NMI,6	00167
690	D(NMI,7)=D(NMI,7)-D(J,7)*D(NMI,J)	00168
691	D(NMI,7)=D(NMI,7)/D(NMI,NMI)	00169
	DO 625 I=4,6	00170
625	D(I,7)=D(I,7)*C(1,3)	00171
C	ADD LEAST SQUARES RESULTS TO CAMERA PARAMETERS IN C ARRAY	00172
	DO 626 J=1,3	00173
	C(1,J)=C(1,J)+D(J+3,7)	00174
	C(4,J)=D(J,7)	00175
	C(5,J)=SQRT(1.-C(4,J)*C(4,J))	00176
	C(6,J)=C(2,J)*C(5,J)+C(3,J)*C(4,J)	00177
	C(7,J)=C(3,J)*C(5,J)-C(2,J)*C(4,J)	00178
	C(2,J)=C(6,J)	00179
626	C(3,J)=C(7,J)	00180
C	TEST MAGNITUDE OF CORRECTIONS FOR ORIENTATION PARAMTERES	00181
	DO 628 I=1,3	00182
	IF (ABS(D(I,7))-0.00001)628,628,610	00183
628	CONTINUE	00184
	IGO=2	00185
	GO TO 610	00186
C	CAMERA PARAMETERS OUTPUT	00187
763	WRITE(02,532)	00188
	WRITE(02,527)	00189

Figure B-3. Listing of subroutines (continued).

WRITE (02,528) IPLATE,(C(1,J),J=1,3)	00190
WRITE (02,529)	00191
WRITE (02,528) IPLATE,(C(2,J),J=1,3)	00192
WRITE (02,528) IPLATE,(C(3,J),J=1,3)	00193
WRITE (02,530) IPLATE	00194
WRITE (02,533) ((C(I,J),J=1,3),I=4,6)	00195
527 FORMAT(/49H PLATE                    XO                    YO                    ZO)	00196
528 FORMAT(/17,3(2X,E14.7))	00197
529 FORMAT(/50H PLATE                    OMEGA                    PHI                    KAPPA)	00198
530 FORMAT(/30H ORIENTATION MATRIX FOR PLATE ,I7)	00199
532 FORMAT(/50H ORIENTATION PARAMETER CORRECTION LIMIT IS 0.00001)	00200
533 FORMAT (1X,3(2X,E14.7))	00201
RETURN	00202
END	00203
SUBROUTINE LEASTFIT (N,NO,B)	00204
DIMENSION XX(10,10),XY(10),B(9),ZITX(10,1)	00205
COMMON X(10,200)	00206
C N=NO OF VARIABLES,NO=NO. OF DATA,B=COFF	00207
KK=N-1	00208
DO 15 J=1,KK	00209
XY(J)=0.	00210
DO 10 I=1,NO,1	00211
XY(J)=XY(J)+X(J,I)*X(N,I)	00212
10 CONTINUE	00213
15 CONTINUE	00214
DO 20 K=1,KK	00215
DO 20 J=1,KK	00216
XX(J,K)=0.	00217
DO 20 I=1,NO	00218
XX(J,K)=XX(J,K)+X(J,I)*X(K,I)	00219
20 CONTINUE	00220
CALL MATINV (XX,KK,ZITX,0,DETERM)	00221
DO 30 J=1,KK	00222
B(J)=0.	00223
DO 30 I=1,KK	00224
B(J)=B(J)+XX(J,I)*XY(I)	00225
30 CONTINUE	00226
WRITE (02,1)	00227
WRITE (02,5) (B(J),J=1,KK)	00228
YY=0.	00229
DO 40 J=1,NO	00230
YY=YY+X(N,J)*X(N,J)	00231
40 CONTINUE	00232
BXX=0.	00233
DO 50 J=1,KK	00234
BXX=BXX+B(J)*XY(J)	00235
50 CONTINUE	00236
IDF=NO-KK	00237
RES=(YY-BXX)/IDF	00238
WRITE (02,3) RES,IDF	00239
1 FORMAT (32H LEAST SQ ESTIMATE OF PARAMETERS )	00240
3 FORMAT (23H MEAN SQ OF RESIDUALS= ,E16.7,5X,4HDF= ,I3)	00241
4 FORMAT (28H VARIANCE-COVARIANCE MATRIX )	00242
5 FORMAT (/4E15.5)	00243
WRITE (02,4)	00244
WRITE (02,5) ((XX(I,J),I=1,KK),J=1,KK)	00245
WRITE (02,7)	00246
7 FORMAT ('                    Y                    EST OF Y                    Y-EST Y')	00247
DO 70 J=1,NO	00248
ESTY=0.0	00249
DO 60 K=1,KK	00250
ESTY=ESTY+B(K)*X(K,J)	00251
60 CONTINUE	00252

Figure B-3. Listing of subroutines (continued).

	DIF=X(N,J)-ESTY	00253
	WRITE (02,6) X(N,J),ESTY,DIF	00254
6	FORMAT(3F15.7)	00255
70	CONTINUE	00256
	RETURN	00257
	END	00258
	SUBROUTINE MATINV(A,N,B,M,DETERM)	00259
C	MATRIX INVERSION WITH ACCOMPANYING SOLUTION OF LINEAR EQUATIONS	00260
	DIMENSION IPIVOT(10), A(10,10), B(10,1), INDEX(10,2), PIVOT(10)	00261
	DETERM=1.0	00262
	DO 20 J=1,N	00263
20	IPIVOT(J)=0	00264
	DO 550 I=1,N	00265
C	SEARCH FOR PIVOT ELEMENT	00266
	AMAX=0.0	00267
	DO 105 J=1,N	00268
	IF (IPIVOT(J)-1) 60, 105, 60	00269
60	DO 100 K=1,N	00270
	IF (IPIVOT(K)-1) 80, 100, 740	00271
80	IF (ABSF(AMAX)-ABSF(A(J,K))) 85, 100, 100	00272
85	IROW=J	00273
	ICOLUM=K	00274
	AMAX=A(J,K)	00275
100	CONTINUE	00276
105	CONTINUE	00277
	IPIVOT(ICOLUM)=IPIVOT(ICOLUM)+1	00278
C	INTERCHANGE ROWS TO PUT PIVOT ELEMENT ON DIAGONAL	00279
	IF (IROW-ICOLUM) 140, 260, 140	00280
140	DETERM=-DETERM	00281
	DO 200 L=1,N	00282
	SWAP=A(IROW,L)	00283
	A(IROW,L)=A(ICOLUM,L)	00284
200	A(ICOLUM,L)=SWAP	00285
	IF(M) 260, 260, 210	00286
210	DO 250 L=1, M	00287
	SWAP=B(IROW,L)	00288
	B(IROW,L)=B(ICOLUM,L)	00289
250	B(ICOLUM,L)=SWAP	00290
260	INDEX(I,1)=IROW	00291
	INDEX(I,2)=ICOLUM	00292
	PIVOT(I)=A(ICOLUM,ICOLUM)	00293
	DETERM=DETERM*PIVOT(I)	00294
C	DIVIDE PIVOT ROW BY PIVOT ELEMENT	00295
	A(ICOLUM,ICOLUM)=1.0	00296
	DO 350 L=1,N	00297
350	A(ICOLUM,L)=A(ICOLUM,L)/PIVOT(I)	00298
	IF(M) 380, 380, 360	00299
360	DO 370 L=1,M	00300
370	B(ICOLUM,L)=B(ICOLUM,L)/PIVOT(I)	00301
C	REDUCE NON-PIVOT ROWS	00302
380	DO 550 L1=1,N	00303
	IF(L1-ICOLUM) 400, 550, 400	00304
400	T=A(L1,ICOLUM)	00305
	A(L1,ICOLUM)=0.0	00306
	DO 450 L=1,N	00307
450	A(L1,L)=A(L1,L)-A(ICOLUM,L)*T	00308
	IF(M) 550, 550, 460	00309
460	DO 500 L=1,M	00310
500	B(L1,L)=B(L1,L)-B(ICOLUM,L)*T	00311
550	CONTINUE	00312
C	INTERCHANGE COLUMNS	00313
	DO 710 I=1,N	00314
	L=N+1-I	00315

Figure B-3. Listing of subroutines (continued).

	IF (INDEX(L,1)-INDEX(L,2)) 630, 710, 630	00316
630	JROW=INDEX(L,1)	00317
	JCOLUMN=INDEX(L,2)	00318
	DO 705 K=1,N	00319
	SWAP=A(K,JROW)	00320
	A(K,JROW)=A(K,JCOLUMN)	00321
	A(K,JCOLUMN)=SWAP	00322
705	CONTINUE	00323
710	CONTINUE	00324
740	RETURN	00325
	END	00326
	FUNCTION REFLECT (AI,AR)	00327
	A=AI-AR	00328
	B=AI+AR	00329
	C=SINF(A)**2	00330
	D=SINF(B)**2	00331
	E=TANF(A)**2	00332
	F=TANF(B)**2	00333
	REFLECT=ABS(A/B+C/D)/2.	00334
	END	00335
	SUBROUTINE TRNCOORD(CAMO,XT,J,FL,IPHOT)	00336
	DIMENSION XT(3),CAMO(3,5,3)	00337
	COMMON X(10,200)	00338
	DO 10 K=1,3	00339
10	XT(K)=CAMO(IPHOT,2,K)*X(1,J)+CAMO(IPHOT,3,K)*X(2,J)+	00340
1	CAMO(IPHOT,4,K)*(-FL)	00341
	XDIS=SQRT(XT(1)**2+XT(2)**2+XT(3)**2)	00342
	DO 20 K=1,3	00343
20	XT(K)=XT(K)/XDIS	00344
	RETURN	00345
	END	00346
	SUBROUTINE GRDCOORD (CAMO,XT,XPG,J,IPHOT)	00347
	DIMENSION CAMO(3,5,3),XT(3),XPG(2)	00348
	XPG(1)=CAMO(IPHOT,1,1)-XT(1)*CAMO(IPHOT,1,3)/XT(3)	00349
	XPG(2)=CAMO(IPHOT,1,2)-XT(2)*CAMO(IPHOT,1,3)/XT(3)	00350
	RETURN	00351
	END	00352
	SUBROUTINE ANGLES(XT,XS,FL,J,CAN,CCA,TAB,SUNR)	00353
	DIMENSION XT(3),XS(9)	00354
	DIV=SQRT(XT(1)**2+XT(2)**2)	00355
	CAN=ABSF(DIV/XT(3))	00356
C	ANGLE BETWEEN RAY IN AIR AND VERTICAL	00357
	CAN=ATANF(CAN)	00358
	SINC=0.75*SINF(CAN)	00359
	COSC=(1.0-SINC**2)**0.5	00360
	TANC=SINC/COSC	00361
C	ANGLE BETWEEN RAY TO CAMERA AND VERTICAL UNDER WATER	00362
	CCA=ATANF(TANC)	00363
	FT=-DIV/TANC	00364
	XDIS=SQRT(XT(1)**2+XT(2)**2+FT**2)	00365
	X1=XT(1)/XDIS	00366
	X2=XT(2)/XDIS	00367
	X3=FT/XDIS	00368
	COSB=X1*XS(1)+X2*XS(2)+X3*XS(3)	00369
	SINB=SQRT(1.0-COSB**2)	00370
	TANB=SINB/ABSF(COSB)	00371
C	ANGLE BETWEEN SUN AND CAMERA RAYS UNDERWATER.	00372
	B=ATANF(TANB)	00373
	B=3.14159265-B	00374
	TAB=B-3.14159/2.	00375
	COSB=-XS(4)*XT(1)-XS(5)*XT(2)+XS(6)*XT(3)	00376
	SINB=SQRT(1.0-COSB**2)	00377
	TANB=SINB/ABSF(COSB)	00378
	SUNR=ATANF(TANB)	00379
	IF (COSB) 260,261,261	00380
260	SUNR=3.14159-SUNR	00381
261	RETURN	00382
	END	00383

Figure B-3. Listing of subroutines (continued).

INPUT LUN 1

000001	000002	000003	000004	000005	000006	000007	000008	000009	000010	000011	000012	000013	000014	000015	000016	000017	000018	000019	000020	000021	000022	000023	000024	000025	000026	000027	000028	000029	000030	000031	000032	000033	000034	000035	000036	000037	000038	000039	000040	000041	000042	000043	000044	000045	000046	000047	000048	000049	000050	000051	000052	000053	000054	000055	000056	000057	000058	000059	000060	000061	000062	000063	000064	000065	000066	000067	000068	000069	000070	000071	000072	000073	000074	000075	000076	000077	000078	000079	000080	000081	000082	000083	000084	000085	000086	000087	000088	000089	000090	000091	000092	000093	000094	000095	000096	000097	000098	000099	000100	000101	000102	000103	000104	000105	000106	000107	000108	000109	000110	000111	000112	000113	000114	000115	000116	000117	000118	000119	000120	000121	000122	000123	000124	000125	000126	000127	000128	000129	000130	000131	000132	000133	000134	000135	000136	000137	000138	000139	000140	000141	000142	000143	000144	000145	000146	000147	000148	000149	000150	000151	000152	000153	000154	000155	000156	000157	000158	000159	000160	000161	000162	000163	000164	000165	000166	000167	000168	000169	000170	000171	000172	000173	000174	000175	000176	000177	000178	000179	000180	000181	000182	000183	000184	000185	000186	000187	000188	000189	000190	000191	000192	000193	000194	000195	000196	000197	000198	000199	000200	000201	000202	000203	000204	000205	000206	000207	000208	000209	000210	000211	000212	000213	000214	000215	000216	000217	000218	000219	000220	000221	000222	000223	000224	000225	000226	000227	000228	000229	000230	000231	000232	000233	000234	000235	000236	000237	000238	000239	000240	000241	000242	000243	000244	000245	000246	000247	000248	000249	000250	000251	000252	000253	000254	000255	000256	000257	000258	000259	000260	000261	000262	000263	000264	000265	000266	000267	000268	000269	000270	000271	000272	000273	000274	000275	000276	000277	000278	000279	000280	000281	000282	000283	000284	000285	000286	000287	000288	000289	000290	000291	000292	000293	000294	000295	000296	000297	000298	000299	000300	000301	000302	000303	000304	000305	000306	000307	000308	000309	000310	000311	000312	000313	000314	000315	000316	000317	000318	000319	000320	000321	000322	000323	000324	000325	000326	000327	000328	000329	000330	000331	000332	000333	000334	000335	000336	000337	000338	000339	000340	000341	000342	000343	000344	000345	000346	000347	000348	000349	000350	000351	000352	000353	000354	000355	000356	000357	000358	000359	000360	000361	000362	000363	000364	000365	000366	000367	000368	000369	000370	000371	000372	000373	000374	000375	000376	000377	000378	000379	000380	000381	000382	000383	000384	000385	000386	000387	000388	000389	000390	000391	000392	000393	000394	000395	000396	000397	000398	000399	000400	000401	000402	000403	000404	000405	000406	000407	000408	000409	000410	000411	000412	000413	000414	000415	000416	000417	000418	000419	000420	000421	000422	000423	000424	000425	000426	000427	000428	000429	000430	000431	000432	000433	000434	000435	000436	000437	000438	000439	000440	000441	000442	000443	000444	000445	000446	000447	000448	000449	000450	000451	000452	000453	000454	000455	000456	000457	000458	000459	000460	000461	000462	000463	000464	000465	000466	000467	000468	000469	000470	000471	000472	000473	000474	000475	000476	000477	000478	000479	000480	000481	000482	000483	000484	000485	000486	000487	000488	000489	000490	000491	000492	000493	000494	000495	000496	000497	000498	000499	000500	000501	000502	000503	000504	000505	000506	000507	000508	000509	000510	000511	000512	000513	000514	000515	000516	000517	000518	000519	000520	000521	000522	000523	000524	000525	000526	000527	000528	000529	000530	000531	000532	000533	000534	000535	000536	000537	000538	000539	000540	000541	000542	000543	000544	000545	000546	000547	000548	000549	000550	000551	000552	000553	000554	000555	000556	000557	000558	000559	000560	000561	000562	000563	000564	000565	000566	000567	000568	000569	000570	000571	000572	000573	000574	000575	000576	000577	000578	000579	000580	000581	000582	000583	000584	000585	000586	000587	000588	000589	000590	000591	000592	000593	000594	000595	000596	000597	000598	000599	000600	000601	000602	000603	000604	000605	000606	000607	000608	000609	000610	000611	000612	000613	000614	000615	000616	000617	000618	000619	000620	000621	000622	000623	000624	000625	000626	000627	000628	000629	000630	000631	000632	000633	000634	000635	000636	000637	000638	000639	000640	000641	000642	000643	000644	000645	000646	000647	000648	000649	000650	000651	000652	000653	000654	000655	000656	000657	000658	000659	000660	000661	000662	000663	000664	000665	000666	000667	000668	000669	000670	000671	000672	000673	000674	000675	000676	000677	000678	000679	000680	000681	000682	000683	000684	000685	000686	000687	000688	000689	000690	000691	000692	000693	000694	000695	000696	000697	000698	000699	000700	000701	000702	000703	000704	000705	000706	000707	000708	000709	000710	000711	000712	000713	000714	000715	000716	000717	000718	000719	000720	000721	000722	000723	000724	000725	000726	000727	000728	000729	000730	000731	000732	000733	000734	000735	000736	000737	000738	000739	000740	000741	000742	000743	000744	000745	000746	000747	000748	000749	000750	000751	000752	000753	000754	000755	000756	000757	000758	000759	000760	000761	000762	000763	000764	000765	000766	000767	000768	000769	000770	000771	000772	000773	000774	000775	000776	000777	000778	000779	000780	000781	000782	000783	000784	000785	000786	000787	000788	000789	000790	000791	000792	000793	000794	000795	000796	000797	000798	000799	000800	000801	000802	000803	000804	000805	000806	000807	000808	000809	000810	000811	000812	000813	000814	000815	000816	000817	000818	000819	000820	000821	000822	000823	000824	000825	000826	000827	000828	000829	000830	000831	000832	000833	000834	000835	000836	000837	000838	000839	000840	000841	000842	000843	000844	000845	000846	000847	000848	000849	000850	000851	000852	000853	000854	000855	000856	000857	000858	000859	000860	000861	000862	000863	000864	000865	000866	000867	000868	000869	000870	000871	000872	000873	000874	000875	000876	000877	000878	000879	000880	000881	000882	000883	000884	000885	000886	000887	000888	000889	000890	000891	000892	000893	000894	000895	000896	000897	000898	000899	000900	000901	000902	000903	000904	000905	000906	000907	000908	000909	000910	000911	000912	000913	000914	000915	000916	000917	000918	000919	000920	000921	000922	000923	000924	000925	000926	000927	000928	000929	000930	000931	000932	000933	000934	000935	000936	000937	000938	000939	000940	000941	000942	000943	000944	000945	000946	000947	000948	000949	000950	000951	000952	000953	000954	000955	000956	000957	000958	000959	000960	000961	000962	000963	000964	000965	000966	000967	000968	000969	000970	000971	000972	000973	000974	000975	000976	000977	000978	000979	000980	000981	000982	000983	000984	000985	000986	000987	000988	000989	000990	000991	000992	000993	000994	000995	000996	000997	000998	000999	001000	001001	001002	001003	001004	001005	001006	001007	001008	001009	001010	001011	001012	001013	001014	001015	001016	001017	001018	001019	001020	001021	001022	001023	001024	001025	001026	001027	001028	001029	001030	001031	001032	001033	001034	001035	001036	001037	001038	001039	001040	001041	001042	001043	001044	001045	001046	001047	001048	001049	001050	001051	001052	001053	001054	001055	001056	001057	001058	001059	001060	001061	001062	001063	001064	001065	001066	001067	001068	001069	001070	001071	001072	001073	001074	001075	001076	001077	001078	001079	001080	001081	001082	001083	001084	001085	001086	001087	001088	001089	001090	001091	001092	001093	001094	001095	001096	001097	001098	001099	001100	001101	001102	001103	001104	001105	001106	001107	001108	001109	001110	001111	001112	001113	001114	001115	001116	001117	001118	001119	00
--------	--------	--------	--------	--------	--------	--------	--------	--------	--------	--------	--------	--------	--------	--------	--------	--------	--------	--------	--------	--------	--------	--------	--------	--------	--------	--------	--------	--------	--------	--------	--------	--------	--------	--------	--------	--------	--------	--------	--------	--------	--------	--------	--------	--------	--------	--------	--------	--------	--------	--------	--------	--------	--------	--------	--------	--------	--------	--------	--------	--------	--------	--------	--------	--------	--------	--------	--------	--------	--------	--------	--------	--------	--------	--------	--------	--------	--------	--------	--------	--------	--------	--------	--------	--------	--------	--------	--------	--------	--------	--------	--------	--------	--------	--------	--------	--------	--------	--------	--------	--------	--------	--------	--------	--------	--------	--------	--------	--------	--------	--------	--------	--------	--------	--------	--------	--------	--------	--------	--------	--------	--------	--------	--------	--------	--------	--------	--------	--------	--------	--------	--------	--------	--------	--------	--------	--------	--------	--------	--------	--------	--------	--------	--------	--------	--------	--------	--------	--------	--------	--------	--------	--------	--------	--------	--------	--------	--------	--------	--------	--------	--------	--------	--------	--------	--------	--------	--------	--------	--------	--------	--------	--------	--------	--------	--------	--------	--------	--------	--------	--------	--------	--------	--------	--------	--------	--------	--------	--------	--------	--------	--------	--------	--------	--------	--------	--------	--------	--------	--------	--------	--------	--------	--------	--------	--------	--------	--------	--------	--------	--------	--------	--------	--------	--------	--------	--------	--------	--------	--------	--------	--------	--------	--------	--------	--------	--------	--------	--------	--------	--------	--------	--------	--------	--------	--------	--------	--------	--------	--------	--------	--------	--------	--------	--------	--------	--------	--------	--------	--------	--------	--------	--------	--------	--------	--------	--------	--------	--------	--------	--------	--------	--------	--------	--------	--------	--------	--------	--------	--------	--------	--------	--------	--------	--------	--------	--------	--------	--------	--------	--------	--------	--------	--------	--------	--------	--------	--------	--------	--------	--------	--------	--------	--------	--------	--------	--------	--------	--------	--------	--------	--------	--------	--------	--------	--------	--------	--------	--------	--------	--------	--------	--------	--------	--------	--------	--------	--------	--------	--------	--------	--------	--------	--------	--------	--------	--------	--------	--------	--------	--------	--------	--------	--------	--------	--------	--------	--------	--------	--------	--------	--------	--------	--------	--------	--------	--------	--------	--------	--------	--------	--------	--------	--------	--------	--------	--------	--------	--------	--------	--------	--------	--------	--------	--------	--------	--------	--------	--------	--------	--------	--------	--------	--------	--------	--------	--------	--------	--------	--------	--------	--------	--------	--------	--------	--------	--------	--------	--------	--------	--------	--------	--------	--------	--------	--------	--------	--------	--------	--------	--------	--------	--------	--------	--------	--------	--------	--------	--------	--------	--------	--------	--------	--------	--------	--------	--------	--------	--------	--------	--------	--------	--------	--------	--------	--------	--------	--------	--------	--------	--------	--------	--------	--------	--------	--------	--------	--------	--------	--------	--------	--------	--------	--------	--------	--------	--------	--------	--------	--------	--------	--------	--------	--------	--------	--------	--------	--------	--------	--------	--------	--------	--------	--------	--------	--------	--------	--------	--------	--------	--------	--------	--------	--------	--------	--------	--------	--------	--------	--------	--------	--------	--------	--------	--------	--------	--------	--------	--------	--------	--------	--------	--------	--------	--------	--------	--------	--------	--------	--------	--------	--------	--------	--------	--------	--------	--------	--------	--------	--------	--------	--------	--------	--------	--------	--------	--------	--------	--------	--------	--------	--------	--------	--------	--------	--------	--------	--------	--------	--------	--------	--------	--------	--------	--------	--------	--------	--------	--------	--------	--------	--------	--------	--------	--------	--------	--------	--------	--------	--------	--------	--------	--------	--------	--------	--------	--------	--------	--------	--------	--------	--------	--------	--------	--------	--------	--------	--------	--------	--------	--------	--------	--------	--------	--------	--------	--------	--------	--------	--------	--------	--------	--------	--------	--------	--------	--------	--------	--------	--------	--------	--------	--------	--------	--------	--------	--------	--------	--------	--------	--------	--------	--------	--------	--------	--------	--------	--------	--------	--------	--------	--------	--------	--------	--------	--------	--------	--------	--------	--------	--------	--------	--------	--------	--------	--------	--------	--------	--------	--------	--------	--------	--------	--------	--------	--------	--------	--------	--------	--------	--------	--------	--------	--------	--------	--------	--------	--------	--------	--------	--------	--------	--------	--------	--------	--------	--------	--------	--------	--------	--------	--------	--------	--------	--------	--------	--------	--------	--------	--------	--------	--------	--------	--------	--------	--------	--------	--------	--------	--------	--------	--------	--------	--------	--------	--------	--------	--------	--------	--------	--------	--------	--------	--------	--------	--------	--------	--------	--------	--------	--------	--------	--------	--------	--------	--------	--------	--------	--------	--------	--------	--------	--------	--------	--------	--------	--------	--------	--------	--------	--------	--------	--------	--------	--------	--------	--------	--------	--------	--------	--------	--------	--------	--------	--------	--------	--------	--------	--------	--------	--------	--------	--------	--------	--------	--------	--------	--------	--------	--------	--------	--------	--------	--------	--------	--------	--------	--------	--------	--------	--------	--------	--------	--------	--------	--------	--------	--------	--------	--------	--------	--------	--------	--------	--------	--------	--------	--------	--------	--------	--------	--------	--------	--------	--------	--------	--------	--------	--------	--------	--------	--------	--------	--------	--------	--------	--------	--------	--------	--------	--------	--------	--------	--------	--------	--------	--------	--------	--------	--------	--------	--------	--------	--------	--------	--------	--------	--------	--------	--------	--------	--------	--------	--------	--------	--------	--------	--------	--------	--------	--------	--------	--------	--------	--------	--------	--------	--------	--------	--------	--------	--------	--------	--------	--------	--------	--------	--------	--------	--------	--------	--------	--------	--------	--------	--------	--------	--------	--------	--------	--------	--------	--------	--------	--------	--------	--------	--------	--------	--------	--------	--------	--------	--------	--------	--------	--------	--------	--------	--------	--------	--------	--------	--------	--------	--------	--------	--------	--------	--------	--------	--------	--------	--------	--------	--------	--------	--------	--------	--------	--------	--------	--------	--------	--------	--------	--------	--------	--------	--------	--------	--------	--------	--------	--------	--------	--------	--------	--------	--------	--------	--------	--------	--------	--------	--------	--------	--------	--------	--------	--------	--------	--------	--------	--------	--------	--------	--------	--------	--------	--------	--------	--------	--------	--------	--------	--------	--------	--------	--------	--------	--------	--------	--------	--------	--------	--------	--------	--------	--------	--------	--------	--------	--------	--------	--------	--------	--------	--------	--------	--------	--------	--------	--------	--------	--------	--------	--------	--------	--------	--------	--------	--------	--------	--------	--------	--------	--------	--------	--------	--------	--------	--------	--------	--------	--------	--------	--------	--------	--------	--------	--------	--------	--------	--------	--------	--------	--------	--------	--------	--------	--------	--------	--------	--------	--------	--------	--------	--------	--------	--------	--------	--------	--------	--------	--------	--------	--------	--------	--------	--------	--------	--------	--------	--------	--------	--------	--------	--------	--------	--------	--------	--------	--------	--------	--------	--------	--------	--------	--------	--------	--------	--------	--------	--------	--------	--------	--------	--------	--------	--------	--------	--------	--------	--------	--------	--------	--------	--------	--------	--------	--------	--------	--------	--------	--------	--------	--------	--------	--------	--------	--------	--------	--------	--------	--------	--------	--------	--------	--------	--------	--------	--------	--------	--------	--------	--------	--------	--------	--------	--------	--------	--------	--------	--------	--------	--------	--------	--------	--------	--------	--------	--------	--------	--------	--------	--------	--------	--------	----

206	1071096	374393	1.3	97.0	1070383	376722	3.1	5.0
207	1072950	373956	42.3	98.0	1070451	376377	3.1	5.0
305	1065334	378561	1.3	98.3	1070456	376273	3.1	5.0
306	1071278	378439	1.3	99.0	1070466	376031	7.4	5.0
307	1073606	377145	75.1	99.8	1070452	375754	6.3	5.0
308	1075864	378167	172.1	100.0	1070449	375885	4.1	5.0
1071900	376300	8500		101.0	1070432	375339	5.0	5.0
0.0	1.0			101.5	1070385	375158	4.1	5.0
306	1071274	378434	1.5	101.8	1070357	375049	13.5	5.0
307	1073606	377145	75.	102.0	1070338	374977	13.5	5.0
308	1075863	378167	172.	103.0	1070250	374629	12.2	5.0
406	1070186	381493	1.5	103.5	1070226	374444	8.5	5.0
407	1074821	381220	61.	104.0	1070201	374258	12.2	5.0
1072200	380000	4500		105.0	1070131	373899	11.0	5.0
0.0	1.0			106.0	1070127	373536	8.5	5.0
205	1068382	375338	1.5	107.0	1070028	373199	8.5	5.0
206	1071096	374493	1.5	108.0	1070028	372866	8.5	5.0
98	1069878	373447	1.5	108.2	1070025	372791	8.5	5.0
99	1070400	376350	1.5	108.5	1070022	372679	3.1	5.0
1070300	374700	4200		109.0	1070015	372491	3.1	5.0
0.0	1.0			110.0	1070201	372379	3.1	5.0
97	1069530	379729	1.5	111.0	1070324	372476	2.0	5.0
99	1070400	376350	1.5	112.0	1070301	372724	3.1	5.0
306	1071274	378439	1.5	113.0	1070261	372937	4.1	5.0
1070700	378400	4200		114.0	1070145	373102	8.5	5.0
0.0	1.0			115.0	1069993	373252	7.4	5.0
94	1072024	381045	1.5	116.0	1069922	373425	4.1	5.0
95	1072223	379452	1.5	116.4	1069866	373484	5.2	5.0
97	1069530	379652	1.5	117.0	1069781	373572	14.8	5.0
406	1070186	381493	1.5	117.5	1069682	373666	16.1	5.0
1071000	381800	4200		118.0	1069583	373760	13.5	5.0
0.0	1.0			118.6	1069463	373865	10.7	5.0

INPUT LUN 3

Figure B-5. Sample input, LUNS 3 and 19.



## APPENDIX C

### PROCESSING 1969 PHOTOGRAPHIC DATA

A general description of the CDC 3300 Computer and special fortran input functions is given in the introduction of Appendix B.

Two main programs were used to process the photos taken in 1969. These were program EDIT, which used the raw data to find film density differences, and the program REMOTE, which used the differences generated by EDIT to find steady and non-steady state diffusion coefficients as well as providing data for symbolic and contour plots of waste concentrations.

#### Program EDIT

A flow diagram for program EDIT is shown in figure C-1. The numbers in parentheses on the diagram refer to the line numbers on the program listing shown in figure C-2.

The input for the program is arranged on three or four LUNS, depending on the number of photographic bands available for each exposure. Each band is on a separate input file. A sample of the coordinate and voltage data is shown in figure C-3. This example shows the beginning of a file of data, with the first three lines being standardization voltages. The format is as listed below.

<u>Column</u>	<u>Data</u>
1	Month photo taken
2-3	Day of month photo taken
4	Flight no. of day
5	Photo no. of flight
6	Blank
7-9	Event no. (see code below)
10	Blank
11-14	y-coordinate of photo
15-18	Voltage value from densitometer

The lines 6-18 are repeated six times across the card. The x coordinate is interpolated across the photo by knowing the number of scan lines and the total distance covered in the x-direction.

<u>Event No.</u>	<u>Description</u>
40-59	Initial red standardization.
60-79	Initial green standardization.
80-99	Initial blue standardization.
100-119	Initial gold standardization.
120-139	Final red standardization.
140-159	Final green standardization.
160-179	Final blue standardization.
180-199	Final gold standardization.
200-299	Normal red color.
300-399	Normal green color.
400-499	Normal blue color.
500-599	Infra-red red color.
600-699	Infra-red green color.
700-799	Infra-red blue color.
800-899	Infra-red black and white.
900-999	Panchromatic black and white.

In running the program, the maximum and minimum voltages must be typed in from the teletype. The program proceeds to read the data, checking to see that it does not read data for a new photo. While reading the input, the number of scan lines are counted and the standardization data is stored. When a new photo is reached, the program backspaces the input LUN to the beginning of the photo. Subroutine LEASTFIT is called, and a least squares adjustment is made of the densitometer voltages to the standard grey scale film densities.

The photo coordinates of the principal point and scan limits are read from LUN 8. The photo coordinate and corresponding voltage are read from the data LUN which was previously backspaced. The film density and x coordinate are computed for each sample point. This process is repeated until one photographic band is completed. The program then goes to the next input LUN, and repeats the process, until all film densities are computed for a single photograph.

The differences between film densities of adjacent photographic bands are found, and the extreme differences are rejected. The remaining differences are printed in an array, from which the general shape of the plume may be found by locating abrupt changes in film density. An example of the output is shown in figure C-4, where the non-zero entries in the array are the differences between film densities of adjacent bands for a particular photo.

The program checks to see if there is another photograph to be processed and if so, the overall process is repeated.

#### Program REMOTE

Program REMOTE is the second program used for processing the photographic data. A flow diagram of program REMOTE is shown in figure C-5. The numbers in parentheses correspond to the line numbers on the listing of the program in figure C-7. The subroutines are listed in figure C-8.

Differences in film densities from program EDIT are on LUNS 1, 2, or 3. The boat data is on LUN 4, general information on LUN 7, photo control coordinates on LUN 8, ground control on LUN 9, and initial orientation parameters on LUN 10. Sample input data is shown in figure C-9.

The program begins by orienting all of the photos. The current velocity and orientation of the plume are then computed. After finding the azimuth and altitude of the sun at the time the photographs were taken, sun ray vectors are computed. The waste concentrations as measured from the boat are read in, and concentration and array indices are computed at 60-ft intervals along the boat's track. These values are saved for later use on scratch LUN 5.

Subroutine PROCESS is called, which reads the photo identification, finds the atmospheric attenuation, and reads in the density difference between adjacent bands which was the output from program EDIT. Ground coordinates, array indices, light values and angles are computed, and the indices, angles, and light values written out. The equation for the light return which would be present in the open sea ( $R_{pho}$ ) is determined. The differences between the open sea values and the values found by measuring the light return on the photograph for each sample point are computed and stored. A flow diagram of PROCESS is given in figure C-6. The subroutine then returns to the main program, which checks to see if the last band was processed. If not, the solution is repeated. When the last band is reached, the program compares the values of waste concentrations found by using various combinations of the photographic bands with those from the boat data. When a good combination is found, coefficients relating the light values to the waste concentrations are typed in, and the waste concentrations for the array are computed. The data generated is then used to form a symbolic plot (see figure 28), and can also be saved for making a

contour plot of waste concentrations (see figure 29). The diffusion coefficients for each flight are computed and when the last flight has been processed, the non-steady state diffusion coefficients are determined.

#### Input Data Description

The input data for program REMOTE is shown in figure C-9. The data displayed as LUN 7 is as follows:

<u>Line</u>	<u>Description</u>
1-2	Approximate difference in orientation between Hasselblads and K-17 in degrees.
3-5	Times of three flights in hours and minutes, P.D.T.
6	Effluent flow rate, gpm.
7-8	Declination of sun, degrees (line 8) and minutes (line 9).
10	Change of declination of sun, minutes per hour.
11-12	Equation of time in minutes (line 11), seconds (line 12) and change in seconds per hour (line 13).
13	Longitude of outfall.
14	Latitude of outfall.
15	The difference between true north and grid north in degrees.
16-23	Each line contains the film gamma, film speed and optical thickness of the atmosphere for each of eight spectral bands.
24-26	Speed and aperture settings for K-17 for three flights.
27-29	Speed and aperture settings for Hasselblad 1 for three flights.

<u>Line</u>	<u>Description</u>
30-32	Speed and aperture settings for Hasselblad 2 for three flights.
33-40	Coefficients for determining atmospheric attenuation from the sea to the camera station.
41	Number indicating whether or not the antivignetting filter is on the K-17, 0 = yes, 1 = no.

The input for LUN 8 contains photo coordinates as measured by the coordinatograph and digitizer. The first five digits of each line are constant data, and represent:

<u>Col.</u>	<u>Data</u>
1	Month photo taken.
2-3	Day of month photo taken.
4	Flight number.
5	Photo number of flight.

After the constant data there are three groups of data on each line, each containing an event number, x-coordinate, y-coordinate, and four zeros where the voltage is normally recorded. The event number coding is as follows:

<u>Event No.</u>	<u>Description</u>
000	Principal point.
001-019	Ground control points (numbers must match those on LUN 9. See below).
020-029	Floats for computing the current velocity.
030-033	Scan limits on photograph.
034	Point near head of plume.
035	Point near tail of plume, which, together with 034 will give orientation of waste plume.

The ground coordinate data is prepared on LUN 9. Each point listed as control on LUN 8 must have ground coordinates on LUN 9. Reading across a line are the point number, the x and y state plane coordinates, and the approximate elevation above mean sea level.

LUN 10 contains the approximate orientation parameters for the camera station relative to the state plane coordinate system. Reading across the line are the photo number, the x and y coordinates, the flying height, and the rotation angles and the x, y, and z axis. These are used in subroutine RESECT as initial conditions for a non-linear least squares solution for the camera station position and orientation.

#### Subroutines for REMOTE

<u>Subroutine</u>	<u>Description</u>
Process	Computes array indices for particular ground coordinates, light values, and sun angles. It also determines the equation for light return from the open sea, and finds the difference between the light return measured and that which would be present if waste area were open sea.
Resect	Determines the orientation of oblique photographs and was modified from USC and GS program RESECTION. Each time the subroutine is called, the camera station coordinates and orientation matrix are printed on LUN 20.
Sunlight	Computes the altitude and azimuth of the sun. Time must be given as Pacific Daylight Time, and all pertinent information dealing with the equation of time must be read in. A value for the longitude and latitude of the area being considered is also necessary.
Trncoord	Converts the photographic vector to a unit vector based on the state plane coordinate system.
Zeroarray	Sets IPHOT, X or CAMO array to zero.
Orimat	Determines orientation matrix.

<u>Subroutine</u>	<u>Description</u>
Interp	Interpolates missing values in IPHOT array.
Average	Averages values in IPHOT array.
Cull	Rejects extreme values in array.
Leastfit	Determines the least squares solution of the regression coefficients for a linear model with one independent and up to nine dependent variables. (See lines 351-422 of EDIT listing and omit lines 393+2, 401+1, 401+2, 405-420).
Matinv	Determines the inverse of a square matrix (see lines 423-490 of EDIT listing).

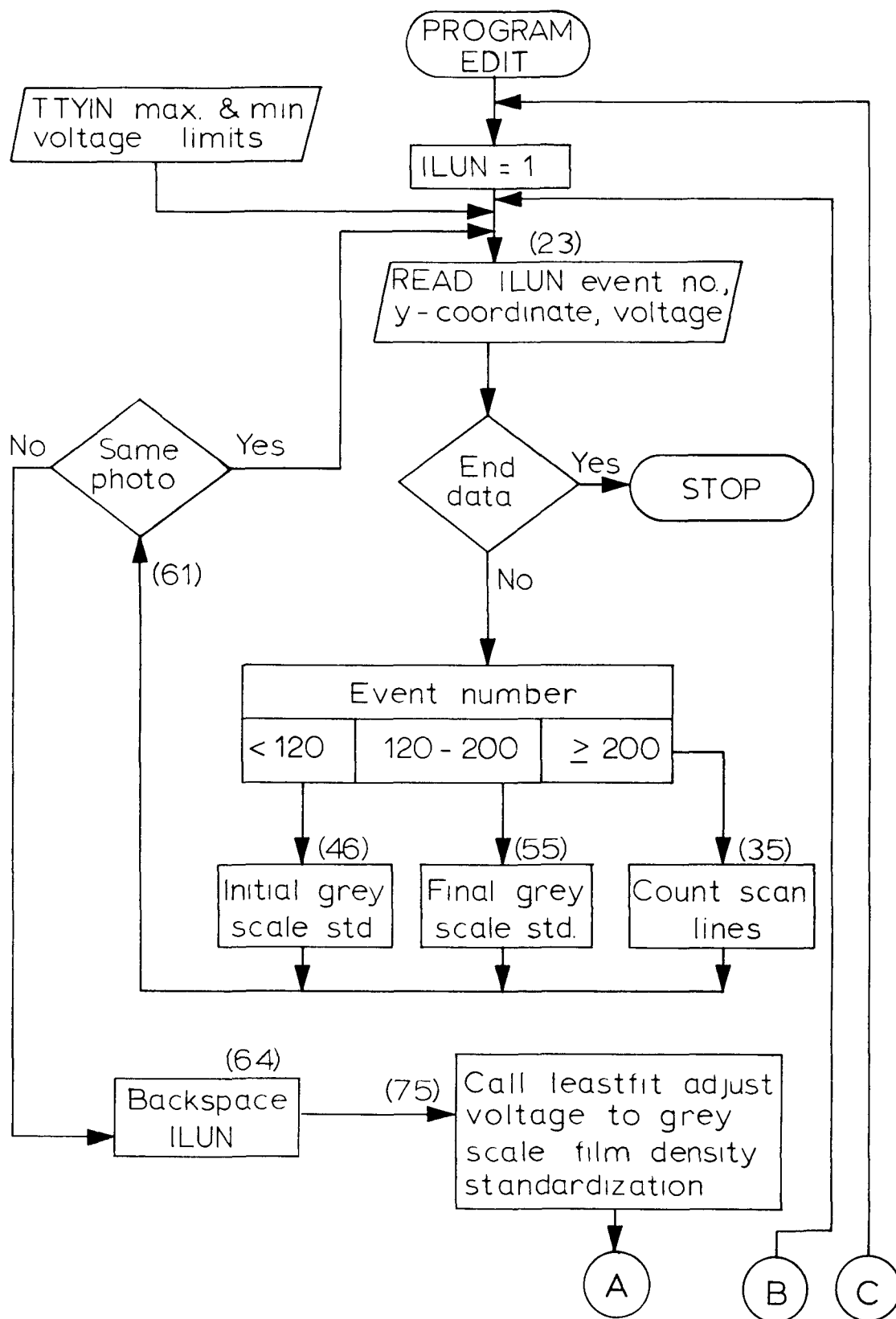


Figure C-1. Flow diagram for computer program EDIT.



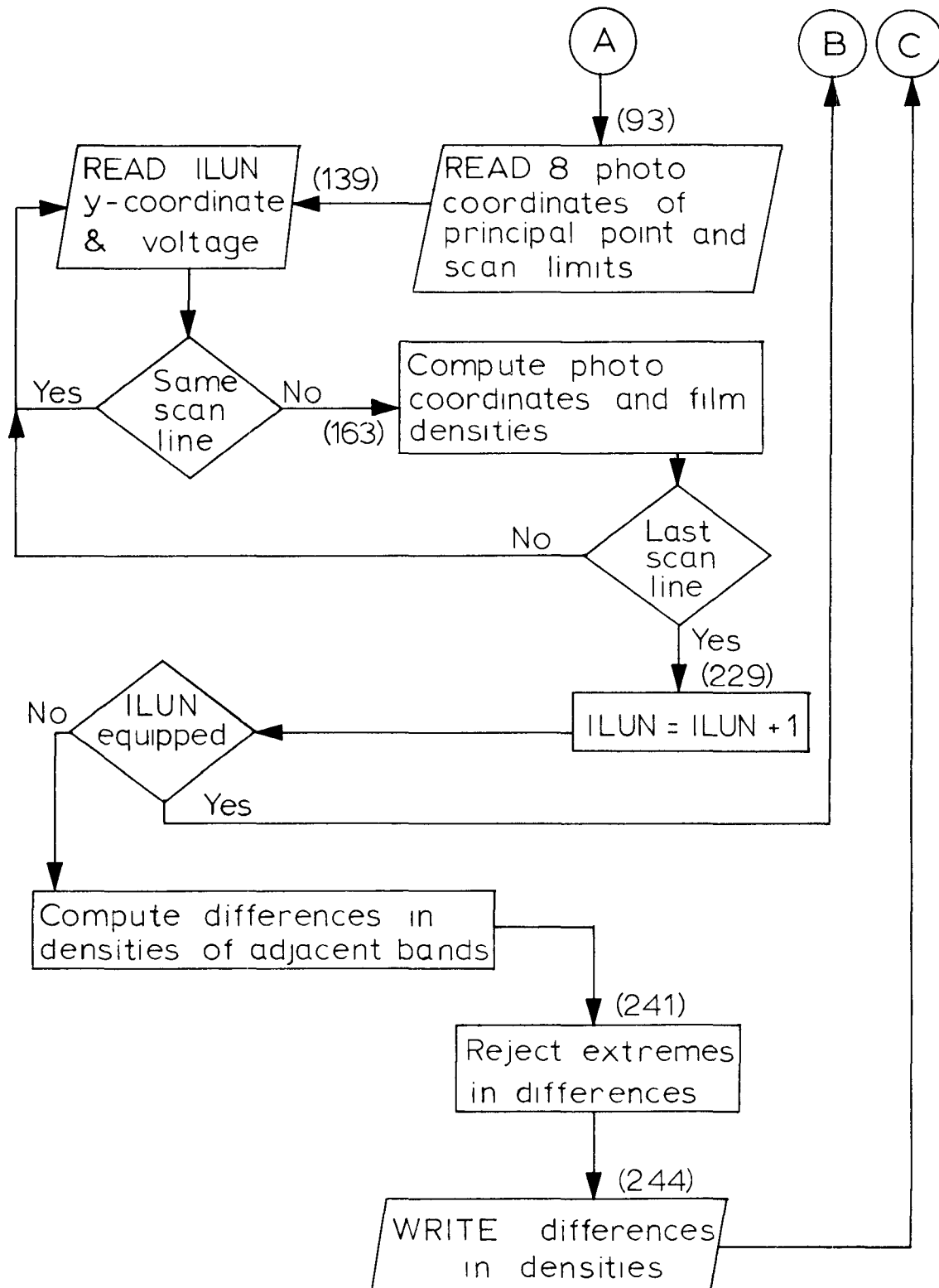


Figure C-1. Flow diagram for computer program EDIT.

PROGRAM EDIT	00001
COMMON IPHOT(4,60,60),X(10,60),B(15,6),IVT(6),BB(9)	00002
INTEGER HARDWARE	00003
10 ILUN=1	00004
DCOOR=C.07	00005
XPH=30.	00006
YPH=30.	00007
NXI=60	00008
NYI=60	00009
KGO=1	00010
DO 90 I=1,NXI	00011
DO 90 J=1,NYI	00012
DO 90 K=1,4	00013
90 IPHOT(K,I,J)=0	00014
95 NOL=0	00015
JNO=0	00016
NOS=0	00017
VOL1=TTYIN(4HLVOL)	00018
VOL2=TTYIN(4HHVOL)	00019
LS=0	00020
K=1	00021
KK=1	00022
100 READ(ILUN,1) IMO,IDATE,IFLT,IPH,(IVT(I),X(10,I),X(9,I),	00023
1I=1,6)	00024
1 FORMAT (I1,I2,2I1,X,6(I3,F5.3,F4.1))	00025
IF (EOF(ILUN)) GO TO 1000	00026
IF (IVT(1).LT.200) GO TO 120	00027
IF (NOL.GE. 1) GO TO 111	00028
IPLATE=(IFLT-1)*10+IPH	00029
IDENT=IFLT*10+IPH	00030
IBAND=IVT(1)/100-1	00031
IF(IPLATE .GT. 30) GO TO 111	00032
XPH=TTYIN(4HPHX=)	00033
YPH=TTYIN(4HPHY=)	00034
111 IF (X(10,2) .GT. X(10,1)) 112,114	00035
112 L=1	00036
GO TO 116	00037
114 L=2	00038
116 NOL=NOL+1	00039
IF(LS-L) 118,100,118	00040
118 NOS=NOS+1	00041
LS=L	00042
WRITE(61,21) LS,NOS,NOL	00043
21 FORMAT(3I5)	00044
GO TO 100	00045
120 IF(IVT(1).GT.119) GO TO 140	00046
DO 132 I=1,6	00047
IF (IVT(I) .EQ.0 ) GO TO 132	00048
X(1,K)=1.0	00049
X(2,K)=X(9,I)	00050
X(3,K)=X(9,I)*X(9,I)	00051
K=K+1	00052
132 CONTINUE	00053
GO TO 100	00054
140 NOL=NOL+1	00055
JNO=JNO+1	00056
DO 142 I=1,6	00057
IF (IVT(I) .EQ. 0) GO TO 142	00058
X(5,KK)=X(9,I)	00059
KK=KK+1	00060
IF (KK-16) 142,142,145	00061
142 CONTINUE	00062
GO TO 100	00063

Figure C-2. Listing of program EDIT.

145	DO 150 I=1,NOL	00064
	BACKSPACE ILUN	00065
150	CONTINUE	00066
	X(4,1)=0.0	00067
	X(4,2)=0.27	00068
	DO 160 I=3,16	00069
	X(4,I)=X(4,I-1)+0.20	00070
160	CONTINUE	00071
	N=4	00072
	NO=16	00073
	IF(K .GT. 16) 170,1000	00074
170	CALL LEASTFIT(N,NO,BB,RES)	00075
	B(1,1)=BB(1)	00076
	B(1,2)=BB(2)	00077
	B(1,3)=BB(3)	00078
	IF(KK .GT. 16) 180,1000	00079
180	DO 190 I=1,16	00080
	X(2,I)=X(5,I)	00081
	X(3,I)=X(2,I)*X(2,I)	00082
190	CONTINUE	00083
	CALL LEASTFIT(N,NO,BB,RES)	00084
	B(2,1)=BB(1)	00085
	B(2,2)=BB(2)	00086
	B(2,3)=BB(3)	00087
	GO TO (195,250),KGO	00088
C	FIND SCAN LIMITS AND PRINCIPLE PT	00089
195	L=0	00090
	K=1	00091
	REWIND 8	00092
200	READ(8,2) IFC,(IVT(I),X(1,I),X(2,I),I=1,3)	00093
	2 FORMAT(3X,I2,3(14,2F6.3,7X))	00094
	IF (EOF(8)) GO TO 1000	00095
	IF (IFC-IDENT) 200,210,200	00096
210	DO 220 I=1,3	00097
	IF (IVT(I).EQ.0.AND.X(1,I).GT.0.1) GO TO 212	00098
	IF (IVT(I).GE.30.AND.IVT(I).LE.33) 216,220	00099
212	XP=X(1,I)	00100
	YP=X(2,I)	00101
	K=2	00102
	GO TO 220	00103
216	J=IVT(I)-19	00104
	B(J,1)=X(1,I)	00105
	B(J,2)=X(2,I)	00106
	L=L+1	00107
220	CONTINUE	00108
	IF(L .GE. 4) 230,200	00109
230	GO TO (232,236),K	00110
232	SUM1=0.0	00111
	SUM2=0.0	00112
	DO 234 I=11,14	00113
	SUM1=SUM1+B(I,1)	00114
	SUM2=SUM2+B(I,2)	00115
234	CONTINUE	00116
	XP=SUM1/4.	00117
	YP=SUM2/4.	00118
236	DO 238 I=11,14	00119
	B(I,1)=B(I,1)-XP	00120
	B(I,2)=B(I,2)-YP	00121
238	CONTINUE	00122
250	AJ=NOS-1	00123
	XADD=0.0	00124
	IF(IFLT.LE.3) GO TO 242	00125
	AJ=AJ+1	00126

Figure C-2. Listing of program EDIT. (Continued)

	XADD=DELX/2.0	00127
242	DELX=(B(14,1)-B(11,1)+B(13,1)-B(12,1))/(AJ*2.)	00128
	DELY1=(B(14,2)-B(11,2))/AJ	00129
	DELY2=(B(13,2)-B(12,2))/AJ	00130
	KNO=NCL-JNO	00131
	WRITE(61,22) KNO,DELX,DELY1,DELY2	00132
22	FORMAT(110,3F10.3)	00133
	K=0	00134
	KK=C	00135
	DO 400 IK=1,KNO	00136
	JS=K+1	00137
	JE=K+6	00138
C	READ AND PROCESS ONE SCAN LINE AT A TIME	00139
	READ(ILUN,3)(X(10,I),X(9,I),I=JS,JE)	00140
3	FORMAT(6X,6(3X,F5.3,F4.1))	00141
	IF(K.GT.0) GO TO 280	00142
	IF(X(10,1)-X(10,2)) 272,272,274	00143
272	L=1	00144
	GO TO 276	00145
274	L=2	00146
276	LS=L	00147
	K=K+6	00148
	GO TO 400	00149
280	IND=K+6	00150
	JS=K+1	00151
	DO 290 J=JS,IND	00152
	IF(X(10,J-1)-X(10,J)) 282,284,286	00153
282	L=1	00154
	GO TO 288	00155
284	GO TO (286,282),L	00156
286	L=2	00157
288	IF(LS.NE.L) GO TO 300	00158
290	CONTINUE	00159
	K=K+6	00160
	GO TO 400	00161
C	PROCESS SCAN LINE	00162
300	LS=L	00163
	IST=J	00164
	IF(J.LT.12) GO TO 392	00165
	ANOS=KK	00166
	KK=KK+1	00167
C	DENSITOMETER STD FOR LINE	00168
	DO 310 I=1,3	00169
	B(3,I)=B(1,I)+(B(2,I)-B(1,I))*ANOS/AJ	00170
310	CONTINUE	00171
	BDIR=(X(10,3)-X(10,2))*100.	00172
	IF(BDIR.LE.0.) GO TO 330	00173
C	PHOTO COORD OF START AND END OF SCAN	00174
	XST=B(12,1)+DELX*ANOS+XADD	00175
	YST=B(12,2)+DELY2*ANOS	00176
	XED=B(11,1)+DELX*ANOS+XADD	00177
	YED=B(11,2)+DELY1*ANOS	00178
	JST=3	00179
	J=IST-3	00180
	KKA=2	00181
	GO TO 340	00182
330	XST=B(11,1)+DELX*ANOS+XADD	00183
	YST=B(11,2)+DELY1*ANOS	00184
	XED=B(12,1)+DELX*ANOS+XADD	00185
	YED=B(12,2)+DELY2*ANOS	00186
	JST=3	00187
	J=IST-3	00188
	KKA=1	00189

Figure C-2. Listing of program EDIT. (Continued)

340	BJ=IST-1	00190
	DELX3=(XED-XST)/BJ	00191
	DELY3=(YED-YST)/BJ	00192
	IF (ABS(DELY3) .GT. 0.15) GO TO 392	00193
	DO 380 I=JST,J	00194
	IF (ABS(X(9,I)-X(9,I+1)) .GT. 10. .AND. ABS(X(9,I)-	00195
	1X(9,I-1)) .GT. 10. .AND. ABS(X(9,I+1)-X(9,I-1))	00196
	2. LT. 10.) GO TO 380	00197
	IF (X(9,I) .LT. VOL1 .OR. X(9,I) .GT. VOL2) GO TO 380	00198
	AAJ=I-1	00199
	AAJ=AAJ+0.5	00200
	XP=XST+DELX3*AAJ	00201
	YP=YST+(X(10,I)-X(10,1))	00202
	LX=XP/DCOOR+XPH+0.5	00203
	LY=YP/DCOOR+YPH+0.5	00204
	DEN=B(3,1)+B(3,2)*X(9,I)+B(3,3)*X(9,I)*X(9,I)	00205
	IF (IBAND .GT. 6) DEN=4.0-DEN	00206
	IF (LX .LE. 0. OR. LX .GT. NXI) GO TO 380	00207
	IF (LY .LE. 0. OR. LY .GT. NYI) GO TO 380	00208
	IPHOT(ILUN,LX,LY)=DEN*100.	00209
380	CONTINUE	00210
392	K=0	00211
	DO 395 J=IST,IND	00212
	K=K+1	00213
	X(10,K)=X(10,J)	00214
	X(9,K)=X(9,J)	00215
395	CONTINUE	00216
400	CONTINUE	00217
	DO 410 I=1,JNO	00218
410	READ(ILUN,1) IMO	00219
	B(7,ILUN)=IFLT	00220
	B(8,ILUN)=IPLATE	00221
	B(9,ILUN)=IBAND	00222
	KND=4	00223
	KDN=4	00224
	NXS=NXI-2	00225
	NYS=NYI-2	00226
	CALL INTERP(NXI,NYI,NXS,NYS,KND,KDN,ILUN)	00227
	CALL CULL(NXI,NYI,ILUN)	00228
	ILUN=ILUN+1	00229
	IF (HARDWARE(ILUN) .EQ. 1) GO TO 95	00230
	IK=ILUN-2	00231
	DO 500 I=1,NXI	00232
	DO 500 J=1,NYI	00233
	DO 500 K=1,IK	00234
	IF (IPHOT(K,I,J) .GT. 0. AND. IPHOT(K+1,I,J) .GT. 0) 490,495	00235
490	IPHOT(K,I,J)=IPHOT(K,I,J)-IPHOT(K+1,I,J)	00236
	GO TO 500	00237
495	IPHOT(K,I,J)=0	00238
500	CONTINUE	00239
	DO 700 K=1,IK	00240
	CALL CULL(NXI,NYI,K)	00241
	LUNO=30+K	00242
	IF (HARDWARE(LJNO) .NE. 1) CALL EQUIP(LUNO,SHFILE)	00243
	WRITE(LUNO,60) IMO,IDATE,B(7,1),IPH,B(8,1),B(9,K),B(9,K+1)	00244
	1,XPH,YPH,DCOOR	00245
60	FORMAT(2I5,F5.0,I5,5F5.0,F5.3)	00246
	IJ=NXI/2	00247
	DO 650 J=1,NYI	00248
650	WRITE(LUNO,61) (IPHOT(K,I,J),I=1,IJ)	00249
	IJ=IJ+1	00250
	DO 660 J=1,NYI	00251
660	WRITE(LUNO,61) (IPHOT(K,I,J),I=IJ,NXI)	00252

Figure C-2. Listing of program EDIT. (Continued)

61	FORMAT(30I4)	00253
700	CONTINUE	00254
	GO TO 10	00255
1000	STOP	00256
	END	00257
	FUNCTION STDDEV(SUM1,SUM2,AJ)	00258
	STDDEV=SGRT((SUM2-SUM1*SUM1/AJ)/(AJ-1.))	00259
	RETURN	00260
	END	00261
	SUBROUTINE INTERP(NXI,NYI,NXS,NYS,KND,KDN,KLUN)	00262
	COMMON IPHOT(4,60,60),X(10,60),B(15,6),IVT(6),JB(9)	00263
	DO 540 I=1,NYI	00264
	DO 540 J=1,NXS	00265
	IF (IPHOT(KLUN,J,1)) 530,540,530	00266
530	IF (IPHOT(KLUN,J+1,1)) 540,532,540	00267
532	DO 534 K=2,KND	00268
	KJ=J+K	00269
	IF (KJ-NXI) 533,533,540	00270
533	IF (IPHOT(KLUN,KJ,1)) 536,534,536	00271
534	CONTINUE	00272
	GO TO 540	00273
536	LJ=KJ-J-1	00274
	DJ=KJ-J	00275
	DIF=IPHOT(KLUN,J,1)-IPHOT(KLUN,KJ,1)	00276
	DO 538 K=1,LJ	00277
	AJ=K	00278
	LLJ=J+K	00279
	IPHOT(KLUN,LLJ,1)=IPHOT(KLUN,J,1)-DIF*AJ/DJ	00280
538	CONTINUE	00281
540	CONTINUE	00282
	DO 520 I=1,NXI	00283
	DO 520 J=1,NYS	00284
	IF (IPHOT(KLUN,I,J)) 510,520,510	00285
510	IF (IPHOT(KLUN,I,J+1)) 520,512,520	00286
512	DO 514 K=2,KDN	00287
	KJ=J+K	00288
	IF (KJ-NYI) 513,513,520	00289
513	IF (IPHOT(KLUN,I,KJ)) 516,514,516	00290
514	CONTINUE	00291
	GO TO 520	00292
516	LJ=KJ-J-1	00293
	DJ=KJ-J	00294
	DIF=IPHOT(KLUN,I,J)-IPHOT(KLUN,I,KJ)	00295
	DO 518 K=1,LJ	00296
	AJ=K	00297
	LLJ=J+K	00298
	IPHOT(KLUN,I,LLJ)=IPHOT(KLUN,I,J)-DIF*AJ/DJ	00299
518	CONTINUE	00300
520	CONTINUE	00301
	RETURN	00302
	END	00303
	SUBROUTINE AVERAGE(NXS,NYS,KLUN)	00304
	COMMON IPHOT(4,60,60),X(10,60),B(15,6),IVT(6),JB(9)	00305
	ITEST=1	00306
	DO 570 I=1,NXS	00307
	DO 560 J=2,NYS	00308
	GO TO (562,564),ITEST	00309
562	X(1,J)=(IPHOT(KLUN,I,J)+IPHOT(KLUN,I,J-1)+IPHOT(KLUN,I,J+1)+	00310
	1 IPHOT(KLUN,I+1,J))/4	00311
564	X(2,J)=(IPHOT(KLUN,I,J)+IPHOT(KLUN,I+1,J)+IPHOT(KLUN,I+2,J)+	00312
	1 IPHOT(KLUN,I+1,J+1)+IPHOT(KLUN,I+1,J-1))/5	00313
560	CONTINUE	00314
	ITEST=2	00315

Figure C-2. Listing of program EDIT. (Continued)

DO 565 J=2,NYS	00316
IPHOT(KLUN,I,J)=X(1,J)	00317
X(1,J)=X(2,J)	00318
565 CONTINUE	00319
570 CONTINUE	00320
RETURN	00321
END	00322
SUBROUTINE CULL(NXI,NYI,KLUN)	00323
COMMON IPHOT(4,60,60),X(10,60),B(15,6),IVT(6),JB(9)	00324
BJ=9.	00325
IX=NXI-2	00326
IY=NYI-2	00327
DO 100 I=1,IX	00328
DO 100 J=1,IY	00329
SUM1=0.0	00330
SUM2=0.0	00331
DO 20 IK=1,3	00332
DO 20 JK=1,3	00333
IP=I+IK-1	00334
JP=J+JK-1	00335
IF(IPHOT(KLUN,IP,JP)) 10,100,10	00336
10 AI=IPHOT(KLUN,IP,JP)	00337
SUM1=SUM1+AI	00338
SUM2=SUM2+AI*AI	00339
20 CONTINUE	00340
SUM2=STDDEV(SUM1,SUM2,BJ)	00341
AI=SUM1/BJ	00342
BI=IPHOT(KLUN,I+1,J+1)	00343
CI=(SUM1-BI)/(BJ-1.)	00344
SUM1=AI-SUM2	00345
SUM2=AI+SUM2	00346
IF(BI.LT.SUM1.OR.BI.GT.SUM2) IPHOT(KLUN,I+1,J+1)=CI	00347
100 CONTINUE	00348
RETURN	00349
END	00350
SUBROUTINE LEASTFIT (N,NO,BB,RES)	00351
COMMON IPHOT(4,60,60),X(10,60),B(15,6),IVT(6)	00352
DIMENSION BB(9),XX(10,10),XY(10),ZITX(10,1)	00353
N=NO OF VARIABLES,NO=NO. OF DATA,B=COEFF	00354
14 KK=N-1	00355
DO 15 J=1,KK	00356
XY(J)=0.	00357
DO 10 I=1,NO,1	00358
XY(J)=XY(J)+X(J,I)*X(N,I)	00359
15 CONTINUE	00360
15 CONTINUE	00361
DO 20 K=1,KK	00362
DO 20 J=1,KK	00363
XX(J,K)=0.	00364
DO 20 I=1,NO	00365
XX(J,K)=XX(J,K)+X(J,I)*X(K,I)	00366
20 CONTINUE	00367
CALL MATINV (XX,KK,ZITX,0,DETERM)	00368
DO 30 J=1,KK	00369
BB(J)=0.	00370
DO 30 I=1,KK	00371
BB(J)=BB(J)+XX(J,I)*XY(I)	00372
30 CONTINUE	00373
WRITE (20,1)	00374
WRITE (20,5) (BB(J),J=1,KK)	00375
YY=0.	00376
DO 40 J=1,NO	00377
YY=YY+X(N,J)*X(N,J)	00378

Figure C-2. Listing of program EDIT. (Continued)

40	CONTINUE	00379
	BXX=0.	00380
	DO 50 J=1, KK	00381
	BXX=BXX+BB(J)*XY(J)	00382
50	CONTINUE	00383
	IDF=NO-KK	00384
	RES=(YY-BXX)/IDF	00385
	WRITE (20,3) RES, IDF	00386
1	FORMAT (32H LEAST SQ ESTIMATE OF PARAMETERS )	00387
3	FORMAT (23H MEAN SQ OF RESIDUALS= ,E16.7,5X,4HDF= ,I3)	00388
4	FORMAT (28H VARIANCE-COVARIANCE MATRIX )	00389
5	FORMAT (/4E15.5)	00390
	WRITE (20,4)	00391
	WRITE (20,5) ((XX(I,J), I=1, KK), J=1, KK)	00392
	WRITE (20,7)	00393
	WRITE (61,17)	(001)
17	FORMAT (' INDEX Y-EST Y')	(002)
7	FORMAT (' Y EST OF Y Y-EST Y')	00394
	DO 70 J=1, NO	00395
	ESTY=0.0	00396
	DO 60 K=1, KK	00397
	ESTY=ESTY+BB(K)*X(K,J)	00398
60	CONTINUE	00399
	DIF=X(N,J)-ESTY	00400
	WRITE (20,6) X(N,J), ESTY, DIF	00401
	WRITE (61,13) J, DIF	(001)
13	FORMAT (I6,F7.3)	(002)
6	FORMAT(3F15.7)	00403
70	CONTINUE	00404
	WRITE (61,8)	00405
8	FORMAT (' ARE THESE OK( TYPE IN 1 FOR YES, 2 FOR NO')	00406
	KTRY=TTYIN(4HTRY=)	00407
	GO TO (100,80), KTRY	00408
80	WRITE (61,9)	00409
9	FORMAT (' WHAT IS THE INDEX OF THE X VALUE TO BE CHANGED(')	00410
	INDX=TTYIN(4HINDX)	00411
	WRITE (61,11)	00413
11	FORMAT (' WHAT IS THE VALUE(')	00414
	X(2, INDX)=TTYIN(4H X= )	00415
	X(3, INDX)=X(2, INDX)*X(2, INDX)	00416
	WRITE (61,12)	00417
12	FORMAT (' ANYMORE CHANGES( 1 FOR YES, 2 FOR NO')	00418
	KTRY=TTYIN(4HTRY=)	00419
	GO TO (80,14), KTRY	00420
100	RETURN	00421
	END	00422
	SUBROUTINE MATINV(A,N,B,M,DETERM)	00423
C	MATRIX INVERSION WITH ACCOMPANYING SOLUTION OF LINEAR EQUATIONS	00424
	DIMENSION IPIVOT(10), A(10,10), B(10,1), INDEX(10,2), PIVOT(10)	00425
	DETERM=1.0	00426
	DO 20 J=1,N	00427
20	IPIVOT(J)=0	00428
	DO 550 I=1,N	00429
C	SEARCH FOR PIVOT ELEMENT	00430
	AMAX=0.0	00431
	DO 105 J=1,N	00432
	IF (IPIVOT(J)-1) 60, 105, 60	00433
60	DO 100 K=1,N	00434
	IF (IPIVOT(K)-1) 80, 100, 740	00435
80	IF (ABS(A(J,K))-AMAX) 85, 100, 100	00436
85	IROW=J	00437
	ICOLUM=K	00438
	AMAX=A(J,K)	00439

Figure C-2. Listing of program EDIT. (Continued)



100	CONTINUE	00440
105	CONTINUE	00441
	IPIVOT(ICOLUM)=IPIVOT(ICOLUM)+1	00442
C	INTERCHANGE ROWS TO PUT PIVOT ELEMENT ON DIAGONAL	00443
	IF (IROW-ICOLUM) 140, 260, 140	00444
140	DETERM=-DETERM	00445
	DO 200 L=1,N	00446
	SWAP=A(IROW,L)	00447
	A(IROW,L)=A(ICOLUM,L)	00448
200	A(ICOLUM,L)=SWAP	00449
	IF(M) 260, 260, 210	00450
210	DO 250 L=1, M	00451
	SWAP=B(IROW,L)	00452
	B(IROW,L)=B(ICOLUM,L)	00453
250	B(ICOLUM,L)=SWAP	00454
260	INDEX(I,1)=IROW	00455
	INDEX(I,2)=ICOLUM	00456
	PIVOT(I)=A(ICOLUM,ICOLUM)	00457
	DETERM=DETERM*PIVOT(I)	00458
C	DIVIDE PIVOT ROW BY PIVOT ELEMENT	00459
	A(ICOLUM,ICOLUM)=1.0	00460
	DO 350 L=1,N	00461
350	A(ICOLUM,L)=A(ICOLUM,L)/PIVOT(I)	00462
	IF(M) 380, 380, 360	00463
360	DO 370 L=1,M	00464
370	B(ICOLUM,L)=B(ICOLUM,L)/PIVOT(I)	00465
C	REDUCE NON-PIVOT ROWS	00466
	DO 550 L1=1,N	00467
	IF(L1-ICOLUM) 400, 550, 400	00468
400	T=A(L1,ICOLUM)	00469
	A(L1,ICOLUM)=0.0	00470
	DO 450 L=1,N	00471
450	A(L1,L)=A(L1,L)-A(ICOLUM,L)*T	00472
	IF(M) 550, 550, 460	00473
460	DO 500 L=1,M	00474
500	B(L1,L)=B(L1,L)-B(ICOLUM,L)*T	00475
550	CONTINUE	00476
C	INTERCHANGE COLUMNS	00477
	DO 710 I=1,N	00478
	L=N+1-I	00479
	IF (INDEX(L,1)-INDEX(L,2)) 630, 710, 630	00480
630	JROW=INDEX(L,1)	00481
	JCOLUM=INDEX(L,2)	00482
	DO 705 K=1,N	00483
	SWAP=A(K,JROW)	00484
	A(K,JROW)=A(K,JCOLUM)	00485
	A(K,JCOLUM)=SWAP	00486
705	CONTINUE	00487
710	CONTINUE	00488
740	RETURN	00489
	END	00490

Figure C-2. Listing of program EDIT. (Continued)

71641	40	60592437	41	60592744	42	60592956	43	60593183	44	60593423	45	60593657
71641	46	60593912	47	60594189	48	60594469	49	60594765	50	60595085	51	60595442
71641	52	60595805	53	60596178	54	60596591	55	60597003	56	60597473	0	0
71641	500	41516924501	40906305502	40166308503	34926218509	34186214510	33406209511	32676221	28216168	37146252		
71641	506	36426258517	35626228508	31046208514	30346194515	25176161522	24626202523	23846190	19666787	23576182		
71641	512	31906212513	26786170520	26026166521	21516252527	20776268528	20066310529	27826160	32336182	36856251		
71641	518	27546147519	22306227526	21376226533	22046208534	26416135540	31546214547	41157256	37806264	33376144		
71641	524	23056210525	20566250532	25766167539	29966187545	35366248552	40466296559	38556264565	34146186571	28916169		
71641	530	19856256531	24986170538	29246176544	33816213550	39046292557	40006293563	35586225569	30276170575			
71641	536	24356178537	29246176544	33816213550	39046292557	40006293563	35586225569	30276170575				
71641	542	28556177543	33816213550	39046292557	40006293563	35586225569	30276170575					
71641	548	33036209549	38346274556	40786302562	36336241568	31806184574						
71641	554	37606275555	40786302562	36336241568	31806184574							
71641	560	41276781561	36336241568	31806184574								
71641	566	37126253567	31806184574									
71641	572	32036176573										

Figure C-3. Sample input for program EDIT.



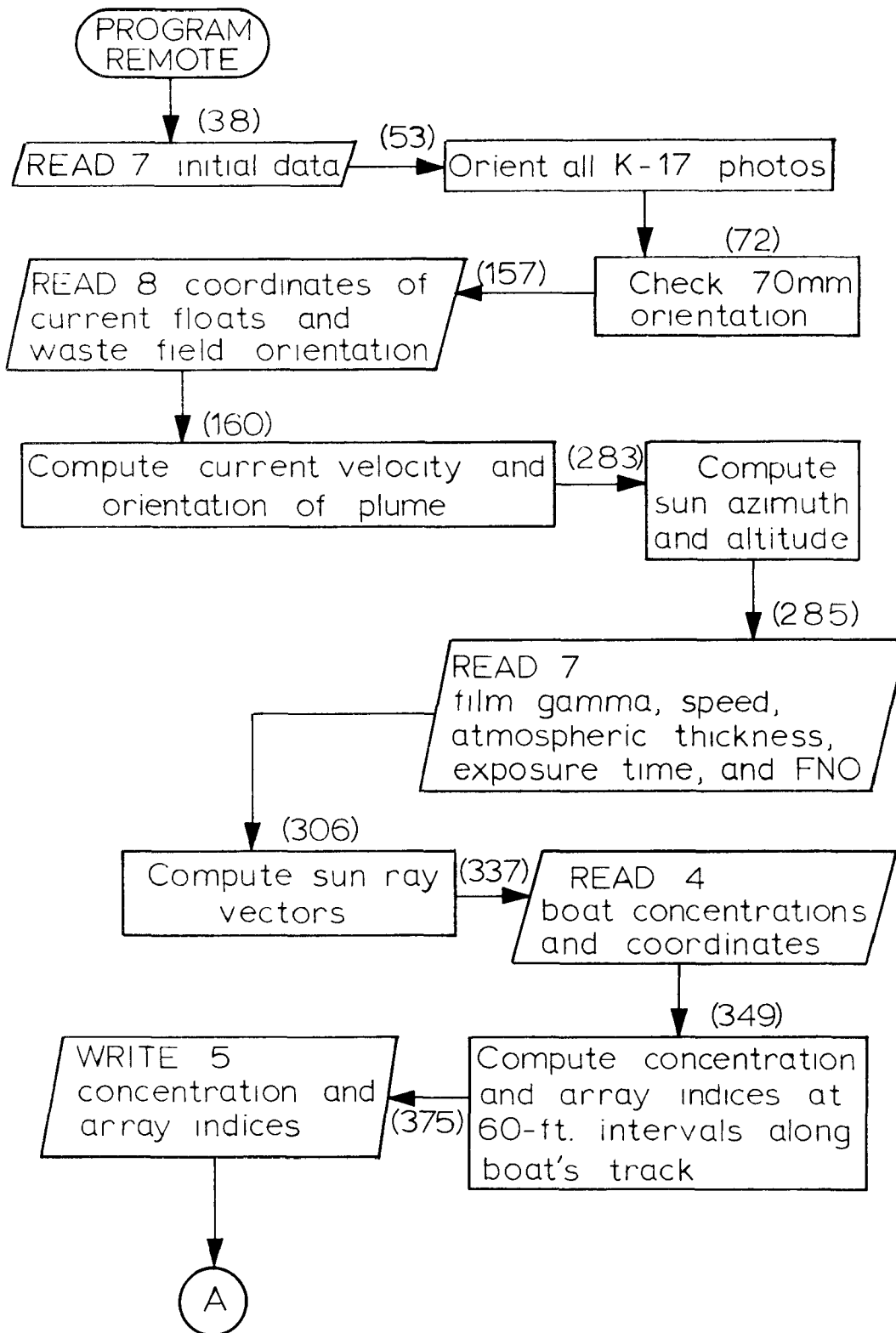


Figure C-5. Flow diagram of program REMOTE.

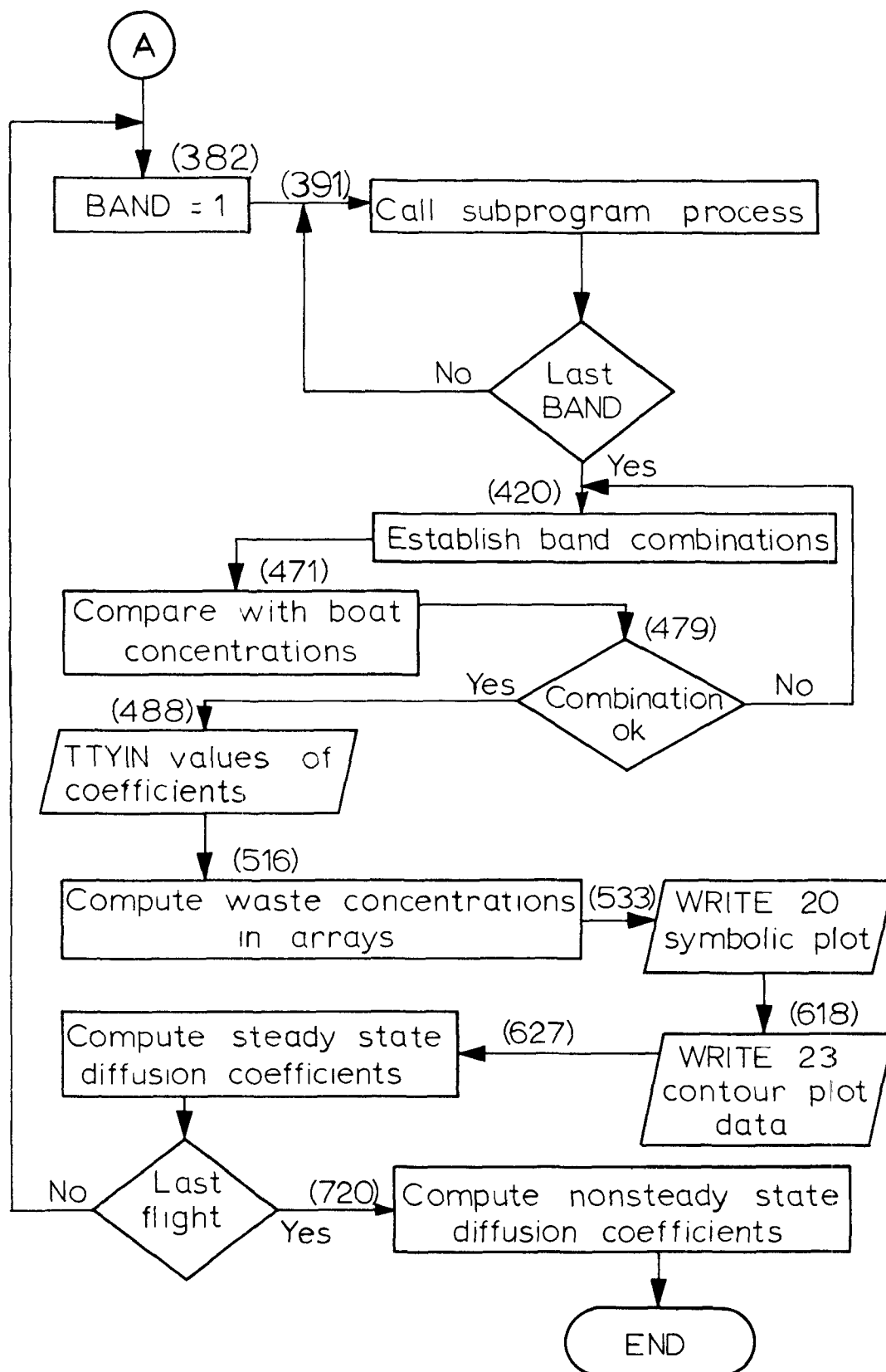


Figure C-5. Flow diagram of program REMOTE.

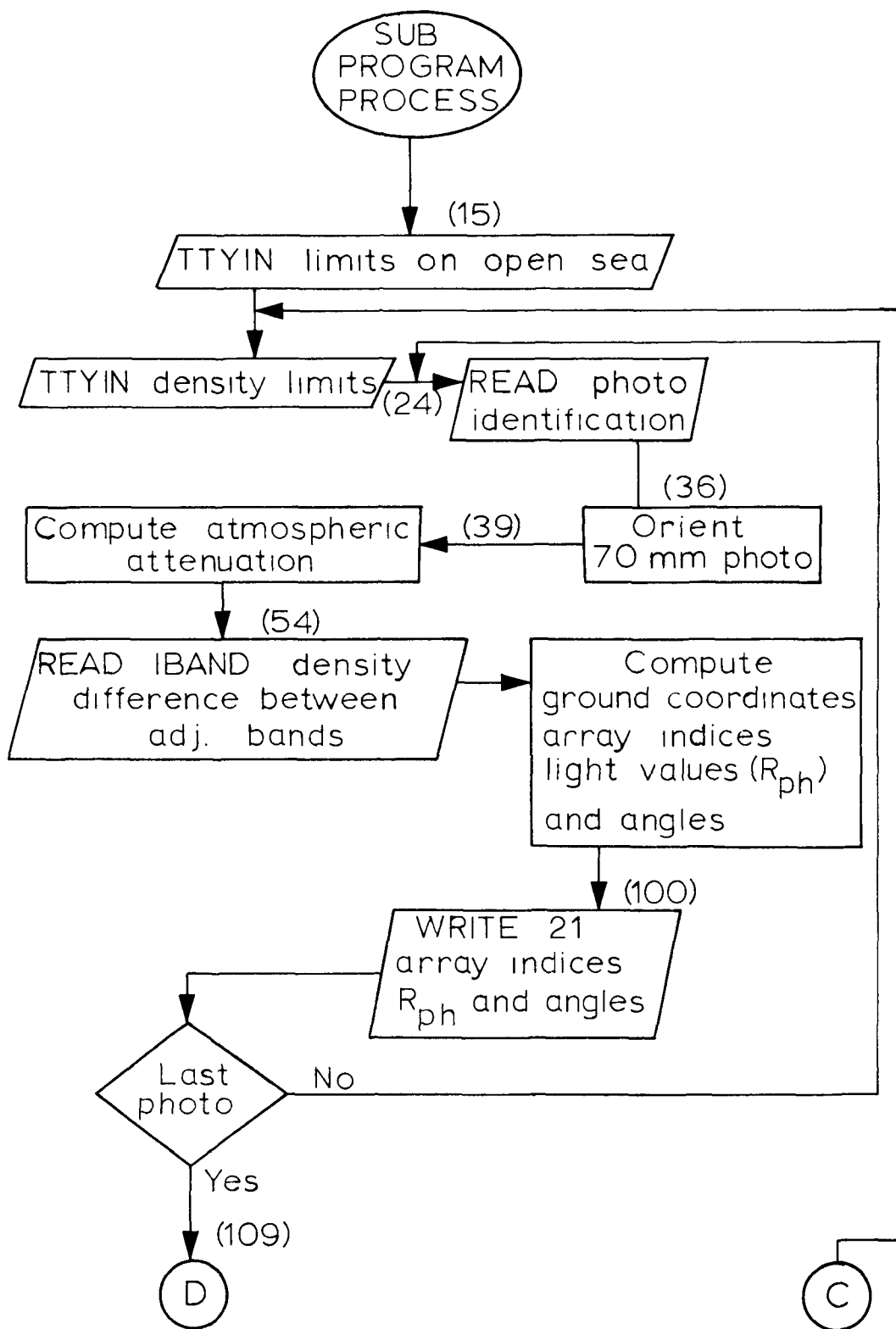


Figure C-6. Flow diagram of subroutine PROCESS.

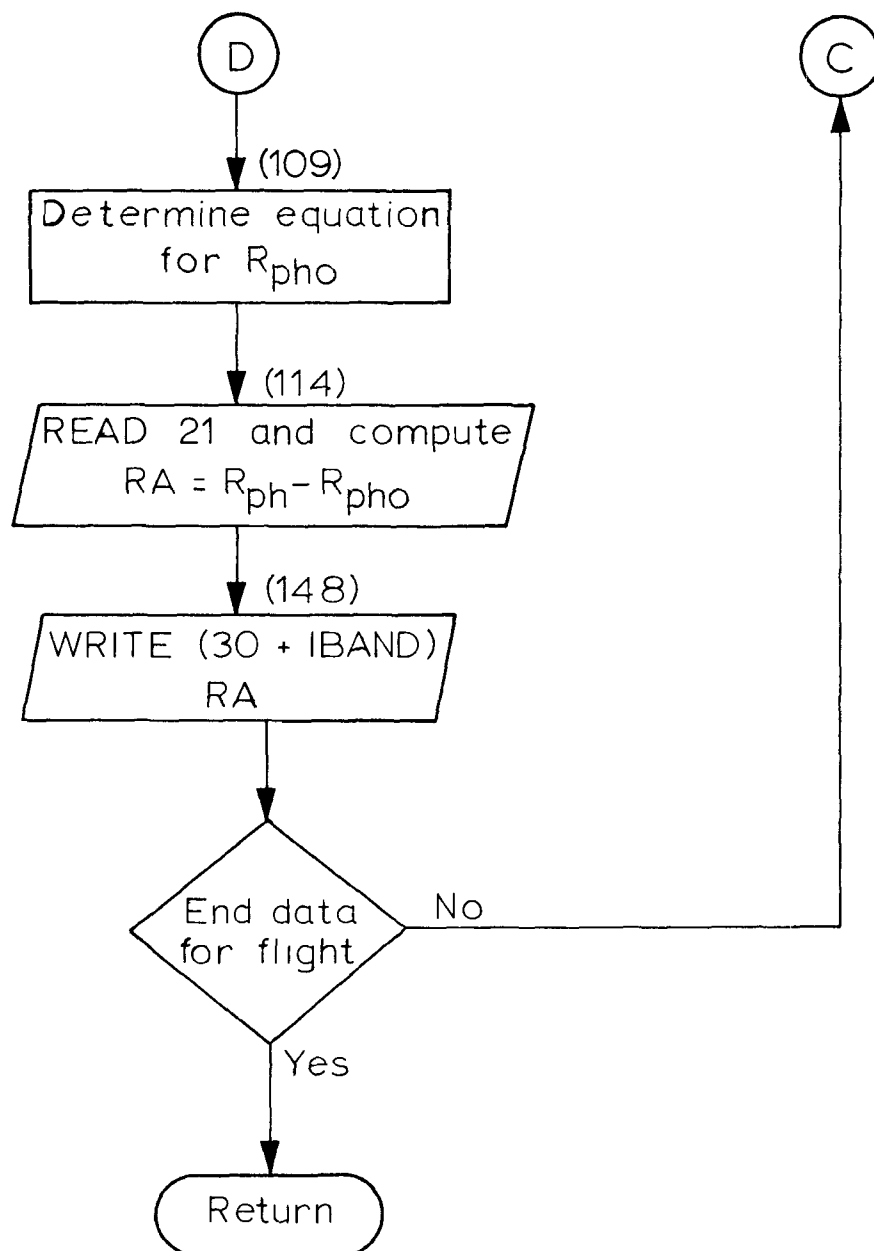


Figure C-6. Flow diagram of subroutine PROCESS.

	DEFINE DECLAR	00001
	COMMON X(10,300),IPHOT(120,80),CAMO(90,6),C(20,3)	00002
	COMMON B(15,6),P(2,8),ANGHB(4),VOLL(2,8)	00003
	END	00004
	DEFINE GROCOORD	00005
	XG(1)=CAMO(IPLATE,1)-CAMO(IPLATE,3)*XT(1)/XT(3)	00006
	XG(2)=CAMO(IPLATE,2)-CAMO(IPLATE,3)*XT(2)/XT(3)	00007
	END	00008
	PROGRAM REMOTE	00009
C	INPUT LUNS ARE	00010
C	1. RED-GREEN FILM DENSITIES	00011
C	2. GREEN-BLUE FILM DENSITIES	00012
C	3. BLUE-GOLD FILM DENSITIES	00013
C	4. BOAT CONCENTRATIONS AND COORDINATES	00014
C	7. GENERAL INFORMATION	00015
C	8. PHOTO COORD. FOR CONTROL, FLOATS, SCAN LIMITS	00016
C	AND WASTE FIELD ORIENTATION	00017
C	9. GROUND CONTROL COORDINATES	00018
C	10 APPROXIMATE ORIENTATION PARAMETERS	00019
	DIMENSION TIMFLT(3),IE(3),XT(3),XG(2),H(3),AZ(3),	00020
	1 X1(3),Y1(3),IBD(8),BB(9)	00021
	INCLUDE DECLAR	00022
	INTEGER HARDWARE	00023
	IF (HARDWARE(7) .EQ. 1) 90,1000	00024
90	REWIND 7	00025
	IF (HARDWARE(20) .EQ. 1) 94,92	00026
92	CALL EQUIP(20,5HFILE)	00027
94	REWIND 20	00028
	FL=6.0	00029
	NXX=10	00030
	NYX=300	00031
	NXI=TTYIN(4HNXI=)	00032
	NYI=TTYIN(4HNYI=)	00033
	IFRA=90	00034
	KOR=6	00035
C	ZERO ARRAYS	00036
	CALL ZEROARRY(NXI,NYI,NXX,NYX,IFRA,KOR)	00037
C	READ FROM LUN 7 HASSELBLAD ORIENTATION ANGLES, TIME	00038
C	OF THREE FLIGHTS IN HOURS AND MIN AND EFFLUENT	00039
C	FLOW RATE IN GPM	00040
	DELOMG=FFIN(7)/57.2958	00041
	DELPHI=FFIN(7)/57.2958	00042
	DO 95 I=1,3,2	00043
	ANGHB(I)=DELOMG	00044
95	ANGHB(I+1)=DELPHI	00045
	DO 100 I=1,3	00046
100	TIMFLT(I)=FFIN(7)+FFIN(7)/60.	00047
	RATE=FFIN(7)/(7.48*60.)	00048
	IF (HARDWARE(8) .NE. 1) GO TO 1000	00049
	IF (HARDWARE(9) .NE. 1) GO TO 1000	00050
	IF (HARDWARE(10) .NE. 1) GO TO 1000	00051
C	ORIENT ALL PHOTOS	00052
	CALL RESECT(FL,DELOMG,DELPHI)	00053
	CALL ZEROARRY(NXI,NYI,NXX,NYX,1,0)	00054
	DO 120 I=1,30	00055
	IF (CAMO(I,3)-1.0) 120,120,110	00056
110	DO 120 J=1,3	00057
	CAMO(I+30,J)=CAMO(I,J)	00058
	CAMO(I+60,J)=CAMO(I,J)	00059
120	CONTINUE	00060
	REWIND 8	00061

Figure C-7. Program listing for REMOTE.



	IGO=1	00062
105	GO TO (122,124,126,300),IGO	00063
122	KHBL=0	00064
	KHBL=4	00065
	GO TO 136	00066
124	KHBL=3	00067
	KHBL=7	00068
	GO TO 136	00069
126	KHBL=6	00070
	KHBL=10	00071
C	CHECK ONE CONTROL PT ON EACH CAMERA	00072
136	XP=0.	00073
	K=0	00074
	J=0	00075
	SUM1=0.0	00076
	SUM2=0.0	00077
140	READ(08,1) IFL,IPH,(IE(I),X1(I),Y1(I),I=1,3)	00078
	1 FORMAT(3X,2I1,3(I4,2F6.3,7X))	00079
	IF (EOF(8)) GO TO 250	00080
	IF (IFL.GT.KHBL.AND.IFL.LT.KHBL) 150,140	00081
150	DO 190 I=1,3	00082
	IF (IE(I) .EQ. 0 .AND. X1(I) .GT. 0.1) GO TO 155	00083
	IF (IE(I) .GE. 1 .AND. IE(I) .LT. 20) 160,170	00084
155	XG(1)=X1(I)	00085
	XG(2)=Y1(I)	00086
	K=1	00087
	GO TO 180	00088
160	IPIN=IE(I)	00089
	XP=X1(I)	00090
	YP=Y1(I)	00091
	IF (K .EQ. 1) GO TO 190	00092
	GO TO 180	00093
170	GO TO (180,171,171),IGO	00094
171	IF(IE(I) .GE. 30 .AND. IE(I) .LE. 33) 172,180	00095
172	J=J+1	00096
	SUM1=SUM1+X1(I)	00097
	SUM2=SUM2+Y1(I)	00098
	IF (J-4) 180,190,190	00099
180	CONTINUE	00100
	GO TO 140	00101
190	IF (XP-0.01) 136,136,192	00102
192	IPLATE=(IFL-1)*10+IPH	00103
	CALL ORIMAT(IPLATE)	00104
	GO TO (197,198,198),IGO	00105
197	SUM1=XG(1)*4.	00106
	SUM2=XG(2)*4.	00107
198	XP=SJM1/4.-XP	00108
	YP=SJM2/4.-YP	00109
	CALL TRNCOORD(YP,XP,FL,XT)	00110
	INCLUDE GRDCOORD	00111
	REWIND 9	00112
194	I=FFIN(9)	00113
	IF (EOF(9)) GO TO 250	00114
	XP=FFIN(9)	00115
	YP=FFIN(9)	00116
	ZP=FFIN(9)	00117
	IF (IPIN-I) 194,196,194	00118
196	DX=XP-XG(1)	00119
	DY=YP-XG(2)	00120
	WRITE (20,2) IPIN,XG(1),XG(2)	00121
	WRITE (20,3) I,XP,YP	00122
	WRITE (20,4) IPLATE,DX,DY	00123

Figure C-7. Program listing for REMOTE. (Continued)

2	FORMAT( # HB PT NO. #, I3, #	X= #, F8.0, #	Y= #, F8.0)	00124
3	FORMAT( # GD PT NO. #, I3, #	X= #, F8.0, #	Y= #, F8.0)	00125
4	FORMAT( # PHOTO NO. #, I3, #	DIFX= #, F5.0, #	DIFY= #, F5.0)	00126
	DIS=)IST(OX,OY)			00127
	IF (JIS-2J.) 136,136,2J0			00128
200	GO TO (136,210,210),IGO			00129
210	J=0			00130
	K=60			00131
	IF (IGO .EQ. 2) K=30			00132
	K=IPLATE-K			00133
220	XG(1)=DY*SIN(CAMO(K,6))+DX*COS(CAMO(K,6))			00134
	XG(2)=DY*COS(CAMO(K,6))-DX*SIN(CAMO(K,6))			00135
	IF (J .EQ. 1) GO TO 230			00136
	DX=XT(1)			00137
	DY=XT(2)			00138
	X1(1)=XG(1)			00139
	X1(2)=XG(2)			00140
	J=J+1			00141
	GO TO 220			00142
230	SUM1=XT(3)/DIST(XG(1),XT(3))			00143
	SUM2=XT(3)/DIST(XG(2),XT(3))			00144
	K=3			00145
	IF (IGO .EQ. 2) K=1			00146
	ANGH3(K+1)=ANGHB(K+1)-X1(1)*SUM1*SUM1/CAMO(IPLATE,3)			00147
	ANGH3(K)=ANGHB(K)+X1(2)*SUM1*SUM2/CAMO(IPLATE,3)/2.			00148
	WRITE(20,30) ANGH3(K),ANGHB(K+1)			00149
30	FORMAT( # DELOMG #, F7.3, / # DELPHI #, F7.3)			00150
	GO TO 136			00151
250	IGO=IGO+1			00152
	REWIND 8			00153
	GO TO 105			00154
300	FL=6.0			00155
C	COMPUTE CURRENTS AND ORIENTATION OF WASTE FIELD FROM K-17			00156
305	READ (8,1) IFL,IPH,(IE(J),X1(J),Y1(J),J=1,3)			00157
	IF (EOF(8)) GO TO 350			00158
	IF (IFL .LE. 3) 310,305			00159
310	IPLATE=(IFL-1)*10+IPH			00160
	DO 340 I=1,3			00161
	IF (IE(I) .EQ. 0 .AND. X1(I) .GT. 0.1) GO TO 320			00162
	IF (IE(I) .LT. 30 .AND. IE(I) .GT. 19) GO TO 324			00163
	IF (IE(I) .EQ. 34 ) GO TO 328			00164
	IF (IE(I) .EQ. 35 ) GO TO 332			00165
	GO TO 340			00166
320	I1=1			00167
	I2=2			00168
	K=IPLATE			00169
	GO TO 338			00170
324	I1=IE(I)			00171
	I2=I1			00172
	K=IPLATE+30			00173
	GO TO 338			00174
328	I1=3			00175
	I2=4			00176
	K=IPLATE			00177
	GO TO 338			00178
332	I1=5			00179
	I2=6			00180
	K=IPLATE			00181
338	IPHOT(IPLATE,I1)=X1(I)*1000.			00182
	IPHOT(K,I2)=Y1(I)*1000.			00183
340	CONTINUE			00184
	GO TO 305			00185

Figure C-7. Program listing for REMOTE. (Continued)

C	COMPUTE ORIENTATION OF WASTE FIELD	00186
350	DO 350 I=1,30	00187
	IF (IPHOT(I,3)) 360,360,352	00188
352	X1(1)=IPHOT(I,2)-IPHOT(I,4)	00189
	X1(2)=IPHOT(I,1)-IPHOT(I,3)	00190
	Y1(1)=IPHOT(I,2)-IPHOT(I,6)	00191
	Y1(2)=IPHOT(I,1)-IPHOT(I,5)	00192
	XP=X1(1)/1000.	00193
	YP=X1(2)/1000.	00194
	CALL ORIMAT(I)	00195
	CALL TRNCOORD(XP,YP,FL,XT)	00196
	IPLATE=I	00197
	INCLUDE GRDCOORD	00198
	C(12,2)=XG(1)	00199
	C(12,3)=XG(2)	00200
	C(14,2)=NYI*30	00201
	XP=Y1(1)/1000.	00202
	YP=Y1(2)/1000.	00203
	CALL TRNCOORD(XP,YP,FL,XT)	00204
	INCLUDE GRDCOORD	00205
	XP=XG(1)-C(12,2)	00206
	YP=XG(2)-C(12,3)	00207
	ROT=ATANF(XP/YP)	00208
	IF (YP) 354,355,355	00209
354	ROT=ROT+3.14159	00210
355	C(13,2)=SINF(ROT)	00211
	C(13,3)=COSF(ROT)	00212
	WRITE(20,5) ROT,C(12,2),C(12,3)	00213
	5 FORMAT(#1 ROTATION ANGLE#,F10.3,# RAD#/,	00214
	1 # ORIGIN X#,F10.0,/# ORIGIN Y#,F10.0)	00215
	GO TO 370	00216
360	CONTINUE	00217
370	K=0	00218
	DO 380 I=1,30	00219
	DO 380 J=20,29	00220
	IF (IPHOT(I,J)) 390,380,375	00221
375	XP=IPHOT(I,2)-IPHOT(I+30,J)	00222
	YP=IPHOT(I,1)-IPHOT(I,J)	00223
	XP=XP/1000.	00224
	YP=YP/1000.	00225
	K=I/10+1	00226
	IF (IPLATE.NE.I) CALL ORIMAT(I)	00227
	CALL TRNCOORD(XP,YP,FL,XT)	00228
	IPLATE=I	00229
	INCLUDE GRDCOORD	00230
	X(J-19,K)=XG(1)	00231
	X(J-19,K+30)=XG(2)	00232
	WRITE(20,6) J,I,XG(1),XG(2)	00233
	6 FORMAT(# FLOAT#,I3,# PLATE#,I3,# X=#,F10.0,	00234
	1 # Y=#,F10.0)	00235
380	CONTINUE	00236
	DO 385 L=1,10	00237
	XP=X(L,1)-X(L,2)	00238
	YP=X(L,31)-X(L,32)	00239
	X1(1)=DIST(XP,YP)	00240
	XP=X(L,1)-X(L,3)	00241
	YP=X(L,31)-X(L,33)	00242
	X(L,1)=DIST(XP,YP)	00243
	XP=X(L,2)-X(L,3)	00244
	YP=X(L,32)-X(L,33)	00245
	X(L,3)=DIST(XP,YP)	00246
	X(L,?)=X1(1)	00247

Figure C-7. Program listing for REMOTE. (Continued)

385	CONTINUE	00248
C	COMPUTE AVERAGE CURRENT VELOCITY	00249
	X1(1)=(TIMFLT(3)-TIMFLT(1))*3600.	00250
	X1(2)=(TIMFLT(2)-TIMFLT(1))*3600.	00251
	X1(3)=(TIMFLT(3)-TIMFLT(2))*3600.	00252
	J=0	00253
	SUM1=0.0	00254
	SUM2=0.0	00255
	DIF=3.0	00256
	AI=0.0	00257
	DO 390 L=1,10	00258
	DO 390 I=1,3	00259
	IF (X(L,I).LT.10..OR.X(L,I).GT.4000.) GO TO 390	00260
	J=J+1	00261
	VEL=X(L,I)/X1(I)	00262
	SUM1=SUM1+VEL	00263
	SUM2=SUM2+VEL*VEL	00264
	K=L+19	00265
	WRITE(20,7) K,I,VEL	00266
7	FORMAT(4 FLOAT NO.,I3,4 I=,I2,4 VEL=,F5.2,4FPS)	00267
	IF (I .NE. 1) GO TO 390	00268
	AI=AI+1	00269
	DIF=DIF+VEL	00270
390	CONTINUE	00271
	IF (J .EQ. 0) GO TO 394	00272
	AJ=J	00273
	VEL=SUM1/AJ	00274
	IF (AJ .GT. 1.0) 392,400	00275
392	SUM2=STDEV(SUM1,SUM2,AJ)	00276
	WRITE(20,8) VEL,SUM2	00277
8	FORMAT(4 MEAN VEL,F5.2,4 STD DEV,F5.2)	00278
	IF (AI .LE. 0.1) GO TO 400	00279
	VEL=DIF/AI	00280
	GO TO 400	00281
394	VEL=TTYIN(4HVEL=)	00282
C	COMPUTE SUN ALTITUDE AND AZIMUTH	00283
400	CALL SUNLITE(TIMFLT,H,AZ)	00284
C	READ FROM LUN 7 VALUES OF FILM GAMMA,FILM SPEED, ATMOS	00285
C	OPTICAL THICKNESS FOR THE EIGHT SPECTRAL BANDS.	00286
	DO 420 J=4,11	00287
	DO 420 I=1,3	00288
	C(J,I)=FFIN(7)	00289
420	CONTINUE	00290
C	READ FROM 7 VALUES OF EXPOSURE TIME AND FNO	00291
C	(NINE VALUES K-17 1,2,3;HB-1 4,5,6; HB-2 7,8,9)	00292
	DO 430 J=12,20	00293
	SUM1=FFIN(7)	00294
	SUM2=FFIN(7)	00295
	C(J,1)=SUM1*SUM2*SUM2	00296
430	CONTINUE	00297
C	READ FROM 7 COEFFS FOR DETERMINING ATMOS ATTEN FROM	00298
C	THE SEA TO THE CAMERA STATION	00299
	DO 440 I=1,8	00300
	DO 440 J=1,2	00301
	P(J,I)=FFIN(7)	00302
440	CONTINUE	00303
C	READ FROM 7 0 IF ANTIVIGNETTING FILTER ON K-17 1 IF NOT	00304
	B(15,6)=FFIN(7)	00305
C	DETERMINE SUNLIGHT VECTORS	00306
	DO 450 I=1,3	00307
	J=3+I	00308
	B(1,J)=SINF(H(I))	00309

Figure C-7. Program listing for REMOTE. (Continued)

B(2,J)=COSF(H(I))	00310
B(13,J)=-SIN(AZ(I))	00311
B(14,J)=-COSF(AZ(I))	00312
B(3,J)=1./B(1,J)	00313
B(4,J)=B(2,J)*B(13,J)	00314
B(5,J)=B(2,J)*B(14,J)	00315
B(6,J)=-B(1,J)	00316
B(8,J)=B(2,J)/1.33	00317
B(7,J)=SQRT(1.0-B(8,J)*B(8,J))	00318
B(9,J)=1.0/B(7,J)	00319
B(10,J)=B(8,J)*B(13,J)	00320
B(11,J)=B(8,J)*B(14,J)	00321
B(12,J)=-B(7,J)	00322
SUM2=ATAN(B(8,J)/B(7,J))	00323
SUM1=1.5708-H(I)	00324
B(15,I)=REFLECT(SUM1,SUM2)	00325
450 CONTINUE	00326
B(15,4)=1.33*1.33	00327
IF (HARDWARE(21).EQ. 1) 460,455	00328
455 CALL EQUIP(21,5HFILE )	00329
460 IF (HARDWARE(22) .EQ. 1) 464,462	00330
462 CALL EQUIP(22,5HFILE )	00331
464 IF (HARDWARE(4) .EQ. 1) 470,1000	00332
470 REWIND 4	00333
IF (HARDWARE(5) .EQ. 1) GO TO 480	00334
CALL EQUIP(5,5HFILE )	00335
480 REWIND 5	00336
READ (4,9) FIX,XL,YL,CONL	00337
500 READ(4,9) FIX,XF,YF,CONF	00338
IF (EOF(4)) GO TO 600	00339
9 FORMAT(F7.1,2F14.0,F10.1)	00340
IF (FIX-0.1) 500,500,505	00341
505 DDEN=CONF-CONL	00342
DKX=XF-XL	00343
DKY=YF-YL	00344
KKX=JIST(DKX,DKY)/60.	00345
IF (KKX .GT. 0.5) GO TO 508	00346
XL=(XF+XL)/2.	00347
YL=(YF+YL)/2.0	00348
CONL=(CONF+CONL)/2.0	00349
GO TO 500	00350
508 KX=KKX	00351
GO TO (510,520),KX	00352
510 X(1,1)=(XL+XF)/2.	00353
X(1,2)=(YL+YF)/2.	00354
X(1,3)=(CONL+CONF)/2.	00355
KX=1	00356
GO TO 530	00357
520 DIV=KX	00358
IF(DIV-8.) 522,522,540	00359
522 DO 524 K=1,KX	00360
YYK=	00361
X(K,1)=XL+DKX*YYK/DIV	00362
X(K,2)=YL+DKY*YYK/DIV	00363
X(K,3)=CONL+DDEN*YYK/DIV	00364
524 CONTINUE	00365
530 DO 540 K=1,KX	00366
X(K,1)=X(K,1)-C(12,2)	00367
X(K,2)=X(K,2)-C(12,3)	00368
XG(1)=X(K,1)*C(13,2)+X(K,2)*C(13,3)	00369
XG(2)=-X(K,1)*C(13,3)+X(K,2)*C(13,2)	00370
LX=XG(1)/60.+0.5	00371

Figure C-7. Program listing for REMOTE. (Continued)

IF(LX .LE. 0 .OR. LX .GT. NXI) GO TO 540	00372
LY=(XG(2)+C(14,2))/60.+0.5	00373
IF (LY .LE. 0 .OR. LY .GT. NYI) GO TO 540	00374
WRITE (5,10) LX,LY,X(K,3)	00375
10 FORMAT(2I4,F6.2)	00376
540 CONTINUE	00377
XL=X <sup>E</sup>	00378
YL=Y <sup>F</sup>	00379
CONL=CONF	00380
GO TO 500	00381
600 JJFL=1	00382
KFLT=1	00383
END FILE 5	00384
602 K=0	00385
ILUN=1	00386
610 IF (HARDWARE(ILUN) .NE. 1) GO TO 630	00387
CALL ZEROARRY(NXI,NYI,1,0,1,0)	00388
FL=6.0	00389
IF (KFLT .GT. 3) FL=150./25.4	00390
CALL PROCESS(KFLT,JJFL,ILUN,FL,NXI,NYI)	00391
K=K+1	00392
WRITE(61,31) K,KFLT,ILUN	00393
31 FORMAT(3I10)	00394
630 ILUN=ILUN+1	00395
KFLT=KFLT+3	00396
GO TO (610,610,610,640),ILUN	00397
640 IF (K .EQ. 0) 642,644	00398
642 L=1	00399
GO TO 901	00400
644 K=0	00401
DO 650 I=1,8	00402
IBD(I)=0	00403
ILUN=I+30	00404
IF (HARDWARE(ILUN) .NE. 1) GO TO 660	00405
REWIND ILUN	00406
K=K+1	00407
IBD(K)=ILUN	00408
J=1	00409
655 READ(ILUN,11) X(K,J)	00410
11 FORMAT(F8.0)	00411
IF (EOF(ILUN)) GO TO 660	00412
J=J+1	00413
IF (J .LT. 300) 655,660	00414
660 CONTINUE	00415
IF (K .LE. 0) GO TO 642	00416
NO=J-1	00417
K<=K	00418
ITRY=1	00419
659 K=KK	00420
WRITE(61,32)(IBD(I),I=1,K)	00421
32 FORMAT(* TYPE IN 1 IF YOU WANT TO USE A PRODUCT,2 IF NOT*/,	00422
1* THE FOLLOWING BANDS ARE USED:*/ ,9I4)	00423
KKGO=TTYIN(4HRAT=)	00424
GO TO (651,663),KKGO	00425
661 K=K+1	00426
WRITE(61,33)	00427
33 FORMAT(* TTYIN NO. OF THE TWO TERMS 1 3 ETC*)	00428
KTOP=TTYIN(4H1ST=)	00429
KBOT=TTYIN(4H2ND=)	00430
DO 662 J=1,NO	00431
X(K,J)=X(KTOP,J)*X(KBOT,J)	00432
662 CONTINUE	00433

Figure C-7. Program listing for REMOTE. (Continued)

663 WRITE(61,34) K	00434
34 FORMAT(1# THERE ARE#,I3,1# VARIABLES USED IN THE EQ#/,	00435
1# ITYIN 1 IF YJU WANT A SQUARED TERM 2 IF NOT#)	00436
KIGO=ITYIN(4HSQU=)	00437
GO TO (664,666),KIGO	00438
664 WRITE(61,35)	00439
35 FORMAT(1# WHAT TERM IS TO BE SQUARED^#)	00440
ISQU=ITYIN(4HSQU=)	00441
K=K+1	00442
K2=K	00443
DO 665 J=1,N0	00444
665 X(K,J)=X(ISQU,J)*X(ISQU,J)	00445
666 K=K+1	00446
N=K	00447
GO TO (672,674),ITRY	00448
672 REWIND 5	00449
DO 667 J=1,N0	00450
READ(5,12)X(K,J)	00451
12 FORMAT(8X,F6.2)	00452
667 CONTINUE	00453
K=0	00454
NKN=N-1	00455
DO 678 J=1,N0	00456
DO 676 I=1,NKN	00457
IF(A3S(X(I,J)).LT..001) GO TO 678	00458
676 CONTINUE	00459
K=K+1	00460
DO 677 I=1,N	00461
X(I,)=X(I,J)	00462
677 CONTINUE	00463
X(9,)=X(N,J)	00464
678 CONTINUE	00465
N0=K	00466
GO TO 671	00467
674 DO 675 J=1,N0	00468
X(N,J)=X(9,J)	00469
675 CONTINUE	00470
671 CALL LEASTFIT(N,N0,88,RES)	00471
KCO=N-1	00472
WRITE(61,37) (88(I),I=1,KCO)	00473
WRITE(61,36) RES	00474
36 FORMAT(1# MEAN SQ#,F10.3,1# IS THIS OK^ #/,	00475
1# ITYIN 1 FOR YES 2 FOR NO.#)	00476
IGO=ITYIN(4HIGO=)	00477
ITRY=2	00478
GO TO (668,659),IGO	00479
668 CALL ZERDARRY(NXI,NYI,1,0,1,0)	00480
IF(HARDWARE(24).NE.1) CALL EQUIP(24,5HFILE )	00481
DO 659 J=1,N0	00482
WRITE(24,37) (X(I,J),I=1,N)	00483
37 FORMAT(9E11.3)	00484
669 CONTINUE	00485
N=N-1	00486
END FILE 24	00487
670 WRITE(61,40)N	00488
40 FORMAT(1# ITYIN VALUES OF COEFFICIENTS#,I4,1# REQUIRED#)	00489
DO 681 I=1,N	00490
681 88(I)=ITYIN(4HCOEF)	00491
DO 682 I=1,KK	00492
ILJN=IBD(I)-20	00493
REWIND ILUN	00494
680 CONTINUE	00495

Figure C-7. Program listing for REMOTE. (Continued)

	LY=0	00496
	LOWX=0	00497
682	DO 684 I=1, KK	00498
	ILUN=IBD(I)-20	00499
	READ(ILUN,13) (X(I,J), J=1,20)	00500
13	FORMAT(X,20F6.0)	00501
	IF (EOF(ILUN)) GO TO 700	00502
684	CONTINUE	00503
	DO 686 J=1,20	00504
	IF (K<GO.EQ.1) X(KK+1,J)=X(KTOP,J)*X(KBOT,J)	00505
	IF (KIGO.EQ.1) X(K2,J)=X(ISQU,J)*X(ISQU,J)	00506
686	CONTINUE	00507
	LY=LY+1	00508
	IF (LY .LE. NYI) GO TO 688	00509
	LOWX=LOWX+20	00510
	LY=1	00511
688	DO 692 J=1,20	00512
	SUM1=0.0	00513
	DO 690 I=1, N	00514
	IF (ABS(X(I,J)) .LE. 0.001) GO TO 692	00515
	SUM1=SUM1+BB(I)*X(I,J)	00516
690	CONTINUE	00517
	LX=LOWX+J	00518
	IF (SUM1 .LT. 0. .OR. SUM1 .GT. 30.) SUM1=0.	00519
	IPLOT(LX,LY)=SUM1*10.	00520
692	CONTINUE	00521
	GO TO 682	00522
700	DO 702 J=1,8	00523
	X(3,J)=0.0	00524
702	CONTINUE	00525
	KND=3	00526
	KON=5	00527
	NXS=NYI-2	00528
	NYS=NYI-2	00529
	CALL INTERP(NXI,NYI,NXS,NYS,KND,KON)	00530
	CALL CULL(NXI,NYI)	00531
	CALL AVERAGE(NXS,NYS)	00532
C	WRITE SYMBOLIC PLOT	00533
704	REWIND 8	00534
	READ(08,14) MO, IDATE	00535
14	FORMAT(I1,I2)	00536
	WRITE (20,15) ROT, JJFL, MO, IDATE	00537
15	FORMAT(1H1,///42X, #AIRPHOTO ANALYSIS OF OCEAN OUTFALL #	00538
	1, #DISPERSION#///,45X, #VOLUMETRIC WASTE CONCENTRATION#	00539
	2, # IN ML/LITER#///,55X, #SKETCH ON 60 - FT GRID#/,49X,	00540
	3#DIRECTION OF PLUME #,F5.2, # RADIANS#/,35X,	00541
	4 #FLIGHT NO.#,I4,30X, #DATE #,I2, #/,I2, #/69#)	00542
	WRITE(20,16)	00543
16	FORMAT( 48X, # CONCENTRATION CODE IN ML/L #/,45X,	00544
	1#) 1 - 2#,15X, #1 1 2 - 4#/,45X, # )#,24X, # 1 #///,45X,	00545
	2#III 4 - 6#,15X, #LLL 6 - 10#/,45X, #III#,24X, #LLL#///,45X,	00546
	3#PPP 10 - 15#,14X, #RRR 15 - 20#/,45X, #PPP#,24X, #RRR#///,45X,	00547
	4#MMM 20 - 25#,14X, #*** GT 25 #/,45X, #MMM#,24X, #***#///)	00548
	WRITE(20,17) C(12,2), C(12,3)	00549
17	FORMAT(60X, #+ X=#,F8.0, #E, Y=#,F7.0, #N#)	00550
	NYS=NYI-10	00551
	IKS=NYI/2	00552
	IEKS=IKS+20	00553
	IKS=IKS-20	00554
	KCO=3	00555
	DO 800 LX=2, NXI	00556
	DO 700 LY=1, NYI	00557

Figure C-7. Program listing for REMOTE. (Continued)



AXZ=IPHOT(LX,LY)	00558
AXZ=AXZ/10.	00559
IF (AXZ-1.0) 710,710,705	00560
705 XL=AXZ/2.+1.	00561
ID0=XL	00562
GO TO (720,730,740,760),ID0	00563
710 X(1,LY)=8H	00564
X(2,LY)=8H	00565
GO TO 790	00566
720 X(1,LY)=8H	00567
X(2,LY)=8H )	00568
X(3,1)=X(3,1)+1.	00569
GO TO 790	00570
730 X(1,LY)=8H1 1	00571
X(2,LY)=8H 1	00572
X(3,2)=X(3,2)+1.	00573
GO TO 790	00574
740 X(1,LY)=8HIII	00575
X(2,LY)=8HIII	00576
X(3,3)=X(3,3)+1.	00577
GO TO 790	00578
750 X(1,LY)=8HLLL	00579
X(2,LY)=8HLLL	00580
X(3,4)=X(3,4)+1.	00581
GO TO 790	00582
760 IF (AXZ-10.) 750,750,770	00583
770 XL=AXZ/5.-1.	00584
ID0=XL	00585
GO TO (775,780,785,788),ID0	00586
775 X(1,LY)=8HPPP	00587
X(2,LY)=8HPPP	00588
X(3,5)=X(3,5)+1.	00589
GO TO 790	00590
780 X(1,LY)=8HRRR	00591
X(2,LY)=8HRRR	00592
X(3,6)=X(3,6)+1.	00593
GO TO 790	00594
785 X(1,LY)=8HMMM	00595
X(2,LY)=8HMMM	00596
X(3,7)=X(3,7)+1.	00597
GO TO 790	00598
788 X(1,LY)=8H***	00599
X(2,LY)=8H***	00600
X(3,8)=X(3,8)+1.	00601
790 CONTINUE	00602
KCO=KCO+1	00603
IF(KCO.NE.4) GO TO 795	00604
WRITE(61,42) (X(1,J),J=1,NYI,3)	00605
42 FORMAT(1X,30A1)	00606
KCO=3	00607
795 WRITE (20,18) (X(1,J),J=IKS,IEKS)	00608
WRITE (20,18) (X(2,J),J=IKS,IEKS)	00609
18 FORMAT (1HW,50A3)	00610
800 CONTINUE	00611
WRITE(61,43)	00612
43 FORMAT(* ARE THE COEFFICIENTS OK^ TTYIN 1=YES, 2=NO*)	00613
KCO=TTYIN(4H GO=)	00614
GO TO (802,670),KCO	00615
802 IF(HARDWARE(23).NE.1) CALL EQUIP(23,5HFILE )	00616
WRITE(61,39)	00617
39 FORMAT(* TTYIN 1 IF WANT DATA FOR CONTOUR PLOT 2 NO*)	00618
JGO=TTYIN(4HPLOT)	00619

Figure C-7. Program listing for REMOTE. (Continued)

GO TO(701,704),JGO	00620
701 DO 703 I=1,NXI	00621
K=NXI-I+1	00622
WRITE (23,28) (J,K,IPHOT(I,J),J=1,NYI)	00623
28 FORMAT(24(15I4/))	00624
703 CONTINUE	00625
END FILE 23	00626
C COMPUTE DIFFUSION COEFFICIENTS	00627
DJKK=0.	00628
SUM2=0.0	00629
DO 810 J=1,8	00630
X(3,J)=X(3,J)*3600.	00631
810 CONTINUE	00632
AMASS=RATE*60./VEL	00633
GO TO (812,820,820),JJFL	00634
812 DO 814 I=4,6	00635
DO 814 J=61,90	00636
CAMO(J,I)=0.0	00637
814 CONTINUE	00638
820 WRITE(20,19) JJFL,MO,IDATE	00639
19 FORMAT(1H1,44X,PRELIMINARY DIFFUSION COMPUTATIONS#/ 1,47X,FLIGHT#,I3,12X,I2,##,I2,#/69#/,19X, 2# SEC. WIDTH EFF DEPTH SIGMA Y COEFFICIENT 3#X#,3X,## DIFF. COEFF.##/,22X,##NO. FT#,7X, 4#FT#,20X,##PPT#,7X,##STATE PLANE COORD FT SQ/SEC#/ L=1 LDST=2.+(TIMFLT(JJFL)-TIMFLT(1))*VEL+0.5 NXS=NXI-2 DO 900 I=LDST,NXS,5 JST=1 LNY=J DIV=J.0 SUM1=0.0 DIF=J.0 DO 830 J=JST,NYI AJ=J*60 ACD=IPHOT(I,J)+IPHOT(I-1,J)+IPHOT(I-2,J)+IPHOT(I+1,J)+ 1 IPHOT(I+2,J) ACD=ACD/50. IF(ACD.LT.1.)GO TO 880 SUM1=SUM1+ACD*AJ DIF=DIF+ACD DIV=DIV+ACD*AJ*AJ IF(IPHOT(I,J).GT.9) LNY=LNY+1 880 CONTINUE IF(DIF.LT.1.)881,882 881 X(10,L)=0.0 X(5,L)=0.0 GO TO 895 882 XMEAN=SUM1/DIF X(10,L)=DIV/DIF-XMEAN*XMEAN X(4,L)=LNY*60 X(5,L)=AMASS/(DIF*3.6) X(6,L)=SQRT(X(10,L)) X(7,L)=DIF*60./(2.51*X(6,L)) RGX=I*60 RGY=XMEAN-C(14,2) XG(1)=+RGX*C(13,2)-RGY*C(13,3) XG(2)=+RGX*C(13,3)+RGY*C(13,2) X(8,L)=XG(1)+C(12,2) X(9,L)=XG(2)+C(12,3) IF(L .EQ. 1) 885,890	00640 00641 00642 00643 00644 00645 00646 00647 00648 00649 00650 00651 00652 00653 00654 00655 00656 00657 00658 00659 00660 00661 00662 00663 00664 00665 00666 00667 00668 00669 00670 00671 00672 00673 00674 00675 00676 00677 00678 00679 00680 00681

Figure C-7. Program listing for REMOTE. (Continued)

885	DJ=0.0	00682
	GO TO 895	00683
890	DJ=VEL*(X(10,L)-X(10,L-1))/600.	00684
895	CAMO(L+60,JJFL+3)=X(10,L)	00685
	IF (X(5,L).GT.0. .AND.X(5,L).LT.20.) 896,897	00686
896	WRITE(20,20) I,(X(KK,L),KK=4,9),DJ	00687
20	FORMAT(19X,I6,F7.0,F9.1,2E11.2,4X,2F9.0,E12.2)	00688
	SUM2=SUM2+DJ	00689
	DJKK=DJKK+1.	00690
897	L=L+1	00691
900	CONTINUE	00692
	SUM2=SUM2/DJKK	00693
	WRITE(20,21) RATE,VEL,AZ(JJFL),H(JJFL),SUM2	00694
21	FORMAT(//20X,#FLOW RATE#,F5.1,# CFS#/,	00695
	120X,#CURRENT VEL#,F5.1,# FPS#/,20X,#SUN AZIMUTH#,	00696
	2F5.1,# RAD#/,20X,#SUN ALTIITUDE#,F5.1,# RAD#/,	00697
	320X,#AVE DIF COEF#,F5.1,# FT SQ/SEC#)	00698
	WRITE(20,22)	00699
22	FORMAT(1H1,56X,#AREA WITHIN EACH CONCENTRATION#,	00700
	1# RANGE#,65X,#RANGE#,13X,#AREA#,65X,	00701
	2#ML/L#,13X,#SQ FT#)	00702
	WRITE(20,23)(X(3,J),J=1,8)	00703
23	FORMAT(65X,#0 - 2#,8X,E11.2/,65X,#2 - 4#,8X,E11.2/,	00704
	1 65X,#4 - 6#,8X,E11.2/,65X,#6 - 10#,8X,E11.2/,	00705
	2 65X,#10-15#,8X,E11.2/,65X,#15-20#,8X,E11.2/,	00706
	3 65X,#20-25#,8X,E11.2/,65X,#GT 25#,8X,E11.2)	00707
901	JJFL=JJFL+1	00708
	KFLT=JJFL	00709
	DO 910 I=1,18	00710
	IF (HARDWARE(I).NE.1) GO TO 905	00711
	CALL UNEQUIP(I)	00712
905	K=I+20	00713
	IF (HARDWARE(K).NE.1) GO TO 910	00714
	CALL UNEQUIP(K)	00715
910	CONTINUE	00716
	H(JJFL-1)=L-1	00717
	GO TO(602,602,602,920),JJFL	00718
920	WRITE(20,24)	00719
24	FORMAT(1H1,///20X,#N O N S T E A D Y S T A T E #,	00720
	1# ) I F F U S I O N C O E F F I C I E N T S #//)	00721
	I=1	00722
	KI=3	00723
	KK=6	00724
	K=2	00725
	NO=1	00726
	L=H(1)	00727
	IF (L .LT. H(2)) L=H(2)	00728
	IF (L .LT. H(3)) L=H(3)	00729
926	DTIM=(TIMFLT(K)-TIMFLT(I))*120.	00730
	DIV=0.	00731
	SUM1=0.	00732
	DO 930 J=1,L	00733
	JK=J+60	00734
	KJ=K+3	00735
	KI=I+3	00736
	IF(CAMO(JK,KJ) .LT.1. .AND. CAMO(JK,KI) .LT.1.)	00737
1	GO TO 928	00738
	X(NO,J)=(CAMO(JK,KJ)-CAMO(JK,KI))/DTIM	00739
	SUM1=SUM1+X(NO,J)	00740
	DIV=DIV+1.	00741
	X(NO+3,J)=1.0	00742
	GO TO 930	00743

Figure C-7. Program listing for REMOTE. (Continued)

928	X(NO ,J)=0.	00744
930	CONTINUE	00745
	X(NO+4,1)=SUM1/DIV	00746
	GO TO (932,934,940),NO	00747
932	NO=NO+1	00748
	K=3	00749
	I=1	00750
	GO TO 926	00751
934	K=3	00752
	I=2	00753
	NO=NO+1	00754
	GO TO 926	00755
940	WRITE(20,25) (TIMFLT(I),I=1,3),MO,DATE	00756
25	FORMAT(20X,#TIMES POT -- FLIGHT 1#,F6.1,5X,	00757
	1#FLIGHT 2#,F6.1,5X,#FLIGHT 3#,F6.1,10X,I2,#/#,I2,	00758
	2#/69#/,23X,#SECTION#,10X,#FLIGHTS 1-2#,10X,	00759
	3#FLIGHTS 1-3#,10X,#FLIGHTS 2-3#/)	00760
	DO 950 I=1,L	00761
	K=2+5*(I-1)	00762
	WRITE(20,26) K,(X(J,I),J=1,NO)	00763
26	FORMAT(25X,I3,3E22.2)	00764
950	CONTINUE	00765
	WRITE(20,27) (X(I,1),I=5, 7)	00766
27	FORMAT(/23X,#MEANS#,3E22.2)	00767
1000	STOP	00768
	END	00769

Figure C-7. Program listing for REMOTE. (Continued)

DEFINE DECLAR	00001
COMMON X(10,300),IPHOT(120,80),CAMO(90,6),C(20,3)	00002
COMMON B(15,6),P(2,8),ANGHB(4),VOLL(2,8)	00003
END	00004
DEFINE GRDCOORD	00005
XG(1)=CAMO(IPLATE,1)-CAMO(IPLATE,3)*XT(1)/XT(3)	00006
XG(2)=CAMO(IPLATE,2)-CAMO(IPLATE,3)*XT(2)/XT(3)	00007
END	00008
SUBROUTINE PROCESS(KFLT,JFLT,ILUN,FL,NXI,NYI)	00009
DIMENSION IVT(6),BB(9),XT(3),XG(2)	00010
INCLUDE DECLAR	00011
INTEGER HARDWARE	00012
REWIND 21	00013
KGO=0	00014
ISEY1=TTYIN(4HSEY1)	00015
ISEY2=TTYIN(4HSEY2)	00016
ISEAX=TTYIN(4HSEAX)	00017
IPHX=TTYIN(4HPOHX)	00018
89 IPLATE=(KFLT-1)*10+1	00019
DENL=TTYIN(4HDNL=)	00020
DENH=TTYIN(4HDNH=)	00021
IEND=1	00022
INK=0	00023
95 READ(ILUN,1) IMO,IDATE,IFLT,IPH,IPLT2,IBD1,IBD2,	00024
1 XPH,YPH,DCOOR	00025
1 FORMAT(7I5,2F5.0,F5.3)	00026
IF(EOF(ILUN)) GO TO 1000	00027
IF(KFLT.NE.IFLT) GO TO 1000	00028
IF(IPLATE-IPLT2) 100,200,150	00029
100 BACKSPACE ILUN	00030
101 IFND=3	00031
GO TO 400	00032
150 IEND=2	00033
BACKSPACE ILUN	00034
GO TO 400	00035
200 CALL ORIMAT(IPLATE)	00036
IBAND=IBD1	00037
SUM1=CAMO(IPLATE,3)/3280.	00038
ATN1=P(1,IBD1)+ALOG(SUM1+1.)+P(2,IBD1)*SUM1*SUM1	00039
ATN2=P(1,IBD2)+ALOG(SUM1+1.)+P(2,IBD2)*SUM1*SUM1	00040
ATN1=ATN1-ATN2	00041
ATN2=(C(IBD1+3,3)-C(IBD2+3,3))*B(3,JFLT+3)	00042
DO 210 I=1,60	00043
YP=I	00044
210 X(9,I)=(XPH+0.5-YP)*DCOOR	00045
DO 300 J=1,120	00046
JK=J	00047
IST=1	00048
IND=30	00049
IF (J.LE.60) GO TO 220	00050
JK=J-60	00051
IST=31	00052
IND=60	00053
220 READ(ILUN,2) (X(10,I),I=IST,IND)	00054
2 FORMAT(30F4.2)	00055
XP=JK	00056
XP=(YPH+0.5-XP)*DCOOR	00057
KGO=1	00058
IF(JK.EQ.ISEY1.OR.JK.EQ.ISEY2) KGO=2	00059
K=0	00060
DO 300 I=IST,IND	00061
IF(X(10,I).LT.DENL.OR.X(10,I).GT.DENH) GO TO 300	00062
IF(.EQ.0.AND.J.LT.60) GO TO 290	00063

Figure C-8. Subroutines used with program REMOTE.

YP=X(9,I)	00064
CALL TRNCOORD(XP,YP,FL,XT)	00065
INCLUDE GRDCOORD	00066
RGX=XG(1)-C(12,2)	00067
RGY=XG(2)-C(12,3)	00068
XG(1)=RGX*C(13,2)+RGY*C(13,3)	00069
XG(2)=-RGX*C(13,3)+RGY*C(13,2)	00070
LX=XG(1)/60.+0.5	00071
IF(LX.LE.0.OR.LX.GT.NXI) GO TO 300	00072
LY=(XG(2)+C(14,2))/60.+0.5	00073
IF(LY.LE.0.OR.LY.GT.NYI) GO TO 300	00074
CAM=ATANF(SQRT(XP*XP+YP*YP)/FL)	00075
C ANGLE BETWEEN RAY IN AIR AND VERTICAL	00076
DIV=SQRT(XT(1)*XT(1)+XT(2)*XT(2))	00077
CAN=ATAN(-DIV/XT(3))	00078
C ANGLE BETWEEN RAY AND VERTICAL UNDERWATE-	00079
SINC=0.75*SINF(CAN)	00080
COSC=SQRT(1.0-SINC*SINC)	00081
C RAY VECTOR UNDERWATER	00082
FT=-DIV*COSC/SINC	00083
SINC=(XT(1)*B(10,JFLT+3)+XT(2)*B(11,JFLT+3)+FT*B(12,JFLT+3)	00084
1 )/1.34	00085
IF(SINC.GT.1.) SINC=1.	00086
FT=SQRT(1.0-SINC*SINC)	00087
TAB=ATAN(-FT/SINC)	00088
CAN=1.0/COS(CAN)	00089
FT=X(10,I)/C(1BD1+3,1)+ATN2+ATN1*CAN	00090
DENS=EXP(FT)*1000.	00091
IF(1.EQ.ISEAX.AND.1PH.EQ.1PHX) GO TO 250	00092
GO TO (260,250),KGO	00093
250 IF (INK.LT.300) INK=INK+1	00094
X(1,INK)=1.0	00095
X(2,INK)=CAM	00096
X(3,INK)=TAB	00097
X(4,INK)=CAN	00098
X(5,INK)=DENS	00099
260 WRITE(21,3)LX,LY,CAM,TAB,CAN,DENS	00100
3 FORMAT(215,5E11.3)	00101
290 K=K+1	00102
300 CONTINUE	00103
IPLATE=IPLATE+1	00104
GO TO 95	00105
400 IF(INK.EQ.0) GO TO 1100	00106
NO=INK	00107
N=5	00108
CALL LEASTFIT(N,NO,BB,RES)	00109
END FILE 21	00110
REWIND 21	00111
410 READ(21,3) LX,LY,CAM,TAB,CAN,DENS	00112
IF(EOF(21)) GO TO 500	00113
1PHCT(LX,LY)=DENS-(BB(1)+BB(2)*CAM+BB(3)*TAB+BB(4)	00114
1 *CAN)	00115
GO TO 410	00116
500 KND=4	00117
KDN=4	00118
NXS=NXI-2	00119
NYS=NYI-2	00120
CALL INTERP(NXI,NYI,NXS,NYS,KND,KDN)	00121
LUNO=IBAND+10	00122
IF (HARDWARE(LUNO).EQ. 1) GO TO 580	00123
CALL EQUIP(LUNO,5HFILE )	00124
580 REWIND LUNO	00125
DO 585 I=1,NXI,5	00126

Figure C-8. Subroutines used with program REMOTE. (Continued)

IMAX=C	00127
DO 583 J=1,NYI	00128
IF (ABS(IPHOT(I,J)).GT.ABS(IMAX)) IMAX=IPHOT(I,J)	00129
583 CONTINUE	00130
WRITE(61,10) IMAX	00131
585 CONTINUE	00132
DO 590 I=1,NXI,20	00133
DO 590 J=1,NYI	00134
KK=I+19	00135
WRITE(LUNO,8) (IPHOT(K,J),K=I,KK)	00136
8 FORMAT(X,20I6)	00137
590 CONTINUE	00138
END FILE LUNO	00139
LUNC=IBAND+30	00140
IF (HARDWARE(LUNO) .EQ. 1) GO TO 592	00141
CALL EQUIP(LUNO,5HFILE )	00142
592 REWIND LUNO	00143
REWIND 5	00144
595 READ(5,9) LX,LY	00145
9 FORMAT(2I4)	00146
IF (EOF(5)) GO TO 598	00147
WRITE(LUNC,10) IPHOT(LX,LY)	00148
10 FORMAT(I8)	00149
GO TO 595	00150
598 END FILE LUNC	00151
GO TO (900,900,1100),IEND	00152
900 CALL ZERGARRY(NXI,NYI,1,C,1,0)	00153
REWIND 21	00154
GO TO 89	00155
1000 BACKSPACE ILUN	00156
IF (KGO.GT. 0) GO TO 101	00157
1100 RETURN	00158
END	00159
..	

Figure C-8. Subroutines used with program REMOTE. (Continued)

DEFINE DECLAR	00001
COMMON X(10,300),IPHOT(120,80),CAMO(90,6),C(20,3)	00002
COMMON B(15,6),P(2,8),ANGHB(4),VOLL(2,8)	00003
END	00004
DEFINE GRDCOORD	00005
XG(1)=CAMO(IPLATE,1)-CAMO(IPLATE,3)*XT(1)/XT(3)	00006
XG(2)=CAMO(IPLATE,2)-CAMO(IPLATE,3)*XT(2)/XT(3)	00007
END	00008
SUBROUTINE RESECT(IFL,DELOMG,DELPHI)	00009
DIMENSION D(6,7)	00010
INCLUDE DECLAR	00011
IEND=1	00012
REWIND 8	00013
5 IGO=0	00014
I=1	00015
C READ PHOTO CONTROL COORDINATES	00016
10 READ (08,1) IFL,IPH,(IPHOT(100,J),X(10,J),X(9,J),J=1,3)	00017
1 FORMAT(3X,2I1,3(I4,2F6.3,7X))	00018
IF (EOF(8)) 15,20	00019
15 IEND=2	00020
GO TO 40	00021
20 IPLT=(IFL-1)*10+IPH	00022
IF (I-1) 21,21,23	00023
21 IPLATE=IPLT	00024
23 IF(IPLT-IPLATE) 24,25,24	00025
24 BACKSPACE 8	00026
GO TO 40	00027
25 DO 38 J=1,3	00028
IF(IPHOT(100,J).EQ. 0 .AND. X(10,J).GT. 0.) GO TO 26	00029
IF(IPHOT(100,J).GT. 0 .AND. IPHOT(100,J).LE.19)GO TO 28	00030
IF(IPHOT(100,J).LE.33 .AND. IPHOT(100,J).GT.29)GO TO 30	00031
GO TO 38	00032
26 XP=X(10,J)	00033
YP=X(9,J)	00034
GO TO 38	00035
28 B(I,1)=IPHOT(100,J)	00036
B(I,2)=X(9,J)	00037
P(I,3)=X(10,J)	00038
I=I+1	00039
GO TO 38	00040
30 K=IPHOT(100,J)-29	00041
X(1,K)=X(10,J)	00042
X(2,K)=X(9,J)	00043
38 CONTINUE	00044
GO TO 10	00045
40 IMAGE=I-1	00046
IF (IMAGE-3) 1002,50,50	00047
50 IF (IPLATE-30) 55,55,52	00048
52 XP=(X(1,1)+X(1,2)+X(1,3)+X(1,4))/4.	00049
YP=(X(2,1)+X(2,2)+X(2,3)+X(2,4))/4.	00050
55 DO 57 I=1,IMAGE	00051
B(I,2)=YP-B(I,2)	00052
B(I,3)=XP-B(I,3)	00053
57 CONTINUE	00054
C READ GROUND CONTROL	00055
DO 100 I=1,IMAGE	00056
REWIND 9	00057
K=B(I,1)	00058
60 J=FFIN(9)	00059
IF(EOF(9)) GO TO 1004	00060
IF (K-J) 70,80,70	00061
70 DO 75 J=1,3	00062
TRASH=FFIN(9)	00063

Figure C-8. Subroutines used with program REMOTE. (Continued)



75	CONTINUE	00064
	GO TO 60	00065
80	DO 90 J=4,6	00066
	B(I,J)=FFIN(9)	00067
90	CONTINUE	00068
100	CONTINUE	00069
C	READ INITIAL RARAMETERS FOR CAMERA PHOTO NO., X,Y,Z IN FT	00070
C	AND OMEGA, PHI , KAPPA IN DEGREES	00071
	REWIND 10	00072
	K=(IPLATE-1)/30+1	00073
	GO TO (102,104,106),K	00074
102	IPLT2=IPLATE	00075
	DEL1=0.	00076
	DEL2=0.	00077
	GO TO 108	00078
104	IPLT2=IPLATE-30	00079
	DEL1=DELOMG	00080
	DEL2=DELPHI	00081
	GO TO 108	00082
106	IPLT2=IPLATE-60	00083
	DEL1=DELOMG	00084
	DEL2=DELPHI	00085
108	IPLT=FFIN(10)	00086
	IF (EOF(10)) GO TO 1006	00087
	IF (IPLT-IPLT2) 110,120,110	00088
110	DO 115 I=1,6	00089
	TRASH=FFIN(10)	00090
115	CONTINUE	00091
	GO TO 108	00092
120	DO 125 J=1,3	00093
	C(1,J)=FFIN(10)	00094
125	CONTINUE	00095
	C(2,1)=FFIN(10)/57.2958+DEL1	00096
	C(2,2)=FFIN(10)/57.2958+DEL2	00097
	C(2,3)=FFIN(10)/57.2958	00098
	DO 130 I=1,3	00099
	C(3,I)=COSF(C(2,I))	00100
	C(2,I)=SINF(C(2,I))	00101
130	CONTINUE	00102
C	ORIENTATION FACTORS IN C ARRAY	00103
610	C(4,1)=C(3,2)*C(3,3)	00104
	C(5,1)=-C(3,2)*C(2,3)	00105
	C(6,1)=C(2,2)	00106
	C(10,1)=-C(2,2)*C(3,3)	00107
	C(11,1)=C(2,2)*C(2,3)	00108
	C(12,1)=C(3,2)	00109
	C(10,2)=C(4,1)*C(2,1)	00110
	C(11,2)=C(5,1)*C(2,1)	00111
	C(12,2)=C(2,1)*C(2,2)	00112
	C(10,3)=-C(4,1)*C(3,1)	00113
	C(11,3)=-C(5,1)*C(3,1)	00114
	C(12,3)=-C(3,1)*C(2,2)	00115
	C(4,2)=C(3,1)*C(2,3)+C(12,2)*C(3,3)	00116
	C(5,2)=C(3,1)*C(3,3)-C(12,2)*C(2,3)	00117
	C(6,2)=-C(2,1)*C(3,2)	00118
	C(4,3)=C(2,1)*C(2,3)+C(10,1)*C(3,1)	00119
	C(5,3)=C(2,1)*C(3,3)+C(11,1)*C(3,1)	00120
	C(6,3)=C(3,1)*C(3,2)	00121
	DO 612 I=7,9	00122
	C(I,1)=0.	00123
	C(I,2)=-C(I-3,3)	00124
	C(I,3)=C(I-3,2)	00125
	C(13,I-6)=C(5,I-6)	00126

Figure C-8. Subroutines used with program REMOTE. (Continued)

	C(14,I-6)=-C(4,I-6)	00127
612	C(15,I-6)=0.	00128
	GO TO (613,763),IGO	00129
C	CLEAR NORMAL EQUATION D ARRAY TO ZERO	00130
613	DO 614 I=1,6	00131
	DO 614 J=I,7	00132
614	D(I,J)=0.	00133
C	COMPUTE P TERMS FOR RESECTION PASS POINTS	00134
	DO 618 NU=1,IMAGE	00135
	DO 619 K=1,3	00136
619	C(16,K)=B(NU,K+3)-C(1,K)	00137
	K=4	00138
	DO 620 L=17,20	00139
	DO 620 I=1,3	00140
	C(L,I)=C(K,1)*C(16,1)+C(K,2)*C(16,2)+C(K,3)*C(16,3)	00141
620	K=K+1	00142
	DO 621 I=1,2	00143
	DO 622 L=1,4	00144
622	P(I,L)=(B(NU,I+1)*C(L+16,3)-(-FL)*C(L+16,I))/C(17,3)	00145
	DO 623 L=5,7	00146
623	P(I,L)=(-B(NU,I+1)*C(6,L-4)+(-FL)*C(I+3,L-4))*C(1,3)/C(17,3)	00147
621	P(I,8)=-P(I,1)	00148
C	CONTRIBUTION TO NORMAL EQUATIONS	00149
	DO 618 I=1,6	00150
	DO 618 J=I,7	00151
	DO 618 K=1,2	00152
618	D(I,J)=D(I,J)+P(K,1+1)*P(K,J+1)	00153
C	FOREWARD SOLUTION	00154
	DO 699 I=1,6	00155
	SQR=SQRT(D(I,I))	00156
	DO 698 J=I,7	00157
698	D(I,J)=D(I,J)/SQR	00158
	IF (I-6)697,696,696	00159
697	IP1=I+1	00160
	DO 699 L=IP1,6	00161
	DO 699 J=L,7	00162
699	D(L,J)=D(L,J)-D(I,L)*D(I,J)	00163
C	BACK SOLUTION	00164
696	D(6,7)=D(6,7)/D(6,6)	00165
	DO 691 I=1,5	00166
	NMI=6-I	00167
	NMI+1=NMI+1	00168
	DO 690 J=NMI+1,6	00169
690	D(NMI,7)=D(NMI,7)-D(J,7)*D(NMI,J)	00170
691	D(NMI,7)=D(NMI,7)/D(NMI,NMI)	00171
	DO 625 I=4,6	00172
625	D(I,7)=D(I,7)*C(1,3)	00173
C	ADD LEAST SQUARES RESULTS TO CAMERA PARAMETERS IN C ARRAY	00174
	DO 626 J=1,3	00175
	C(1,J)=C(1,J)+D(J+3,7)	00176
	C(4,J)=D(J,7)	00177
	C(5,J)=SQRT(1.-C(4,J)*C(4,J))	00178
	C(6,J)=C(2,J)*C(5,J)+C(3,J)*C(4,J)	00179
	C(7,J)=C(3,J)*C(5,J)-C(2,J)*C(4,J)	00180
	C(2,J)=C(6,J)	00181
626	C(3,J)=C(7,J)	00182
C	TEST MAGNITUDE OF CORRECTIONS FOR ORIENTATION PARAMTERES	00183
	DO 628 I=1,3	00184
	IF (ABS(D(I,7))-0.00001)628,628,610	00185
628	CONTINUE	00186
	IGO=2	00187
	GO TO 610	00188
C	CAMERA PARAMETERS OUTPUT	00189

Figure C-8. Subroutines used with program REMOTE. (Continued)

763	WRITE(20,532)	00190
	WRITE(20,527)	00191
	WRITE (20,528) IPLATE,(C(1,J),J=1,3)	00192
	WRITE (20,529)	00193
	WRITE (20,528) IPLATE,(C(2,J),J=1,3)	00194
	WRITE (20,528) IPLATE,(C(3,J),J=1,3)	00195
	WRITE (20,530) IPLATE	00196
	WRITE (20,533) ((C(I,J),J=1,3),I=4,6)	00197
527	FORMAT(/49H PLATE                   XO                   YO                   ZO)	00198
528	FORMAT(17,3(2X,E14.7))	00199
529	FORMAT(/50H PLATE                   OMEGA                   PHI                   KAPPA)	00200
530	FORMAT(/30H ORIENTATION MATRIX FOR PLATE ,17)	00201
532	FORMAT(/50H ORIENTATION PARAMETER CORRECTION LIMIT IS 0.00001)	00202
533	FORMAT (1X,3(2X,F14.7))	00203
	DO 710 I=1,3	00204
	CAMO(IPLATE,I)=C(1,I)	00205
	TAN=ATANF(C(2,I)/C(3,I))	00206
	IF (C(3,I)) 702,704,704	00207
702	TAN=3.14159+TAN	00208
704	CAMO(IPLATE,I+3)=TAN	00209
710	CONTINUE	00210
	GO TO (5,1100),IEND	00211
1002	WRITE(20,1003) IPLATE	00212
1003	FORMAT(' INSUFFICIENT CONTROL,PLT',I6)	00213
	GO TO (5,1100),IEND	00214
1004	WRITE (20,1005) K	00215
1005	FORMAT(' GRD CONTROL MISSING',I6)	00216
	GO TO (5,1100),IEND	00217
1006	WRITE (20,1007) IPLATE	00218
1007	FORMAT(' INITIAL PARAMETERS NOT ON FILE',I6)	00219
	GO TO(5,1100),IEND	00220
1100	RETURN	00221
	END	00222

Figure C-8. Subroutines used with program REMOTE. (Continued)

```

SUBROUTINE SUNLITE(TIMFLT,H,AZ)                                00001
DIMENSION H(3),AZ(3),TIMFLT(3)                                00002
C   COMPUTE THE ALTITUDE AND AZIMUTH OF THE SUN                00003
C   TIME IS PACIFIC DAYLIGHT TIME                              00004
C   READ IN DECLINATION OF SUN IN DEGREES (AA),AND MIN (B)    00005
C   AND CHANGE IN MIN PER HOUR (CC). EQUATION OF TIME         00006
C   IN MINUTES (DD), SECONDS (E), AND CHANGE PER HOUR (F)    00007
C   LONGITUDE (WLOH) AND LATITUDE (ALAT).                      00008
AA=FFIN(7)                                                    00009
B=FFIN(7)                                                       00010
CC=FFIN(7)                                                       00011
DD=FFIN(7)                                                       00012
E=FFIN(7)                                                       00013
F=FFIN(7)                                                       00014
WLOH=FFIN(7)                                                    00015
ALAT=FFIN(7)                                                    00016
ALAT=ALAT*3.14159/180.                                         00017
APANG=FFIN(7)                                                    00018
DO 200 I=1,3                                                    00019
GCT=TIMFLT(I)+7.                                                00020
DEC=(AA+(B+CC*GCT)/60.)*3.14159/180.                          00021
EQT=(DD+(E+F*GCT)/60.)/60.                                     00022
GHA=(GCT+EQT)*15.0-180.                                         00023
TT=GHA-WLOH                                                    00024
TT=TT*3.14159/180.                                             00025
T=ABS(TT)                                                       00026
Z=SINF(T)/(COSF(ALAT)*TANF(DEC)-SINF(ALAT)*COSF(T))           00027
AZ(I)=ATANF(Z)                                                  00028
IF (TT) 120,120,123                                           00029
120 IF (AZ(I)) 121,121,126                                     00030
121 AZ(I)=3.14159+AZ(I)                                         00031
GO TO 126                                                       00032
123 IF (AZ(I)) 124,124,125                                     00033
124 AZ(I)=3.14159-AZ(I)                                         00034
GO TO 126                                                       00035
125 AZ(I)=6.28318-AZ(I)                                         00036
126 CONTINUE                                                    00037
SINH=SINF(ALAT)*SINF(DEC)+COSF(ALAT)*COSF(DEC)*COSF(T)       00038
COSH=SINF(T)*COSF(DEC)/SINF(AZ(I))                             00039
ALT=ABS(SINH/COSH)                                              00040
HH=ATANF(ALT)                                                  00041
REF=((1.+25./60.)/60.)*3.14159/180.                           00042
H(I)=HH+REF                                                    00043
AZ(I)=AZ(I)-APANG/57.2958                                       00044
200 WRITE (20,1) H(I),REF,AZ(I)                                00045
1 FORMAT(11H SUN'S ALT. ,F10.6,12H REFRACTION ,F10.6,         00046
1/16H AZIMUTH OF SUN ,F10.6)                                  00047
RETURN                                                         00048
END                                                             00049

..

DEFINE DECLAR                                                  00001
COMMON X(10,300),IPHOT(120,80),CAMO( 0,6),C(20,3)           00002
COMMON B(15,6),P(2,8),ANGHB(4),VOLL(2,8)                     00003
END                                                             00004
DEFINE GRDCOORD                                                00005
XG(1)=CAMO(IPLATE,1)-CAMO(IPLATE,3)*XT(1)/XT(3)              00006
XG(2)=CAMO(IPLATE,2)-CAMO(IPLATE,3)*XT(2)/XT(3)              00007
END                                                             00008

```

Figure C-8. Subroutines used with program REMOTE. (Continued)

SUBROUTINE TRNCOCRD(XP,YP,FL,XT)	00009
DIMENSION XT(3)	00010
INCLUDE DECLAR	00011
DO 10 K=1,3	00012
XT(K)=C(1,K)*XP+C(2,K)*YP+C(3,K)*(-FL)	00013
10 CONTINUE	00014
XDIS=SQRT(XT(1)*XT(1)+XT(2)*XT(2)+XT(3)*XT(3))	00015
DO 20 K=1,3	00016
XT(K)=XT(K)/XDIS	00017
20 CONTINUE	00018
RETURN	00019
END	00020
SUBROUTINE ZEROARRY(NXI,NYI,NXX,NYX,IFRA,KOR)	00021
INCLUDE DECLAR	00022
DO 100 I=1,NXI	00023
DO 100 J=1,NYI	00024
IPHOT(I,J)=0	00025
100 CONTINUE	00026
DO 200 I=1,NXX	00027
DO 200 J=1,NYX	00028
X(I,J)=0.0	00029
200 CONTINUE	00030
DO 300 I=1,IFRA	00031
DO 300 J=1,KOR	00032
CAMO(I,J)=0.0	00033
300 CONTINUE	00034
RETURN	00035
END	00036
SUBROUTINE ORIMAT(IPLATE)	00037
INCLUDE DECLAR	00038
DIMENSION AC(3,3),BC(3,3)	00039
IF (IPLATE.GT. 30.AND.IPLATE.LE.60) GO TO 100	00040
IF (IPLATE.GT. 60.AND.IPLATE.LE.90) GO TO 200	00041
IGO=1	00042
K=IPLATE	00043
GO TO 300	00044
100 IGO=2	00045
K=IPLATE-30	00046
GO TO 300	00047
200 IGO=3	00048
K=IPLATE-60	00049
300 SINW=SINF(CAMO(K,4))	00050
COSW=COSF(CAMO(K,4))	00051
SINP=SINF(CAMO(K,5))	00052
COSP=COSF(CAMO(K,5))	00053
SINK=SINF(CAMO(K,6))	00054
COSK=COSF(CAMO(K,6))	00055
C(1,1)=COSP*COSK	00056
C(1,2)=COSW*SINK+SINW*SINP*COSK	00057
C(1,3)=SINW*SINK-COSW*SINP*COSK	00058
C(2,1)=-COSP*SINK	00059
C(2,2)=COSW*COSK-SINW*SINP*SINK	00060
C(2,3)=SINW*COSK+COSW*SINP*SINK	00061
C(3,1)=SINP	00062
C(3,2)=-SINW*COSP	00063
C(3,3)=COSW*COSP	00064
GO TO (100,400,500,600),IGO	00065
400 CAMO(90,4)=ANGHB(1)	00066
CAMO(90,5)=ANGHB(2)	00067
CAMO(90,6)=0.0	00068
410 DO 420 I=1,3	00069
DO 420 J=1,3	00070
AC(I,J)=C(I,J)	00071

Figure C-8. Subroutines used with program REMOTE. (Continued)

420	CONTINUE	00072
	K=0	00073
	IGO=4	00074
	GO TO 300	00075
500	CAYC(90,4)=ANGHB(3)	00076
	CAYC(90,5)=ANGHB(4)	00077
	CAYC(90,6)=0.0	00078
	GO TO 410	00079
600	DO 620 I=1,3	00080
	DO 620 J=1,3	00081
	BC(I,J)=C(I,J)	00082
620	CONTINUE	00083
	DO 700 I=1,3	00084
	DO 700 J=1,3	00085
	C(I,J)=0.	00086
	DO 700 K=1,3	00087
	C(I,J)=C(I,J)+AC(K,J)*BC(I,K)	00088
700	CONTINUE	00089
1000	RETURN	00090
	END	00091
	FUNCTION DIST(XP,YP)	00092
	DIST=SQRT(XP*XP+YP*YP)	00093
	RETURN	00094
	END	00095
	FUNCTION STDEV(SUM1,SUM2,AJ)	00096
	STDEV=SQRT((SUM2-SUM1*SUM1/AJ)/(AJ-1.))	00097
	RETURN	00098
	END	00099
	FUNCTION REFLECT(AI,AR)	00100
	A=AI-AR	00101
	B=AI+AR	00102
	C=SINF(A)	00103
	D=SINF(B)	00104
	E=C/COSF(A)	00105
	F=D/COSF(B)	00106
	REFLECT=1.-((F*F)/(F*F)+(C*C)/(D*D))/2.0	00107
	RETURN	00108
	END	00109
	SUBROUTINE INTERP(NXI,NYI,NXS,NYS,KND,KDN)	00110
	INCLUDE DECLAR	00111
	DO 540 I=1,NYI	00112
	DO 540 J=1,NXS	00113
	IF (IPHOT(J,I)) 530,540,530	00114
530	IF (IPHOT(J+1,I)) 540,532,540	00115
532	DO 534 K=2,KND	00116
	KJ=J+K	00117
	IF (KJ-NXI) 533,533,540	00118
533	IF (IPHOT(KJ,I)) 536,534,536	00119
534	CONTINUE	00120
	GO TO 540	00121
536	LJ=KJ-J-1	00122
	DJ=KJ-J	00123
	DIF=IPHOT(J,I)-IPHOT(KJ,I)	00124
	DO 538 K=1,LJ	00125
	AJ=K	00126
	LLJ=J+K	00127
	IPHOT(LLJ,I)=IPHOT(J,I)-DIF*AJ/DJ	00128
538	CONTINUE	00129
540	CONTINUE	00130
	DO 520 I=1,NXI	00131
	DO 520 J=1,NYS	00132
	IF (IPHOT(I,J)) 510,520,510	00133
510	IF (IPHOT(I,J+1)) 520,512,520	00134

Figure C-8. Subroutines used with program REMOTE. (Continued)

512	DO 514 K=2,KDN	00135
	KJ=J+K	00136
	IF (KJ-NYI) 513,513,520	00137
513	IF (IPHOT(I,KJ)) 516,514,516	00138
514	CONTINUE	00139
	GO TO 520	00140
516	LJ=KJ-J-1	00141
	DJ=KJ-J	00142
	DIF=IPHOT(I,J)-IPHOT(I,KJ)	00143
	DO 518 K=1,LJ	00144
	AJ=K	00145
	LLJ=J+K	00146
	IPHOT(I,LLJ)=IPHOT(I,J)-DIF*AJ/DJ	00147
518	CONTINUE	00148
520	CONTINUE	00149
	RETURN	00150
	END	00151
	SUBROUTINE AVERAGE(NXS,NYS)	00152
	INCLUDE DECLAR	00153
	ITEST=1	00154
	DO 570 I=1,NXS	00155
	DO 560 J=2,NYS	00156
	GO TO (562,564),ITEST	00157
562	X(1,J)=(IPHOT(I,J)+IPHOT(I,J-1)+IPHOT(I,J+1)+	00158
	1 IPHOT(I+1,J))/4	00159
564	X(2,J)=(IPHOT(I,J)+IPHOT(I+1,J)+IPHOT(I+2,J)+	00160
	1 IPHOT(I+1,J+1)+IPHOT(I+1,J-1))/5	00161
560	CONTINUE	00162
	ITEST=2	00163
	DO 565 J=2,NYS	00164
	IPHOT(I,J)=X(1,J)	00165
	X(1,J)=X(2,J)	00166
565	CONTINUE	00167
570	CONTINUE	00168
	RETURN	00169
	END	00170
	SUBROUTINE CULL(NXI,NYI)	00171
	INCLUDE DECLAR	00172
	BJ=9.	00173
	IX=NXI-2	00174
	IY=NYI-2	00175
	DO 100 I=1,IX	00176
	DO 100 J=1,IY	00177
	SUM1=0.0	00178
	SUM2=0.0	00179
	DO 20 IK=1,3	00180
	DO 20 JK=1,3	00181
	IP=I+IK-1	00182
	JP=J+JK-1	00183
	AI=IPHOT(IP,JP)	00184
	SUM1=SUM1+AI	00185
	SUM2=SUM2+AI*AI	00186
20	CONTINUE	00187
	SUM2=STDEV(SUM1,SUM2,BJ)	00188
	AI=SUM1/BJ	00189
	BI=IPHOT(I+1,J+1)	00190
	CI=(SUM1-BI)/(BJ-1.)	00191
	SUM1=AI-SUM2	00192
	SUM2=AI+SUM2	00193
	IF(BI.LT.SUM1.OR.BI.GT.SUM2) IPHOT(I+1,J+1)=CI	00194
100	CONTINUE	00195
	RETURN	00196
	END	00197

Figure C-8. Subroutines used with program REMOTE. (Continued)

0	80711 000 04240 03335 0000	001 03901 04321 0000	004 07136 03545 0000
A.A	80711 010 05225 01200 0000	011 02211 01241 0000	021 04239 04272 0000
15 15	80711 030 02664 04823 0000	031 02660 02982 0000	032 08031 02844 0000
15 21	80711 033 08023 06454 0000	034 03350 04044 0000	035 08030 04776 0000
15 50	80721 000 04241 03405 0000	001 03825 04424 0000	004 06301 03982 0000
9000	80721 010 05156 01841 0000	011 02603 01699 0000	021 04503 04413 0000
	80721 030 03348 04720 0000	031 03320 03101 0000	032 04246 03220 0000
22	80721 033 08277 06745 0000		
31.63	80722 000 04205 03435 0000	001 01595 04312 0000	004 04157 03982 0000
-0.285	80722 009 06913 01616 0000	010 03629 01917 0000	011 01204 01801 0000
-4	80731 000 04241 03435 0000	001 03918 04540 0000	004 06494 03928 0000
-51.6	80731 009 08528 01362 0000	010 05080 01868 0000	011 02545 01903 0000
-0.39	80731 021 05631 04356 0000	030 03227 04908 0000	031 03237 03081 0000
124.0667	80731 032 08065 03121 0000	033 08079 04326 0000	
46.64	80732 000 04240 03392 0000	001 02314 04098 0000	004 04919 03598 0000
-2.53	80732 009 07481 01214 0000	010 04071 01648 0000	011 01640 01627 0000
-1.3 0.0 0.252	80733 000 04240 03403 0000	001 00960 03934 0000	004 03419 03514 0000
-1.3 0.0 0.331	80733 009 06461 01291 0000	010 03149 01671 0000	011 00805 01635 0000
-1.3 0.0 0.619	80751 001 01126 04512 0000	021 01785 04501 0000	030 00574 05535 0000
-1.7 1.0 0.187	80751 031 00507 03368 0000	032 02647 03345 0000	033 02647 05528 0000
-2.1 0.4 0.252	80752 004 01488 01455 0000	030 00512 03032 0000	031 00513 00861 0000
-1.3 0.4 0.331	80752 032 02661 00840 0000	033 02662 03005 0000	
0.82 -0.9 .252	80761 001 03198 06472 0000	030 02499 07411 0000	031 02472 05238 0000
0.91 -0.9 .187	80761 032 04639 05202 0000	033 04641 07365 0000	
200 6.3	80762 004 04040 03091 0000	021 03176 03451 0000	030 02444 04930 0000
200 6.3	80762 031 02434 02753 0000	032 04601 02704 0000	033 04640 04868 0000
250 5.6	80763 004 02623 00566 0000	030 02431 02485 0000	031 02414 00321 0000
250 5.6	80763 032 04577 00275 0000	033 04602 02437 0000	
250 5.6	80791 001 03241 06329 0000	030 02502 07273 0000	031 02514 05104 0000
250 5.6	80791 032 04679 05091 0000	033 04680 07257 0000	
250 5.6	80792 004 04123 02991 0000	021 03239 03338 0000	030 02516 04314 0000
250 5.6	80792 031 02504 02640 0000	032 04669 02617 0000	033 04678 04797 0000
250 5.6	80793 004 02716 00381 0000	030 02507 02320 0000	031 02437 00146 0000
0.163 -0.005	80793 032 04649 00133 0000	033 04662 02291 0000	
0.188 -0.005			
0.272 -0.003			
0.143 -0.005			
0.163 -0.005			
0.163 -0.005			
0.143 -0.005			
1			

LUN 7			
1	1069310 375760 0.0	1	1066500 375800 3000 0 -45 0
4	1069540 373540 0.0	11	1066500 375000 4000 0 -45 0
9	1072951 369571 130	12	1066000 373500 4000 0 -45 0
10	1072949 373966 42	21	1066500 375800 3000 0 -45 0
11	1073606 377145 75	22	1066500 374000 3000 0 -45 0
		23	1066500 372000 3000 0 -45 0

LUN 9			
LUN 10			

LUN 8			
-------	--	--	--

Figure C-9. Sample input data for REMOTE.



## APPENDIX D

### PROCESSING OF 1970-71 PHOTOGRAPHIC DATA

A general description of the CDC 3300 Computer and special fortran input functions is given in the introduction of Appendix B.

The program used for processing the data collected in 1970 and 1971 was program INSHORE. The program delineates the plume outline from coordinates measured from the aerial photography and determines the area of the waste field. The direction and velocity of the current and the diffusion coefficients are determined from the dye patch. In the process, state plane coordinates of the points around the plume were computed, and these were saved for later plotting on the Tektronix graphic-scope. See figure D-1 for a flow diagram of program INSHORE. The numbers in parentheses on the flow diagram correspond to line numbers on the program listing in figure D-2.

#### Program

Program INSHORE first orients the photo found on LUN 8 by calling RESECT2, a version of the subroutine RESECT used in processing the data in 1968 and 1969. After the orientation is completed, the coordinates of the points on the photograph are read in, and the state plane coordinates of each point are computed. As this is done, the data is sorted according to the event number so that it is known whether the point is a plume point, a point in the foam or kelp, a dye patch point, or a point representing the apparent position of the outfall.

If the point is on the plume, a code number is assigned to indicate that a continuous line is to be drawn from the previous point when the data is plotted. Therefore, IDO is set to equal 1. If the point is the first point, a line from the origin to that point is not desired, and IPEN = 0. For all other plume points, the line is required and IPEN = 1. When the last plume point is reached, the area of the plume is computed by calling subroutine SECPROP. The area is converted to acres, and is stored for later print out. As each point is assigned the proper code, the code and the coordinate are written on LUN 23.

The points indicating the foam, kelp, and the outfall are coded separately, and are also written out with their respective coordinates and codes.

The dye points are read, and as the last point is reached, section properties needed for the computation of diffusion coefficients are calculated. This is also done by subroutine SECPROP.

After the end of file has been reached on LUN 8, the time elapsed between flights is typed in. If there are two photos on file, the current velocity and direction are computed, using section properties of

the dye patch. A current vector is then generated, and the coordinates needed to plot the vector are written on LUN 23.

Diffusion coefficients are then computed and all of the general information is written on LUN 20.

Normally the data on LUN 23 is saved to be used as input for the plotting program. The data on LUN 20 is sent to the line printer and is used for reference purposes.

#### Input Description

The input on LUN 8 consists of photo coordinates, with the format being the same as in the previous year (see Appendix C, figure C-8). As shown below, the event number coding differs from that listed in Appendix C.

<u>Event No.</u>	<u>Description</u>
000	Principal point.
001-019	Ground control.
100-498	Plume points.
499	Last plume point (always).
500-599	Foam points.
600-699	Kelp points.
700-898	Dye patch points.
899	Last dye patch point (always).
999	Outfall.

It should be noted that the control point numbers must correspond to the ground control numbers on LUN 9.

Data on LUNS 8 and 9 are exactly the same as listed in Appendix C. The data on LUN 9 is ground control, listing the point number, the x and y coordinates and the elevation above mean sea level. LUN 10 contains the initial orientation parameters for the camera station, and are arranged as follows: photo number, x and y coordinates, state plane coordinates, flying height, omega, phi and kappa rotation angles in degrees.

#### Output Description

The major output is a listing of coordinates for each point which is

to be plotted, along with a title for the plot. This is all written on LUN 23, and saved for later plotting. General information such as orientation for the photo, dye patch centroids, date, area of plume, current velocity, and diffusion coefficients are written on LUN 20, and are not saved except as hard copy. The area of the plume and date are also written on the teletype so that the operator may have a check to see if the program is operating correctly.

#### Plotting of Data

The data is plotted using a program which utilizes the Tektronix T-4002 slope. A grid is drawn and the axes are labeled. The data is then plotted and the plot labeled. A polaroid photograph is taken of the plot for a permanent record. Examples of these plots are shown in Section X.

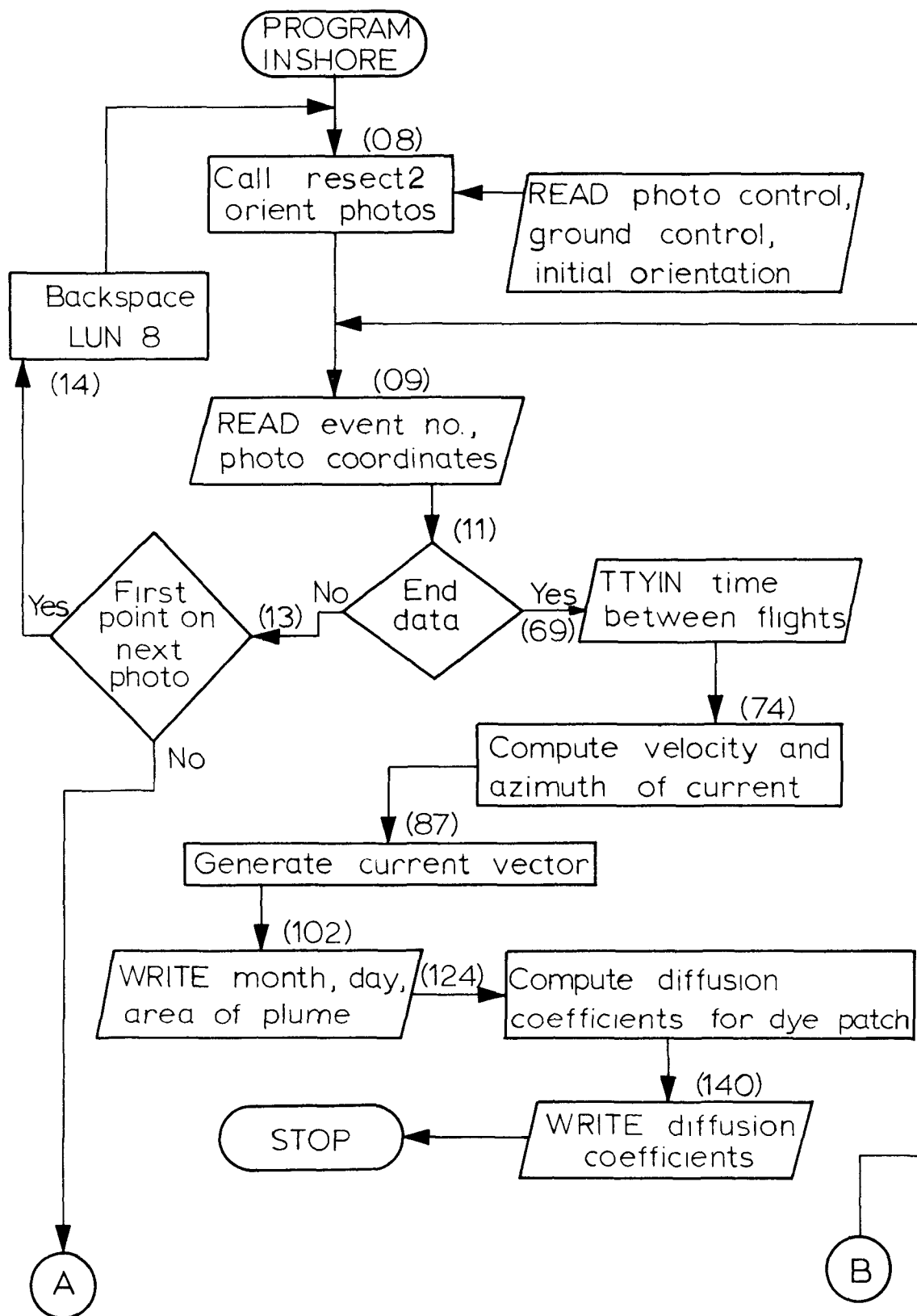


Figure D-1 Flow diagram for computer program INSHORE.

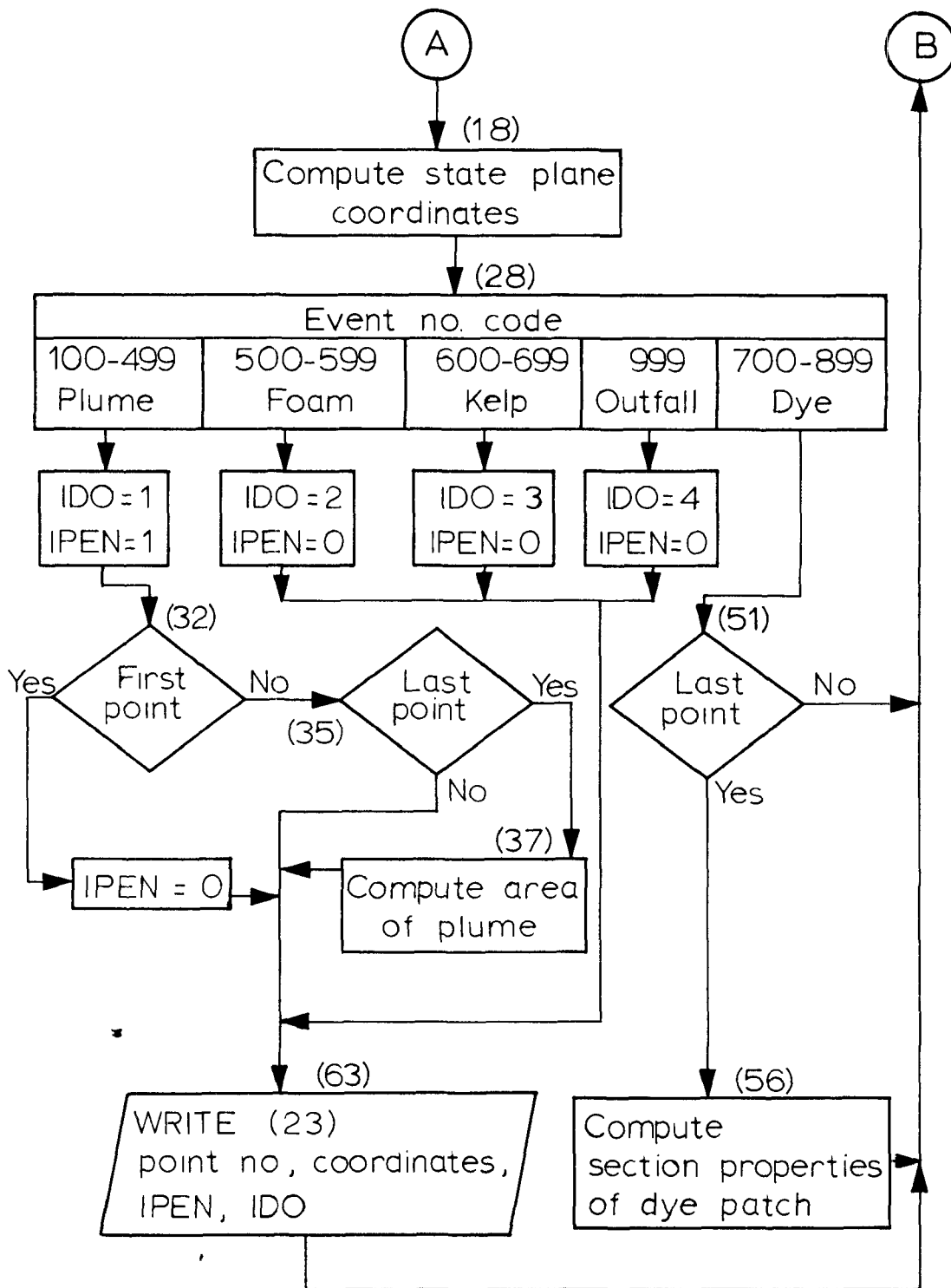


Figure D-1. Flow diagram for computer program INSHORE.

PROGRAM SHORE	00001
CJMMN C(2J,3),IP(3),XF(3),YF(3)	00002
DIMENSION XPL(2J0,2),XJ(2J0,2),XT(3),DYE(15,2,6),VEL(15),AZI(15)	00003
LFLT=1	00004
INO=1	00005
IFL1=1	00006
ICHECK=1	00007
100 CALL RESECT2(FL,XP,YP)	00008
110 READ(9,1) IPLATE,(IP(J),XF(J),YF(J),J=1,3)	00009
1 FORMAT(4X,I1,3(I4,2F6.3,6X))	00010
IF(E)F(8)) GO TO 10J0	00011
IF(IP(1).GT.99) GO TO 10	00012
IF(XF(1).LT.0.001) GO TO 110	00013
BACKSPACE 8	00014
GO TO 100	00015
10 DO 2J J=1,3	00016
IF(IP(J).EQ.0.AND.XF(J).EQ.0.) GO TO 110	00017
X1=YJ-YF(J)	00018
Y1=XJ-XF(J)	00019
DO 2J0 K=1,3	00020
210 XT(K)=C(4,K)*X1+C(5,K)*Y1+C(6,K)*(-FL)	00021
XDIS=SQRT(XT(1)*XT(1)+XT(2)*XT(2)+XT(3)*XT(3))	00022
DO 2J0 K=1,3	00023
220 XT(K)=XT(K)/XDIS	00024
XPG1=C(1,1)-XT(1)*C(1,3)/XT(3)	00025
XPG2=C(1,2)-XT(2)*C(1,3)/XT(3)	00026
IGO=IP(J)/100	00027
GO TO (2J,2J,2J,2J,3J,40,50,50,60) IGO	00028
20 XPL(IJO,1)=XPG1	00029
XPL(INO,2)=XPG2	00030
IPEN=1	00031
IF(IJO.EQ.1) IPEN=0	00032
IDO=1	00033
INO=INO+1	00034
IF(IP(J).NE.499) GO TO 300	00035
N=INO-1	00036
CALL SECPROP(XPL,N,15,1,DYE)	00037
PAREA=DYE(15,1,3)	00038
AO=PAREA/43560.	00039
INO=1	00040
GO TO 300	00041
30 IDO=2	00042
IPEN=0	00043
GO TO 300	00044
40 IDO=3	00045
IPEN=0	00046
GO TO 300	00047
50 XD(IFLAG,1)=XPG1	00048
XD(IFLAG,2)=XPG2	00049
IFLAG=IFLAG+1	00050
IF(IP(J).NE.899) GO TO 200	00051
N=IFLAG-1	00052
IFLT=1	00053
IF(IPLATE.GT.5) IFLT=2	00054
IF(IFLT.NE.LFLT) ICHECK =1	00055
CALL SECPROP(XD,N,ICHECK,IFLT,DYE)	00056
LFLT=IFLT	00057
IFLAG=1	00058
ICHECK=ICHECK+1	00059
GO TO 200	00060
60 IPEN=0	00061

Figure D-2. Listing of program INSHORE.

100=4	00062
300 WRITE(23,2) IP(J),XPG1,XPG2,IPEN,IDO	00063
2 FORMAT(X,I5,2F10.0,2I5)	00064
200 CONTINUE	00065
GO TO 110	00066
1000 WRITE(61,3)	00067
3 FORMAT(* TIME ELAPSED IN MINUTES*)	00068
TIME=TTYIN(4*TIME)	00069
TIME=TIME*60.	00070
ICOUNT=ICHECK-1	00071
SUMVE=0.0	00072
VELNO=0.0	00073
DO 400 I=1,ICOUNT	00074
XDIST=(DYE(I,2,1)-DYE(I,1,1))	00075
YDIST=(DYE(I,2,2)-DYE(I,1,2))	00076
AZI(I)=ATAN(XDIST/YDIST)	00077
IF(YDIST.LT.0.) AZI(I)=AZI(I)+3.14159	00078
IF(AZI(I).LT.0.) AZI(I)=AZI(I)+6.28318	00079
XDIST=SQR(XDIST*XDIST+YDIST*YDIST)	00080
IF(XDIST.GT.50.) GO TO 370	00081
VEL(I)=0.0	00082
GO TO 390	00083
370 IF(XDIST.LT.5000.) GO TO 380	00084
GO TO 400	00085
380 VEL(I)=XDIST/TIME	00086
CALL ARROW(VEL(I),DYE(I,1,1),DYE(I,1,2),AZI(I))	00087
SUMVE=SUMVE+VEL(I)	00088
390 VELNO=VELNO+1.	00089
400 CONTINUE	00090
REWIND 8	00091
VELM=0.0	00092
IF(VELNO.GT.0.1) VELM=SUMVE/VELNO	00093
READ(8,4) MO,IDAY	00094
4 FORMAT(2I2)	00095
WRITE(61,5)	00096
5 FORMAT(* TYPE IN YEAR IN WHICH PHOTO WAS TAKEN*)	00097
IYR=TTYIN(4*HYR= )	00098
WRITE(61,6)	00099
6 FORMAT(* PLUME DATA*)	00100
WRITE(20,6)	00101
WRITE(20,7) MO,IDAY,PAREA,AC	00102
WRITE(61,7) MO,IDAY,PAREA,AC	00103
7 FORMAT(* MONTH#,I4,/* DAY#,I6,/* AREA# ,E11.3,/* SQ. FT.#,/	00104
1# AREA#,F6.1,/* ACRES#)	00105
IF(VELNO.GT.0.1) GO TO 410	00106
WRITE(23,8) AC,MO,IDAY ,IYR	00107
8 FORMAT(* AREA OF PLUME#, F6.1,/* ACRES#,20X,2(I2,*/#),I2)	00108
GO TO 420	00109
410 WRITE(23,14) AC,VELM,MO,IDAY,IYR	00110
14 FORMAT(* AREA OF PLUME#,F6.1,/* ACRES#,	00111
1# VELOCITY#,F5.2,/* FPS #, 2(I2,*/#),I2)	00112
420 END FILE 23	00113
WRITE(20,9)	00114
9 FORMAT(* DYE PATCH DATA*)	00115
WRITE(20,12)(I,((DYE(I,J,K),K=1,3),J=1,2),VEL(I),AZI(I),	00116
5I=1,ICOUNT)	00117
12 FORMAT(* NO#,I2,/* XCENTROID-1#,F10.0,/* YCENTROID-1#,F10.0,/*	00118
C# AREA-1#,F15.2,/* XCENTROID-2#,F10.0,/* YCENTROID-2#,F10.0,/*	00119
C# AREA-2#,F15.2,/* VELOCITY#,F13.2,/* FPS#,/* AZIMUTH#	00120
C# FROM NORTH#,F8.5,/* RADIANS#)	00121
WRITE(20,13) TIME,VELM	00122
13 FORMAT(* TIME FOR VEL.#,F6.0,/* VELOCITY= #,F5.2)	00123

Figure D-2. Listing of program INSHORE. (Continued)

DO 430 I=1,ICOUNT	00124
RATIO=SQRT(DYE(I,1,4)/DYE(I,1,5))	00125
RAT2=DYE(I,1,3)/3.14159	00126
ASQ1=RAT2*RATIO	00127
BSQ1=RAT2/RATIO	00128
RATIO=SQRT(DYE(I,2,4)/DYE(I,2,5))	00129
RAT2=DYE(I,2,3)/3.14159	00130
ASQ2=RAT2*RATIO	00131
BSQ2=RAT2/RATIO	00132
RTA1=SQRT(ASQ1)	00133
RTA2=SQRT(ASQ2)	00134
RTB1=SQRT(BSQ1)	00135
RTB2=SQRT(BSQ2)	00136
DIV=1.385*TIME*2.	00137
DX=(ASQ2-ASQ1)/DIV	00138
DY=(BSQ2-BSQ1)/DIV	00139
430 WRITE(20,15) DX,DY,RTA1,RTA2,RTB1,RTB2	00140
15 FORMAT(///# D I F F U S I O N S T U D Y# /	00141
1# DX= #,F10.2,# FT SQ / SEC# /	00142
2# DY= #,F10.2,# FT SQ / SEC# /	00143
3# A1=#,F6.0,#, A2=#,F6.0,#, B1=#,F6.0,#, B2=#,F6.0)	00144
END FILE 20	00145
STOP	00146
END	00147
SUBROUTINE ARROW(SCAF,XDYE,YDYE,BZI)	00148
COMMON/DATA/A	00149
DIMENSION A(10,2)	00150
DATA((A(I,J),I=1,10),J=1,2)=0.,0.,30.,100.,30.,0.,-30.,	00151
1-100.,-30.,0.,0.,1000.,900.,800.,900.,1000.,900.,800.,900.,	00152
2)00.)	00153
AZI=-BZI	00154
S=SIGN(AZI)	00155
C=COS(AZI)	00156
IDO=5	00157
DO 10 J=1,2	00158
DO 10 I=1,10	00159
10 A(I,J)=A(I,J)*SCAF	00160
IPEN=0	00161
DO 20 I=1,10	00162
Y=YDYE+A(I,2)*C+A(I,1)*S	00163
X=XDYE-A(I,2)*S+A(I,1)*C	00164
IF(I.NE.1)IPEN=1	00165
20 WRITE(23,1)X,Y,IPEN,IDO	00166
1 FORMAT(6X,2F10.0,2I5)	00167
RETURN	00168
END	00169
SUBROUTINE SECPROP(X,N,N0,IFLT,DYE)	00170
C.....PROGRAMMED MARCH 1971	00171
C.....XSY= COORDS OF POINTS DEFINING CLOCKWISE PATH AROUND	00172
C.....BOUNDARY, N=NUMBER OF POINTS, CLOSURE FROM PT N TO PT 1	00173
C.....IS AUTOMATIC (POINT 1 IS READ IN ONLY ONCE).	00174
C.....IGX,IGY,IGXY ARE ABOUT CENTROIDAL AXES PARALLEL TO XSY.	00175
C.....THETA IS CLOCKWISE ANGLE FROM X AXIS TO MAJOR PRINC AXIS.	00176
REAL IX,IY,IXY,IGX,IGY,IGXY,IMAX,IMIN	00177
DIMENSION X(200,2),DYE(15,2,6)	00178
XLOW=X(1,1)	00179
YLOW=X(1,2)	00180
DO 10 I=1,N	00181
X(I,1)=X(I,1)-XLOW	00182
X(I,2)=X(I,2)-YLOW	00183
10 CONTINUE	00184
XI=X(N,1)	00185

Figure D-2. Listing of program INSHORE. (Continued)



XM=X(1,1)	00186
XMSQ=XM*XM	00187
T2X=XI+XM	00188
YI=X(N,2)	00189
YI=X(1,2)	00190
YMSQ=YI*YI	00191
T2Y=YI+YI	00192
A=AXBAR=AYBAR=IX=IY=IXY=0.	00193
DO 3 I=1,N	00194
IF(I.NE.N)GO TO 1	00195
M=1	00196
GO TO 2	00197
1 M=I+1	00198
2 XL=XI	00199
XI=XI	00200
XM=X(M,1)	00201
C.....XL=X(I-1), XI=X(I), XM=X(I+1), Y=S SIMILAR.	00202
T1X=T2X	00203
T2X=XI+XM	00204
T3X=XI-XI	00205
XISQ=XMSQ	00206
XMSQ=XM*XM	00207
YL=YI	00208
YI=YI	00209
YM=X(M,2)	00210
T1Y=T2Y	00211
T2Y=YI+YM	00212
T3Y=YI-YI	00213
YISQ=YMSQ	00214
YMSQ=YI*YI	00215
A=A+XI*(YL-YM)	00216
C.....ADJUSTULATE 2*A, 6*A*XBAR, 12*IX, 72*IXY, ETC.	00217
AXBAR=AXBAR-YI*(XL*T1X-XM*T2X)	00218
AYBAR=AYBAR+XI*(YL*T1Y-YM*T2Y)	00219
IX=IX+T3X*(YISQ+YMSQ)*T2Y	00220
IY=IY+T3Y*(XISQ+XMSQ)*T2X	00221
3 IXY=IXY-T3Y*(18.*XISQ*T2Y+T3X*(T3X*T3Y+4.*(2.*XI+XM)*(YI+2.*YM)))	00222
A=A*.5	00223
AXBAR=AXBAR/6.	00224
AYBAR=AYBAR/6.	00225
XBAR=AXBAR/A	00226
YBAR=AYBAR/A	00227
IX=IX/12.	00228
IY=IY/12.	00229
IXY=IXY/72.	00230
C.....TRANSFER TO CENTROIDAL AXES.	00231
IGX=IX-AYBAR*YBAR	00232
IGY=IY-AXBAR*XBAR	00233
IGXY=IXY-AXBAR*YBAR	00234
T1=(IGX-IGY)*.5	00235
T2=(IGX+IGY)*.5	00236
T3=SQRT(T1*T1+IGXY*IGXY)	00237
C.....COMPUTE PRINC MOMENTS OF INERTIA AND ORIENTATION OF	00238
C.....PRINC AXES.	00239
IF(T2.LT.1.)T3=-T3	00240
IMAX=T2+T3	00241
IMIN=T2-T3	00242
THETA=28.6479*ATAN(IGXY/T1)	00243
IF(T1.LT.0.)THETA=THETA+90.	00244
DYE(10,IFLT,1)=XBAR+XLOW	00245
DYE(10,IFLT,2)=YBAR+YLOW	00246
DYE(10,IFLT,3)=ABS(A)	00247

Figure D-2. Listing of program INSHORE. (Continued)

DYE(N0,IFLT,4)=ABS(IMAX)	00248
DYE(N0,IFLT,5)=ABS(IMIN)	00249
DYE(N0,IFLT,6)=THETA	00250
WRITE(20,6) IX,IY,IGX,IGY,IXY,IGXY,T1,T2,T3	00251
FORMAT(E13.4)	00252
WRITE(20,5)(N0,IFLT,I,DYE(N0,IFLT,I),I=1,6)	00253
5 FORMAT(* DYE(I2,I2,I2,I2)=#,F18.2)	00254
RETURN	00255
END	00256
SUBROUTINE RESECT2 (FL,XP,YP)	00257
COMMON C(2J,3), IP(3), XF(3), YF(3)	00258
DIMENSION B(15,6), P(2,9), D(6,7)	00259
INPUT LUNS ARE:	00260
8 PHOTO COORDINATES	00261
9 GROUND CONTROL	00262
10 INITIAL ORIENTATION PARAMETERS	00263
OUTPUT DATA ON LUN 20	00264
K=6.0	00265
IG0=J	00266
I=1	00267
READ PHOTO CONTROL COORDINATES	00268
10 READ(18,1)IPLATE,(IP(J), XF(J), YF(J), J=1,3)	00269
1 FORMAT(4X,I1,3(I4,2F6.3,6X))	00270
IF (IP(1) .LT. 20) GO TO 25	00271
BACKSPACE 8	00272
GO TO 40	00273
25 DO 33 J=1,3	00274
IF (IP(J) .EQ. 0 .AND. XF(J) .GT. 0.001) GO TO 26	00275
IF (IP(J) .EQ. 0) GO TO 38	00276
GO TO 28	00277
YP=YF(J)	00278
GO TO 38	00279
28 B(I,1)=IP(J)	00280
B(I,2)=YF(J)	00281
B(I,3)=XF(J)	00282
I=I+1	00283
38 CONTINUE	00284
GO TO 10	00285
40 IMAGE = I-1	00286
IF (IMAGE.LT.3) GO TO 10J2	00287
DO 57 I=1,IMAGE	00288
B(I,2)=YP-B(I,2)	00289
B(I,3)=XP-B(I,3)	00290
57 CONTINUE	00291
C READ GROUND CONTROL	00292
DO 100 I=1,IMAGE	00293
REWIND 9	00294
K=7(I,1)	00295
60 J=FFIN(9)	00296
IF (EJF(9)) GO TO 1004	00297
IF (K-J) 70,80,70	00298
70 DO 75 J=1,3	00299
TRAS=FFIN(9)	00300
75 CONTINUE	00301
GO TO 60	00302
80 DO 90 J=4,6	00303
B(I,J)=FFIN(9)	00304
90 CONTINUE	00305
100 CONTINUE	00306
C READ INITIAL PARAMETERS FOR CAMERA PHOTO NO., X,Y,Z IN FT	00307
C AND OMEGA, PHI , KAPPA IN DEGREES	00308
	00309

Figure D-2. Listing of program INSHORE. (Continued)

	REWIND 10	00310
108	IPLT=FFIN(10)	00311
	IF (EOF(10)) GO TO 1006	00312
	IF (IPLT-IPLATE) 110,120,110	00313
110	DO 115 I=1,6	00314
	TRAS4=FFIN(10)	00315
115	CONTINUE	00316
	GO TO 108	00317
120	DO 125 J=1,3	00318
	C(1,J)=FFIN(10)	00319
125	CONTINUE	00320
	C(2,1)=FFIN(10)/57.2958	00321
	C(2,2)=FFIN(10)/57.2958	00322
	C(2,3)=FFIN(10)/57.2958	00323
	DO 130 I=1,3	00324
	C(3,I)=COSF(C(2,I))	00325
	C(2,I)=SINF(C(2,I))	00326
130	CONTINUE	00327
C	ORIENTATION FACTORS IN C ARRAY	00328
610	C(4,1)=C(3,2)*C(3,3)	00329
	C(5,1)=-C(3,2)*C(2,3)	00330
	C(6,1)=C(2,2)	00331
	C(10,1)=-C(2,2)*C(3,3)	00332
	C(11,1)=C(2,2)*C(2,3)	00333
	C(12,1)=C(3,2)	00334
	C(10,2)=C(4,1)*C(2,1)	00335
	C(11,2)=C(5,1)*C(2,1)	00336
	C(12,2)=C(2,1)*C(2,2)	00337
	C(10,3)=-C(4,1)*C(3,1)	00338
	C(11,3)=-C(5,1)*C(3,1)	00339
	C(12,3)=-C(3,1)*C(2,2)	00340
	C(4,2)=C(3,1)*C(2,3)+C(12,2)*C(3,3)	00341
	C(5,2)=C(3,1)*C(3,3)-C(12,2)*C(2,3)	00342
	C(6,2)=-C(2,1)*C(3,2)	00343
	C(4,3)=C(2,1)*C(2,3)+C(10,1)*C(3,1)	00344
	C(5,3)=C(2,1)*C(3,3)+C(11,1)*C(3,1)	00345
	C(6,3)=C(3,1)*C(3,2)	00346
	DO 612 I=7,9	00347
	C(I,1)=0.	00348
	C(I,2)=-C(I-3,3)	00349
	C(I,3)=C(I-3,2)	00350
	C(13,I-6)=C(5,I-6)	00351
	C(14,I-6)=-C(4,I-6)	00352
612	C(15,I-6)=0.	00353
	GO TO (613,763),IGO	00354
C	CLEAR NORMAL EQUATION D ARRAY TO ZERO	00355
613	DO 614 I=1,6	00356
	DO 614 J=I,7	00357
614	D(I,J)=0.	00358
C	COMPUTE P TERMS FOR RESECTION PASS POINTS	00359
	DO 618 NU=1,IMAGE	00360
	DO 619 K=1,3	00361
619	C(16,K)=P(NU,K+3)-C(1,K)	00362
	K=4	00363
	DO 620 L=17,20	00364
	DO 620 I=1,3	00365
	C(L,I)=C(K,1)*C(16,1)+C(K,2)*C(16,2)+C(K,3)*C(16,3)	00366
620	K=K+1	00367
	DO 621 I=1,2	00368
	DO 622 L=1,4	00369
622	P(I,L)=(P(NU,I+1)*C(L+16,3)-(-FL)*C(L+16,I))/C(17,3)	00370
	DO 623 L=5,7	00371

Figure D-2. Listing of program INSHORE. (Continued)

623	P(I,L)=(-B(NU,I+1)*C(6,L-4)+(-FL)*C(I+3,L-4))*C(1,3)/C(17,3)	00372
621	P(I,3)=-P(I,1)	00373
C	CONTRIBUTION TO NORMAL EQUATIONS	00374
	DO 613 I=1,6	00375
	DO 613 J=I,7	00376
	DO 613 K=1,2	00377
613	J(I,J)=D(I,J)+P(K,I+1)*P(K,J+1)	00378
C	FORWARD SOLUTION	00379
	DO 639 I=1,6	00380
	SQR=SQRT(D(I,I))	00381
	DO 633 J=I,7	00382
693	D(I,J)=D(I,J)/SQR	00383
	IF (I-6) 697,696,696	00384
697	IP1=I+1	00385
	DO 633 L=IP1,6	00386
	DO 633 J=L,7	00387
699	D(L,J)=D(L,J)-D(I,L)*D(I,J)	00388
C	BACK SOLUTION	00389
696	D(6,7)=D(6,7)/D(6,6)	00390
	DO 631 I=1,5	00391
	NMI=6-I	00392
	NMIP1=NMI+1	00393
	DO 633 J=NMI+1,6	00394
699	D(NMI,7)=D(NMI,7)-D(J,7)*D(NMI,J)	00395
691	D(NMI,7)=D(NMI,7)/D(NMI,NMI)	00396
	DO 625 I=4,6	00397
625	D(I,7)=D(I,7)*C(1,3)	00398
C	ADD LEAST SQUARES RESULTS TO CAMERA PARAMETERS IN C ARRAY	00399
	DO 626 J=1,3	00400
	C(1,J)=C(1,J)+D(J+3,7)	00401
	C(4,J)=D(J,7)	00402
	C(5,J)=SQRT(1.-C(4,J)*C(4,J))	00403
	C(6,J)=C(2,J)*C(5,J)+C(3,J)*C(4,J)	00404
	C(7,J)=C(3,J)*C(5,J)-C(2,J)*C(4,J)	00405
	C(2,J)=C(6,J)	00406
626	C(3,J)=C(7,J)	00407
C	TEST MAGNITUDE OF CORRECTIONS FOR ORIENTATION PARAMETERES	00408
	DO 628 I=1,3	00409
	IF (ABS(D(I,7))-0.00001) 628,628,610	00410
628	CONTINUE	00411
	ISO=2	00412
	GO TO 610	00413
C	CAMERA PARAMETERS OUTPUT	00414
763	WRITE(20,532)	00415
	WRITE(20,527)	00416
	WRITE (20,528) IPLATE,(C(1,J),J=1,3)	00417
	WRITE (20,528)	00418
	WRITE (20,528) IPLATE,(C(2,J),J=1,3)	00419
	WRITE (20,528) IPLATE,(C(3,J),J=1,3)	00420
	WRITE (20,530) IPLATE	00421
	WRITE (20,533) ((C(I,J),J=1,3),I=4,6)	00422
527	FORMAT(/49H PLATE                   XO                   YO                   ZO)	00423
528	FORMAT(I7,3(2X,E14.7))	00424
529	FORMAT(/50H PLATE                   OMEGA                   PHI                   KAPPA)	00425
530	FORMAT(/30H ORIENTATION MATRIX FOR PLATE ,I7)	00426
532	FORMAT(/50H ORIENTATION PARAMETER CORRECTION LIMIT IS 0.00001)	00427
533	FORMAT (1X,3(2X,E14.7))	00428
	GO TO 1100	00429
1002	WRITE(20,1003) IPLATE	00430
1003	FORMAT(* INSUFFICIENT CONTROL,PLT#,I6)	00431
	GO TO 1100	00432
1004	WRITE (20,1005) K	00433
1005	FORMAT(* GRO CONTROL MISSING#,I6)	00434
	GO TO 1100	00435
1006	WRITE (20,1007) IPLATE	00436
1007	FORMAT(* INITIAL PARAMETERS NOT ON FILE#,I6)	00437
	GO TO 1100	00438
1100	RETURN	00439
	END	00440

Figure D-2. Listing of program INSHORE. (Continued)

## APPENDIX E

### Streamlines For A Source In A Uniform Flow

A general description of the CDC 3300 Computer and special fortran input functions is given in the introduction of Appendix B.

Program FLOWNET was used for generating the coordinates for plotting a flownet for a line source oriented perpendicular to a uniform stream. The program used the equation:

$$\psi = -UY + \alpha \left[ \left( Y + \frac{b}{2} \right) \theta_1 - \left( Y - \frac{b}{2} \right) \theta_2 - X \ln \frac{r_1}{r_2} \right]$$

which was derived in Section XI as equation 112.

The variables in the equation correspond to those shown in figure 96.

A flow diagram for program FLOWNET is shown in figure E-1 and the numbers in parentheses correspond to line numbers in the program listing of figure E-2.

### Program

Program FLOWNET requires that the velocity and azimuth from the north of the uniform flow, as well as the flow rate, estimated dilution over the outfall, the depth of the waste field and the length of the diffuser section be typed in. The maximum value of  $\psi$  is then computed and the y coordinate for a point 6000 ft downstream on the outermost streamline is determined. Using this as a starting point, the coordinates for successive points along one half of a stream line are computed by incrementing  $\theta$  and checking the new y value against the estimated value of y. After one side of a streamline is generated, the coordinates are rotated and the mirror image is computed. These are written on LUN 2 and the process is repeated for the next streamline until three streamlines and the centerline are computed.

The data on LUN 2 is saved and used as input for a plotting program which utilizes the Tektronix T-4002 graphic-scope. Two examples of plots generated using program FLOWNET are shown in figure 97 (a and b) with uniform flow velocities of 0.1 and 0.5 ft/sec respectively.

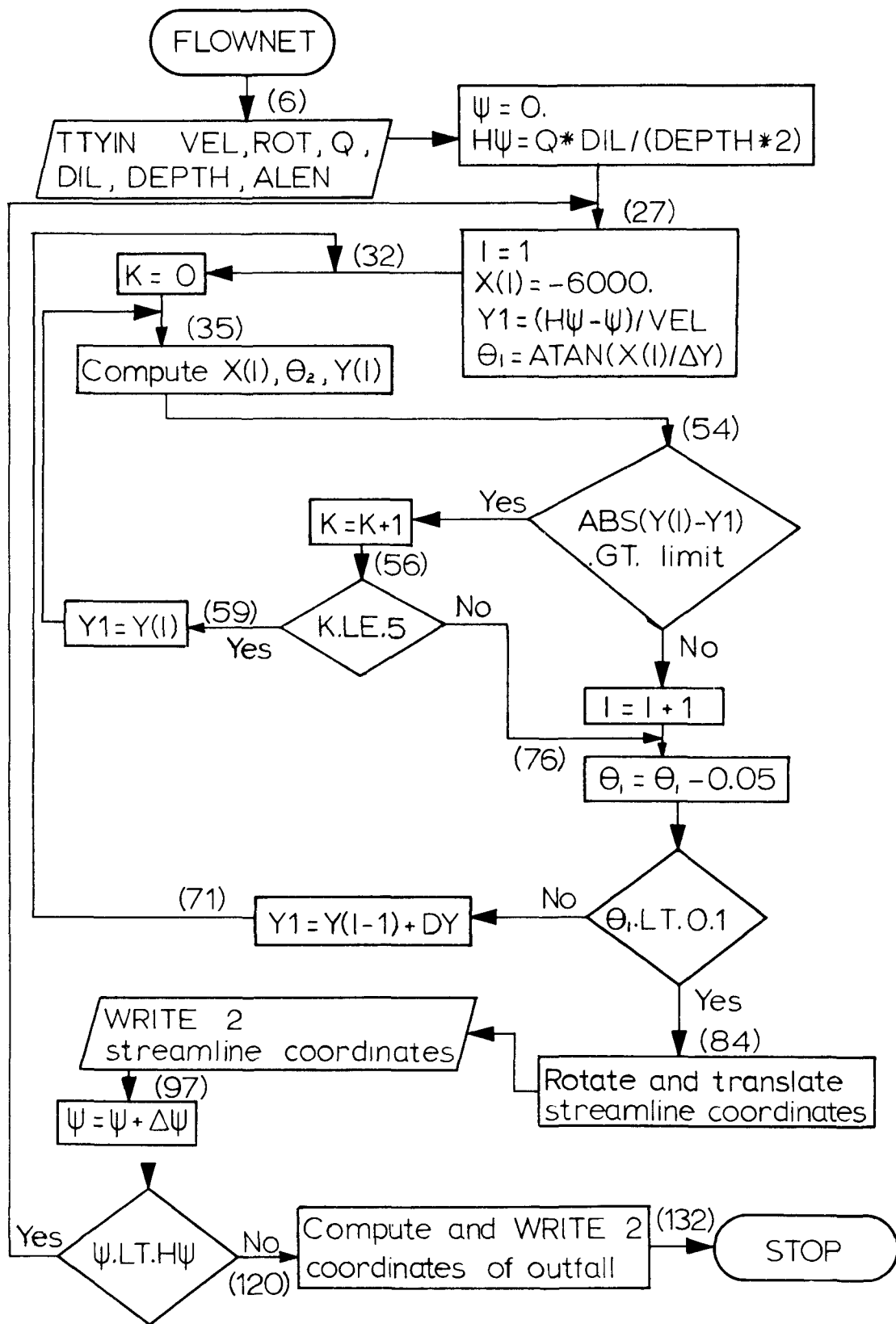


Figure E-1. Flow diagram of program FLOWNET.

PROGRAM FLOWNET	00001
DIMENSION X(250),Y(250),IPEN(250)	00002
1000 K60=0	00003
XCUT=1069450.	00004
YCUT=375770.	00005
U=TTYIN(4HVEL=)	00006
RCT=TTYIN(4HAZ= )	00007
ANG=RCT-1.5*3.1416	00008
Q=TTYIN(4HCFS=)	00009
DIL=TTYIN(4HDIL=)	00010
DEPT=TTYIN(4HDEP=)	00011
QDD=Q*DIL/DEPTH	00012
WRITE(2,3) U,QDD	00013
3 FORMAT(F10.2,F10.0)	00014
ALEN=TTYIN(4HLEN=)	00015
ALPHA=QDD/ALEN	00016
ALEN2=ALEN/2.	00017
COS1=COS(ANG)	00018
SIN1=SIN(ANG)	00019
CONST=ALPHA/(3.14159*2.*U)	00020
HPSI=QDD/2.	00021
DPSI=-HPSI/3.	00022
AFST=0.0	00023
XH11=0.	00024
XH1=0.	00025
THEL=4.71	00026
15 X(1)=-6000.	00027
I=1	00028
YI=(HPSI-AFST)/U	00029
BY=0.0	00030
YLIM=1.0.	00031
25 YL=YI	00032
K=0	00033
IPEN(I)=1	00034
50 IF(I.GT.1) GO TO 60	00035
RCT=ALEN2+YI	00036
THETR=-ATAN(X(I)/RCT)	00037
IF(RCT.GT.0) THETR=3.14159+THETR	00038
IF(THETR.LT.0.) THETR=6.28318+THETR	00039
GO TO 70	00040
60 X(I)=-SIN(THETR)/COS(THETR)	00041
X(I)=X(I)*(YI+ALEN2)	00042
70 RCT=ALEN2-YI	00043
THETA=ATAN(X(I)/RCT)	00044
IF(RCT.LT.0.) THETA=THETA+3.14159	00045
IF(THETA.LT.0.) THETA=THETA+6.28318	00046
SINA=SIN(THETA)	00047
SIN2=SIN(THETR)	00048
CONST2=ARS(SIN2/SINA)	00049
CON3=THETA+THETR-3.14159	00050
Y(I)=(-AFST/U+CONST*(ALEN2*CON3+X(I)*	00051
1 ALOG(CONS12)))/(1.+CONST*(THETA-THETR))	00052
YDIF=Y(I)-YI	00053
IF (ARS(YDIF) .LT. YLIM) GO TO 100	00054
K=K+1	00055
GO TO (90,91,92,92,92,110) K	00056
90 YST=YI	00057
YST1=Y(I)	00058
YI=Y(I)	00059
GO TO 50	00060
91 YND=YI	00061
YND2=Y(I)	00062
DIF1=YND2-YST1	00063
DIF2=YND-YST	00064
DIF3=YST-YST1	00065
DIF4=YND-YND2	00066

Figure E-2. Listing of program FLOWNET.

IF (ABS(DIF3).LT.ABS(DIF4)) GO TO 97	00067
Y1=YND+DIF2*ABS(DIF4/(DIF3-DIF4))	00068
GO TO 50	00069
97 Y1=YST-DIF2*ABS(DIF3/(DIF3-DIF4))	00070
GO TO 50	00071
92 YST=YND	00072
YST1=YND2	00073
GO TO 91	00074
100 IF (Y(I).GT.0..AND.X(I).LT.2000.) I=I+1	00075
110 THETR=THETB-0.05	00076
THEL=THETA	00077
IF (K.GT.5) GO TO 120	00078
DY=Y(I-1)-YL	00079
120 YI=Y(I-1)+DY	00080
IF (THETR.GT. 1.6) GO TO 25	00081
130 IPEN(I)=0	00082
K=I-1	00083
210 DO 300 I=1,K	00084
FACT1=X(I)*COSI	00085
IF (X(I).GT.2000.) IPEN(I)=0	00086
IF (X(I).LT.-6000.) X(I)=-6000.	00087
FACT2=Y(I)*SINI	00088
FACT3=-X(I)*SINI	00089
FACT4=Y(I)*COSI	00090
XG1=XOUT+FACT1+FACT2	00091
YG1=YOUT+FACT3+FACT4	00092
X(I)=XOUT+FACT1-FACT2	00093
Y(I)=YOUT+FACT3-FACT4	00094
WRITE(2,1) XG1,YG1,IPEN(I)	00095
1 FORMAT(2F10.,15)	00096
300 CONTINUE	00097
2 FORMAT(F5.0)	00098
IF (KGO.GT.0) GO TO 450	00099
DO 400 I=1,K	00100
WRITE(2,1) X(I),Y(I),IPEN(I)	00101
400 CONTINUE	00102
APSI=APSI+DPSI	00103
IF (APSI.LT.HPSI-0.1) GO TO 15	00104
450 KGO=KGO+1	00105
GO TO (500,700,900),KGO	00106
500 X(1)=0.0	00107
Y(1)=0.0	00108
K=7	00109
DO 600 I=2,7	00110
X(I)=X(I-1)-1000.	00111
Y(I)=0.0	00112
600 IPEN(I)=1	00113
IPEN(I)=0	00114
APSI=HPSI	00115
IPEN(K)=2	00116
GO TO 210	00117
700 CONTINUE	00118
WRITE(2,2) APSI	00119
Y(1)=-ALENZ	00120
Y(2)=ALENZ	00121
Y(3)=Y(2)	00122
Y(4)=Y(1)	00123
X(1)=20.	00124
X(2)=20.	00125
X(3)=-20.	00126
X(4)=-20.	00127
K=4	00128
GO TO 210	00129
900 END FILE 2	00130
GO TO 1000	00131
STOP	00132
END	00133

Figure E-2. Listing of program FLOWNET. (Continued)



<b>1</b>	Accession Number  <b>W</b>	<b>2</b>	Subject Field & Group  <b>SELECTED WATER RESOURCES ABSTRACTS INPUT TRANSACTION FORM</b>
<b>5</b>	Organization  Oregon State University, Corvallis, Oregon 97331		
<b>6</b>	Title  AIRPHOTO ANALYSIS OF OCEAN OUTFALL DISPERSION		
<b>10</b>	Author(s)  Burgess, Fred J.  James, Wesley P.	<b>16</b>	Project Designation 16070 ENS, Federal Water Quality Office
		<b>21</b>	Note
<b>22</b>	Citation Water pollution Control Research Series 16070 ENS, WQO, EPA. June 1971. 102 figs, 12 tables, 47 ref. 312 p.		
<b>23</b>	Descriptors (Starred First) * Aerial photography/ *Waste water disposal/ *Oceans/ *Coasts/ * Remote sensing/ industrial waste/ sewage effluents/ outlets/ mixing/ diffusion/ currents (water).		
<b>25</b>	Identifiers (Starred First)  *Ocean outfall/ *Marine disposal		
<b>27</b>	Abstract Aerial photography was taken of the ocean outfall waste plume at Newport, Oregon, during the summers of 1968, 1969, and the period extending from September, 1970 through May 1971. This remote sensing system involving multispectral photography was utilized to compute waste concentrations, water currents and diffusion coefficients in the outfall area. Conventional boat sampling of the waste field was conducted concurrently with the photography during the 1968 and 1969 field seasons. The waste concentrations determined by the two methods were compared by matching ground coordinates. The correlation coefficient for the comparison ranged from 0.85 to 0.95. The water current velocity was found to be the dominant factor in the surface plume pattern. The steady state form of the Fickian diffusion equation with a unidirectional transport velocity was not applicable to the majority of the observations. The equation for a line source in a uniform stream provided the x and y velocity components for a two-dimensional diffusion model with the losses to the lower layers being considered by including a decay coefficient. This second model was found to be more applicable to the diffusion process. Characteristic airphoto pattern elements are given for visual interpretation of the photography. Wind velocity, sea state, current velocity wave height and diffusion coefficients can be estimated from the aerial photography.		
Abstractor		Institution Oregon State University	

WR 102 (REV JULY 1969)  
WRSIC

SEND, WITH COPY OF DOCUMENT, TO: WATER RESOURCES SCIENTIFIC INFORMATION CENTER  
U.S. DEPARTMENT OF THE INTERIOR  
WASHINGTON, D. C. 20240